TABLE OF CONTENTS

TABLE OF CONTENTS (Continued)

NASA Contractor Report 2957



# Design and Fabrication of a Radiative Actively Cooled Honeycomb Sandwich Structural Panel for a Hypersonic Aircraft

D. A. Ellis, L. L. Pagel,
and D. M. Schaeffer

CONTRACT NAS1-13939
MARCH 1978

NASA

NASA Contractor Report 2957

# Design and Fabrication of a Radiative Actively Cooled Honeycomb Sandwich Structural Panel for a Hypersonic Aircraft

D. A. Ellis, L. L. Pagel,
and D. M. Schaeffer
*McDonnell Douglas Corporation*
*McDonnell Aircraft Company*
*St. Louis, Missouri*

Prepared for
Langley Research Center
under Contract NAS1-13939

NASA
National Aeronautics
and Space Administration

**Scientific and Technical
Information Office**

1978

Blank Page

# FOREWORD

This report was prepared by McDonnell Aircraft Company (MCAIR), St. Louis, Missouri, for the Langley Research Center of the National Aeronautics and Space Administration.

The purpose of this program was to design and optimize a radiative actively cooled panel compatible with the available hydrogen fuel heat sink for a hypersonic transport aircraft and to substantiate the panel structural integrity by tests. The program was conducted in accordance with the requirements and instructions of NASA RFP 1-31-5303 and McDonnell Technical Proposal Report MDC A3280, with minor revisions mutually agreed on by NASA and MCAIR. Customary units were used for the principal measurements and calculations. Results were converted to the International System of Units (SI) for the final report.

Mr. Leland C. Koch was the MCAIR Program Manager, with Mr. David A. Ellis as Principal Investigator. Mr. D. M. Schaeffer was responsible for the detail strength analysis and liaison between Engineering and Manufacturing. Mr. L. L. Pagel was responsible for thermodynamic analyses.

Blank

Page

LIST OF ILLUSTRATIONS AND TABLES

LIST OF ILLUSTRATIONS AND TABLES (Continued)

LIST OF TABLES

SUMMARY

Feasibility of combining radiative and convective cooling in a structural system suitable for hydrogen fueled hypersonic cruise vehicles was investigated by designing and optimizing a 0.61 by 6.1 m (2 by 20 ft.) radiative convectively cooled panel. The system was designed for a uniform uniaxial, in-plane limit load of ±210 kN/m (±1200 lbf/in), a uniform limit pressure of ±6.89 kPa (±1.0 psi), a fatigue life of 5000 fully reversed load cycles and for aerodynamic heating conditions equivalent to 136 kW/m$^2$ (12 Btu/ft$^2$ sec) to a 422 K (300°F) surface temperature. Based on factors such as mass, performance and integrity, durability, producibility, inspectability, and cost, a Rene'41 corrugation stiffened, beaded heat shield with a Min-K insulation blanket was selected as the radiative concept to reduce the heat flux to the convectively cooled honeycomb sandwich structural panel. The optimized combined radiative actively cooled configuration which absorbs 9.1 kW/m$^2$ (0.8 Btu/ft$^2$ sec) offers a 7 percent mass savings over an unshielded system which absorbs the full 136 kW/m$^2$ (12 Btu/ft$^2$ sec) heat flux when the mass of a distribution system to supply coolant to the panels is included.

Sensitivity studies indicate that the mass of the honeycomb sandwich panel is unaffected by biaxial in-plane loading (transverse load ≤ 50 percent of longitudinal load) but increases by 11 percent when shear loads (50 percent of longitudinal load) are combined with a uniaxial in-plane load. Additionally, the combined system can accommodate variations in the aerodynamic heating conditions of 25 to 200 percent without changing the concept significantly i.e., by resizing or material substitutions.

A 0.30 by 0.61 m (1 by 2 ft.) heat shield thermal restraint specimen and a 0.61 by 1.22 m (2 by 4 ft.) test panel which incorporates the major design features of the full scale panel were designed, fabricated, and delivered to NASA for tests to determine the thermal/mechanical performance and structural integrity of the combined system.

Black Page

# INTRODUCTION

Design of structures to operate efficiently for long periods in the severe thermal environment encountered by hypersonic cruise aircraft requires careful selection of materials and structural concepts. In Reference 1 an actively cooled aluminum panel which absorbs all of the incident heat load was designed for hypersonic aircraft application. Hydrogen fuel was used as the ultimate heat sink to cool the aluminum structure to relatively low temperatures so that long life could be achieved. However, since cooling of the engines and the inlets requires a high percentage of the available heat sink it was doubtful that the remaining available heat sink would be sufficient for airframe cooling. A solution to this problem is the design of a radiative actively cooled panel (figure 1) which uses heat shields and insulation on the outer surface of the structural actively cooled panel. Such a system permits operation of the outer surface at high temperatures which radiates an appreciable amount of the incident heat load back to the atmosphere and reduces the heat load that must be absorbed by the hydrogen fuel. The present study uses the actively cooled panel concept from reference 1, i.e., a honeycomb sandwich concept with coolant passages in contact with the outer skin. However, the panel was optimized to be compatible with a radiative thermal protection system and the heat sink available for a representative hypersonic vehicle described in reference 2.

A primary purpose of this study was to compare the mass of a radiative actively cooled panel to the mass of a bare actively cooled panel designed to the same conditions and constraints, thus adding to the existing experimental technology base for cooling hypersonic aircraft structures. The approach was to design and optimize a 0.61 x 6.1m (2 x 20 ft) full scale panel which innovatively combines radiative and active cooling to control structural temperatures to levels compatible with use of lightweight materials and to fabricate a 0.61 x 1.22 m (2 x 4 ft) panel for performance testing by NASA.

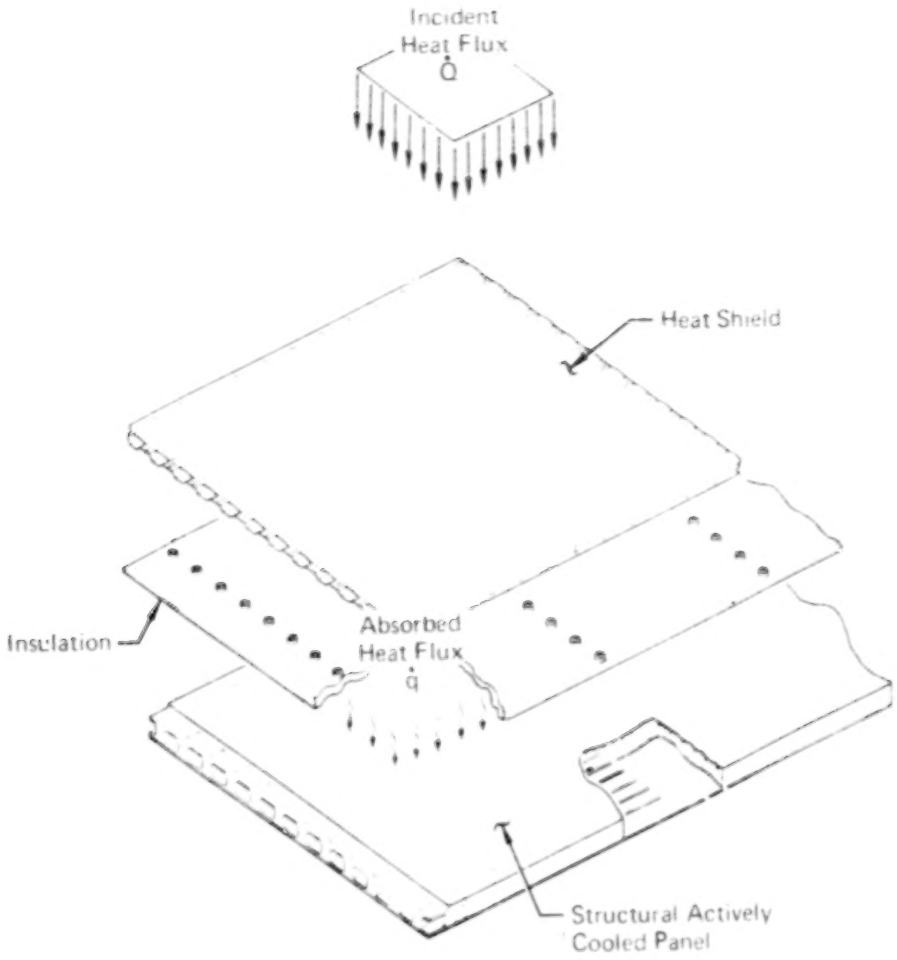


**FIGURE 1 - RADIATIVE ACTIVELY COOLED PANEL CONCEPT**

Results of the design and optimization of the full scale radiative actively cooled structural panel, including radiative concept selection, sensitivity of configuration mass to variation in panel mechanical and thermal loads, final configuration details, test panel description, and conclusions of the study are summarized in the main body of the report. Supporting details are presented in appendices.

Use of commercial products or names of manufacturers in this report does not constitute official endorsement of such products or manufacturers, either expressed or implied, by the National Aeronautics and Space Administration.

## SYMBOLS AND PARAMETERS

| | |
|---|---|
| a | Crack depth, cm (in.) |
| A | Preloaded dome width or length, cm (in.) |
| ACP | Actively cooled panel |
| ACS | Active cooling system |
| APS | Auxiliary power system |
| Btu | British thermal units |
| b | Length of panel edge, m (in.) |
| $C_p$ | Material specific heat, J/kg.K (Btu/lbm °F) |
| C | One half of crack length, cm (in.) |
| D | Tube inside diameter, cm (in.), Drag, N(lbf) |
| da/dN | Crack growth rate |
| E | Young's modulus of elasticity, Pa (psi) |
| E' | Effective modulus of elasticity of face sheet, Pa (psi) |
| $E_c$ | Effective modulus of core, Pa (psi) |
| EDM | Electrical discharge machined |
| F | Pumping power conversion factor, g/kW.s (lbm fuel/Hp-hr) |
| Fcc | Crippling stress, Pa (psi) |
| $F_c$ | Core flatwise compression strength or compression stress, Pa (psi) |
| $F_{cy}$ | Compression yield stress, Pa (psi) |
| $F_I$ | Allowable working stress of inner face sheet, Pa (psi) |
| $F_o$ | Allowable working stress of outer face sheet, Pa (psi) |
| $F_{tu}$ | Tensile ultimate stress, Pa (psi) |
| $F_{ty}$ | Tensile yield stress, Pa (psi) |
| $F_w$ | Face wrinkling stress, Pa (psi) |
| FWD | Forward |
| f | Fanning friction factor |

| | |
|---|---|
| H | Actively cooled panel height, cm (in.) |
| $H_b$ | Beaded skin height, cm (in.) |
| $H_c$ | Corrugation height, cm (in.) |
| $H_D$ | Hydraulic diameter, cm (in.) |
| HP | Horsepower |
| h | Heat transfer coefficient, preloaded dome height, cm (in.) |
| Hr | Hour |
| I | Moment of inertia |
| in. | Inch |
| K | Panel buckling coefficient |
| $K_c$ | Critical stress intensity factor, $MP\sqrt{m}$ ($KSI\sqrt{in.}$) |
| $K_T$ | Loss coefficient, stress concentration factor |
| k | Thermal conductivity, W/m·K (Btu·in./hr·ft$^2$ °F) |
| ksi | Thousand pound force per square inch |
| L | Length, m (in.); lift, N (lbf) |
| lbf | Pounds force |
| lbm | Pounds mass |
| M | Mach |
| MCAIR | McDonnell Aircraft Company |
| $\dot{m}_c$ | Coolant mass flow rate, g/s (lbm/hr) |
| N/A | Not available |
| N | Compression load per unit length N/m (lb/in.); cycles |
| $N_x$ | Axial load per unit length N/m (lbf/in.) |
| $N_{xy}$ | Shear load per unit length N/m (lbf/in.) |
| $N_y$ | Axial load per unit length N/m (lbf/in.) |

SYMBOLS AND PARAMETERS (Continued)

| | |
|---|---|
| OASPL | Overall sound pressure level, dB |
| O.D. | Outside diameter, cm (in.) |
| OWE | Operational weight empty, g (lbm) |
| P | Tube pitch, cm (in.); beaded skin pitch, cm (in.); load, N (lbf) |
| psi | Pounds force per square inch |
| P | Pressure, Pa (psi) |
| $P_r$ | Prandtl number |
| $\dot{Q}$ | Incident heat flux |
| Q | Flaw shape parameter |
| q | Dynamic pressure |
| $\dot{q}$ | Heat flux, $kW/m^2$ ($Btu/ft^2$ sec) |
| $\dot{q}_{ref}$ | Reference aerodynamic heat flux of 136 $kW/m^2$ (12 $Btu/ft^2$ sec) |
| R | Stress ratio - minimum stress divided by maximum stress; reaction, N (lbf); radius, cm (in.) |
| RACP | Radiative actively cooled panel |
| RT | Room temperature, K (°F) |
| $R_e$ | Reynolds number |
| $R_{e_L}$ | Critical Reynolds number for laminar flow |
| $R_{e_T}$ | Critical Reynolds number for turbulent flow |
| S | Honeycomb cell size, cm (in.) |
| T | Temperature, K (°F), thrust, N (lbf) |
| TPS | Thermal protection system |
| $T_{co}$ | Temperature of coolant at outlet, K (°F) |
| $T_o$ | Temperature in outer skin, K (°F) |
| $T_{ref}$ | Reference wall temperature of 422K (300°F) |
| $T_w$ | Local wall temperature, K (°F) |

| | |
|---|---|
| TOGW | Takeoff gross weight |
| $t$ | Thickness, cm (in.) |
| $t_b$ | Thickness of beaded skin, cm (in.) |
| $t_c$ | Thickness of corrugation, cm (in.) |
| $t_I$ | Thickness of inner skin, cm (in.) |
| $t_o$ | Thickness of outer skin, cm (in.) |
| $t_t$ | Thickness of Dee tube wall, cm (in.) |
| V | Velocity of fluid |
| W | Mass |
| $\alpha$ | Coefficient of thermal expansion |
| $\delta$ | Initial deflection of facing waviness; thickness, cm (in.) |
| $\Delta$ | Delta; difference |
| $\Delta K$ | Stress intensity factor difference |
| $\varepsilon$ | Surface emissivity |
| $\mu$ | Poisson's ratio, fluid viscosity, $10^{-6}$ |
| $\mu_s$ | Fluid viscosity evaluated at wall temperature |
| $\rho$ | Density, $kg/m^3$ ($lbm/ft^3$) |
| $\psi$ | Deflection or stress due to combined edgewise and normal loadings, cm (in.) |
| $\psi_o$ | Deflection or stress, due to panel normal load only, cm (in.) |
| $\theta$ | Time, hour |

SUBSCRIPTS

| | |
|---|---|
| a | Ambient |
| abs | Absorbed |
| all. | Allowable |
| aw | Adiabatic wall |

## SUBSCRIPTS

| | |
|---|---|
| b | Beaded skin |
| C | Compression |
| c | Coolant, corrugation, honeycomb core |
| cr | Critical |
| I | Inner |
| L | Laminar |
| MAX | Maximum |
| s | Skin |
| SLS | Sea level static |
| T | Turbulent |
| t | tube |

## SI UNITS

| | |
|---|---|
| g | Gram (mass) |
| K | Kelvin (temperature) |
| m | Meter (length) |
| N | Newton (force) |
| Pa | Pascal (pressure and stress) |
| W | Watt (power) |
| s | Second (time) |

## SI PREFIXES

| | |
|---|---|
| m | Milli ($10^{-3}$) |
| c | Centi ($10^{-2}$) |
| k | Kilo ($10^{3}$) |
| M | Mega ($10^{6}$) |
| G | Giga ($10^{9}$) |

Blank

Page

## STATEMENT OF PROBLEM

### Generai Problem

The problem was to demonstrate the feasibility of integrating a radiative thermal protection system with an actively cooled structural panel which could be used on hypersonic cruise transpo't aircraft. Design problems include matching airframe cooling flow requirements with engine fuel flow requirements, integration of the cooling system into the primary structure, and integration of heat shield attachments into the panel.

### Design Conditions and Requirements

General requirements to ensure that the panel design was representative of a hypersonic transport aircraft structure were:

- Failure due to cracks and fatigue must be avoided.
- The panel must be designed to avoid catastrophic failure in the event of loss of coolant supply to a panel.
- The panel must withstand the acoustic and aerodynamic environment of a hypersonic aircraft.
- The panel must be optimized for minimum mass within practical limitations.
- The coolant manifolds must be terminated at the panel edge.

Actively cooled panel - The full scale panel design limit loads and heat flux are presented in figure 2. The actively cooled panel was designed to sustain cyclic in-plane limit loading, parallel to the 6.1m (20 ft) edge, of ±210 kN/m (±1200 lbf/in.), combined with a uniform panel pressure of ±6.89 kPa (±1.0 psi), while subjected to an undetermined uniform heat flux which results in minimum system mass.

Provisions were made for attachment to the adjacent panels on all edges and for attachment to fuselage frames located at 0.61m (2 ft) spacing.

The active cooling system was designed with a coolant outlet pressure of at least 344.7 kPa (50 psi).

The structural panel was designed to sustain 10,000 hours exposure to maximum temperatures and to sustain 20,000 cycles

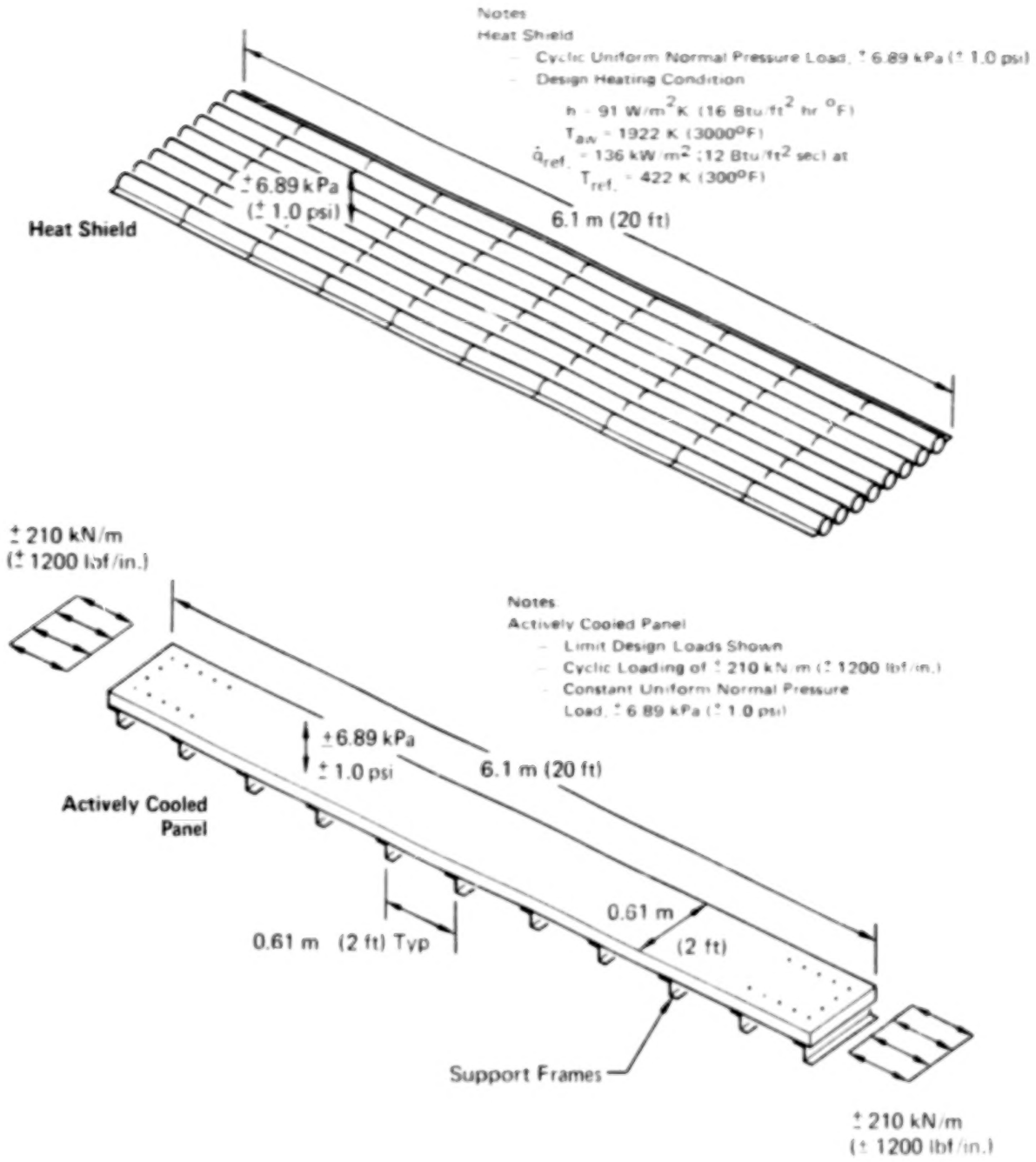


**FIGURE 2 - RADIATIVE ACTIVELY COOLED PANEL DESIGN LOADS AND HEAT FLUX**

(5000 cycles with a scatter factor of four) of design limit loads and temperatures without fatigue failure, without crack growth to a critical length in the skins, and without surface flaw growth through the thickness of the coolant passages (see Appendix A). The scatter factor of four is consistent with the

requirements of MIL-A-008866A (reference 3) and is used to protect against fatigue failure for aircraft that experience a service-load spectrum more severe than the design service-load spectrum.

Heat shield loads and temperatures - The heat shields were designed to sustain 20,000 cycles (including a scatter factor of four) of design limit pressures of ±6.89 kPa (±1.0 psi) and aerodynamic heating conditions equivalent to 136 $kW/m^2$ (12 $Btu/ft^2$ sec) to a 422K (300°F) surface temperature. The thermal cycle used in the design of the heat shield and the actively cooled panel was compatible with the flight profile of a representative hypersonic aircraft described in Appendix B.

Factors of safety - The factors of safety on loads, temperatures, and stresses shown in table 1 are the same as used in the study described in reference 1 and are based on the recommendations of Federal Air Regulations, Part 25 (reference 4). A factor of safety of 1.5 was applied to in-plane loads, coolant pressures, and aerodynamic pressures when sizing the panel to prevent failure (an ultimate strength check). A factor of

**TABLE 1 - FACTORS OF SAFETY**

| Static Strength Design Conditions | Factor of Safety | |
|---|---|---|
| | Limit | Ultimate |
| In-Plane Axial Load | 1.0 | 1.5 |
| Lateral Pressure | 1.0 | 1.5 |
| Thermal Stress | 1.0 | 1.0 |
| Temperature | 1.0 | 1.0 |
| Temperature Gradient | 1.0 | 1.0 |
| Coolant Pressures[a] | 1.0 | 1.5 |

(a) Burst pressure (acting alone) factor of safety for coolant passages, manifolds and fittings is 4.0

safety of four was used on the coolant operating pressures when analyzing the manifolds, coolant system passages and fittings for a burst condition (pressure acting alone). Factors of safety of one were applied to temperature, temperature gradients, and thermal stresses (based on the recommendations in reference 5) for both limit and ultimate strength checks. Using these factors of safety, the panel was designed for any combination of limit

loads and temperatures without yielding or significant permanent set, and for any combination of ultimate loads and temperatures without failure.

Deviation from moldline contour - The panel surface deviation from contour (in streamwise direction) of +0.051 cm (0.020 in.) and -0.102 cm (-0.040 in.) is the same as that used for the forward fuselage of the F-15, where good surface smoothness is required to minimize the aerodynamic drag. This flatness requirement was selected because, although surface smoothness at hypersonic speeds is not as important as it is in the Mach .60 to Mach 3.0 range, a hypersonic aircraft would be penalized as it passed through the subsonic and supersonic region if the aircraft surface was not reasonably smooth in the streamwise direction.

Dynamics and acoustics - The heat shields were designed to be free of flutter throughout the flight envelope (Appendix B) enlarged by 20 percent equivalent airspeed consistent with the requirements of Federal Air Regulation Part 25 (reference 4). The acoustic environment on the lower surface of the fuselage 3.05 m (10 ft.) aft of the nose of the representative hypersonic aircraft was used for acoustic design of the heat shields. Heating conditions at this location matched those specified in figure 2.

## RADIATIVE ACTIVELY COOLED PANEL OPTIMIZATION AND DESIGN SEQUENCE

The procedure used to optimize the radiative actively cooled panel design is illustrated in figure 3. The predominant flow of the design process is indicated by the direction of the arrows. Several engineering disciplines were involved in each phase of the study, with the primary interaction occurring between structural and thermal analysis in the parametric and trade study phase. Subsequent paragraphs present a synopsis of each phase.

Select representative aircraft - A representative hypersonic aircraft (see Appendix B) was selected to provide a realistic flight profile and design conditions for input to thermal, structural, and dynamic analyses.

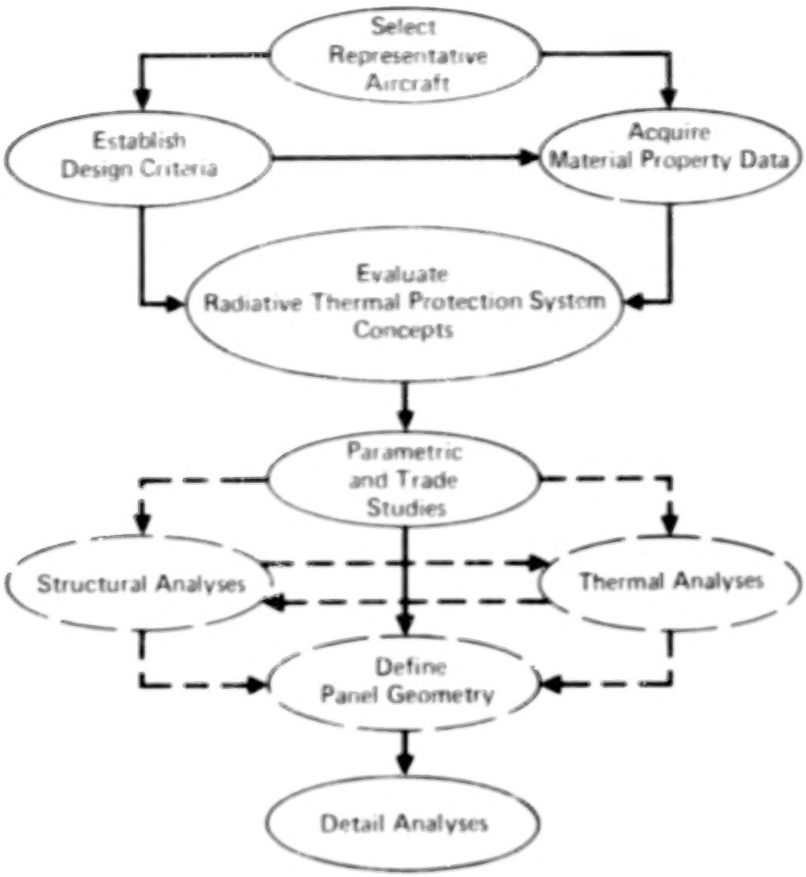


**FIGURE 3 - PANEL OPTIMIZATION AND DESIGN SEQUENCE**

Establish design criteria - Panel design criteria and requirements were established consistent with those for the selected representative aircraft.

Acquire material property data - Materials were selected which satisfied the requirements and criteria established for the representative aircraft. Appropriate material property data were collected and operating allowables established for the aluminums, superalloys, insulations, and the coolant.

Evaluate radiative thermal protection system concepts - Nine radiative thermal protection systems were evaluated to permit selection of a concept which offered the most potential for providing a minimum mass design when combined with an actively cooled panel.

Parametric and trade studies - The actively cooled panel, active cooling system, insulation, and heat shield were optimized

during this phase to minimize mass. Primary elements of each component, i.e., skin gage; tube size, wall thickness, and tube spacing; corrugation thickness, height, and spacing; beaded skin thickness and spacing; insulation thickness, etc., were considered in the optimization. The optimization involved determining the minimum mass of each component versus absorbed heat flux ($\dot{q}_{abs}$) and then summing the total to determine the absorbed heat flux for least total mass. Once the primary elements were optimized, the frame attachments, edge joints, manifolds, supports, and insulation packages were sized and integrated in the design such that least additional mass resulted.

Sizing a radiative actively cooled panel for minimum mass involved selecting materials, establishing allowables, and defining the geometry. This involved thirty-six different parameters and their impact on panel mass. Table 2 lists these parameters and identifies those that were selected based on results from reference 1.

**TABLE 2 - RADIATIVE ACTIVELY COOLED PANEL PARAMETERS**

| Varied During Study | Fixed, Based on Actively Cooled Panel Program |
|---|---|
| Outer Face Sheet Thickness | Outer Face Sheet Material and Allowable Stresses |
| Inner Face Sheet Thickness | Inner Face Sheet Material and Allowable Stresses |
| Tube Diameter | Tube Material and Allowable Stresses |
| Tube Pitch | Honeycomb Core Material |
| Tube Wall Thickness | Tube to Outer Skin Adhesive |
| Honeycomb Core Density | Interface Conductance of Tube to Outer Skin Bond Joint |
| Honeycomb Core Height | Honeycomb Core to Outer Skin and Tube Adhesive |
| Heat Shield | Honeycomb to Inner Skin Adhesive |
| Corrugation Thickness | Manifold Material |
| Bead and Corrugation Pitch | Manifold Configuration |
| Beaded Skin Thickness | Coolant |
| Bead Height | Coolant Inlet Temperature |
| Corrugation Height | Maximum Panel Operating Temperature |
| Heat Shield Support Spacing | |
| Insulation Material | |
| Insulation Thickness | |
| Absorbed Heat Flux | |
| Coolant Mass Flow Rate | |
| Coolant Pressure | |

The steps followed in the Parametric and Trade Studies are shown in figure 4. In Step 1 the combination of outer skin thickness ($t_o$), tube diameter (D), and tube pitch (P) that yielded a specified maximum panel temperature was calculated for different values of absorbed heat flux. A specific coolant with preselected inlet and outlet temperatures was used in the calculations. The maximum structural temperature occurs in the outer skin midway between tubes at the coolant exit end of the panel. Thus, the results were based on a steady-state heat balance neglecting longitudinal temperature gradients which are small relative to lateral gradients. Under these conditions all of the heat impinging on a unit length of panel of width (P) is transferred to the coolant. Expressions defining heat conduction in the outer skin and across the tube/skin interface, and convection between the tube wall and coolant were derived to solve for geometric combinations that satisfy the boundary conditions (coolant and maximum panel temperatures).

Using these geometric combinations, the structural mass of the panel was calculated as a function of absorbed heat flux and tube pitch (P). This mass was determined for specific combinations of P, D, and $t_o$ (generated in Step 1) by varying the inner skin thickness and computing the honeycomb core height that satisfied panel strength and buckling requirements when subjected to the design panel pressure, inplane loads and temperatures. Total mass of the panel was found by adding individual masses of the panel elements including the coolant mass in the tubes which varies with tube diameter and spacing. Several inner skin thicknesses were used for discrete values of absorbed heat flux ($q_{abs}$) until a minimum mass panel was found for each value of $q_{abs}$. The variation of panel mass with $q_{abs}$ for various tube spacings (Step 2) permits selection of tube spacing for minimum panel mass as a function of $q_{abs}$.

The mass increment required to pump the coolant through the panel (pumping power penalty) as a function of absorbed heat flux was calculated in Step 3. The pumping power penalty is directly

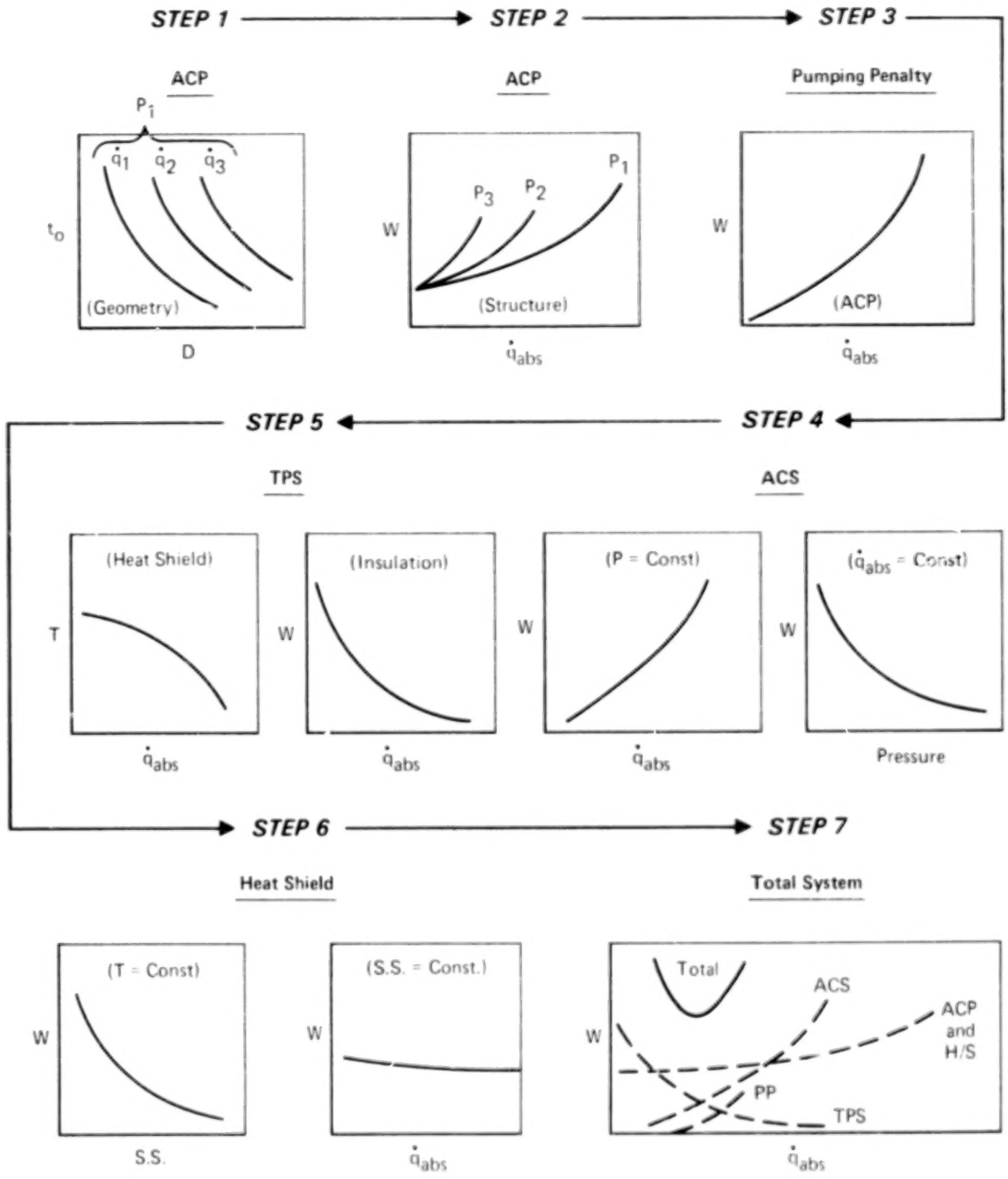


FIGURE 4 - PARAMETRIC AND TRADE STUDIES

proportional to the product of coolant mass flow rate and pressure drop in the panel. Therefore, the coolant mass flow rate (hence, pressure drop and pumping power penalty) was calculated as a function of $\dot{q}_{abs}$ for the combination of P, D, and $t_o$ (from Steps 1 and 2), which satisfied heat transfer requirements.

The objective of Step 4 was to establish the sensitivity of active cooling system (ACS) mass to absorbed heat flux. The active cooling system includes the mass of distribution lines, pumps, reservoir, heat exchanges, coolant inventory, and the fuel and oxidizer required to pump the coolant through the system. Most of these component masses are pressure or pressure drop dependent. Mass of the ACS as a function of pressure was calculated to establish the system operating pressure which minimizes ACS mass for a representative temperature rise in the coolant. For the fixed system pressure, ACS mass was then calculated as a function of absorbed heat flux. Results from reference 2 served as a data base for computing the mass of ACS components.

The thermal protection system (i.e., heat shields and insulation) was sized in Steps 5 and 6. Heat shield temperatures and insulation mass were calculated as a function of absorbed heat flux from a steady-state heat balance between the incident aerodynamic heat, heat radiated to space, and heat conducted through the insulation material to a constant (average) temperature panel (Step 5). Variation of the heat shield surface temperature with the absorbed heat flux permitted structural sizing of the heat shield in Step 6. Material allowables were determined for the candidate materials for different temperatures and/or absorbed heat fluxes. The material with the most potential for yielding a minimum mass heat shield was used when sizing the heat shield for both the pressure loading and thermal stresses. Heat shield geometry and support spacing were varied to obtain a minimum mass material/configuration. The thickness, spacing, and height of the crown in the beaded skin were varied until both fatigue and static strength requirements in the transverse direction were satisfied. Then the thickness and height of the corrugation and the support spacing were varied until strength and fatigue require-

ments in the longitudinal direction were satisfied. The mass of the heat shields was calculated for different temperatures and gave the sensitivity of heat shield mass to absorbed heat flux.

The last step in the parametric and trade studies, Step 7, consisted of adding the mass of each item (i.e., the mass of the actively cooled panel from Step 2; the mass of the pumping penalties from Step 3; the mass of the active cooling system from Step 4; and the mass of the thermal protection system, insulation and heat shield, from Steps 5 and 6, respectively), for discrete values of absorbed heat flux to identify the absorbed heat flux which yields a minimum mass radiative actively cooled panel design.

The procedure was used to size a radiative actively cooled panel for normal cruise operation and for abnormal conditions such as loss of coolant supply to a panel.

Detail Analyses - Detail analyses were performed to substantiate the design and size manifolds, splices, and local attachments.

RADIATIVE THERMAL PROTECTION SYSTEM CONCEPT EVALUATION

Nine radiative thermal protection system (TPS) concepts were investigated for use on a hypersonic cruise transport aircraft. These concepts were: 1) RSI (LI900), 2) Metal Wool, 3) SLA-220 (silica filled elastomeric silicon), 4) Foamed metals, 5) Preloaded dome, 6) Screen sandwich, 7) Astroquartz, 8) Beaded skin, and 9) Corrugated stiffened beaded skin. The concepts were evaluated and compared on the basis of mass, cost, producibility, inspectability, maintainability, durability, volumetric efficiency, performance and integrity, resistance to hot gas influx, tolerance to overheat, and development needs. Weighting factors, agreed upon between MCAIR and NASA, were applied to realistically assess the significance of each of the above figures of merit to the overall mass, cost, and performance of a hypersonic aircraft. The concept designs were developed in sufficient detail to permit a reasonable comparison of each concept for each figure of merit.

A first order assessment eliminated the RSI, the metal wool, and the foamed metals. The RSI was eliminated because of its

poor durability, which would require high maintenance if used on a transport aircraft. Durability was also a reason for eliminating the metal wool concept. Thermal and structural performance of the metal wool when subjected to a hypersonic environment was also questionable. The foamed metals were eliminated because of their water absorption characteristics and questionable performance in service, i.e., the ability to withstand hypersonic flow.

The six remaining concepts shown in figure 5 were then evaluated in more detail. The corrugated stiffened beaded skin concept was selected for optimization with the actively cooled

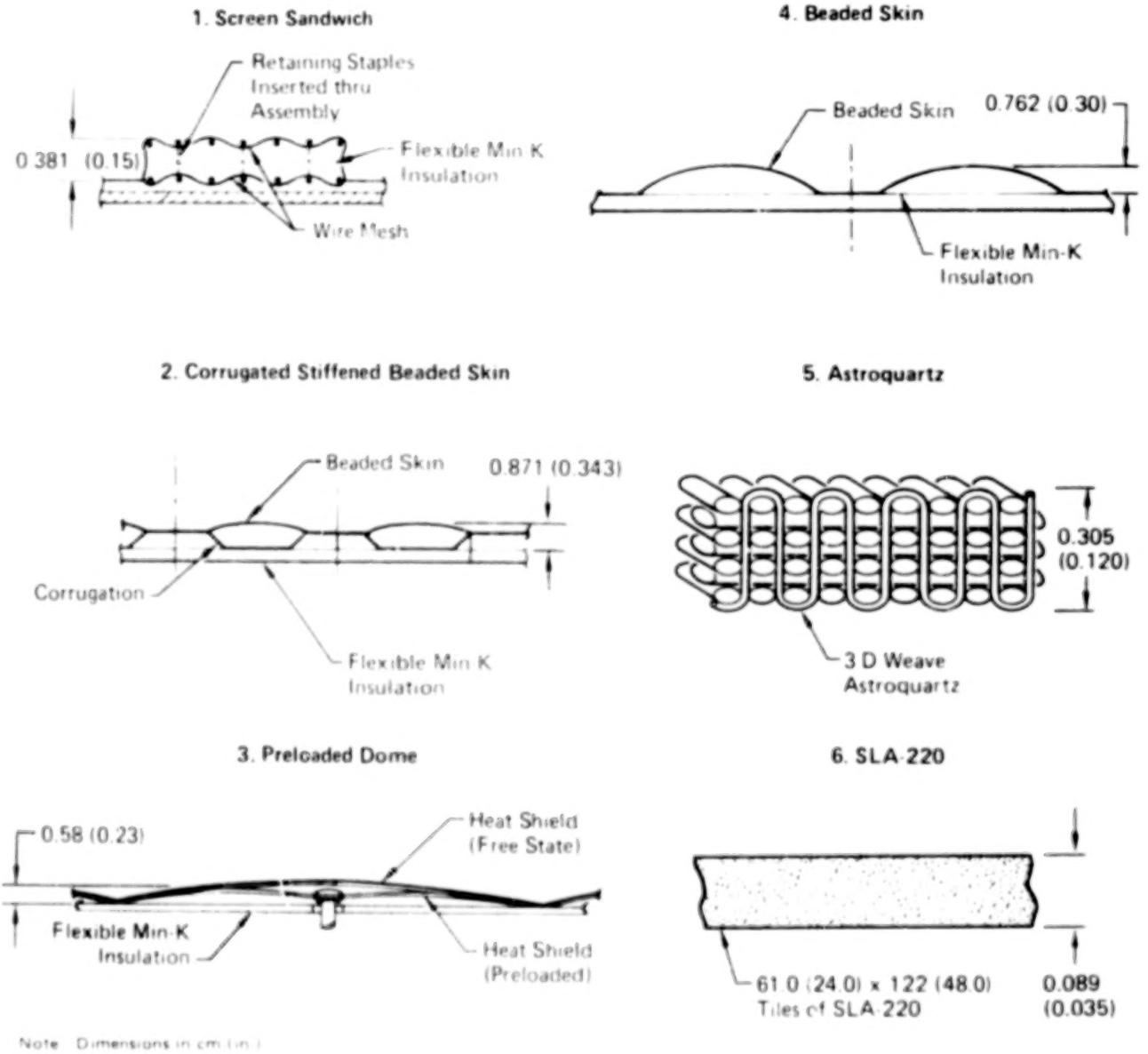


Note: Dimensions in cm (in.)

FIGURE 5 - FINAL HEAT SHIELD CONCEPTS EVALUATED

panel. This concept was selected since it received uniformly high ratings for all figures of merit and was considered the most reliable of all the concepts evaluated.

Details of the rating system used and a description of each concept evaluated are presented in Appendix C.

## PARAMETRIC AND TRADE STUDIES

During this phase of the program, structural and thermal aspects of the panel design were continuously re-evaluated to ensure that a thermally and structurally compatible design was achieved. Analyses, using the material property data presented in Appendix A, determined the mass and associated geometry of the insulation packages, the active cooling system, the auxiliary power system, the actively cooled panel, and the heat shield. The mass of each item was calculated versus absorbed heat flux to identify the configurations yielding a minimum mass radiative actively cooled panel and its operating absorbed heat flux level. Radiative actively cooled panels were sized for a normal cruise condition and also for a condition in which loss of coolant supply to a panel would not result in catastrophic failure of the panel. Once the radiative actively cooled panel was optimized, sensitivity studies determined the effect on the actively cooled panel mass of increased inplane loading, combined bi-axial loading and shear, and higher and lower heating rates.

### Insulation and Active Cooling System Mass Versus Heat Flux

The radiative actively cooled panel concept employs an external thermal protection system to reduce the aerodynamic heat load that must be absorbed by the coolant. Added thermal resistance (insulation) between the external moldline (heat shield) and panel increases the heat shield temperature and a larger percentage of the aerodynamic heat load is radiated to space. This trend is illustrated in figure 6; as insulation mass and heat shield temperature increase the heat flux absorbed by the coolant decreases. Reducing insulation mass increases the amount of heat absorbed by the coolant and increases the mass of the active cooling system.

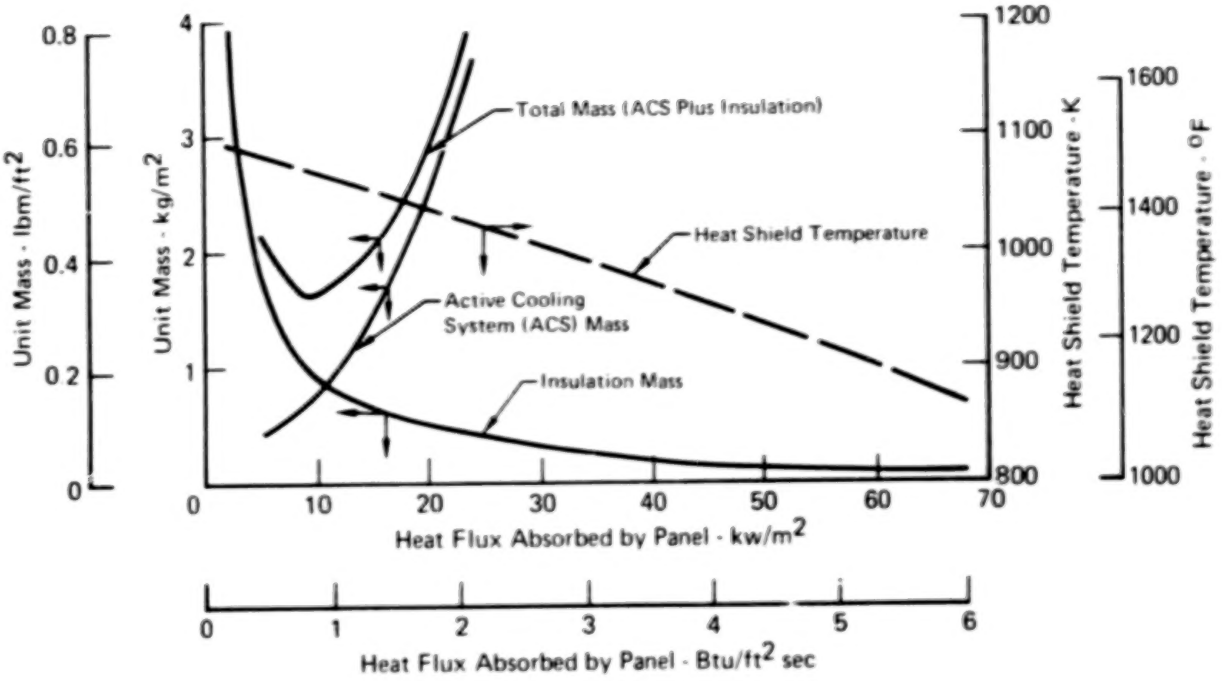


**FIGURE 6 - COMBINED MASS OF ACTIVE COOLING SYSTEM AND INSULATION OPTIMIZE AT LOW HEAT FLUX LEVEL**

A closed loop active cooling system (ACS) distributes the coolant to the panels, collects, and returns the coolant to the heat exchanger, where the heat absorbed in cooling the structure is rejected to the hydrogen fuel. The active cooling system includes all mass elements external to the panel (distribution lines, dual pumps, reservoir, heat exchanger, coolant inventory, and the APS propellant consumed in pumping the coolant through the ACS).

As shown in figure 6, the combined mass of insulation and active cooling system is a minimum at an absorbed heat flux of about 9.1 $kW/m^2$ (0.8 $Btu/ft^2$ sec). Insulation and active cooling system mass are the driving factors that determine the absorbed heat flux level for minimum system mass. Variations in the mass of the heat shield and panel with absorbed heat flux have a small compensating effect but the location of the minimum point does not shift. The absorbed heat flux at the minimum mass point (figure 6) is approximately 13 percent of the maximum heat flux that could be absorbed by the hydrogen heat sink

available for structural cooling of a representative hypersonic aircraft (see Appendix B).

Insulation mass presented in figure 6 is based upon the properties of 256 kg/m$^3$ (16 lbm/ft$^3$) flexible Min-K manufactured by the Johns-Manville Corporation (see Appendix A). This material is representative of the type of high temperature Aerospace insulation material that would be used on a hypersonic aircraft. The material's low thermal conductivity minimizes overall thickness of the thermal protection system and maximizes the volumetric efficiency of the aircraft. Flexible Min-K is a proprietary silica based material that is faced with Astroquartz cloth and stitched together in a quilted blanket configuration. Standard blanket thicknesses range from 0.32 cm (0.125 in.) to 1.27 cm (0.5 in.), in 0.32 cm (0.125 in.) increments. Nonstandard thicknesses are available on special order. The minimum mass point of figure 6 corresponds to an insulation thickness of 0.38 cm (0.15 in.) and accounts for 4.4% of the total panel mass.

Active cooling system mass and its sensitivity to pressure are discussed in Appendix D. It was found that the mass decreases by 30% when ACS pressure increases from 680 kPa (100 lbf/in$^2$) to 1448 kPa (210 lbf/in$^2$) and is insensitive to further increases in the pressure level.

### Skin Thickness, Tube Size, and Tube Spacing Versus Heat Flux

Since the optimized panel design must satisfy both thermal and structural requirements, combinations of outer skin thickness, tube size, and tube spacing satisfying thermal requirements were identified in order to limit the number of combinations to be analyzed parametrically.

Extensive trade studies in reference 1 determined combinations of coolant inlet temperature nad maximum panel temperature that result in minimum system mass. These studies demonstrated that coolant requirements and system mass were minimized by designing for a maximum allowable panel temperature of 422K (300°F). Further, a 60/40 mass solution of ethylene glycol and

water coolant minimizes system mass for coolant inlet and outlet temperature of approximately 283K (50°F) and 322K (120°F), respectively. Due to similarity of panel designs (reference 1 and present study) these coolant temperatures were used in thermally analyzing the panel to identify combinations of skin thickness, tube size, and tube pitch, as presented in figure 7 for a maximum panel temperature of 422K (300°F). At a given pitch and heat flux the curves approach a vertical slope with decreasing tube diameter. This is due to the large thermal resistance of the FM-400 adhesive used to attach coolant tubes to the outer skin. As the temperature drop across the skin/tube interface increases with decreasing tube diameter (less area for heat transfer across interface), the temperature difference in the outer skin must decrease due to an increase in outer skin thickness ($t_o$). The impact of increasing tube pitch is shown in figure 7. Note that at a given skin thickness and tube diameter (point where curves cross) the heat flux which can be absorbed for a maximum panel temperature of 422K (300°F) decreases approximately 60% when the tube pitch is doubled.

## Actively Cooled Panel Mass Versus Heat Flux

Starting with the combinations of tube pitch (P), tube diameter (D), and outer skin thickness ($t_o$) shown in figure 7, the actively cooled panel was optimized for minimum mass. The inner skin thickness and honeycomb sandwich panel height were varied until the lightest actively cooled panel was found for each particular combination of P, D, and $t_o$ and absorbed heat flux. The results of this analysis are presented in figure 8. The actively cooled panel geometry was optimized using 2024-T81 skins and a maximum temperature of 422K (300°F). The 2024-T81 aluminum was used since reference 1 indicated that the mass difference was less than 2% if either 2024-T81, 6061-T6, or 2219-T87 aluminum facesheets were used. The lowest mass was obtained with the 2219-T87, but due to procurement problems with the 2219-T87 and the desire to have a direct comparison of the

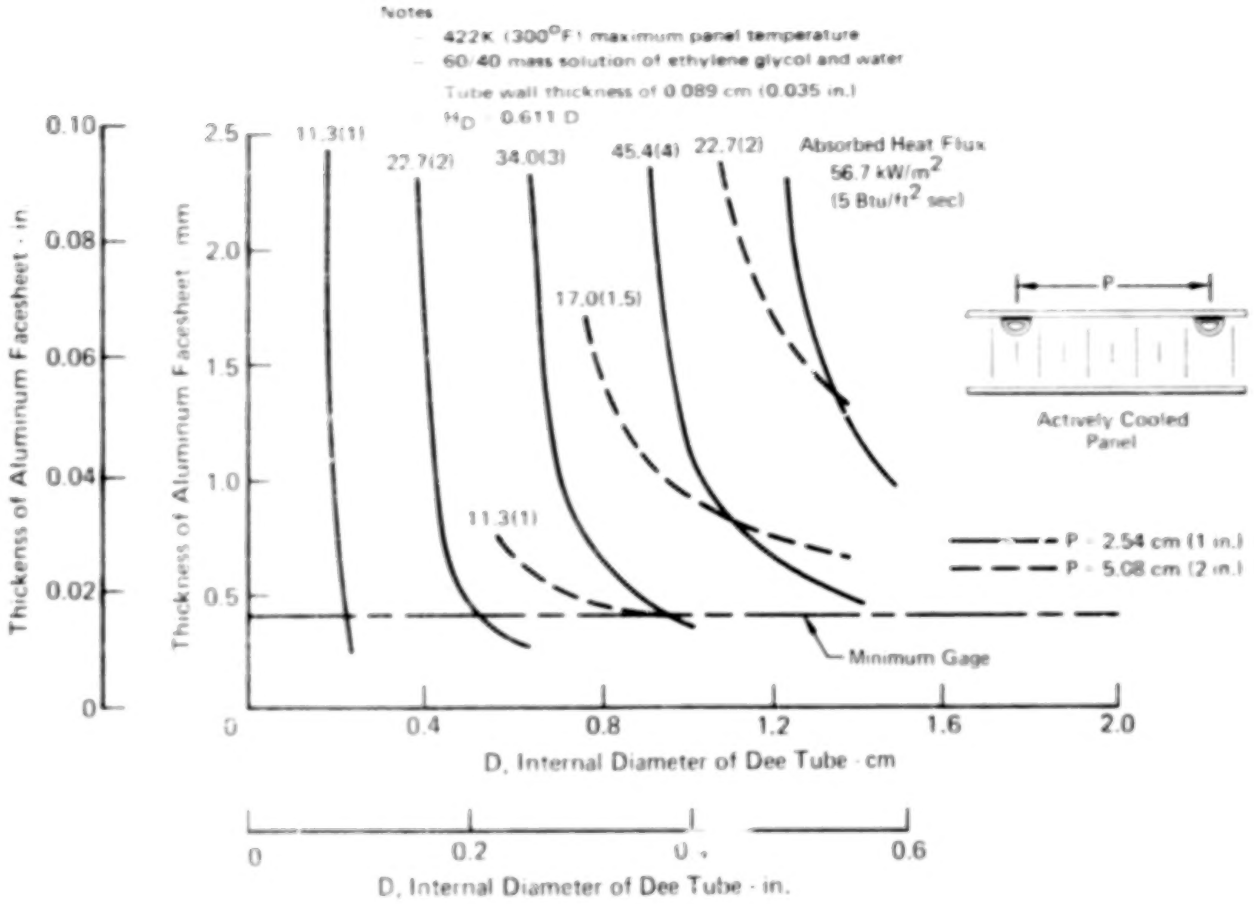


**FIGURE 7 - COMBINATIONS OF SKIN THICKNESS, TUBE DIAMETER, TUBE PITCH, AND ABSORBED HEAT FLUX LEVEL FOR A 422K (300°F) PANEL TEMPERATURE**

test panel with the full scale panel design, the full scale panel was optimized using 2024-T81 skins. The maximum permissible operating temperature of the aluminum was limited to 422K (300°F) because reference 1 shows that operation at higher temperatures does not save significant additional mass and because of concern of overheating the structure at off-design conditions.

As shown in figure 8, a minimum mass actively cooled panel is obtained in the 5.7 to 22.7 kW/m$^2$ (0.5 to 2 Btu/ft$^2$ sec) absorbed heat flux range. As the tube pitch is decreased, the panel mass becomes less sensitive to absorbed heat flux and the mass for a 2.54 cm (1.0 in.) pitch is essentially constant for heat fluxes up to 22.7 kW/m$^2$ (2 Btu/ft$^2$ sec). For a given tube pitch, decreasing the tube diameter reduces panel mass primarily because the coolant in the tube is reduced but also because of a

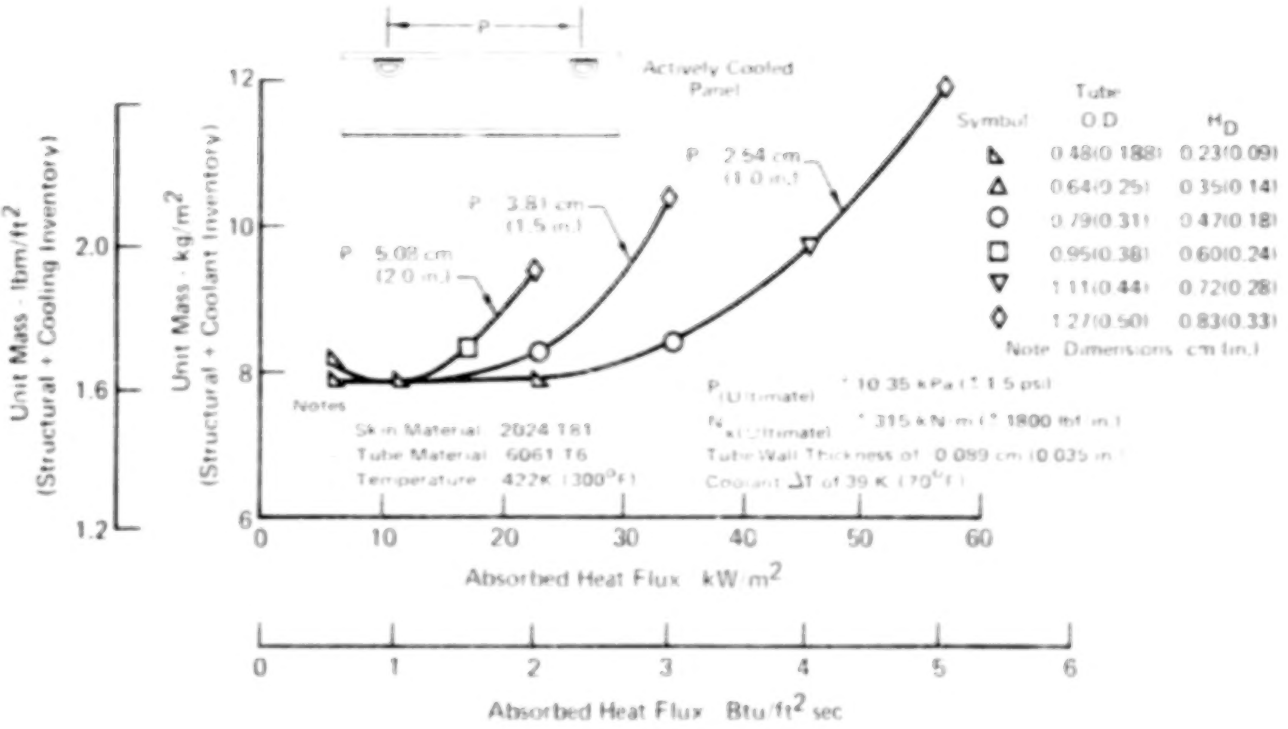


**FIGURE 8 - ACTIVELY COOLED PANEL MASS vs ABSORBED HEAT FLUX**

reduction in tube size and an increase of inner skin thickness results in a more efficient structural cross section. At this point in the sensitivity studies the actively cooled panel geometry (Appendix D) was selected, i.e., 3.01 cm (1.185 in.) for the height of the panel, 0.48 cm (0.188 in.) for the coolant tube diameter, 0.10 cm (0.04 in.) for the inner and outer skin thickness, and a 2.54 cm (1.0 in.) tube pitch.

### Heat Shield Mass Versus Heat Flux

The sensitivity of the corrugated stiffened beaded skin heat shield mass to absorbed heat flux is shown in figure 9 for a span-wise support spacing of 30.48 cm (12 in.) and for corrugation pitches of 5.08 cm and 7.62 cm (2 in. and 3 in.). The mass of the heat shield includes the mass of the standoff posts and local doublers at the supports. It reflects the use of Rene'41 super-alloy skins and corrugations. Rene'41 was found to be the most efficient, of the superalloys investigated (see Appendix A), in the 811K (1000°F) to 1117K (1550°F) temperature range.

The heat shield mass is essentially a constant, over most

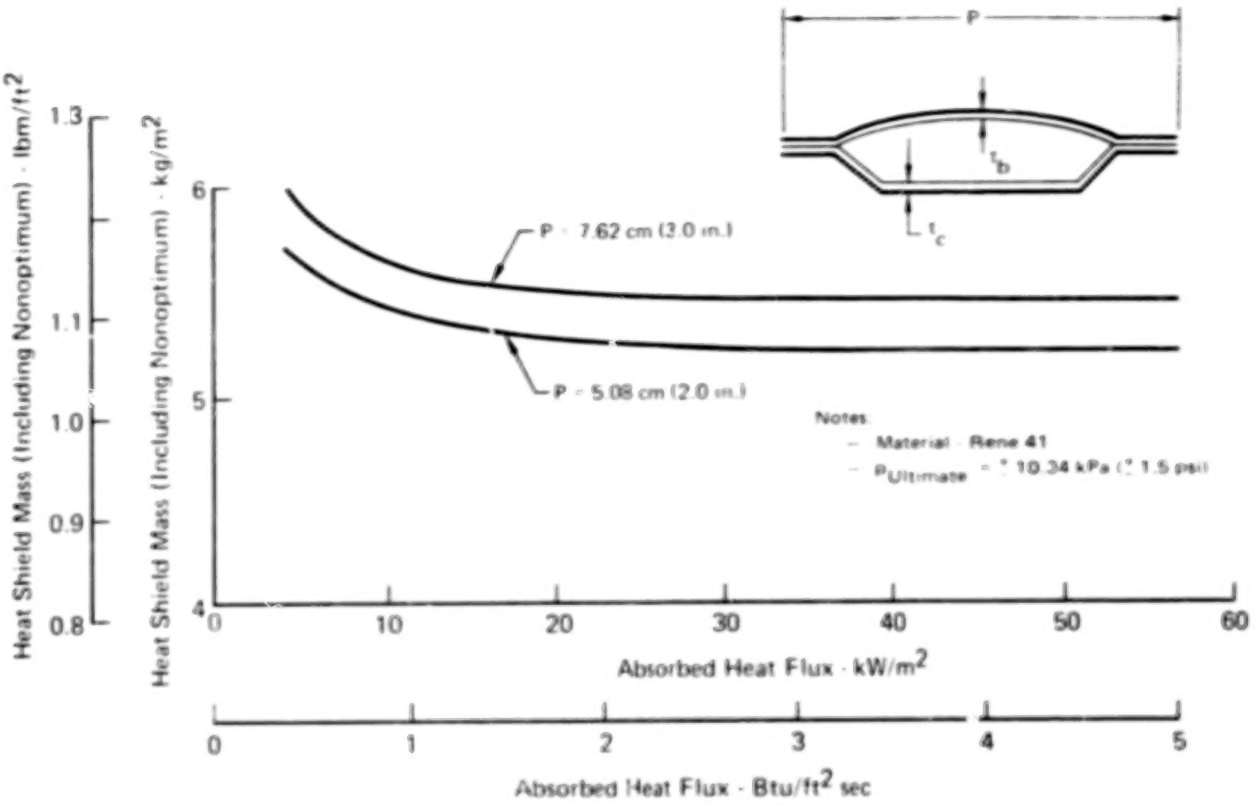


**FIGURE 9 - HEAT SHIELD MASS vs ABSORBED HEAT FLUX**

of the temperature range, but does increase slightly for absorbed heat fluxes less than 22.7 kW/m$^2$ (2 Btu/ft$^2$ sec) due to an increase in heat shield temperatures and a reduction in mechanical properties of the Rene'41. The mass shown is based on a spanwise support spacing of 30.48 cm (12 in.) since trade studies (Appendix D) showed this yielded a low mass design and permitted maximum use of existing fasteners in the actively cooled panel.

The mass of the heat shield reduces slightly as the pitch of the beaded skin decreases from 7.62 cm to 4.08 cm (3 in. to 2 in.) because of the reduced mass of local doublers required to carry the concentrated loads at the support posts. Bead/currgation pitches of less than 5.08 cm (2 in.) were not considered because of difficulty in integrating the heat shield supports into the actively cooled panel to clear the coolant tubes. Details of the calculations to determine the beaded skin and corrugation thicknesses of 0.25 cm (0.010 in.) and 0.02 cm (0.008 in.), respectively, and the 0.32 cm (0.125 in.) crown in the beaded skin and the 0.53 cm (0.208 in.) corrugation height are given in Appendix D.

## Radiative Actively Cooled Panel Total Mass Versus Heat Flux

A summary of results from the thermal and structural trade studies is given in figure 10 which shows the mass of the actively cooled panel (including coolant in tubes), heat shield, insulation,

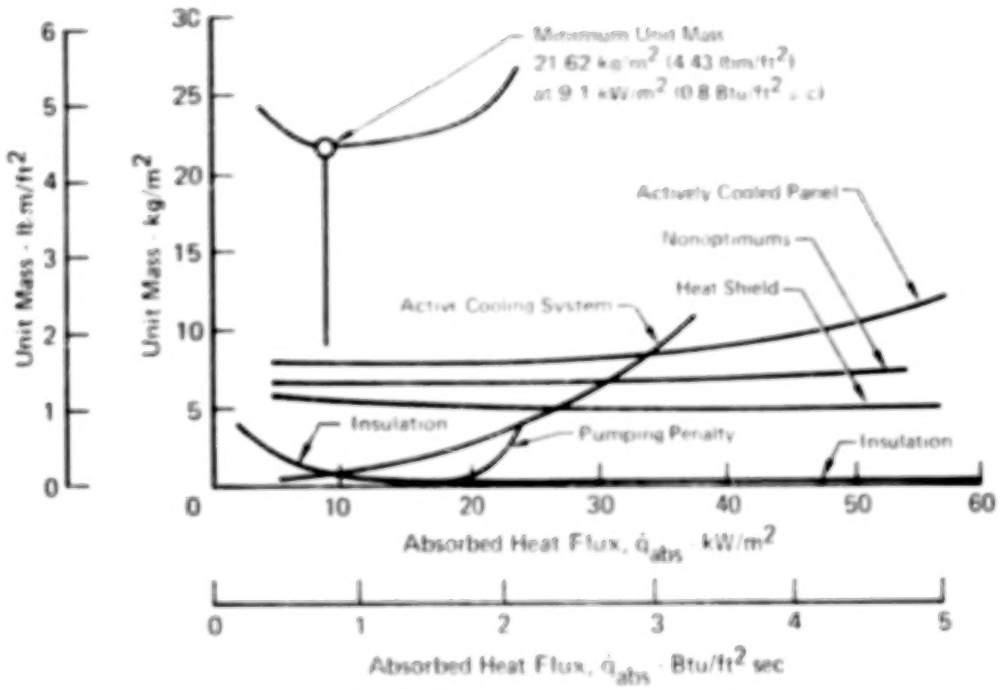


**FIGURE 10 - MASS OF A RADIATIVE ACTIVELY COOLED PANEL AS A FUNCTION OF ABSORBED HEAT FLUX FOR NORMAL CRUISE**

nonoptimums (fasteners, adhesives, etc.), active cooling system, and the panel pumping power penalty as a function of absorbed heat flux.

A minimum mass design occurs at an absorbed heat flux of 9.1 kW/m$^2$ (0.8 Btu/ft$^2$ sec). The mass of the insulation dominates for heat fluxes less than this value and the mass of the active cooling system dominate above this point. Consequently, the minimum mass for a radiative actively cooled panel designed for normal cruise only, is 21.62 kg/m$^2$ (4.43 lbm/ft$^2$). Refer to Appendix D for details of heat shield and actively cooled panel geometry and skin gages associated with the absorbed heat flux of 9.1 kW/m$^2$ (0.8 Btu/ft$^2$ sec).

## Impact of Loss of Coolant to Panel

Three different methods of ensuring a safe return if the cooling system fails were evaluated and the results are presented in figure 11. The methods are: (a) cruise/abort, (b) precooled/abort, and (c) incorporation of a redundant active cooling system. With the cruise/ abort method, insulation is added so that starting with a normal maximum panel temperature of 422K (300°F) during cruise, the mission can be aborted without exceeding a panel temperature of 478K (400°F). This method increases the mass of the panel by 0.6 kg/$m^2$ (0.12 lbm/$ft^2$), relative to the cruise only condition, as shown by the left plot in figure 11. Adding insulation to protect the panel during the abort reduces the cruise only absorbed heat flux level by approximately 50%. After a cooling system failure is detected, the aircraft decelerates

| Maximum Panel Temperatures | | | | |
|---|---|---|---|---|
| Method | Cruise | | Failed | |
| | K | °F | K | °F |
| Cruise/Abort | 422 | 300 | 478 | 400 |
| Precooled/Abort | 400 | 260 | 478 | 400 |
| Redundant Active Cooling System | 422 | 300 | 464 | 375 |

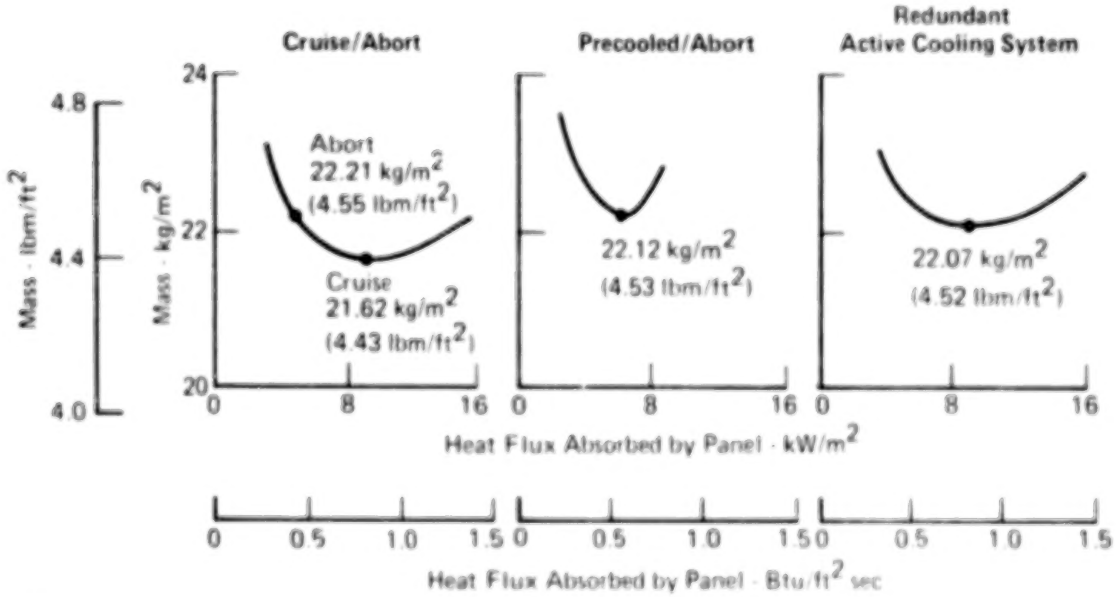


Notes:
- 60/40 Mass Solution of Ethylene Glycol and Water
- Coolant Inlet Temperature of 283 K (50°F)

**FIGURE 11 - IMPACT OF LOSS OF COOLANT SUPPLY ON RADIATIVE ACTIVELY COOLED PANEL MASS**

and descends along a load factor limited trajectory which minimizes the abort heat load as discussed in Appendices B and D.

The precooled/abort method trades-off the mass effects of increasing the heat sink capacity of the panel (precooling) versus additional insulation, to ensure that panel temperatures do not exceed 478K (400°F) during abort. As shown in the insert of figure 11, precooling the panel to 400K (260°F) during cruise, limits panel temperatures to 478K (400°F) in the failed condition. The minimum mass for the precooled/abort method is 22.12 kg/m$^2$ (4.53 lbm/ft$^2$) which is 0.1 kg/m$^2$ (0.02 lbm/ft$^2$) lighter than the cruise/abort method.

The third method incorporates a redundant active cooling system (right hand plot of figure 11) and was selected as the preferred method of ensuring a safe return if the cooling system fails. The redundant active cooling system consists of two independent coolant circuits, dual inlet and outlet plumbing to unitized "y" fittings at the panel manifolds, and a check valve arrangement that prevents loss of coolant from the operative coolant loop if a failure occurs. With this method, no abort maneuvers are required since the panel continues to receive 50% of the design coolant mass flow rate which is sufficient to limit the panel maximum temperature to 464K (375°F). In practice, the flight would probably continue at a reduced Mach number.

Selection of the redundant cooling system method was based primarily upon operational considerations (ability to continue mission at a reduced Mach number without subjecting passengers to a high load factor abort), rather than the slight mass savings indicated in figure 11.

### Effect of Increasing Panel Loads

Sensitivity studies of the effect on actively cooled panel mass and geometry of increasing the in-plane loading and of applying combined biaxial loading and shear loads to the panel showed that panel mass and geometry were unaffected by biaxial loading for Ny/Nx = 0.5 and that the application of shear loads (Nxy/Nx = 0.5) with a uniaxial in-plane loading results in a bout an 11% increase in panel mass. Panel mass was found to increase approx-

imately linearly with increasing uniaxial in-plane loads. Appendix D gives details of the studies.

### Effect of Variations in External Heating

Results of an analysis of variations in the external heat transfer coefficient on the full scale panel design are presented in figure 12. Results are shown for variations ranging from 1/4 to twice the design value. Reducing the heat transfer coefficients to 1/4 of the design value lowers heat shield temperatures by 278K (500°F), reduces the absorbed heat flux by 33%, and reduces panel temperatures by 40K (72°F). The present panel design could be operated at this reduced heating condition or re-sized to take advantage of the mass savings resulting from a reduction in insulation thickness and/or coolant mass flow rates. Increasing the heat transfer coefficient to twice the design value increases the absorbed heat flux 18% and would require an increase in insulation requirements and/or coolant flow rates to prevent overheating of the panel. These changes could be readily incorporated.

As indicated in figure 12, a 20% increase in the heat transfer coefficient causes the temperature limit of Rene'41 heat shields to be exceeded, necessitating a material change. Except for this change, which requires redesign of the heat shield, the present radiative actively cooled panel design can readily accomplish large variations in the external heat transfer coefficient.

## FINAL DESIGN

The geometry and materials of the heat shield, the insulation packages, and the actively cooled panel for the selected minimum mass redundant radiative actively cooled panel, operating at an absorbed heat flux of 9.1 $kW/m^2$ (0.80 $Btu/ft^2$ sec), are shown in figure 13. The panel consists of an actively cooled aluminum honeycomb structural panel; insulation packages; and Rene'41 superalloy heat shields. The heat shields consist of a 0.025 cm (0.010 in.) beaded skin and a 0.02 cm (0.008 in.) corrugation spot welded together. Pitch of the beaded skin/corrugation is 5.08 cm (2 in.). The crown in the beaded skin is 0.32 cm (0.125 in.), the width of the lands between beads is 2.03 cm (0.8 in.),

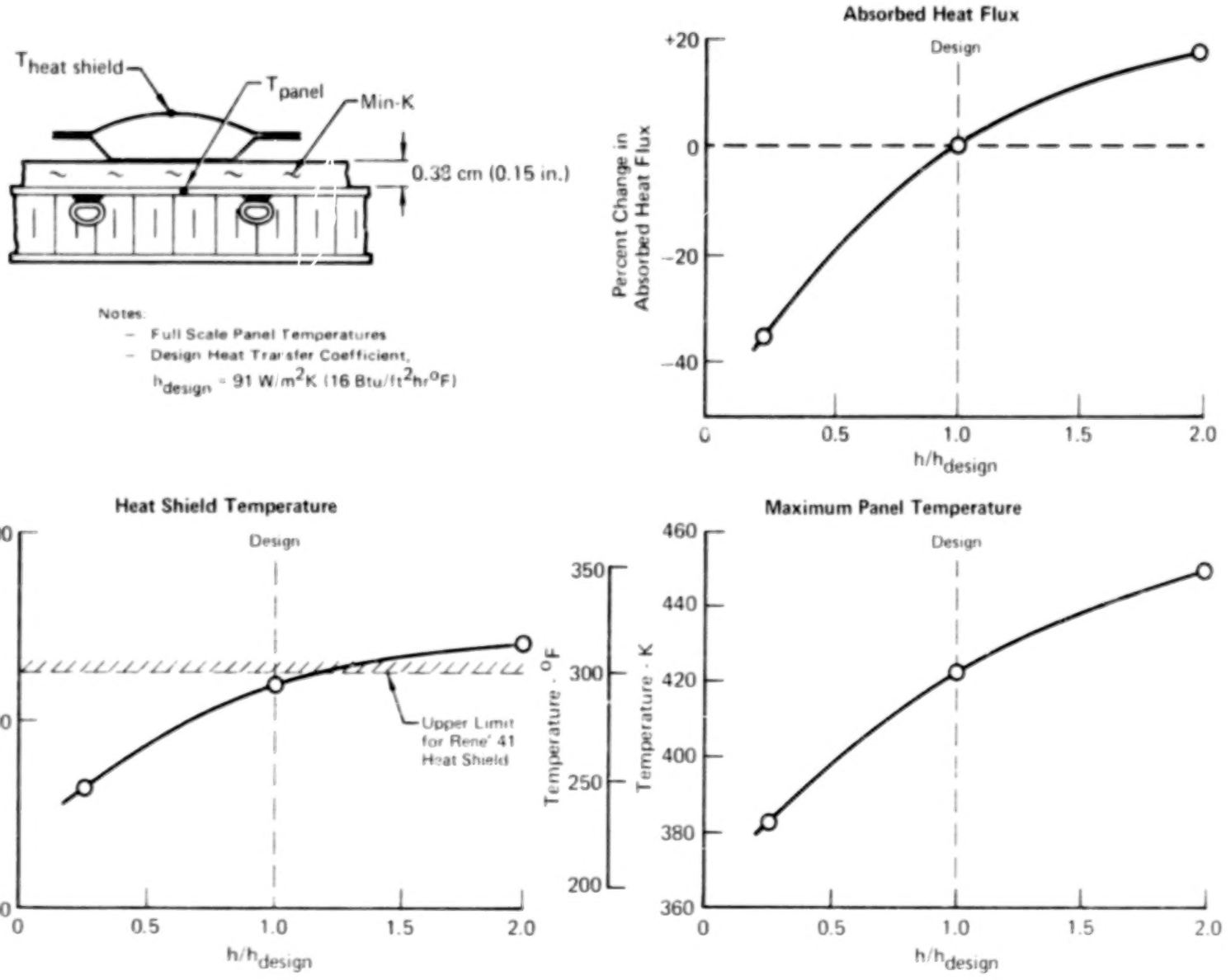


**FIGURE 12 - SENSITIVITY OF PANEL TEMPERATURES AND ABSORBED HEAT FLUX TO VARIATIONS IN EXTERNAL HEAT TRANSFER COEFFICIENT**



33

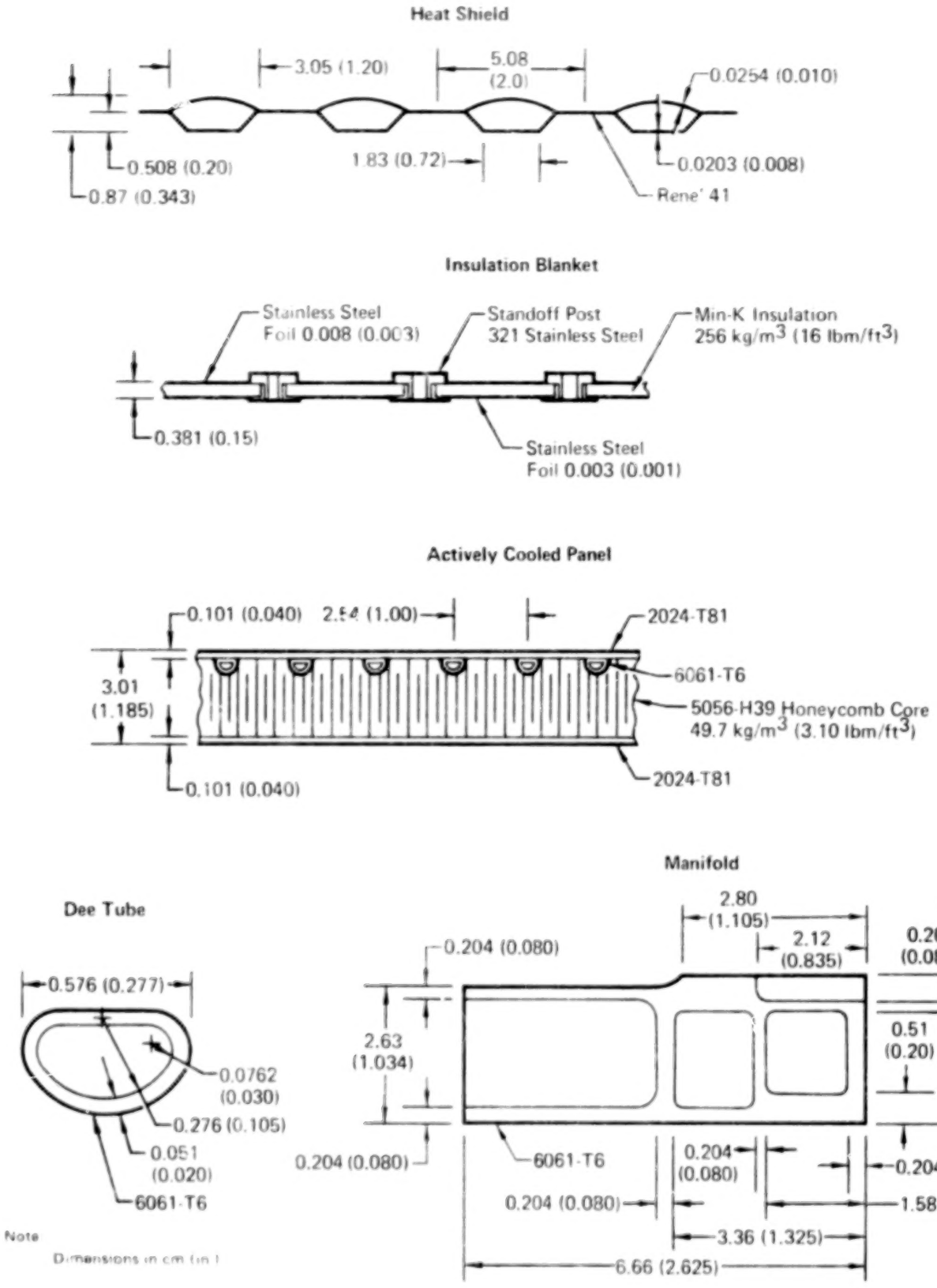


FIGURE 13 - RADIATIVE ACTIVELY COOLED PANEL MATERIALS AND GEOMETRY

and the height of the corrugation is 0.508 cm (0.2 in.). The insulation packages is 256 kg/m$^3$ (16 pcf) Min-K insulation, 0.38 cm (0.15 in.) thick and packaged in 0.008 cm (0.003 in.) and 0.003 cm (0.001 in.) stainless steel foil on the outer and inner surfaces, respectively.

Machined and crimped stainless steel standoff posts are a part of the insulation packages. These posts support the heat shields and provide the required buildup to accept the insulation packages between the heat shilds and the structural panel.

The actively cooled panel is composed of 0.101 cm (0.04 in.) thick 2024-T81 outer and inner face sheets and 49.7 kg/m$^3$ (3.1 pcf) 5056-H39 aluminum honeycomb core. The overall height of the panel is 3.01 cm (1.185 in.). The coolant tubes are formed into the Dee shape from 0.48 cm (0.188 in.) diameter, 0.051 cm (0.02 in.) wall, 6061-0 aluminum tubing and are then heat treated to the T6 condition. The manifolds are finished machined from 6061-T6 aluminum extrusions.

The method of attaching the heat shields and the insulation packages to the actively cooled panel is shown in figure 14. Machined A-286 stainless steel shoulder bolts pass through the heat shields, the standoff posts and the actively cooled panel and are retained by plate nuts attached to the inner skin of the actively cooled panel. The shoulder on the A-286 bolts provides a controlled gap to prevent clamping of the heat shields so that they can thermally expand. At the transverse splice, the forward (relative to the airstream) heat shield overlaps the aft heat shield. Consequently, the corrugations and the beaded skin on the forward and aft heat shields, respectively, are cut away and the fastener holes slotted. This allows the forward heat shield (beaded skin and corrugations) to rest on the aft heat shield all along the transverse edge. The slotted holes are long enough to accommodate thermal expansion of one half of the length of the panel. (It is restrained at midspan and permitted to grow in both directions, i.e., forward and aft.) No provisions are made at the fasteners to accommodate thermal expansion in the transverse direction since the crown in the beaded skin and the height

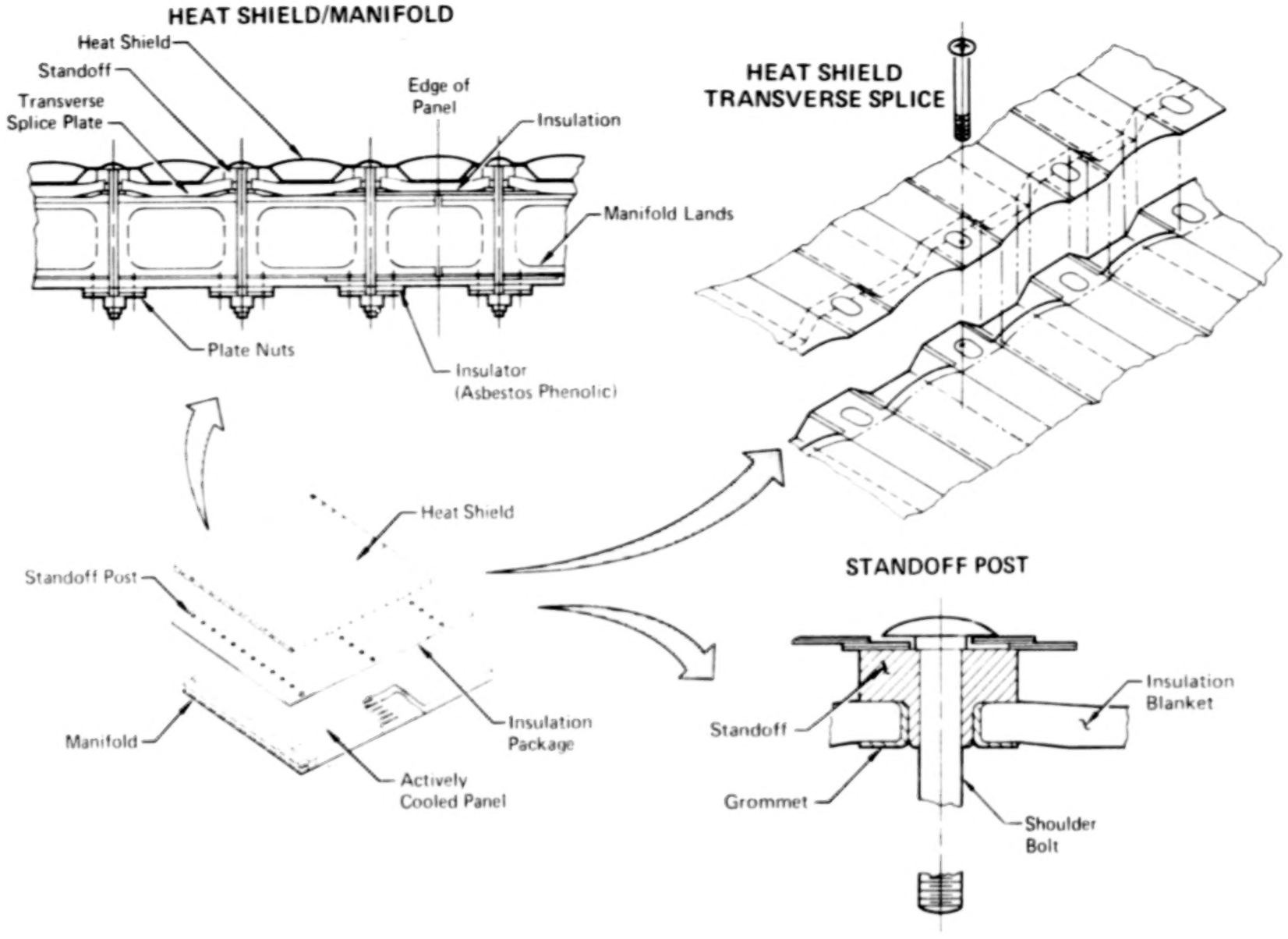


FIGURE 14 - RADIATION SYSTEM JOINT DETAILS

of the corrugations were designed (see Appendix D) to relieve the induced thermal stresses by bending/bowing. Consequently, the heat shields could be fabricated to any practical width and fastened rigidly along the longitudinal edges to the adjacent heat shields. However, the maximum length is 61 cm (24 in.), with transverse supports at 30.5 cm (12 in.) results in a minimum mass heat shield. Refer to Appendix D for impact of frame spacing on heat shield mass.

The full scale actively cooled panel is shown in figure 15. It is a 0.61 x 6.1 m (2 x 20 ft) aluminum honeycomb sandwich panel with coolant manifolds, tube/tab assemblies, and honeycomb core adhesively bonded to the inner and outer skins. It is supported by frames spaced at 0.61 m (2 ft) intervals.

The manifolds located at the panel ends are machined from 6061-T6 aluminum extrusions and have welded end caps. Dual chambers provide uniform cooling across the width of the panel. The coolant enters and exits at the panel centerline through the chamber closest to the panel support bulkhead. The ends of the manifold are cooled as the coolant turns the corner into the second chamber and is distributed into the individual tube/tab assemblies. Provisions to accept two supply and/or exit lines are provided by unitized "Y" fitting, with internal pressure operated valves. These valves prevent loss of coolant from the operative line/system in the event of complete failure of the other line.

Brazed tube/tab assemblies, nested in machined pockets, are adhesively bonded with American Cyanamide FM-400 to the manifolds. The individual tube/tab assemblies made it possible to more closely control the tube straightness and obtain a bondline thickness no greater than 0.025 cm (0.010 in.). If the bondline thickness exceeds this value, the interface conductance becomes too low to prevent the aluminum structure from exceeding the 422K (300°F) design temperature.

The skins are adhesively bonded to an aluminum honeycomb core and to the manifolds with FM-400 film type adhesive. FM-400 was used because it had high strength and sufficient thermal

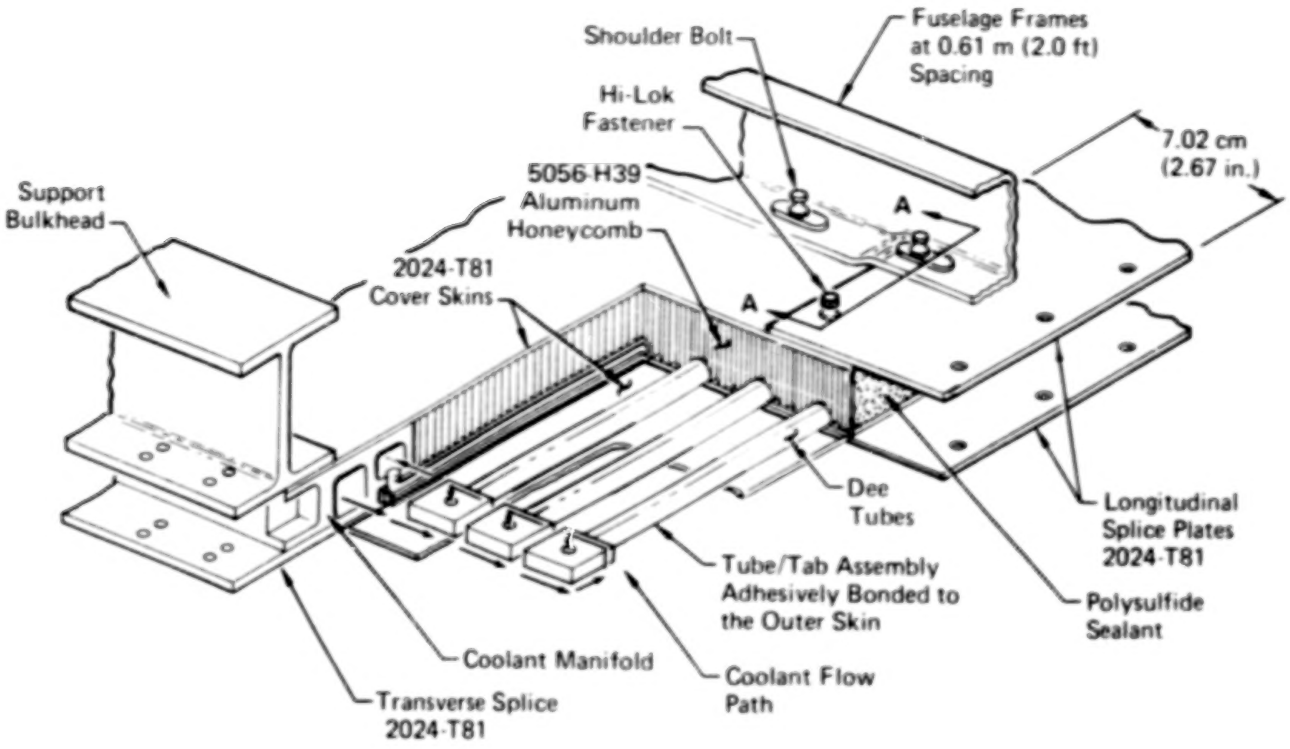


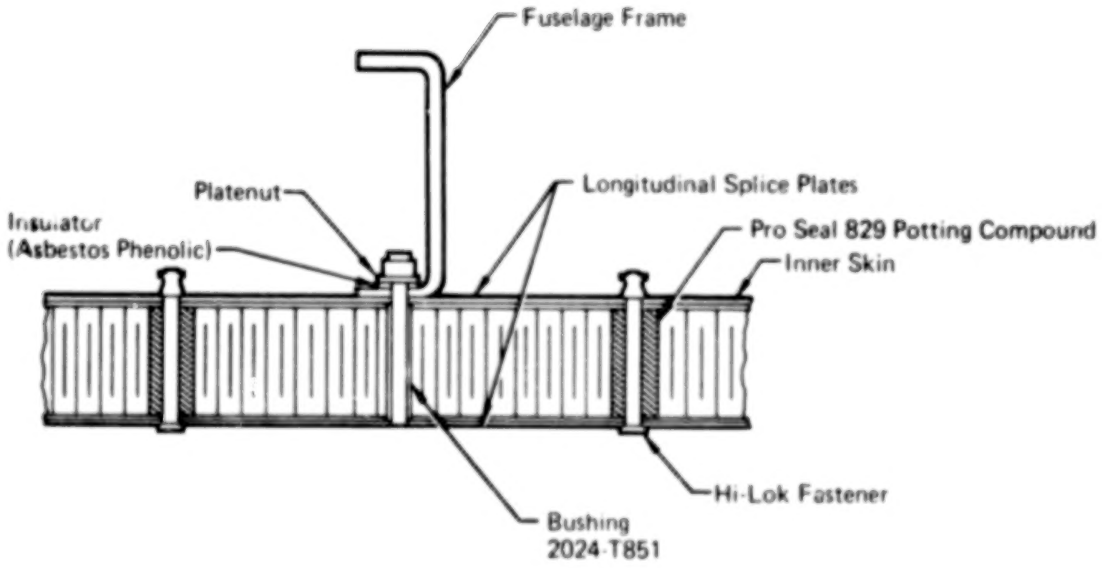


Section A-A

**FIGURE 15 - FULL SCALE ACTIVELY COOLED PANEL DETAILS**

conductivity (Appendix A) to conduct the heat from the skins to the coolant. FM-404 foaming adhesive is used to bond the Dee tubes and the manifolds to the honeycomb core.

The 2024-T81 aluminum longitudinal and transverse splice plates are 0.082 cm (0.032 in.) and 0.254 cm (0.10 in.) thick, respectively, and provide attachment to adjacent panels. Both are mechanically fastened and bonded with RTV 560 adhesive to the actively cooled panel. The adhesive provides the needed conductivity to prevent the splice plates from exceeding the 422K (300°F) design temperature. The fasteners were designed to carry all of the loads since the RTV 560 has a low shear modulus.

Two different methods are used to provide good clamp-up at the fasteners and to prevent crushing the aluminum honeycomb core during fastener installation. In areas where heat shield stand-off posts are required and good conduction is needed, an aluminum bushing is used. Away from the standoff posts, the honeycomb core is locally filled with a potting compound, which cures solid during bonding of the skins to the honeycomb core. The potting compound is used to reduce cost and simplify fabrication.

The panel is cooled by pumping a 60/40 mass solution of ethylene glycol/water through the coolant passages at a mass flow rate of 9.6 g/s (76 lbm/hr) per tube with an inlet coolant temperature of 283K (50°F). The use of ethylene glycol/water as the coolant and the 283K (50°F) inlet temperature was based on results from reference 1.

Temperatures and stresses in both the heat shields and the actively cooled panel are presented in Appendix D.

### RACP and ACP Mass Comparison

The total mass of a radiative actively cooled panel (RACP) is 7% less than the mass of a bare actively cooled panel (ACP). Figures 16 and 17 give a mass breakdown of both panels.

The total mass of the radiative actively cooled panel is 22.07 kg/m$^2$ (4.52 lbm/ft$^2$). Of this total, 56% is attributed to

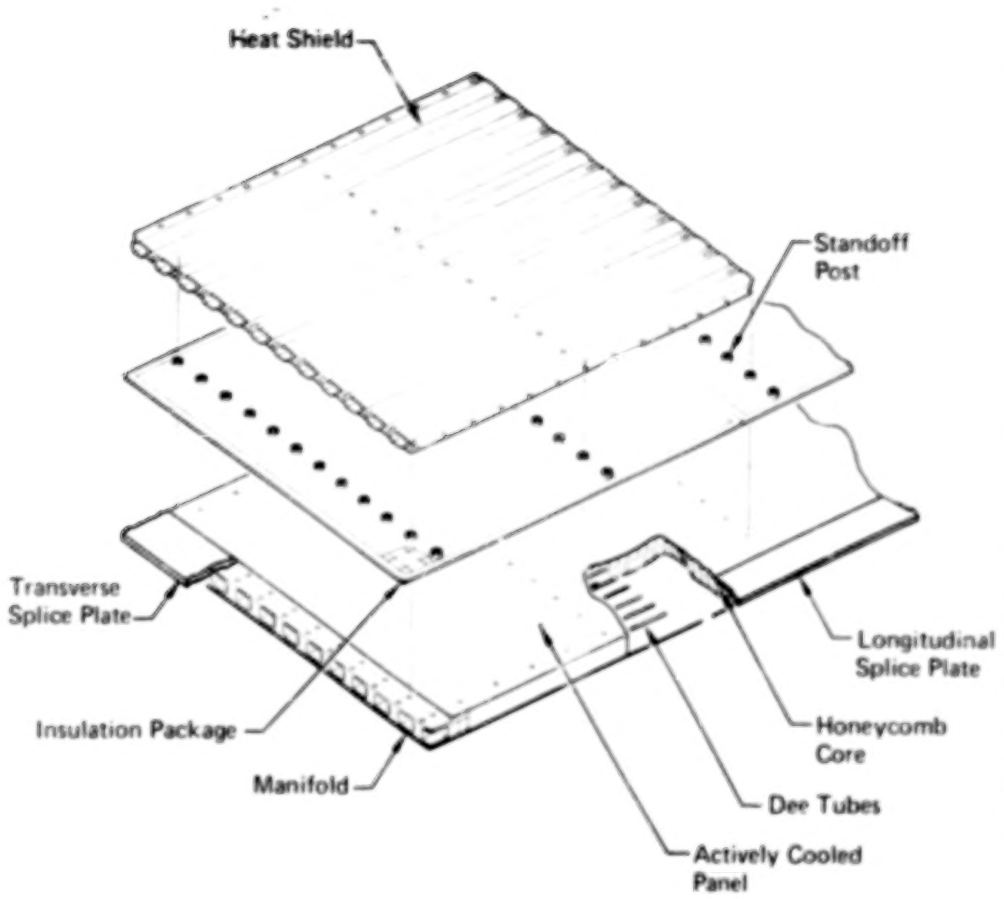


| Component | Unit Mass | |
|---|---|---|
| | $kg/m^2$ | $lbm/ft^2$ |
| Actively Cooled Panel | | |
| Skins (2024-T81) | 5.86 | 1.20 |
| Dee Tubes (6061-T6) | 0.78 | 0.16 |
| Honeycomb (5056-H39) | 1.42 | 0.29 |
| Manifolds (6061-T6) | 0.63 | 0.13 |
| Splice Plates (2024-T81) | 0.63 | 0.13 |
| Bushings/Fasteners | 0.63 | 0.13 |
| Plumbing | 0.15 | 0.03 |
| Adhesives | 1.95 | 0.40 |
| Potting Compound | 0.39 | 0.08 |
| Subtotal | 12.44 | 2.55 |
| Radiation System | | |
| Heat Shield (Rene' 41) | 4.34 | 0.89 |
| Insulation Package | 1.86 | 0.38 |
| Support Posts (321 Stn Stl) | 0.44 | 0.09 |
| Fasteners (A-286) | 0.63 | 0.13 |
| Subtotal | 7.27 | 1.49 |
| Active Cooling System | 1.37 | 0.28 |
| Panel Fluid Penalties | 1.00 | 0.20 |
| Total | 22.07 | 4.52 |

**FIGURE 16 - RADIATIVE ACTIVELY COOLED PANEL MASS BREAKDOWN**

| Component | [a] Unit Mass | |
|---|---|---|
| | $kg/m^2$ | $lbm/ft^2$ |
| Skins (2219-T87) | 3.77 | 0.77 |
| Dee Tubes (6061-T6) | 2.75 | 0.56 |
| Honeycomb (5056-H39) | 1.34 | 0.27 |
| Closure Angles (2219-T87) | 0.85 | 0.18 |
| Manifolds (6061-T6) | 0.69 | 0.12 |
| Splice Plates (2219-T87) | 0.89 | 0.18 |
| Bushings/Fasteners | 0.50 | 0.10 |
| Bellmouth | 0.04 | 0.01 |
| Connectors | 0.01 | 0.01 |
| Adhesives | 2.09 | 0.43 |
| Subtotal | 12.80 | 2.62 |
| Active Cooling System | 8.64 | 1.77 |
| Panel Fluid Penalties | 2.25 | 0.46 |
| Total | 23.68 | 4.85 |

Note
[a] Information obtained from Reference 1

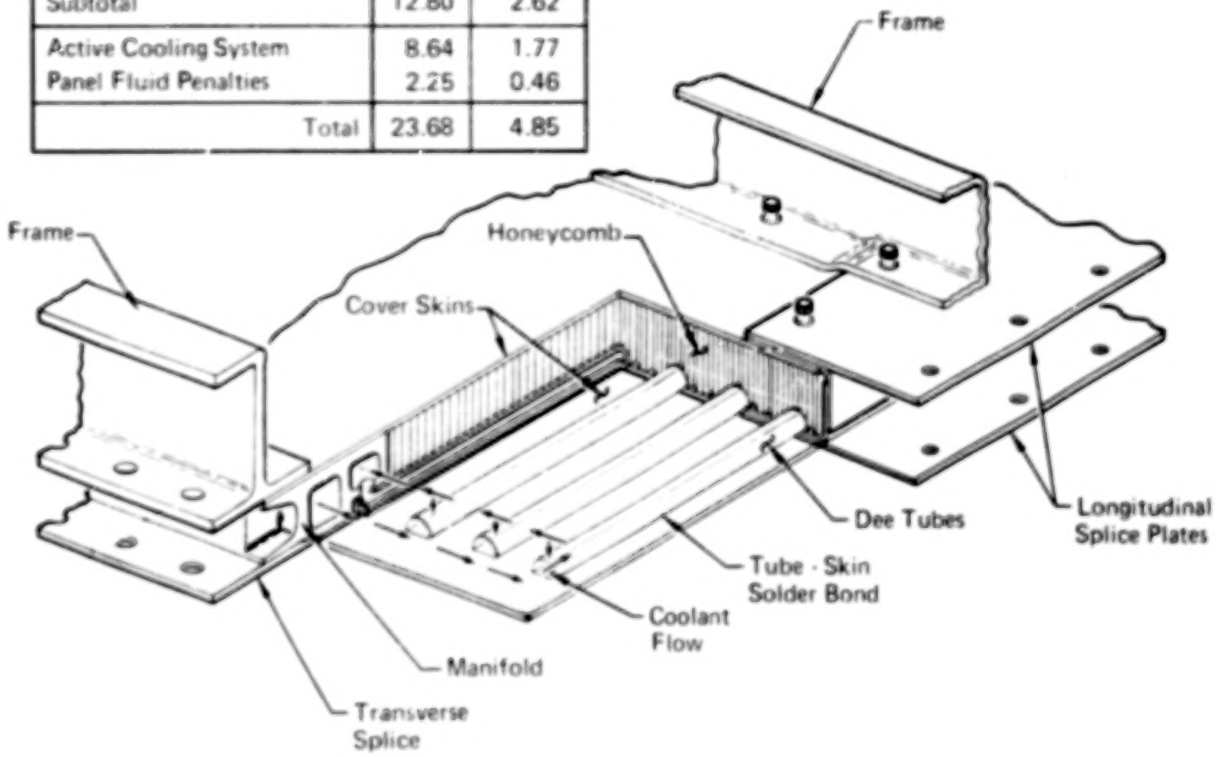


**FIGURE 17 - ACTIVELY COOLED PANEL MASS BREAKDOWN**

the actively cooled panel, 33% to the radiative thermal protection system (heat shields and insulation packages) and only 11% to the active cooling system and panel fluid penalties. In contrast, a bare (i.e., no thermal protection system) actively cooled panel requires 46% of the total 23.68 $kg/m^2$ (4.85 $lbm/ft^2$) mass for the active cooling system and fluid penalties, and 54% to the actively cooled panel.

The lower mass of the radiative actively cooled panel as compared to a bare actively cooled panel is attributed to the

reduced mass of the active cooling system, which more than offsets the mass of the heat shield and insulation packages.

## TEST PANEL DESIGN AND FABRICATION

A .61 x 1.22 m (2 x 4 ft) radiative actively cooled test panel, representing a section of the optimized full scale panel, was designed, fabricated and delivered to NASA, along with hardware required to mate with the NASA fatigue/radiant test facility and 8 foot High Temperature Structures Wind Tunnel test fixture. The purpose of the test panel was to demonstrate the thermal and structural integrity and performance of the design by simulating full scale panel inlet and exit conditions.

### Test Panel

The test panel is made up of four Rene'41 corrugated stiffened beaded skin heat shields, two insulation blankets, an aluminum honeycomb sandwich actively cooled panel, and three support frames. A photograph of test panel components is shown in figure 18. Two heat shields and one insulation blanket

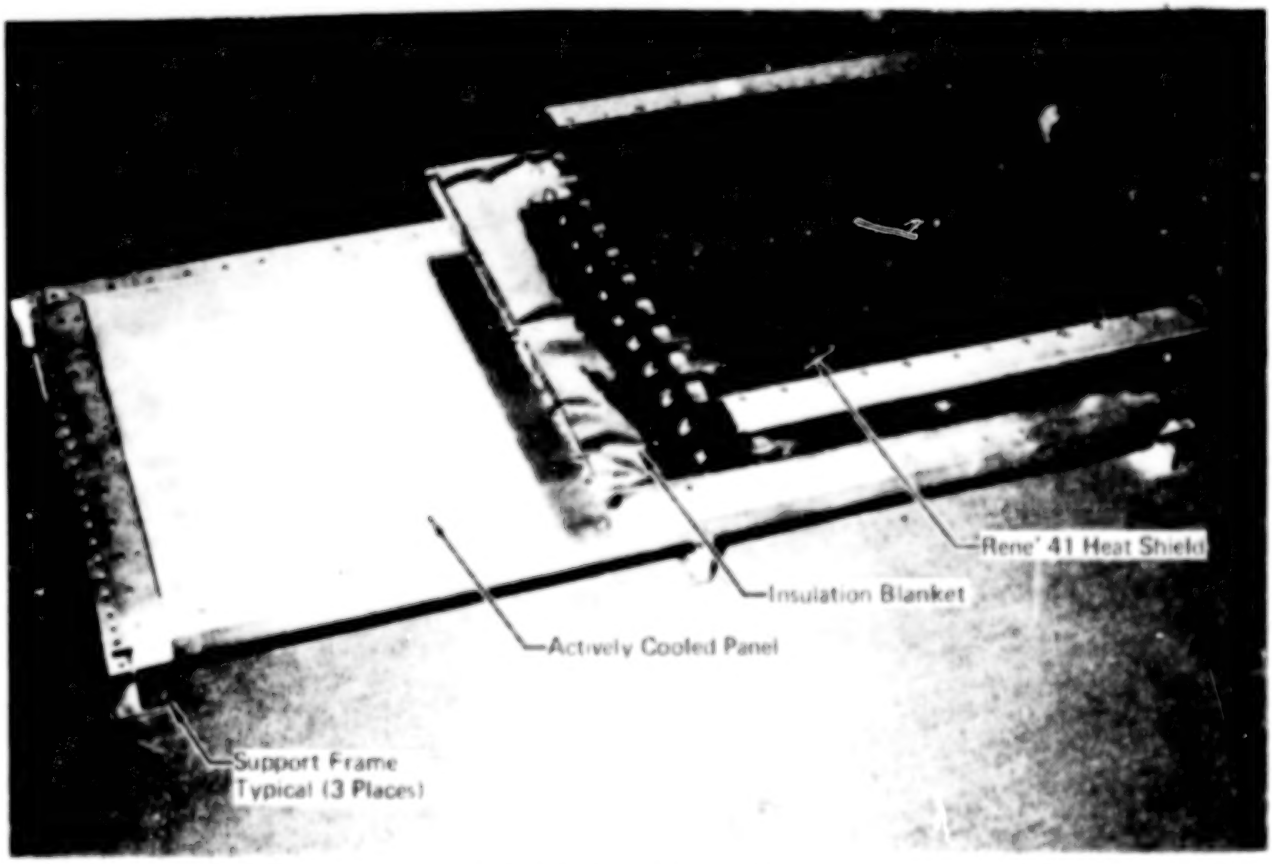


FIGURE 18 - TEST PANEL

have been removed to expose the actively cooled panel.

Deviation from the full scale panel design - The details of the test panel represent those of the full scale panel as far as practical. Some deviations were required because of material procurement problems. However, no deviations were made w adversely affect the thermal and structural performance and integrity of the concept.

There were six areas where the test panel differed from the full scale panel design: (1) heat shield corrugation thickness, (2) heat shield shoulder bolt head diameter, (3) heat shield longitudinal joing fastener material, (4) insulation package thickness (5) coolant manifolds raw material and fabrication method, and (6) actively cooled panel size.

The thickness of the Rene'41 material used for the heat shield corrugations was 0.0254 cm (0.01 in.) rather than the design nominal thickness of 0.02 cm (0.008 in.). Procurement problems prevented obtaining the 0.02 cm (0.008 in.) gage material.

Since the shoulder bolts were machined from standard A-286 corrosion resistant NAS 1218 bolts, the diamter of the head was smaller than desired. Consequently, washers were used under the heads to provide equivalent fastener head/heat shield bearing area and close the gap over the slotted holes in the heat shield.

The full scale panel design called for Hastelloy X fasteners to join longitudinal edges of adjacent heat shields. Corrosion resistant steel A286 fasteners were used except for twelve (all that were readily available) fasteners which were Hastelloy X. The two different materials will provide a comparison of the erosion characteristics in a simulated hypersonic environment.

The Min-K insulation blankets were standard 0.318 cm (0.125 in.) thickness rather than the full scale panel design thickness of 0.381 cm (0.15 in.). Analyses in Appendix F showed that the desired full scale panel temperatures can be readily simulated by adjusting coolant temperatures.

The test panel manifolds were fabricated as a three piece weldment of machined 6061-T5611 bar stock whereas the full scale

panel specified 6061-T6 extrusions. This deviation had no impact on the panel design since the manifolds were finish machined to the full scale panel manifold dimensions.

The actively cooled test panel was 0.61 x 1.22 m (2 x 4 ft) and the full scale panel was 0.61 x 6.1 m (2 x 20 ft). Analyses showed that the temperatures and stresses corresponding to the inlet and exit conditions of the full scale panel can be reasonably simulated with the 1.22 m (4 ft) test panel.

Unique fabrication problems - Although state of the art fabrication techniques were used for the test panel, some unique fabrication problems were encountered. Most of these problems could be attributed to incorporation of the coolant passages into the panel. Tube straightness was essential to maintain a thin uniform bondline between the outer skin and the tubes and assure adequate interface conductance to prevent overheating the structure. To simplify the process of straightening the Dee tubes individual tube/tab assemblies were fabricated by hand brazing the tabs to the tubes. The rejection rate for the assemblies was high because of porosity in the braze alloy which caused leaks and entrapped flux which could create corrosion problems if exposed to the coolant. Therefore, the assemblies were pressure checked and then visually inspected for porosity around the surface of the coolant passage holes.

The tube/tab assemblies were adhesively bonded to the manifolds at the same time the tubes and tabs were bonded to the outer skin. Careful dimensional control of tab thicknesses and the corresponding pockets in the manifolds was required to provide a leak free joint.

Incorporation of these coolant passages into the honeycomb sandwich concept considerably increased the fabrication complexity over that of a honeycomb sandwich panel and/or a conventional skin/stringer design without coolant passages.

## Fatigue/Radiant Heating Test Configuration

The test panel, load adapters, side fairings and support frames for the fatigue/radiant heating test configuration are shown in figure 19. The in-plane loads are applied to the

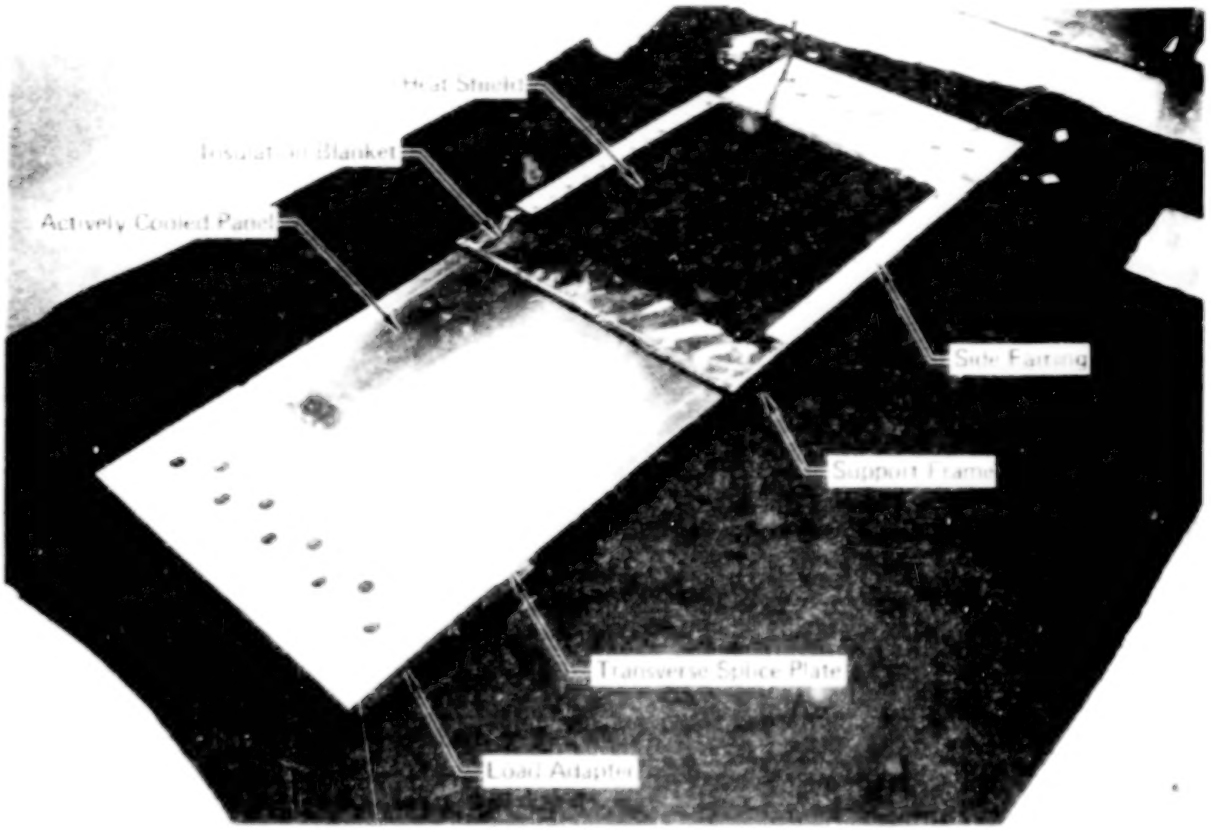


FIGURE 19 FATIGUE/RADIANT HEATING/TEST PANEL CONFIGURATION

actively cooled panel through 3.18 cm (1.25 in.) thick aluminum load adapters attached to the panel transverse splice plates with a row of 0.48 cm (0.189 in.) fasteners. The load adapters are insulated from the splice plates by 0.06 cm (0.032 in.) asbestos insulation strips to properly simulate panel temperatures.

The Rene'41 side fairings are attached directly to the heat shield and protect the longitudinal edges of the panel from direct exposure to the radiant heat. The insulation blankets extend beyond the transverse and longitudinal splice plates. Along the longitudinal edges, the insulation is tucked under the lip of the side fairings.

Four thermocouples are installed on one tube, two each approximately 12.7 cm (5.0 in.) from the inlet and exit manifolds. The thermocouple leads extend through the nearest honeycomb cell and through small holes drilled in the inner skin. Additional instrumentation will be installed on the insulation blankets, heat shields, and actively cooled panel by NASA.

## Wind Tunnel Test Configuration

A photograph of the wind tunnel test configuration with the test panel, forward, aft, and side fairings, and the wind tunnel closeout fairing is shown in figure 20. The wind tunnel closeout fairing was designed to fit NASA's wind tunnel fixture

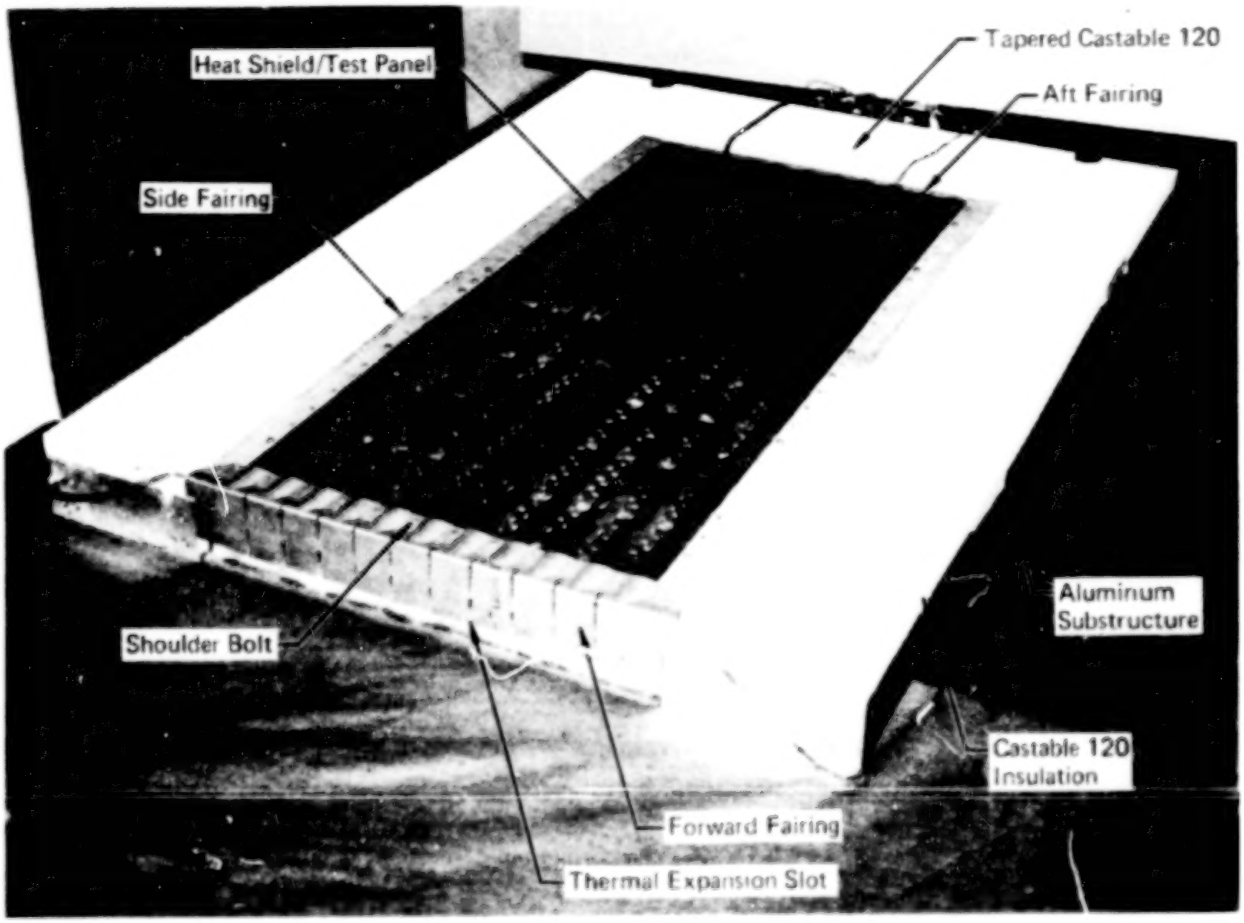


**FIGURE 20 - WIND TUNNEL/TEST PANEL CONFIGURATION**

and consists of 2.54 cm (1.0 in.) thick Thermo-Sil Castable 120 insulation, bonded with RTV 560 adhesive to an aluminum sub-structure. The Castable 120 insulation at the aft end of the panel is tapered to mate with the aft fairing, which was designed to allow venting of the air between the heat shield and the actively cooled panel during tunnel start-up. The forward fairing was designed to have the tops of the beads flush with

NASA's fairing moldline (not shown) and provide a smooth transition from NASA's flat surface to the beaded skin of the heat shield. Relative motion due to differential thermal expansion between the fairing and the heat shield leading edge is accommodated by slots cut in the crests of the fairing. To prevent separation of the fairing from the heat shield surface, the flats in the fairing are held in place by the shoulder bolts used to attach the heat shields. Discussion of the test panel design and fabrication is presented in Appendices F and G, respectively.

### Test Simulation of Full Scale Panel Temperatures

Analyses have shown that full scale panel temperatures can be adequately simulated on the test panel by adjusting test coolant temperatures to compensate for the difference in panel length and the difference in insulation thickness. For example, as shown in figure 21, full scale panel inlet temperatures can be simulated by decreasing the test coolant temperature 11K (20°F). Similarly, full scale panel temperatures at other locations can be duplicated by properly adjusting test coolant temperatures.

As shown, no adjustment of test coolant temperature is required to simulate full scale exit temperatures. At this location, the increase in coolant side heat transfer coefficient as a result of a factor of 5 difference in the respective panel lengths, compensates for the 20% decrease in test panel insulation thickness.

As shown in figure 21, the heat short effect (of heat shield attachments) locally increases outer skin temperature ($T_o$) by approximately 28K (50°F). Although shown only for the full scale panel, similar peaks will be experienced on the test panel. An assessment of the effects of heat shorts is presented in Appendix D. It was found that heat short effects significantly impact active cooling system requirements (44% increase in ACS mass) but only increase the mass of the radiative actively cooled panel by approximately 2%.

Test panel temperatures, including the variation with coolant

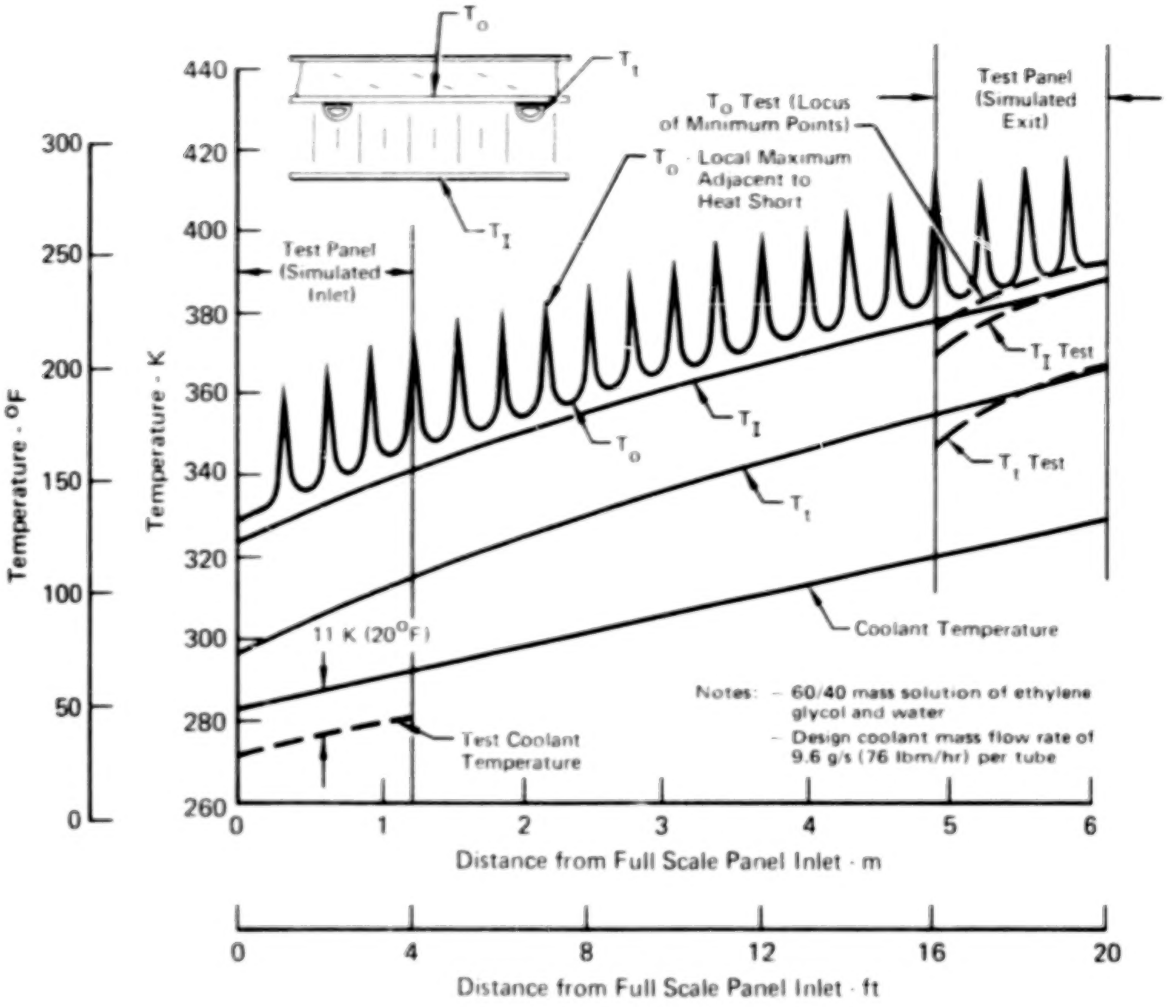


**FIGURE 21 - COMPARISON OF TEST AND FULL SCALE ACTIVELY COOLED PANEL TEMPERATURES**

temperature are discussed in Appendix F.

## CONCLUDING REMARKS

This report presents the results of a program in which a full scale 0.61 m x 6.1 m (2 ft x 20 ft) radiative actively cooled panel was designed and optimized and a 0.30 m x 0.61 m (1 ft x 2 ft) heat shield fatigue specimen and a 0.61 m x 1.22 m (2 ft x 4 ft) radiative actively cooled panel were fabricated and delivered to NASA for testing. The design loading conditions, heat flux, and thermal/structural requirements were representative of those for a Mach 6 to 8 hypersonic cruise transport aircraft. The concept developed in this program has a corrugated stiffened beaded skin superalloy heat shield, an insulation package comprised

of Min-K insulation wrapped in astroquartz cloth and stainless steel foil, and an adhesively bonded aluminum honeycomb sandwich structural panel with aluminum manifolds and Dee shaped coolant tubes nested in the honeycomb and in contact with the outer skin.

Overall conclusions of this program are: (1) the significant reduction in heat load to the cooling system offered by a combined radiative-actively cooled panel will permit matching of the instantaneous heat load and available fuel flow heat sink for hypersonic aircraft, (2) a radiative actively cooled panel is 7% lighter than a bare actively cooled panel designed to the same conditions and constraints, (3) the increase in mass of a radiative actively cooled panel designed both with and without provisions to prevent catastrophic failure in the event of loss of coolant supply is only 0.60 $kg/m^2$ (0.12 $lbm/ft^2$) or 2.5% of the total mass of the panel, and (4) fabrication of an actively cooled panel, incorporating the coolant passages, is considerably more difficult than conventional aluminum honeycomb sandwich structure.

The following paragraphs present specific conclusions related to the thermal and structural aspects of a radiative actively cooled panel.

## Thermodynamics

The mass of the active cooling system is reduced 30% by increasing the system pressure from 689 kPa (100 $lbf/in^2$) to 1448 kPa (210 $lbf/in^2$) and is insensitive to additional increases in the pressure level.

Heat shorts due to heat shield attachments increase the mass of the active cooling system by 44% but has a small impact (2%) on the mass of the radiative actively cooled panel design.

The full scale panel design can readily accommodate large variations in the external heat transfer coefficient by proper selection of heat shield material.

Full scale panel temperatures can be readily simulated during tests of the 0.61 m x 0.61 m (2 ft x 4 ft) panel by regulating test coolant temperatures.

Of the superalloys evaluated, Rene'41 yielded the minimum mass heat shield in the 811K (1000°F) to 1117K (1550°F) temperature range. The mass of the Rene'41 corrugated stiffened beaded skin heat shields is essentially constant in this temperature range.

A minimum mass actively cooled panel is obtained with a minimum practical tube diameter, 0.48 cm (0.188 in.), and spacing 2.54 cm (1.0 in.). As the tube spacing is reduced to 2.54 cm (1.0 in.) the panel mass becomes less sensitive to absorbed heat flux and is essentially a constant between 5.67 and 22.7 $kW/m^2$ (0.5 and 2 $Btu/ft^2$ sec).

The mass of the honeycomb sandwich actively cooled panel concept is unaffected by biaxial loading, for Ny/Nx = 0.5, but is increased by approximately 11% when shear loads, Nxy/Nx = 0.5, are combined with a uniaxial in-plane load.

# APPENDIX A

## MATERIAL DATA

This appendix presents the material property data used to select the metals, coolants, adhesives, and insulation for the radiative actively cooled panel.

Material property data were collected for two aluminum alloys (2024-T81 and 6061-T6) and five superalloy candidates (Hastelloy X, Inconel 625, L-605, Haynes 188, and Rene'41). Plots of the strength efficiencies ($F_{tu}/\rho$, $F_{ty}/\rho$, and $F_{cy}/\rho$), stiffness efficiency ($E_c/\rho$), crippling efficiency ($E_c^{.225} F_{ty}^{.325}/\rho$), and specific heat are presented in figures 22 through 27. The aluminum data are for long time exposure (10,000 hours) at temperatures up to 589K (600°F) whereas the superalloy data are for short time exposure (less than one hour) at temperatures up to 1144K (1600°F). Data for long time exposure are not available for the superalloys. Figure 28 shows the variation in coefficient of thermal expansion vs temperature for the aluminum and superalloy material candidates.

Crack growth rates, da/dN, for the two aluminum alloy candidates are presented in figure 29 versus $\Delta K$ (change in stress intensity factor). This data is for thin sheet at room temperature (elevated temperature da/dN was not available) and a stress ratio R (minimum stress divided by maximum stress) = -1.0 for 2024-T81 and R = -0.09 for 6061-T6.

### Material Allowables

The maximum operating stress levels which satisfied the requirement that cracks growing from the edge of fastener holes would not grow to critical length and surface flaws would not grow through the thickness of coolant tubes or manifolds in 20,000 cycles (including a scatter factor of four) were developed for each aluminum material. The allowable for 2024-T81 facesheets was developed for an initial flaw size of 0.013 cm (0.005 in.) at the edge of a fastener hole, an infinitely wide plate, and R = -1. The initial flaw size was based on results from Reference 6, where probable flaw sizes in holes in F-4 airplane

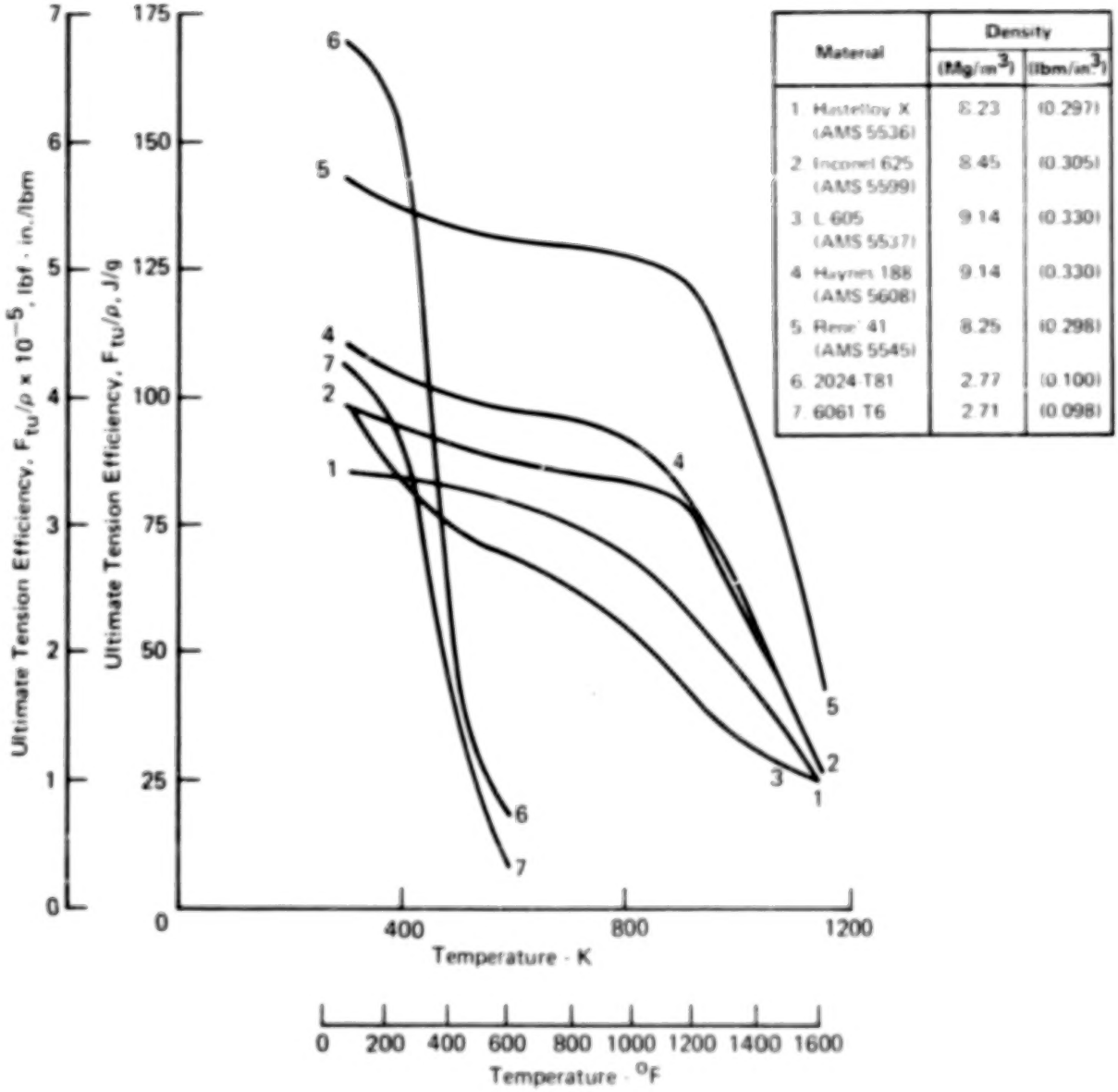


| Material | Density | |
|---|---|---|
| | ($Mg/m^3$) | ($lbm/in^3$) |
| 1. Hastelloy X (AMS 5536) | 8.23 | (0.297) |
| 2. Inconel 625 (AMS 5599) | 8.45 | (0.305) |
| 3. L-605 (AMS 5537) | 9.14 | (0.330) |
| 4. Haynes 188 (AMS 5608) | 9.14 | (0.330) |
| 5. Rene' 41 (AMS 5545) | 8.25 | (0.298) |
| 6. 2024-T81 | 2.77 | (0.100) |
| 7. 6061-T6 | 2.71 | (0.098) |

**FIGURE 22 - TENSION EFFICIENCY vs TEMPERATURE**

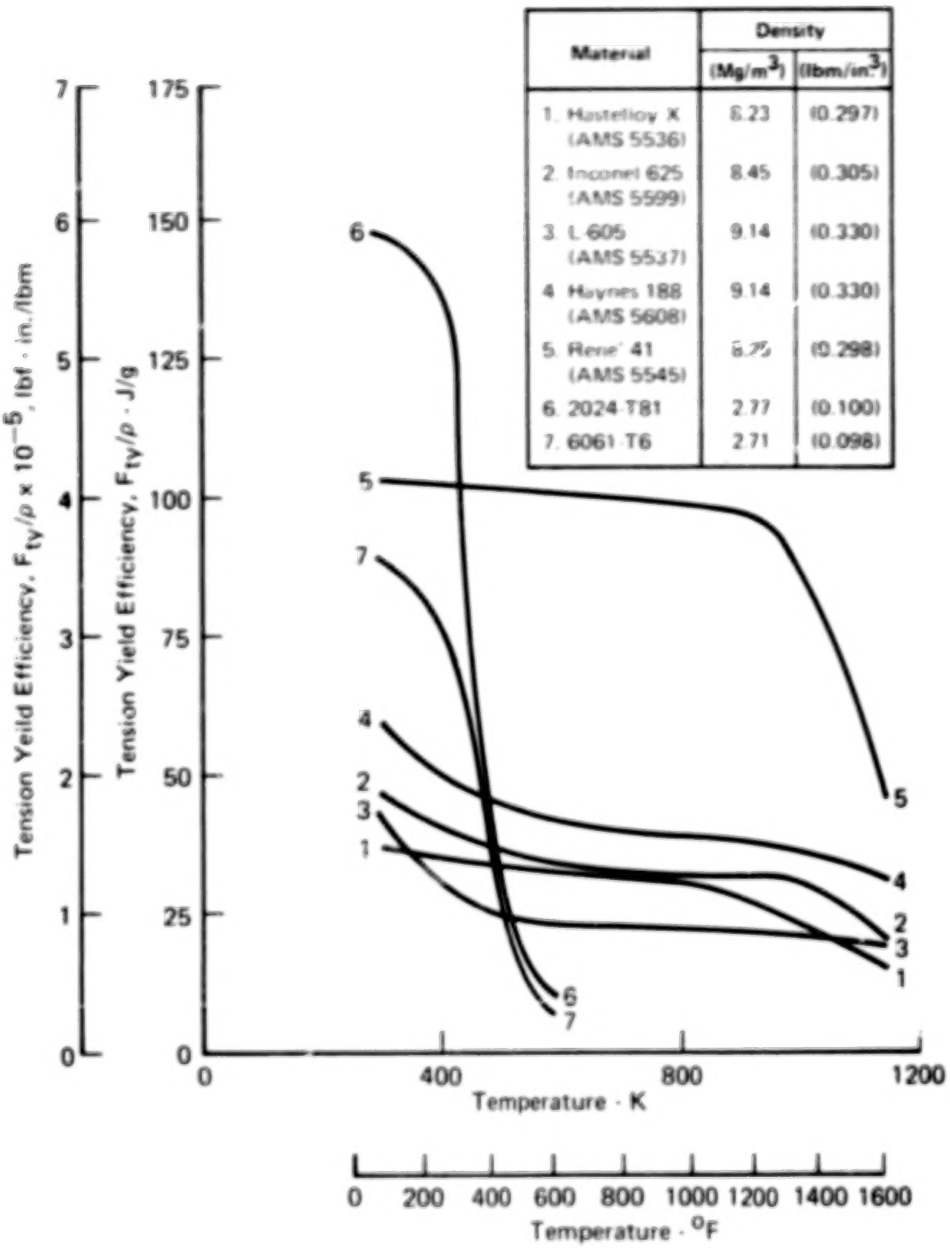


**FIGURE 23 - YIELD EFFICIENCY vs TEMPERATURE**

| Material | Density | |
|---|---|---|
| | ($Mg/m^3$) | ($lbm/in.^3$) |
| 1. Hastelloy X (AMS 5536) | 8.23 | (0.297) |
| 2. Inconel 625 (AMS 5599) | 8.45 | (0.305) |
| 3. L-605 (AMS 5537) | 9.14 | (0.330) |
| 4. Haynes 188 (AMS 5608) | 9.14 | (0.330) |
| 5. Rene' 41 (AMS 5545) | 8.25 | (0.298) |
| 6. 2024-T81 | 2.77 | (0.100) |
| 7. 6061-T6 | 2.71 | (0.098) |

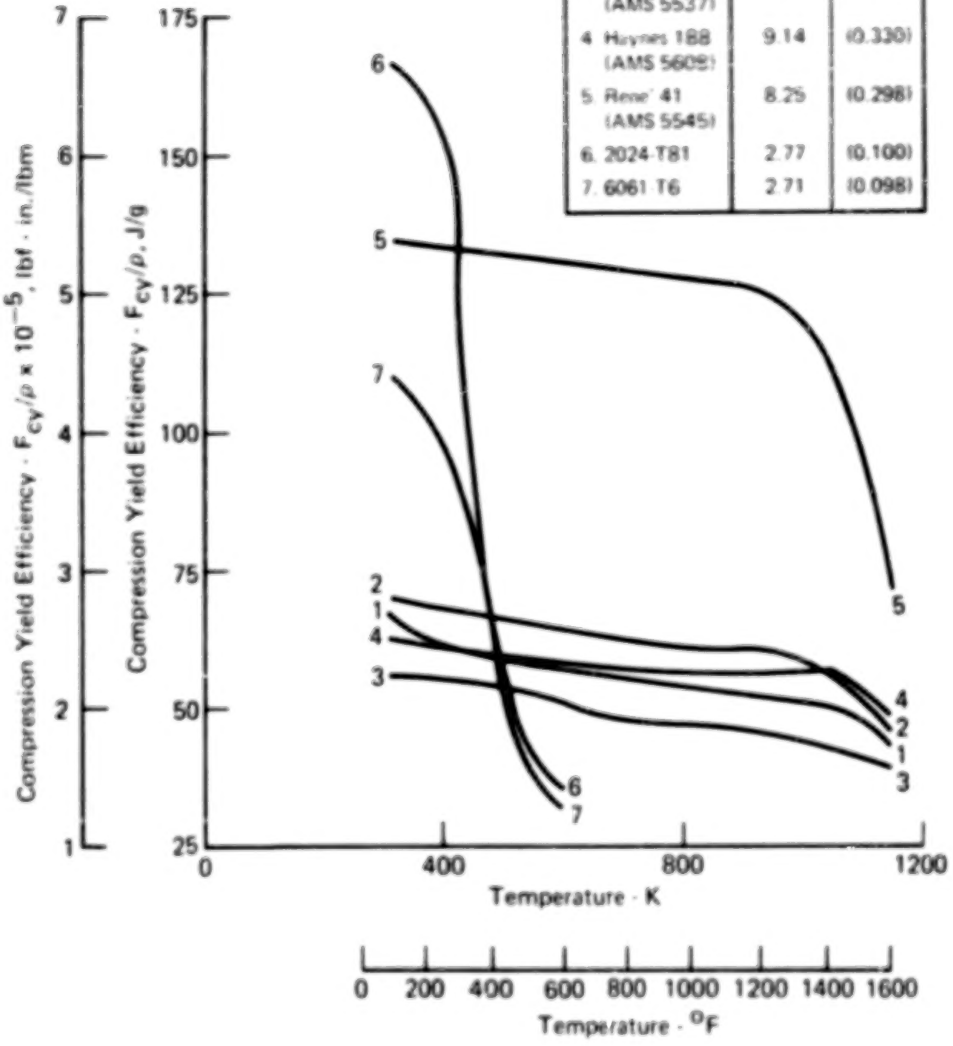


**FIGURE 24 - COMPRESSION YIELD EFFICIENCY vs TEMPERATURE**

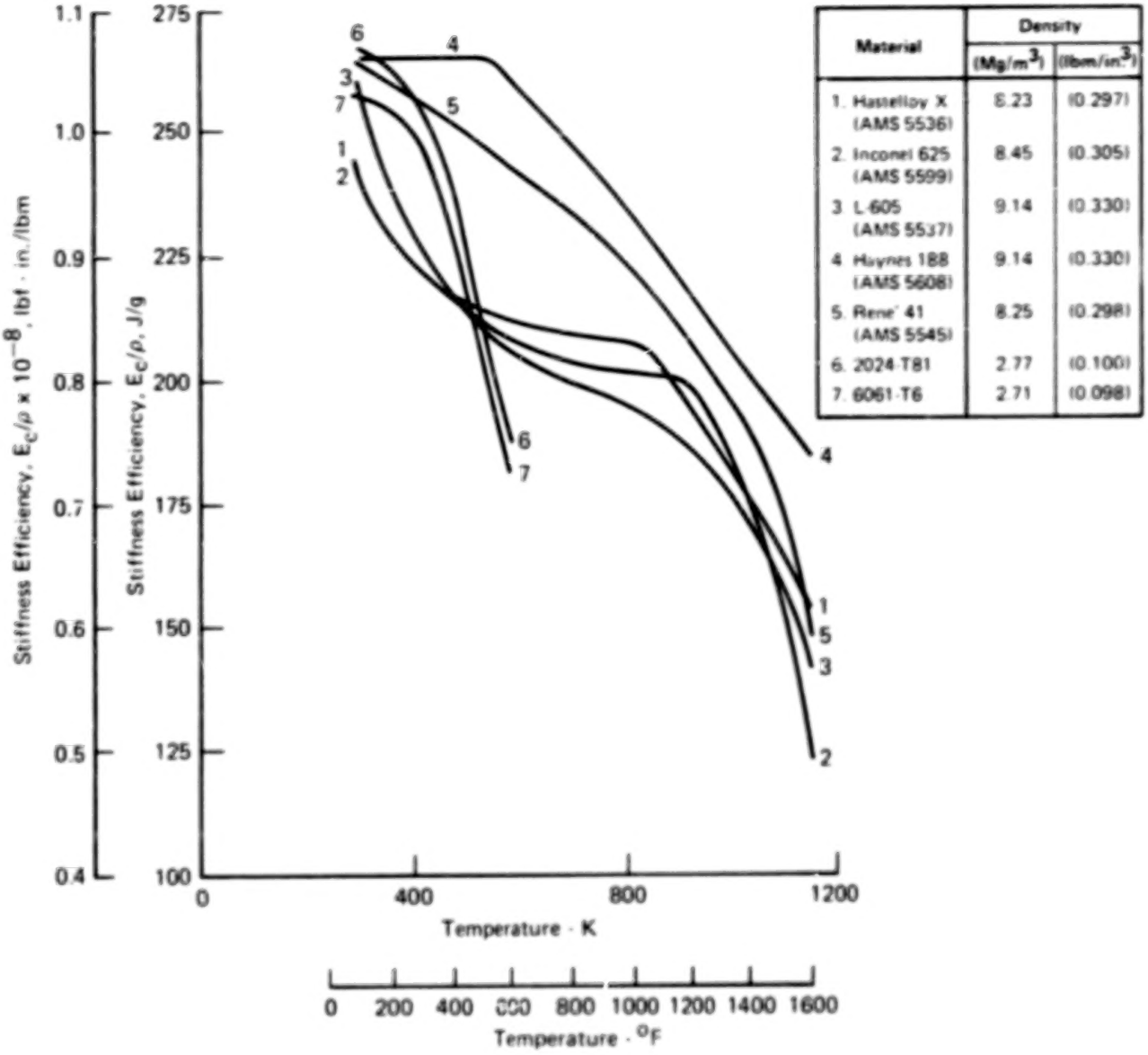


| Material | Density | |
|---|---|---|
| | ($Mg/m^3$) | ($lbm/in.^3$) |
| 1. Hastelloy X (AMS 5536) | 8.23 | (0.297) |
| 2. Inconel 625 (AMS 5599) | 8.45 | (0.305) |
| 3. L-605 (AMS 5537) | 9.14 | (0.330) |
| 4. Haynes 188 (AMS 5608) | 9.14 | (0.330) |
| 5. Rene' 41 (AMS 5545) | 8.25 | (0.298) |
| 6. 2024-T81 | 2.77 | (0.100) |
| 7. 6061-T6 | 2.71 | (0.098) |

**FIGURE 25 - STIFFNESS EFFICIENCY vs TEMPERATURE**

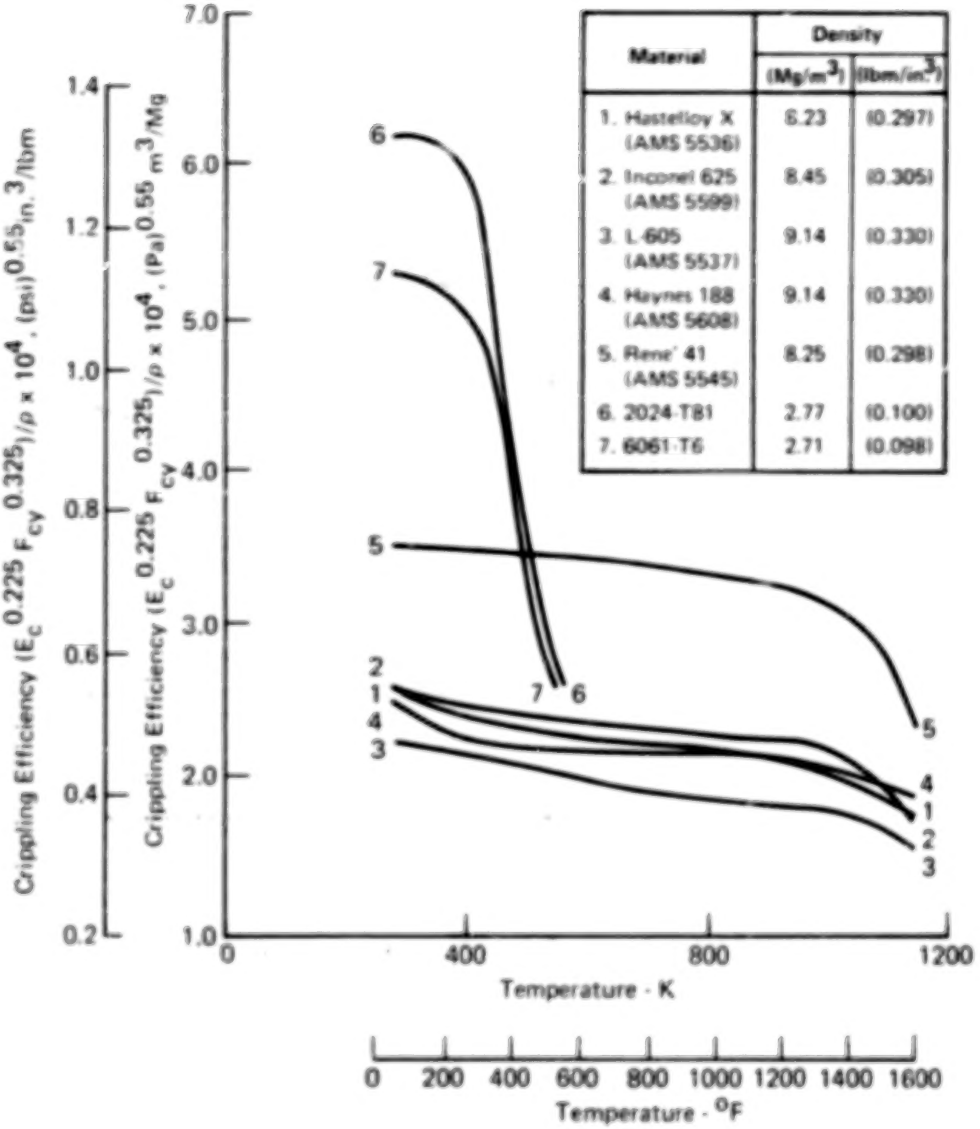


**FIGURE 26 - CRIPPLING EFFICIENCY vs TEMPERATURE**

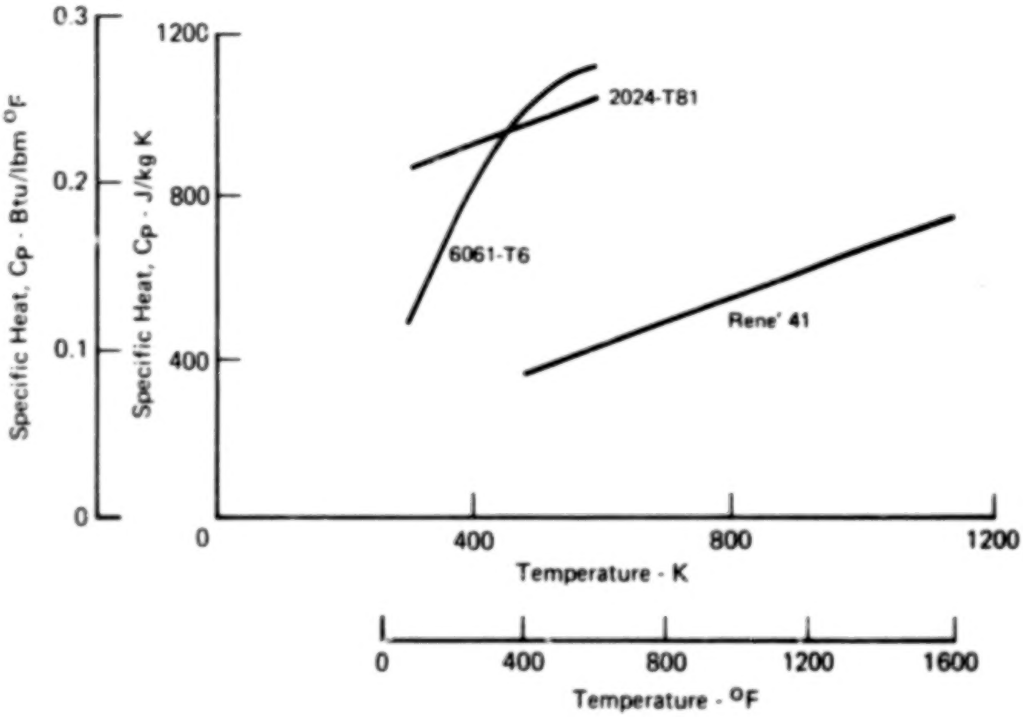


**FIGURE 27 - SPECIFIC HEAT vs TEMPERATURE**

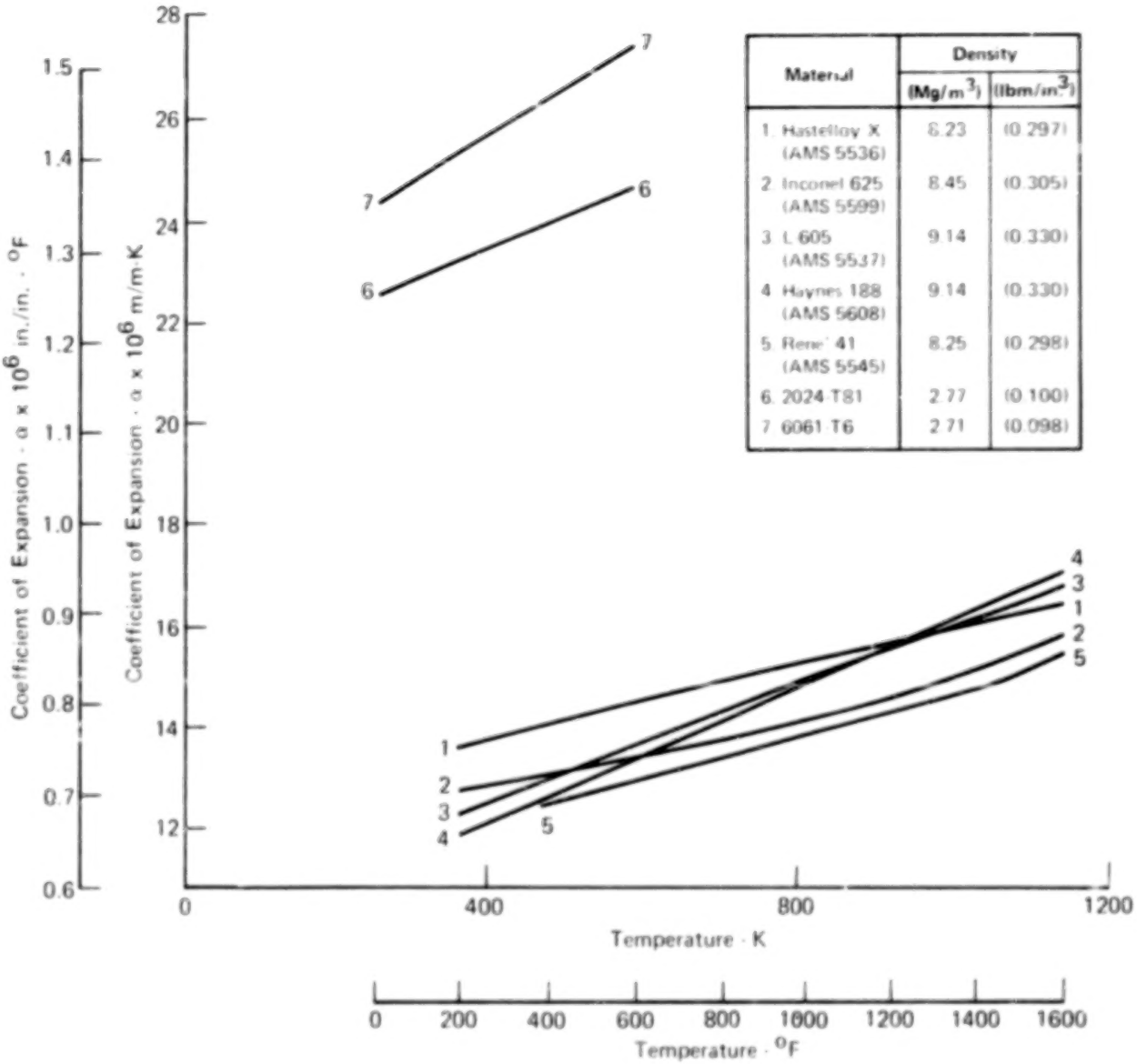


| Material | Density | |
|---|---|---|
| | ($Mg/m^3$) | ($lbm/in^3$) |
| 1. Hastelloy X (AMS 5536) | 8.23 | (0.297) |
| 2. Inconel 625 (AMS 5599) | 8.45 | (0.305) |
| 3. L-605 (AMS 5537) | 9.14 | (0.330) |
| 4. Haynes 188 (AMS 5608) | 9.14 | (0.330) |
| 5. Rene' 41 (AMS 5545) | 8.25 | (0.298) |
| 6. 2024-T81 | 2.77 | (0.100) |
| 7. 6061-T6 | 2.71 | (0.098) |

**FIGURE 28 - COEFFICIENT OF EXPANSION vs TEMPERATURE**

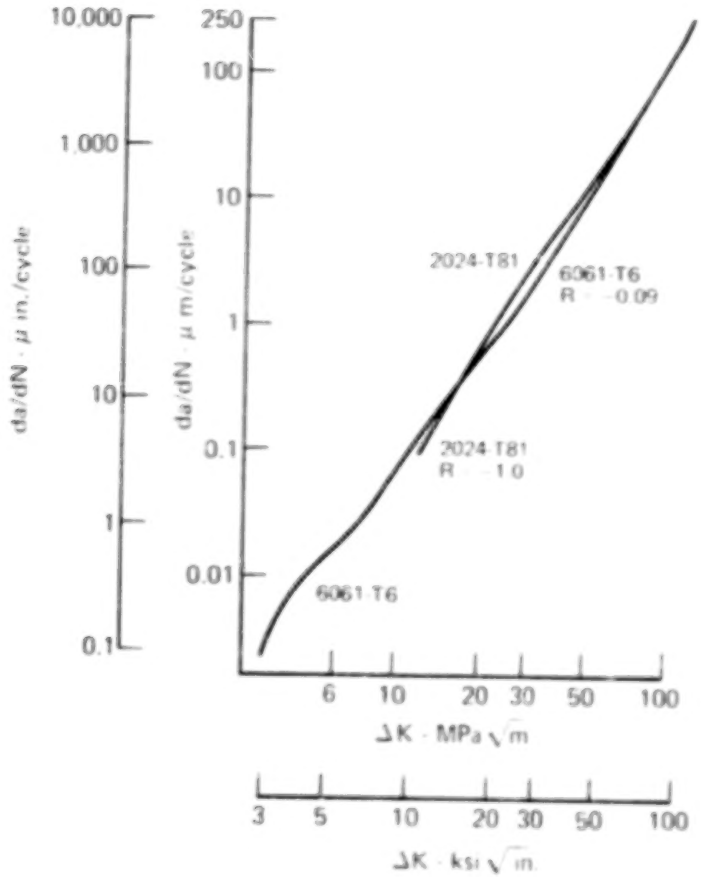


**FIGURE 29 - ALUMINUM CRACK GROWTH RATE vs STRESS INTENSITY RANGE**

wing skins were identified. The results of the analysis, based on the analytical method for predicting crack growth described in Reference 6, show that the 2024-T81 material has a 20,000 cycle life at a 106.9 MPa (15,500 psi) stress level. This is also the allowable established in reference 1.

The allowable for 6061-T6 coolant tubing was developed for an initial surface flaw 0.0220 cm (0.009 in.) deep and 0.456 cm (0.018 in.) long in a plate width equal to the tube circumference, and R = -0.09. This stress ratio is based on the stress levels in the coolant tube where, for a typical flight envelope, the cyclic mechanical stress levels are combined with the constant thermal stress, resulting in a maximum tensile stress of 171 MPa (23,810 psi limit) and a maximum compressive stress of 15.2 MPa (2210 psi limit).

Thermal stresses have a more significant affect on the cyclic stress levels in the coolant tubes than they do in the skins. The results of the analysis were substantiated by tests (Appendix E) and showed that the 6061-T6 material achieves more than the required 20,000 cycles at an operating stress level of 163.0 MPa (23,860 psi) and an R = 0.09.

Figure 30 shows the fatigue allowables for R = 0 and a life of 20,000 cycles versus $K_t$ for Rene'41 superalloy at 1144K (1600°F). This data was obtained from reference 7. Figure 31 shows the fatigue allowables versus $K_T$ for the two aluminum alloys for a R = -1.0 and a life of 20,000 cycles.

## Coolants

The coolant fluid used in this program was a 60/40 mass solution of ethylene glycol/water. Viscosity, vapor pressure, density, specific heat, and thermal conductivity for this coolant were obtained from Union Carbide Corporation and are presented in figures 32 through 36.

## Insulation

Insulation property data were collected for various candidates and are shown in table 3.

## Adhesives

Shear strength, peel strength, and thermal conductivity for FM 400 and FM 404 at various temperatures and exposure times are shown in table 4. These data were obtained from references 8 and 9. Thermal conductivity for RTV 560 was obtained from reference 10 and is also included in table 4.

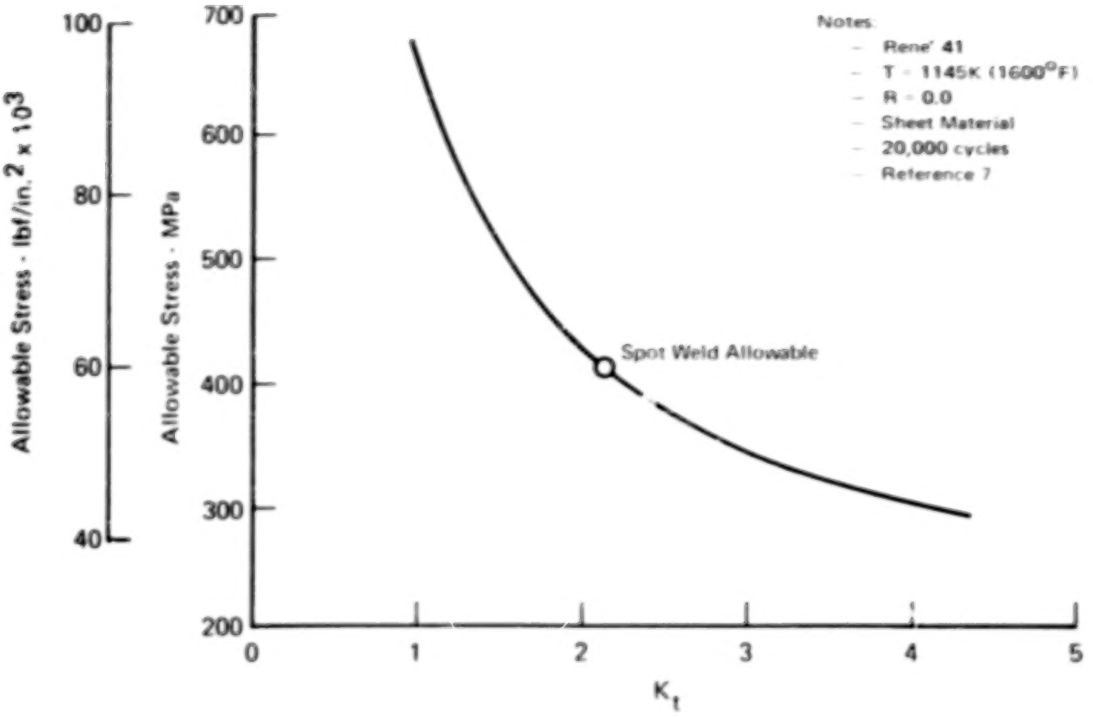


**FIGURE 30 - RENE' 41 ALLOWABLE STRESS vs STRESS CONCENTRATION FACTORS**

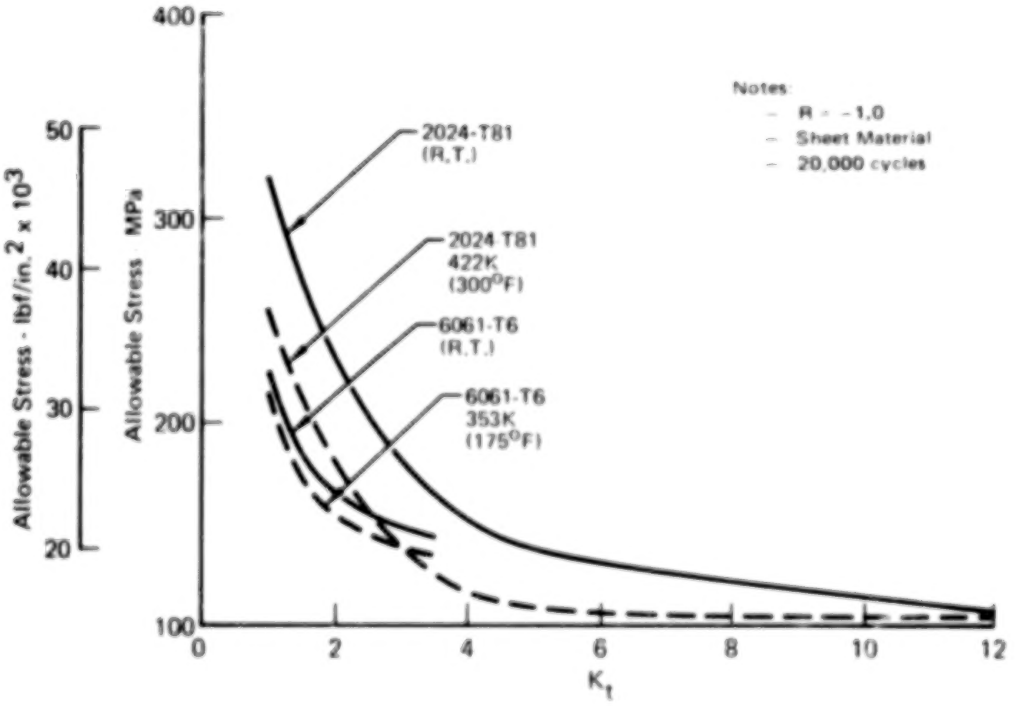


**FIGURE 31 - ALUMINUM ALLOWABLE STRESS vs CONCENTRATION FACTOR**

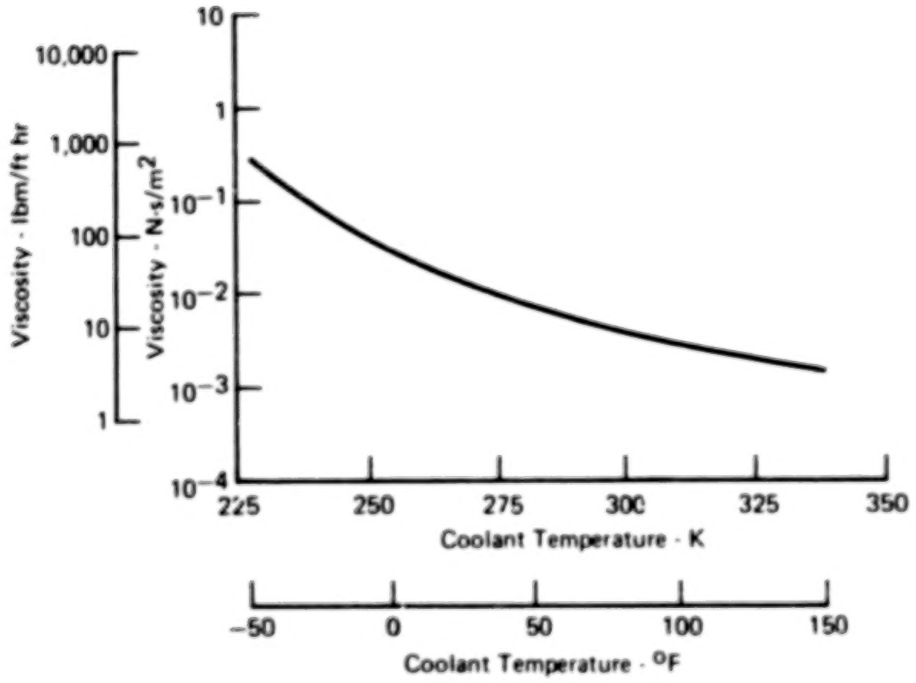


**FIGURE 32 · VISCOSITY vs TEMPERATURE FOR A 60/40 MASS SOLUTION OF ETHYLENE GLYCOL AND WATER**

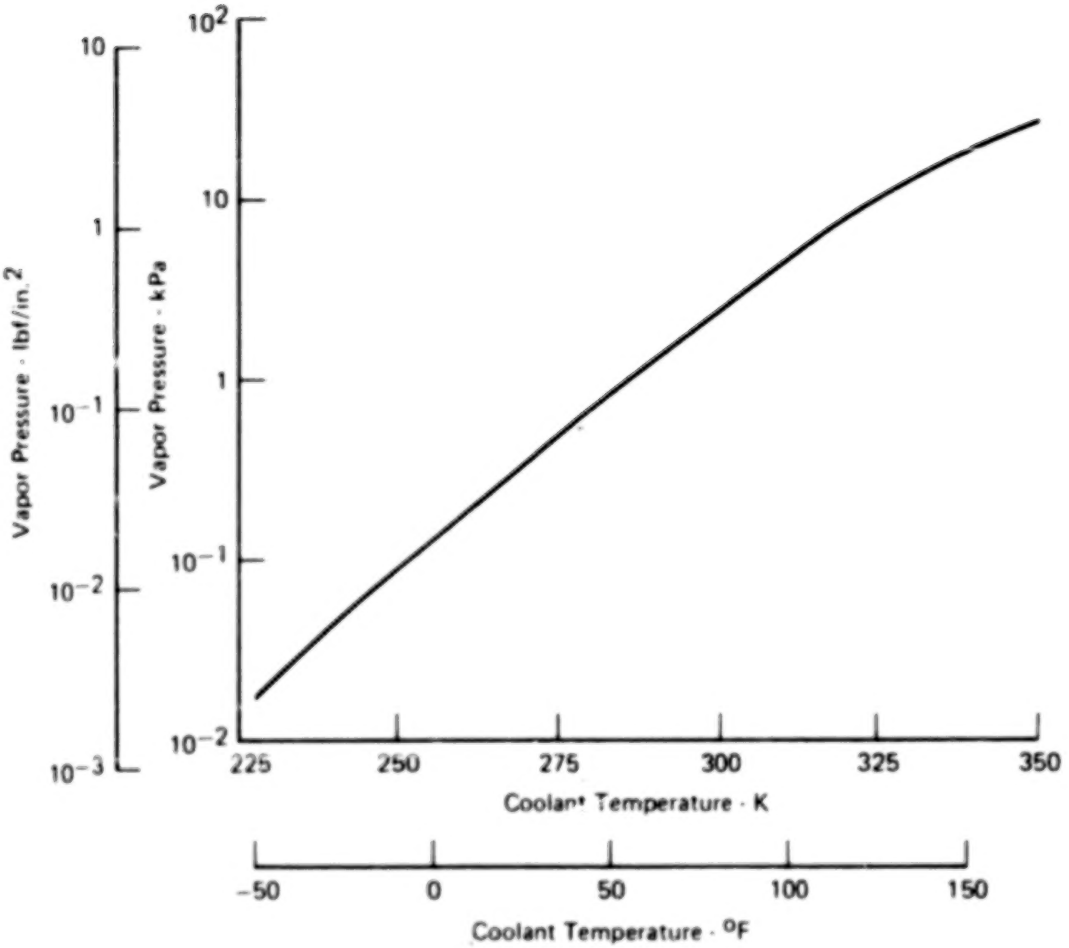


FIGURE 33 - VAPOR PRESSURE vs TEMPERATURE FOR A 60/40 MASS SOLUTION OF ETHYLENE GLYCOL AND WATER

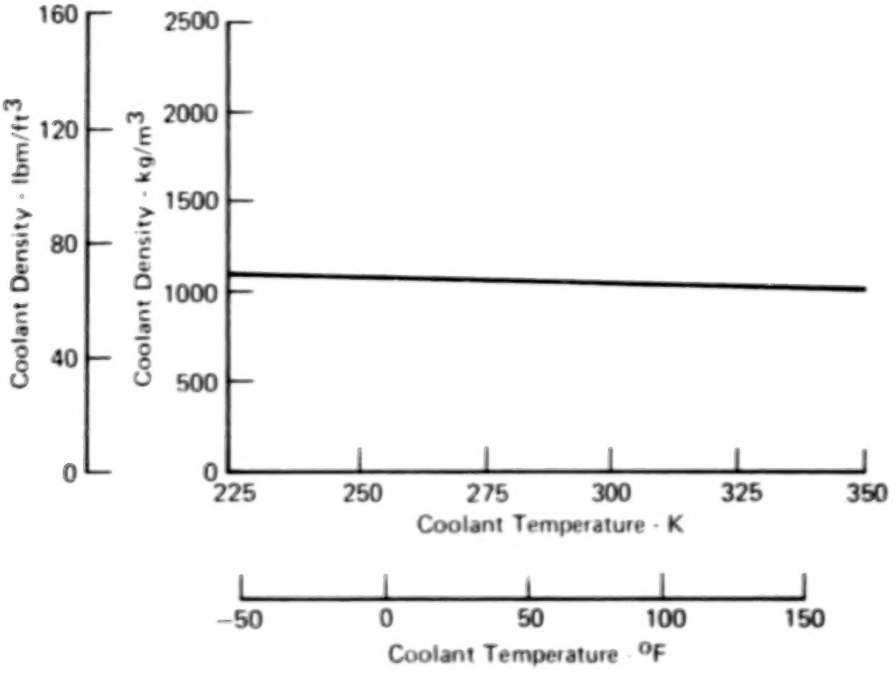


**FIGURE 34 - DENSITY vs TEMPERATURE FOR A 60/40 MASS SOLUTION OF ETHYLENE GLYCOL AND WATER**

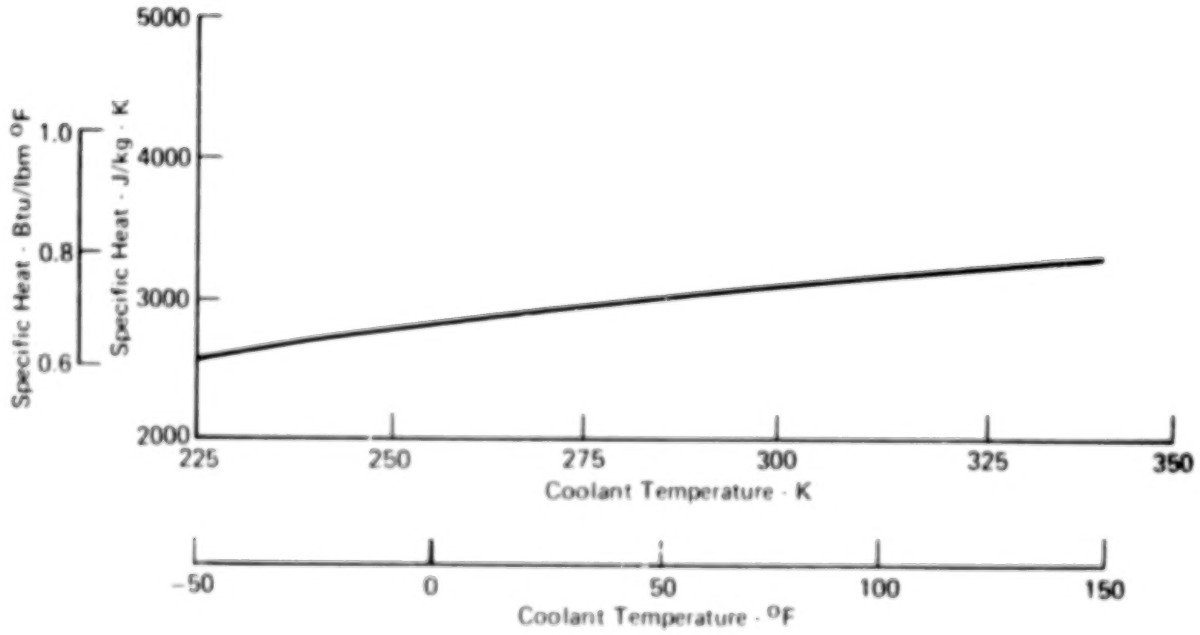


**FIGURE 35 - SPECIFIC HEAT vs TEMPERATURE FOR A 60/40 MASS SOLUTION OF ETHYLENE GLYCOL AND WATER**

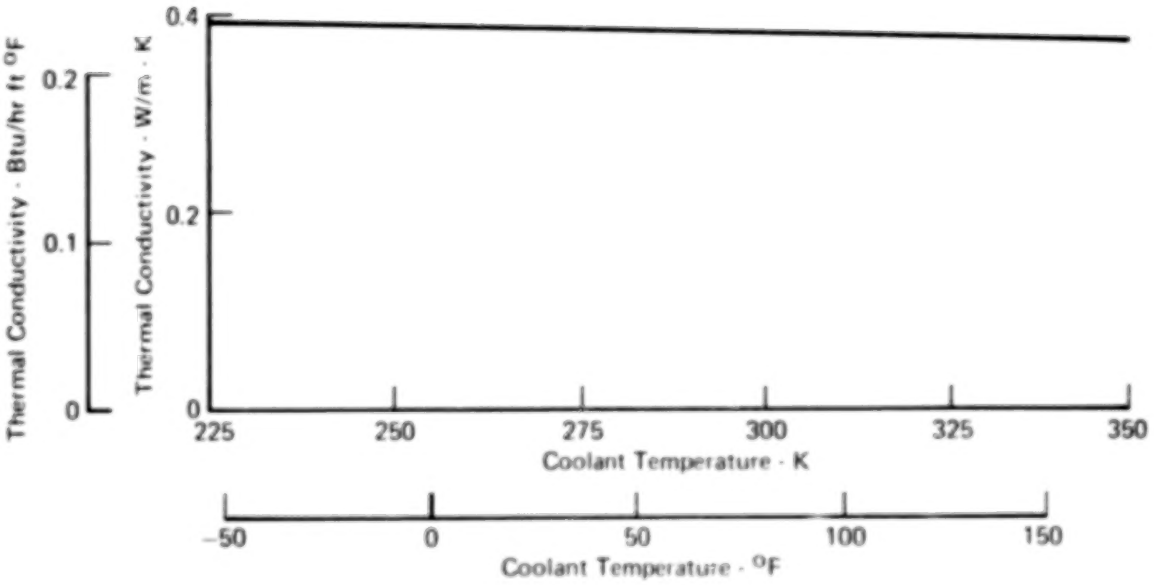


**FIGURE 36 - THERMAL CONDUCTIVITY vs TEMPERATURE FOR A 60/40 MASS SOLUTION OF ETHYLENE GLYCOL AND WATER**

## TABLE 3 – INSULATION PROPERTY DATA

| Material | Description | Density $kg/m^3$ ($lbm/ft^3$) | Thermal Conductivity W/m K @ 811 K (Btu in./$ft^2$ hr°F @1000°F) | Min Available Thickness cm (in.) | Maximum Continuous Use Temp K (°F) | Vendor | Characteristics |
|---|---|---|---|---|---|---|---|
| High Temp Flexible Min-K | Proprietary Silica Based Material | 256 (16) | 0.052 (0.36) | 0.318 (0.125) | 1250 (1800) | Johns-Manville | • Flexible with moderate load bearing capability |
| Thermoflex RF Felt | Fibrous Alumina-Silica Batting | 224 (14)<br>384 (24) | 0.101 (0.70)<br>0.095 (0.66) | 0.318 (0.125)<br>0.318 (0.125) | 1530 (2300)<br>755 (900) | Johns-Manville | • Semi-rigid with some load-bearing capability<br>• Contains organic binder which "burns out" at approx 755 K (900°F) |
| Li-900 | Ultra Pure Silica Hardened Compacted Fibers | 144 (9) | 0.137 (0.95) | 0.635 (0.25) | 1530 (2300) | Lockheed | • Requires the use of a strain isolator (Nomex felt, RL 1973 sponge rubber or equivalent) at the interface when bonded to structure. Normally bonded with RTV silicone.<br>• Requires coating (silicon carbide or equivalent) for improved handling and reduced water absorption.<br>• Machinable to shapes with smooth surfaces. |
| Marimet-45 | Heat Treated Calcium Silicate Board | 720 (45) | 0.121 (0.84) | 1.27 (0.50) | 1140 (1600) | Johns-Manville | • Machinable to shapes with smooth surfaces<br>• Rigid with load-bearing capability |

## TABLE 4 - ADHESIVE PROPERTY DATA

| Bonding Material | Exposure | | Test Temp | | Peel Strength[b] | | Shear Strength[b] | | Thermal Conductivity | |
|---|---|---|---|---|---|---|---|---|---|---|
| | Time | Temp | K | (°F) | kN/m | (lbf/in.) | MPa | (ksi) | W/m·K | $\left(\frac{\text{Btu·in.}}{\text{hr·ft}^2\cdot{}^\circ\text{F}}\right)$ |
| FM-400[a] | None | | 297 | ( 75) | 3.3 | (19.0) | 23.7 | (3.44) | 0.37 | (2.6) |
| | 10 min at 218 | (–67) | 218 | (–67) | – | – | 24.6 | (3.56) | 0.37 | (2.6) |
| | 18 hrs at 458 | (365) | 297 | ( 75) | – | – | 27.8 | (4.03) | 0.37 | (2.6) |
| | 18 hrs at 458 | (365) | 458 | (365) | 1.3 | ( 7.2) | 21.2 | (3.08) | 0.37 | (2.6) |
| | 3 hrs at 489 | (420) | 489 | (420) | – | – | 12.6 | (1.82) | 0.37 | (2.6) |
| FM-404[a] | None | | 297 | ( 75) | – | – | 3.4 | (0.50) | – | – |
| RTV-560[c] | (N/A) | | 367 | (200) | (N/A) | | (N/A) | | 0.31 | (2.16) |

Notes:

a Thermal conductivity obtained during Reference 1 Program

b Peel and shear strengths obtained from References 7 and 8

c Thermal conductivity obtained from Reference 9



67

Blank

Page

## APPENDIX B

## OPERATIONAL CONSIDERATIONS

A representative hydrogen fueled hypersonic cruise aircraft (figure 37) and flight envelope (figure 38) were selected for the purpose of this program to establish:

(a) The panel location and local flow conditions for thermal, structural, and structural dynamic analyses,

(b) The hydrogen heat sink available for airframe cooling,

(c) An operational climb profile for transient temperature analyses, and

(d) A representative cruise Mach/altitude condition for conducting abort heating analyses.

Aircraft Concept Number 3 from reference 2 was selected as representative of the class of aircraft employing radiative actively cooled structure. Satisfying the design requirement for a 1922K (3000°F) adiabatic wall temperature (for turbulent flow and a recovery factor of 0.9) yields a cruise Mach number of 6.7. The Mach 6 flight envelope for the aircraft was then extended to Mach 6.7, as indicated by the dashed lines on figure 38. As shown, the climb profile is constrained by sonic boom over-pressure up to Mach 2, dynamic pressure between Mach 2 and 4, a duct pressure limit between Mach 4 and 6.2, and aerodynamic heating between Mach 6.2 and the cruise Mach number of 6.7. The aerodynamic heating constraint was selected so heat shield temperatures during climb do not exceed the steady state cruise value.

Based upon conical flow and the Spalding and Chi turbulent heating relation (reference 11) it was determined that, at the start-of-cruise condition, the aircraft experiences an aero-dynamic heat transfer coefficient equal to the design value of 91 $W/m^2K$ (16 $Btu/ft^2$ hr°F) at a location 3 m (10 ft) aft of the nose on the lower fuselage centerline. At this location the flow deflection angle is 15 degrees (8 degrees of body contour plus 7 degrees angle of attack). This established the local flow conditions used in structural dynamic analyses.

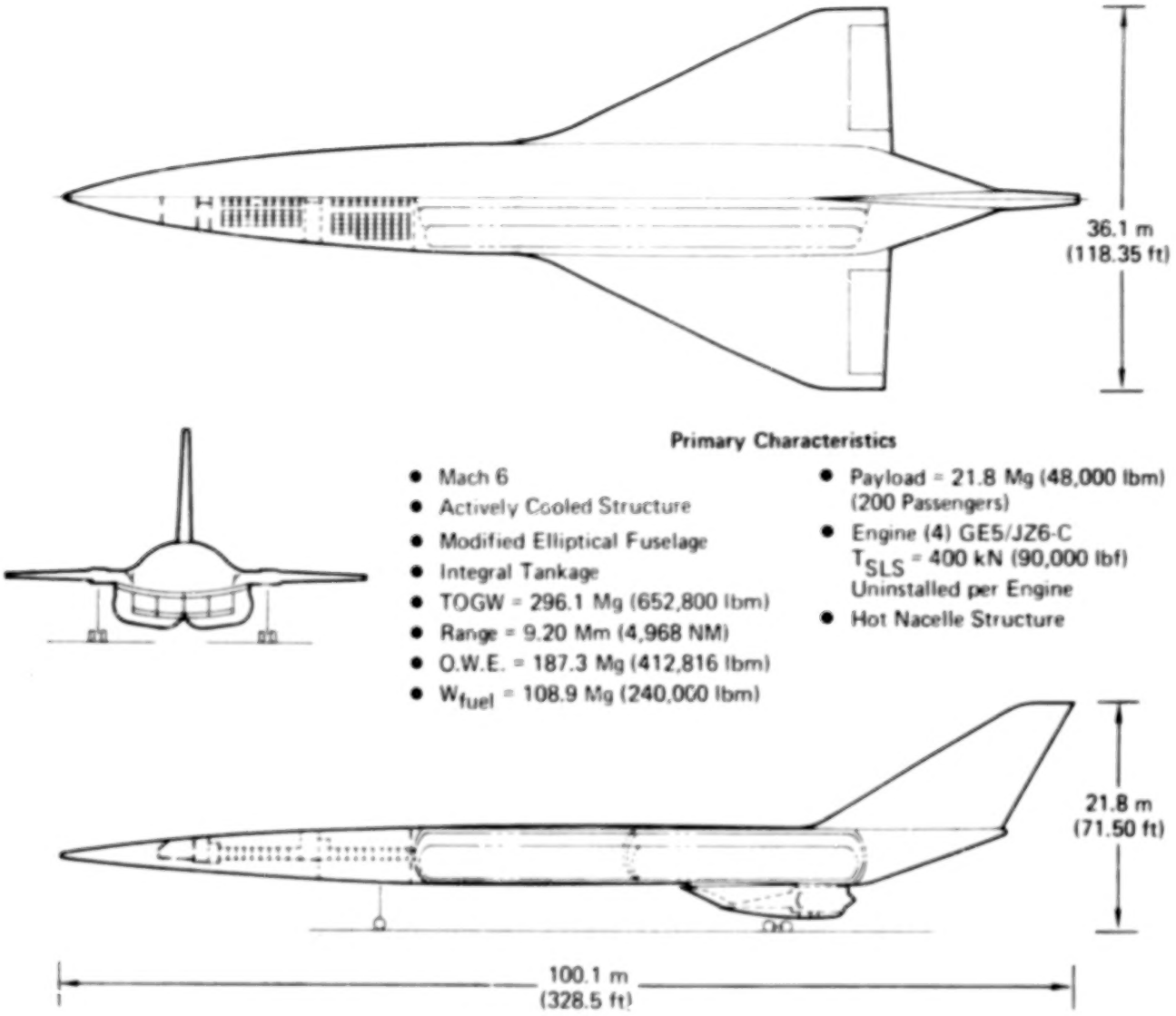


**FIGURE 37 - BASELINE AIRCRAFT**

The amount of hydrogen heat sink available for structural cooling was determined utilizing a statistically averaged aerodynamic heat load and hydrogen fuel flow rate, as presented in figures 39 and 40, respectively. Adjusting the results of figure 39 to a 422K (300°F) wall temperature, indicates that the average aerodynamic heat load to the aircraft is 36.2 $kW/m^2$ (3.2 $Btu/ft^2$ sec). Assuming a lift-to-drag ratio of 4.5, figure 40 indicates that the hydrogen fuel flow rate at Mach 6.7 is 3.7 $kg/m^2$ hr (0.756 $lbm/ ft^2$ hr). Assuming that the hydrogen fuel can be heated from 33 K (-400°F) to 311 K (100°F) indicates

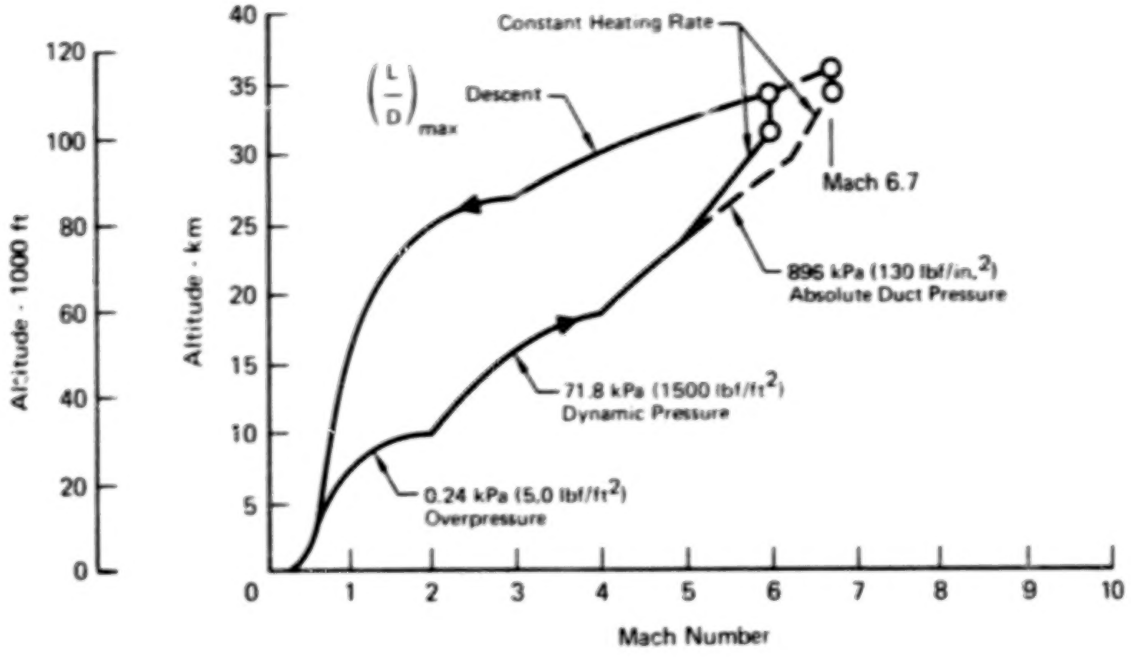


**FIGURE 38 - MACH 6 BASELINE FLIGHT ENVELOPE AND EXTENSION TO MACH 6.7**

that 18.7 kW/m$^2$ (1.65 Btu/ft$^2$ sec) of hydrogen heat sink is available for active cooling of the structure, which is approximately 50% of the above aerodynamic heat load. During the present program, parametric analyses were performed over a range of absorbed heat flux levels up to a maximum of 68 kW/m$^2$ (6 Btu/ft$^2$ sec), 50% of the reference value.

For abort heating analyses a failure was assumed at the start-of-cruise condition. After detecting a cooling system failure, the aircraft decelerates and descends along a load-factor-limited trajectory (figure 41), constrained as follows:

- o Load factor limit - - - - - - - - - - 2.5
- o Angle-of-attack limit - - - - - - - - 20 degrees
- o Bank angle limit - - - - - - - - - - 40 degrees
- o Minimum dynamic pressure - - - - - 4.8 kPa (100 lbf/ft$^2$)

Reference 17 results previously demonstrated that a load-factor-limited descent minimizes the abort heat load and established that 15 seconds was sufficient time to detect a failure and start the abort maneuver.

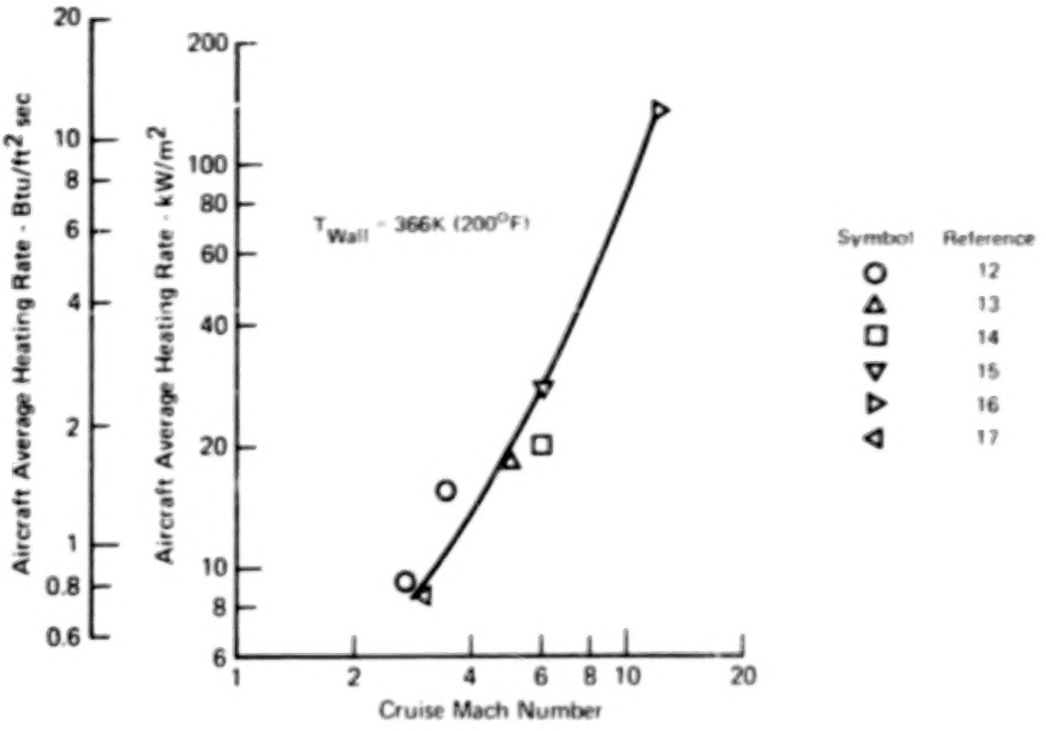


**FIGURE 39 · INCREASE IN AERODYNAMIC HEATING RATES AS A FUNCTION OF CRUISE MACH NUMBER**

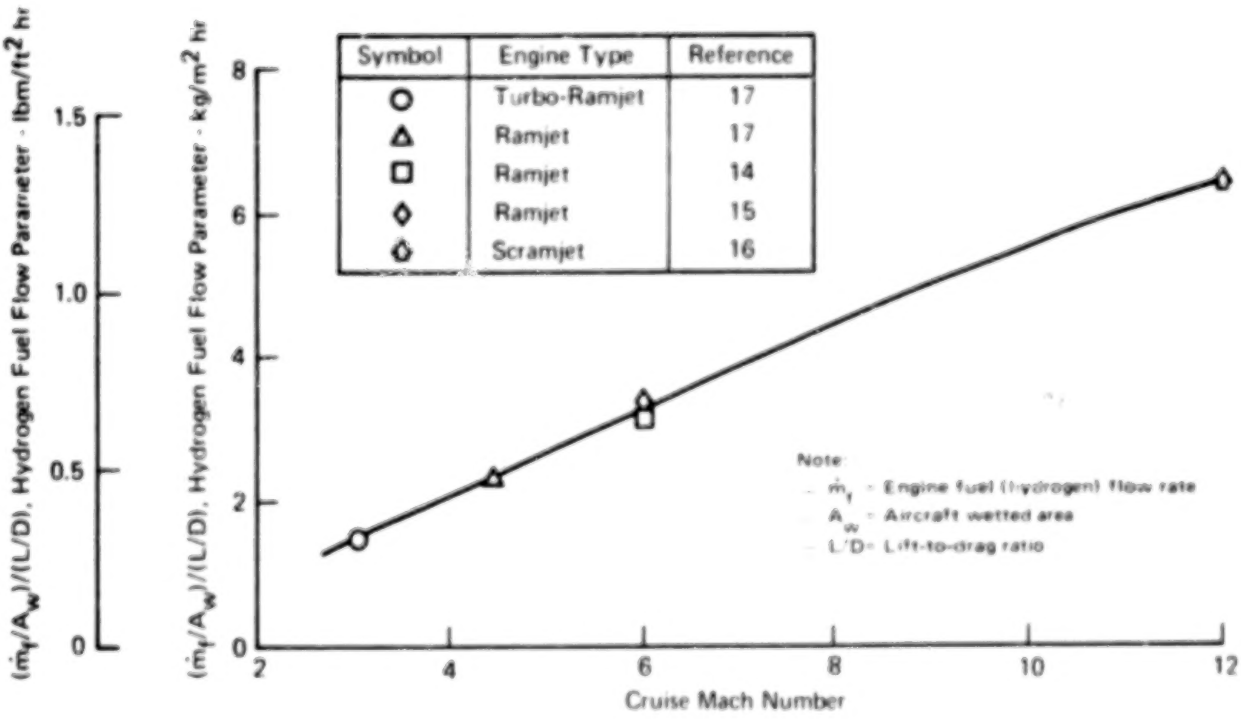


**FIGURE 40 · HYDROGEN FUEL FLOW REQUIREMENTS FOR HIGH MACH NUMBER CRUISE AIRCRAFT**

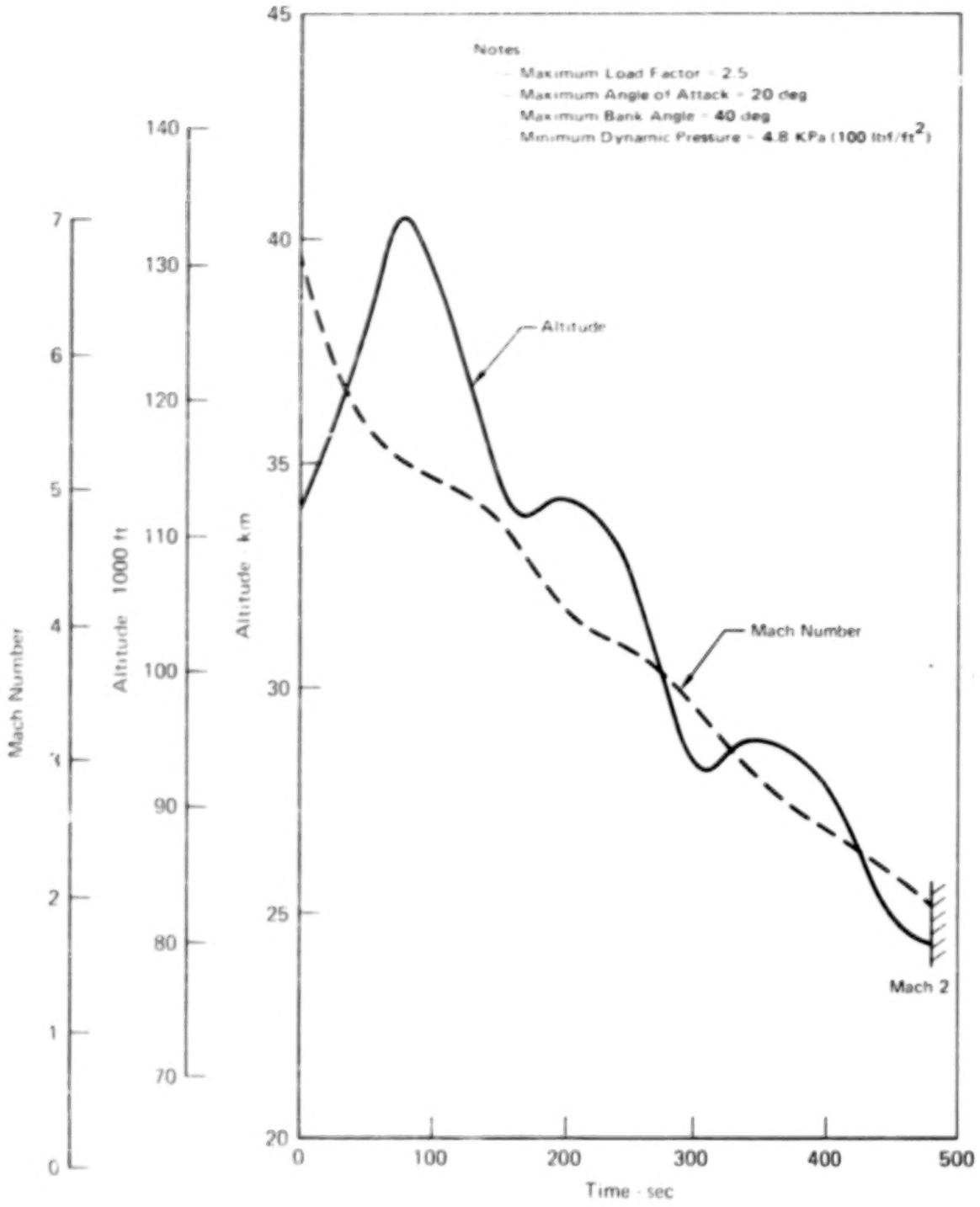


FIGURE 41 - MINIMUM HEAT LOAD/LOAD FACTOR LIMITED ABORT TRAJECTORY

Blank Page

## APPENDIX C

## RADIATIVE THERMAL PROTECTION SYSTEM CONCEPT EVALUATION

Nine radiative heat shield concepts were evaluated to identify the concept with the most potential for providing a minimum mass configuration when combined with an actively cooled panel. The heat shield concepts, shown in figure 42, were; (1) RSI (LI900), (2) Metal Wool, (3) SLA-220 (silica filled elastomeric silicon), (4) Foamed metals, (5) Preloaded dome, (6) Screen sandwich, (7) Astroquartz, (8) Beaded skin, and (9) Corrugated stiffened beaded skin.

All concepts were evaluated for eleven figures of merit; mass, cost, producibility, inspectability, maintainability, durability, volumetric efficiency, performance and integrity, resistance to hot gas influx, tolerances to overheat, and development needs. Considerations in these evaluations were as follows:

- Mass - mass of the heat shield, heat shield supports, insulation package, actively cooled panel (including readily identifiable provisions such as adhesives and fasteners), and the active cooling system.
- Cost - tooling and recurring manufacturing labor cost.
- Producibility - fabrication complexity of curved and flat surfaces.
- Inspectability - ease and reliability of inspection of radiation system concept components and actively cooled panel.
- Maintainability - cost and down-time required for routine and emergency maintenance.
- Durability - resistance to foreign objects and environmental damage.
- Volumetric efficiency - volume of airplane without radiation system divided by the volume of airplane with radiation system.
- Thermal/structural performance and integrity - predictability of performance and extent of unproven details.

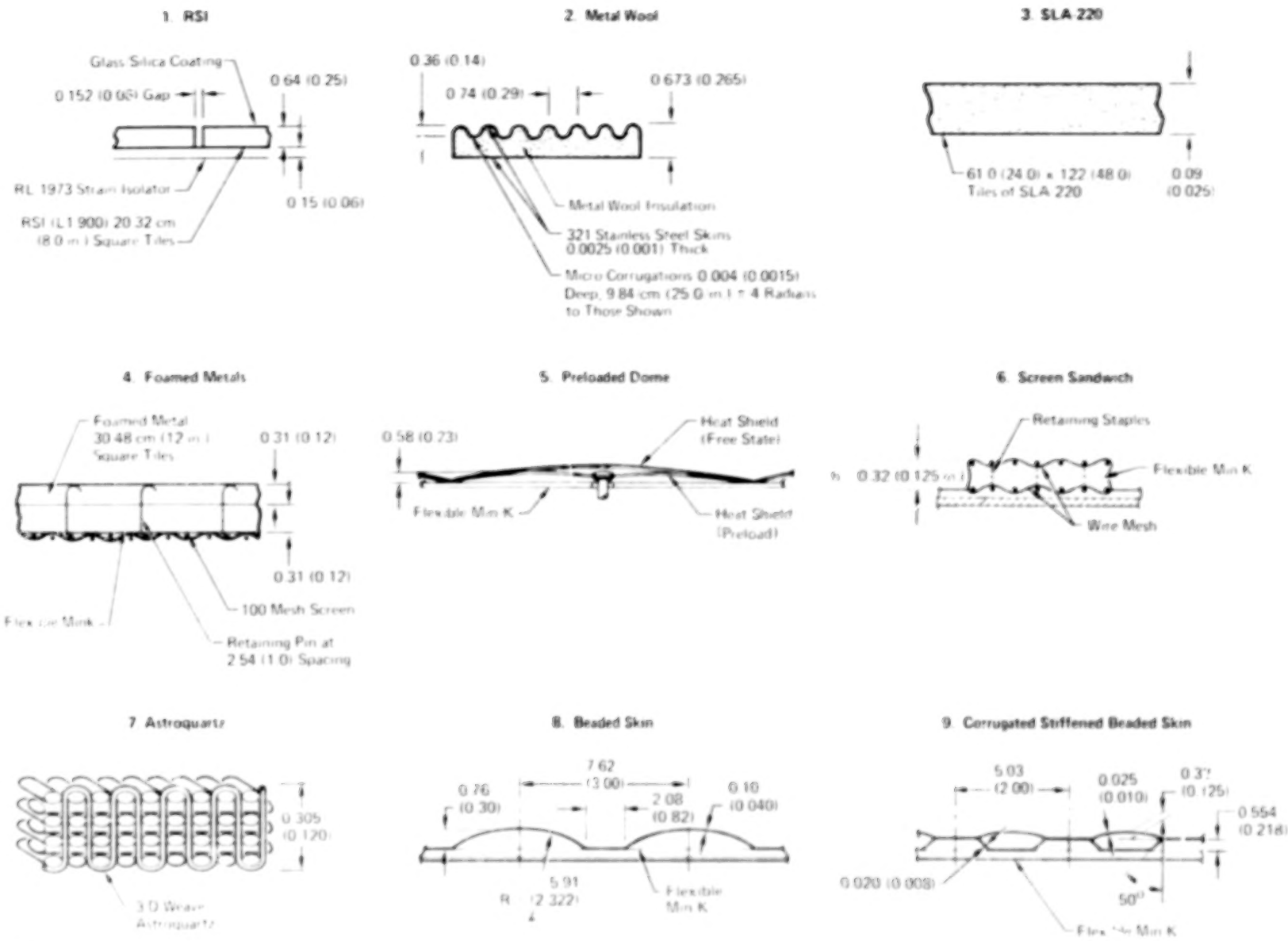


**FIGURE 42 RADIATIVE HEAT SHIELD DESIGNS**

- o Advanced Development Needs - required materials and manufacturing development compared with current state of the art.
- o Resistance to hot gas influx - requirement for barriers to prevent boundary layer gases from impinging on the actively cooled panel.
- o Tolerance to overheating - ability of the radiative system to sustain over design temperatures without refurbishment.

Grades were given to each concept for each figure of merit. The grades were the result of inputs received from several engineering disciplines after their review of drawings (the result of preliminary sizing) showing pertinent details. The grades ranged between ten (the best) and zero (the worst). Weighting factors, agreed upon between NASA and MCAIR, were applied to each figure of merit to properly assess the significance of each relative to the overall weight, cost, and performmance of a hypersonic airplane. A score was then computed for each concept and figure of merit by multiplying the weighting factor times the grade. The figure of merit scores were then added and the concept having the highest sum was ranked number one. The subjective nature of all figures of merit, except mass and cost, causes problems for this type of evaluation, i.e., the wrong concept may be selected if only the ranking is used for the selection without application of common sense and engineering judgement. However, the evaluation does identify promising concepts, their strong and weak points and an indication of their relative ranking.

A first order assessment was made, using preliminary drawings of each concept, to quickly identify the concepts with most potential for application on a hypersonic transport vehicle. Those concepts were reanalyzed, refined, and reevaluated for each of the eleven figures of merit. Following paragraphs present a description of all concepts and the results of the evaluation of the final six concepts.

## Description of Thermal Protection System Concepts

The reusable surface insulation (RSI) evaluated was the LI900 type used on the Space Shuttle, reference 18. The RSI concept is 20.32 cm (8.0 in.) square and 0.64 cm (0.25 in.) thick, and is bonded to a 0.15 cm (0.06 in.) thick strain isolator which is bonded to an actively cooled panel. The strain isolator, bonded with a silicon type adhesive, prevents cracking of the brittle RSI due to strains caused by temperature differences and mechanical loading.

The metal-wool heat shield concept was proposed for use on the Space Shuttle in reference 19. The concept consists of a 0.0025 cm (0.001 in.) thick corrugated stainless steel foil with micro-corrugations 0.004 cm (0.0015 in.) deep at 0.01 cm (0.04 in.) spacing. The micro-corrugations are oriented at 45° to the primary corrugations, which have a 0.74 cm (0.29 in.) pitch and a 0.36 cm (0.14 in.) height. The cavity between corrugations and the 0.0025 cm (0.001 in.) stainless steel inner skin is filled with metal wool insulation. These packages are bonded to the actively cooled panel with a room temperature curing silicon adhesive.

The SLA-220 (see reference 20) has a maximum continuous use temperature of 867 K (1100°F). Its primary advantages are low cost and ease of application. The SLA-220 could be fabricated in 0.61 x 1.22m (2 x 4 ft) sheets 0.09 cm (0.025 in.) thick and bonded to the actively cooled panel.

Two Rene'41 foamed metal concepts were considered. One uses the foamed metal, bonded directly to the actively cooled panel, as the sole insulator. Due to its poor insulating characteristics a thickness of 3.05 cm (1.2 in.) is required to prevent overheating the silicon bonding agent and the actively cooled panel. It was therefore, approximately 60% heavier than the second system which uses a 0.31 cm (0.12 in.) thick 256 kg/m$^3$ (16 pcf) Min-K insulation package wrapped in 0.0025 cm (0.001 in.) stainless steel foil sandwiched between a stainless steel screen wire and 0.31 cm (0.12 in.) thick foamed metal. Retaining pins which pass through the foamed metal, the Min-K package, and a 100 mesh wire screen (which prevents the retaining pins from

pulling through the fragile Min-K insulation) hold the concept together. This complete 30.48 cm (12 in.) square by 0.61 cm (0.24 in.) thick package (foamed metal, insulation, wire screen) is bonded to the actively cooled panel with a silicon adhesive.

The preloaded dome concept is a thin skin superalloy sheet formed to a spherical shape. The edges of the heat shield are trimmed to a square plan form. When the dome is not preloaded and is placed on a flat surface, only the corners touch the surface. The domed heat shield is preloaded by a single bolt through the apex of the sphere. In the preloaded condition, the edges of the heat shield are in contact with the insulation package and maintains a positive bearing pressure all along the perimeter.

The size, thickness, radius of curvature, and required preload was varied until a minimum mass heat shield design was obtained. The insulation package consists of 0.32 cm (0.125 in.) thick flexible 256 kg/m$^3$ (16 pcf) Min-K insulation wrapped in 0.0025 cm (0.001 in.) stainless steel foil. A solid insulative washer, fabricated as a part of the insulation package, provides a solid stop, directly under the head of the fastener, to prevent "snap through" during fastener installation.

The screen sandwich concept consists of 0.32 cm (0.125 in.) thick 256 kg/m$^3$ (16 pcf) flexible Min-K insulation wrapped in 0.0025 in. (0.001 in.) thick stainless steel foil encased in 100 mesh screen wire. The screen wire is held in place with retaining pins inserted through the package and crimped over the wire screen. The 30.5 x 30.5 cm (12 x 12 in.) square by 0.3 cm (0.135 in.) thick packages are bonded to the actively cooled panel with a silicon adhesive. The packages are butted together with no joint gap to allow for expansion; thermal expansion is accommodated by flexing of the 0.001 cm (0.0045 in.) diameter screen wire.

The Astroquartz concept is simply a layer of silica type insulation bonded directly to the outer surface of the actively cooled panel. The required 0.32 cm (0.12 in.) thickness is obtained by three dimensional weaving of the silica fibers into

0.61 x 1.22m (2 x 4 ft) sections.

The beaded skin concept consists of a 0.10 cm (0.040 in.) thick (to prevent flutter) superalloy sheet formed into 0.76 cm (0.30 in.) high beads, in the longitudinal direction, with a 7.62 cm (3 in.) spacing. The heat shield is supported every 30.5 cm (12 in.), with slotted holes (relative to the direction of airflow) at the ends to allow for thermal expansion. The insulation package consists of 0.32 cm (0.125 in.) thick flexible 256 $kg/m^3$ (16 pcf) Min-K insulation, a 0.0025 cm (0.001 in.) stainless steel foil wrapper, and 0.64 cm (0.25 in.) high standoff posts.

The corrugated stiffened beaded skin concept consists of an 0.025 cm (0.010 in.) thick beaded superalloy skin with a 0.32 cm (0.125 in.) bead height at a 5.08 cm (2 in.) spacing. The 0.02 cm (0.008 in.) thick corrugations are spot welded to the 2.03 cm (0.80 in.) wide lands in the beaded skin. The heat shields are 0.61 x 0.61 m (2 x 2 ft) square, supported at each land in the transverse direction, and at 30.48 cm (12 in.) spacing in the longitudinal direction. The heat shield geometry was optimized to provide minimum mass when considering support spacing, local concentrated loads at the supports, and the increased heating which results from flow angularity and bead protrusion outside of the moldline. The insulation package is the same as that used for the beaded skin concept.

## Results of Concept Evaluation

The first assessment eliminated the RSI, the metal wool, and the foamed metals. The RSI received low scores in inspectability, maintainability and durability. However, the primary reason for its elimination was its inherent brittleness, which is a major disadvantage if used on a transport aircraft where long life and low maintenance are desired.

The metal wool concept received low scores in cost, producibility, inspectability, maintainability, durability, and performance and integrity. Its only real advantage was its reported (reference 19) low mass, which was due to its thin 0.0025 cm

(0.001 in.) outer skin. However, the thin outer skin durability was judged to be extremely poor, making its use on a hypersonic aircraft impractical. If the outer skin thickness is increased to what is considered more practical, i.e., 0.025 cm (0.01 in.), it would lose its low mass advantage. Also, the ability of the concept to withstand hypersonic flow is doubtful.

The foamed metals received low scores in cost, inspectability, and volumetric efficiency. In general they were rated uniformly low for all figures of merit. However, they were eliminated primarily because their thermal performance in service was questionable, especially in light of their water absorption characteristics.

Evaluation of the six remaining radiative heat shield concepts, indicated that the metallic (corrugated stiffened beaded skin, preloaded dome, and the beaded skin) and the non-metallic (SLA-220, Astroquartz, and screen sandwich) concepts each have certain unique characteristics. The metallic concepts are generally easier to inspect and maintain, primarily because of their mechanical attachment (adhesive bonding prevents heat shield removal without destroying the heat shield). Metallic heat shields are also more durable and their performance in service is more predictable, because of knowledge gained from past hardware programs. The non-metallic heat shields are generally lightweight, have a high resistance to hot gas influx, and have a high tolerance to overheating (except the SLA-220).

The results of the evaluation of the six radiative heat shield concepts presented in table 5, show that all concepts, except the SLA-220, are competitive with a maximum spread in scores of 0.86. The top five radiative heat shield concepts were; the screen sandwich, the corrugated stiffened beaded skin, the preloaded dome, the beaded skin, and the Astroquartz concepts, respectively.

Screen sandwich - The primary advantage of this concept, as reflected by its high score, is its low mass. Inspection of the primary structure is poor because it is bonded rather than mechanically fastened to the actively cooled panel. Removal of

TABLE OF CONTENTS

TABLE OF CONTENTS (Continued)

TABLE 5 - RESULTS OF RADIATIVE HEAT SHIELD CONCEPTS EVALUATION

| Concepts | Figures of Merit: Mass | Cost | Producibility | Inspectability | Maintainability | Durability | Volumetric Efficiency | Performance & Integrity | Development Needs | Resistance to Gas Influx | Tolerance to Overheat | Cumulative Score | Ranking |
|---|---|---|---|---|---|---|---|---|---|---|---|---|---|
| | Weighting Factors: 0.35 | 0.15 | 0.06 | 0.07 | 0.06 | 0.11 | 0.04 | 0.04 | 0.02 | 0.06 | 0.04 | | |
| | Grade (Score) | | | | | | | | | | | | |
| Screen Sandwich | 10.0 (3.5) | 6.0 (0.90) | 7.0 (0.42 | 2.8 (0.20) | 4.2 (0.25) | 6.2 (0.68) | 2.2 (0.09) | 5.6 (0.22) | 6.7 (0.13) | 7.8 (0.47) | 8.8 (0.35) | (7.21) | 1 |
| Corrugated Stiffened Beaded Skin | 6.8 (2.4) | 7.0 (1.05) | 7.0 (0.42) | 8.0 (0.56) | 8.3 (0.50) | 8.0 (0.88) | 0.7 (0.03) | 9.7 (0.39) | 9.4 (0.19) | 7.3 (0.44) | 7.8 (0.31) | (7.17) | 2 |
| Preloaded Dome | 4.3 (1.5) | 10.0 (1.50) | 9.0 (0.54) | 9.3 (0.65) | 9.7 (0.58) | 8.8 (0.97) | 1.0 (0.04) | 8.9 (0.36) | 8.3 (0.17) | 7.5 (0.45) | 7.3 (0.29) | (7.05) | 3 |
| Beaded Skin | 4.7 (1.6) | 9.0 (1.35) | 8.0 (0.48) | 8.5 (0.60) | 8.5 (0.51) | 9.8 (1.08) | 0.7 (0.03) | 9.8 (0.39) | 9.2 (0.18) | 7.3 (0.44) | 8.3 (0.33) | (6.99) | 4 |
| Astroquartz | 6.8 (2.4) | 7.0 (1.05) | 10.0 (0.60) | 3.3 (0.23) | 4.0 (0.24) | 4.8 (0.53) | 2.9 (0.12) | 5.6 (0.22) | 3.2 (0.06) | 8.3 (0.50) | 10.0 (0.40) | (6.35) | 5 |
| SLA-220 | 3.8 (1.3) | 4.0 (0.60) | 9.5 (0.57) | 3.7 (0.26) | 3.6 (0.22) | 2.9 (0.32) | 10.0 (0.40) | 5.7 (0.23) | 9.3 (0.19) | 9.8 (0.59) | 1.2 (0.05) | (4.73) | 6 |

this type heat shield for inspection, maintenance or replacement would result in complete destruction and would require a new heat shield. Consequently, it received a low grade for maintainability. Its low score for volumetric efficiency, even though it is only 0.32 cm (0.125 in.) thick, is due to the fact that the SLA-220 concept was used as a base since it was only 0.09 cm (0.035 in.) thick. However, the low grade received for volumetric efficiency has little impact on its overall rating since all concepts were equally penalized. The total score was 7.21 and resulted in the concept being rated number one.

Corrugated stiffened beaded skin - This concept had a total score of 7.17 and was ranked number two. It received uniformly high scores for all figures of merit. The cross-section was sized to provide a minimum mass configuration when considering

support spacing, local concentrated loads at the supports, and varying heating rates resulting from the flow angularity and bead protrusion outside of the moldline. The thermal stresses resulting from the temperature gradients, combined with the 10.3 kPa (1.5 psi) ultimate normal airloading, resulted in the concept being strength critical rather than flutter critical. This concept was not penalized for surface roughness because the beads in the outer skin are generally parallel to the direction of the air flow. This concept's performance in service is more predictable than the other concepts and, based on current knowledge, was considered the most reliable of all the concepts evaluated.

Preloaded dome - The preloaded dome concept was ranked number three and received high scores except for volumetric efficiency and mass. Large mass prevented this concept from being rated number one. The large mass results from penalizing the concept because of increased airplane drag due to surface irregularities. Figure 43 shows the results of the performance study which evaluated the impact on range of the baseline aircraft for different dome shapes, i.e. h/A (deviation outside of moldline divided by heat shield size). As shown, the maximum penalty occurred during climb and acceleration. For an h/A of 0.023 (selected geometry), an additional 7.26 Mg (16,000 lbm) of fuel was necessary for the required 4,968 NM range. This increased fuel requirement causes an increase in the operational weight empty (O.W.E.) of the representative airplane of 13.93 Mg (30,708 lbm). When the preloaded dome heat shield was penalized for this additional mass of 18 $kg/m^2$ (3.69 $lbm/ft^2$) its effective mass increased to 38.5 $kg/m^2$ (7.90 $lbm/ft^2$) compared to the baseline screen sandwich heat shield mass of 16.49 $kg/m^2$ (3.38 $lbm/ft^2$).

Beaded skin - The beaded skin concept was rated number four and received high scores for all figures of merit except volumetric efficiency and weight. Panel flutter prevention for flow angularities greater than 5° required a 0.10 cm (0.04 in.) outer skin and a 30.48 cm (12 in.) support span. Consequently, the mass required to prevent panel flutter, resulting from this

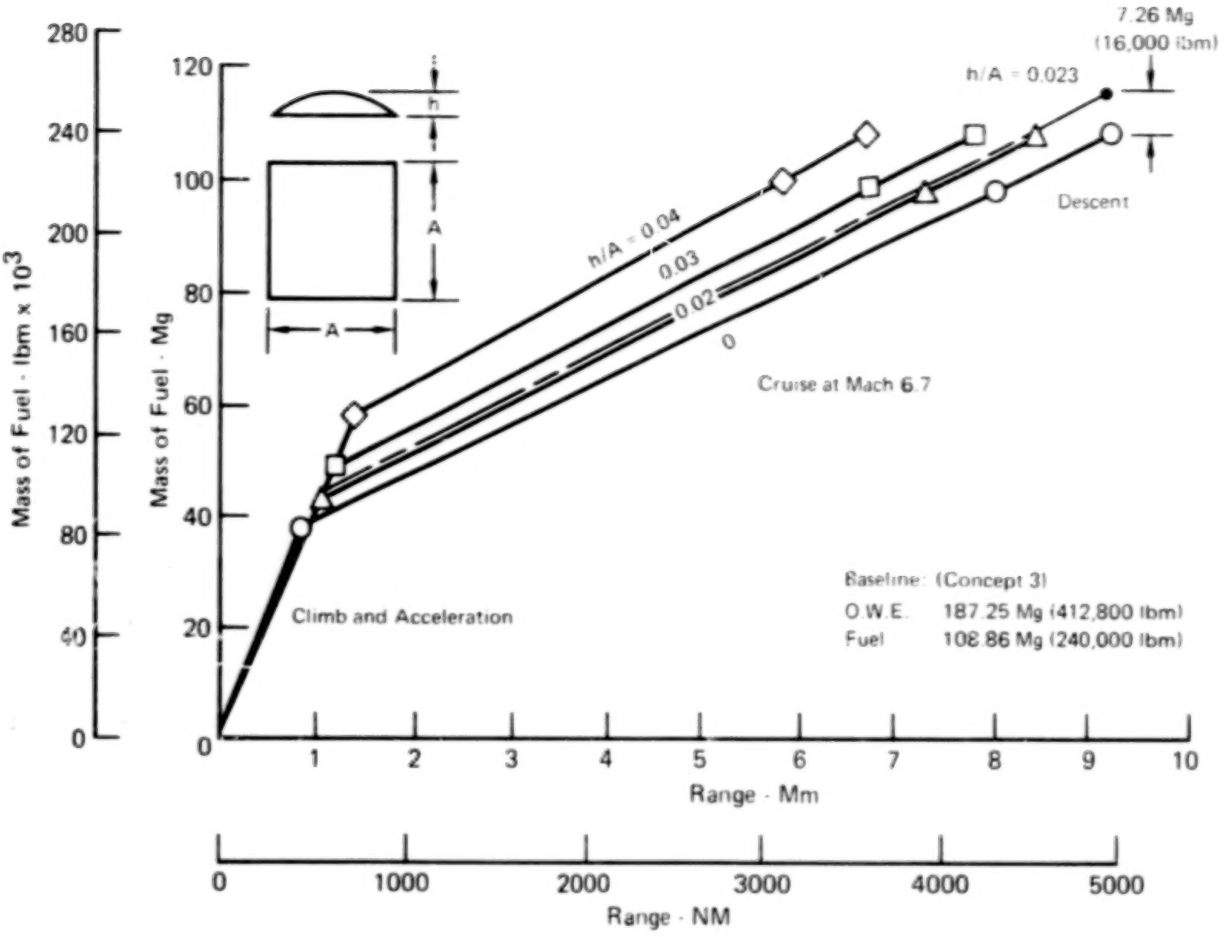


**FIGURE 43 - AIRCRAFT FUEL USAGE AS A FUNCTION OF HEIGHT OF PRELOADED DOME**

concept's inherently low torsional stiffness, is its primary drawback.

Astroquartz - The major advantages of the Astroquartz concept, rated number five, are its producibility and its tolerance to overheating. Fabrication of a 3-D woven Astroquartz heat shield up to 0.61m (2 ft) wide and almost any reasonable length is considered state of the art. A major drawback of this concept is that it readily absorbs liquids. MCAIR tests on Astroquartz with an effective density of 1000 $kg/m^3$ (62.5 $lbm/ft^3$) indicate it will readily absorb up to 30% of its weight if subjected to water spray. Another area of concern is the inability of unimpregnated Astroquartz to withstand surface

erosion. There are no known techniques for surface protection.

SLA-220 - The SLA-220 was rated number six. It was not competitive with the other heat shield concepts, primarily because of the requirement to limit maximum surface temperature to 867K (1100°F) to prevent excessive mass loss of the material. The surface temperature could be maintained at 867 K (1100°F) only by absorbing 68 $kW/m^2$ (6 $Btu/ft^2$ sec), which would use virtually all of the heat sink available and require a heavy active cooling system and a heavy actively cooled panel. Consequently, the large mass penalty charged to the SLA-220, and the inherent disadvantages of a nonmetallic bond on heat shield, eliminated this concept early in the evaluation of the six candidate heat shield concepts.

Although ranked number two, high reliability and state-of-the-art fabrication techniques led to selection of the corrugated stiffened beaded skin concept rather than the screen sandwich concept (ranked number one). Fabrication of the screen sandwich concept would require further development to properly seal the insulation from moisture.

Blank

Page

# APPENDIX D

## FULL SCALE PANEL OPTIMIZATION AND DETAIL DESIGN

Optimization of the radiative actively cooled panel includes the sensitivity of, active cooling system mass to operating pressure, absorbed heat flux, structural operating temperatures, and the effects of heat shorts. Further, the sensitivity of the structural mass of the heat shield and the actively cooled panel to geometrical changes was included to identify the geometry yielding a minimum mass design. Following sections present the results of the thermal and structural analyses to determine these sensitivities including the presentation of detail temperatures and stresses in both the heat shield and the actively cooled panel.

### Thermal Analyses

Thermal analyses determined, (a) panel temperature and temperature gradients for the structural optimization studies, (b) coolant mass flow requirements, pressure drops, and pumping power penalties, (c) active cooling system mass, (d) the impact of designing for a cooling system failure, and (d) the effect of heat shorts. Methods used and the results of these analyses are discussed in the sections which follow.

### Method of Analyses

A three-dimensional finite difference computer program with a fluid flow subroutine was used for detailed thermal analyses. Along with the physical dimensions, the thermal model defines materials, external heating or cooling conditions, and the modes of heat transfer between temperature nodes. Variation in material properties with temperature are included since all thermal resistance and capacitance terms are recomputed for each time step.

Laminar and turbulent coolant side heat transfer coefficients for each fluid volume element were computed from the following expressions from references 21 and 22, respectively:

$$\text{Laminar:}\quad h_L = 1.86 \frac{k}{H_D}\left[(R_e)(P_r)\left(\frac{H_D}{L}\right)\right]^{1/3}\left(\frac{\mu}{\mu_s}\right)^{0.14} \tag{1}$$

$$\text{Turbulent:}\quad h_T = 0.027 \frac{k}{H_D}(R_e)^{0.8}(P_r)^{1/3}\left(\frac{\mu}{\mu_s}\right)^{0.14} \tag{2}$$

Where the Reynolds number range of each expression is specified by the user. The condition that the flow is laminar at coolant Reynolds numbers below 2100 and fully turbulent for Reynolds numbers greater than 3000 was used in the analyses. No factor of safety was placed upon laminar heat transfer coefficients defined by equation (1). Turbulent heat transfer coefficients from equation (2) were reduced 20%. Heat transfer coefficients in the transition region were determined by logarithmically interpolating between laminar and turbulent values.

The pressure drop for each fluid element was computed from equation (3) and summed to determine the total pressure drop in the panel.

$$\Delta p = \frac{4f}{H_D}(1/2\rho\, V^2)(\Delta L) \tag{3}$$

Friction factors (f) were determined from the correlations of reference 23, presented herein as equations (4) through (6).

$$f = \frac{16}{R_e} \qquad R_e \leq 2100 \tag{4}$$

$$f = \frac{0.0791}{(R_e)^{0.25}} \qquad R_e = 3000 \text{ to } 10{,}000 \tag{5}$$

$$f = \frac{0.046}{(R_e)^{0.2}} \qquad R_e = 10{,}000 \text{ to } 200{,}000 \tag{6}$$

Friction factors in the region between Reynolds numbers of 2100 and 3000 were determined by linearly interpolating between the corresponding values of f from equations (4) and (5), respectively. Friction factors were not corrected for viscosity effects. For heating of a liquid, neglecting the viscosity correction results

in conservative predictions of friction factor and pressure drop (see references 22, 24, and 25).

Auxiliary Power System (APS) propellant requirements (pumping power penalty) were determined from the procedure of reference 26 as follows:

$$\text{APS PROPELLANT} = \frac{F \cdot \dot{m}_c \cdot \Delta p \cdot \theta}{\rho_c} \qquad (7)$$

Where F is the propellant consumption rate of the APS required to generate a unit of power. The flight time, $\theta$, was a constant, one hour. Since F and $\theta$ are constants, variations in APS propellant requirements are directly proportional to the product of coolant mass flow rate ($\dot{m}_c$) and pressure drop ($\Delta p$) and inversely proportional to coolant density ($\rho_c$). A value of F = 0.34 g/kW.s (2 lbm/HP hr) was used in the current study.

## Active Cooling System

The active cooling approach employs an intermediate heat transport fluid (coolant) to cool the structure and transport the airframe heat load, via a heat exchanger, to the hydrogen fuel. A closed loop active cooling system (ACS) is used to distribute the coolant to the actively cooled panels and to collect and return it to the heat exchanger. All fluid flow elements external to the panel (distribution lines, dual pumps, reservoir, heat exchanger, coolant inventory, and APS propellant required to pump the coolant through the ACS) are included in the mass of the active cooling system. Coolant in the panel and the panel pumping power penalty are included in the mass of the panel.

Active cooling system masses determined by MCAIR and others (see figure 44) were found to be in good agreement and were used as a data base during the present study. The linear correlation of active cooling system mass with coolant mass flow rate ($\dot{m}_c$) presented in figure 45 was derived for a 60/40 mass solution of ethylene glycol and water by assuming the coolant is heated from 283K (50°F) to 322K (120°F) in absorbing the airframe heat load. This linear correlation was used in preliminary panel

| Symbol | Reference (Contractor) | Design Mach Number | Heat Load MW ($10^6$ Btu/hr) | Mass[a] Mg (lbm) |
|---|---|---|---|---|
| △ | 12 (Lockheed) | 2.7 | 8.7 (29.6) | 1.34 (2,962) |
| ▲ | | 3.2 | 17.5 (59.7) | 2.31 (5,088) |
| □ | 14 (Bell) | 6.0 | 67.9 (232) | 5.68 (12,520) |
| ■ | | 6.0 | 104.6 (357) | 8.52 (18,780) |
| ○ | 17 (MCAIR) | 3.0 | 25.2 (86) | 3.30 (7,285) |
| ● | | 4.5 | 63.6 (217) | 6.16 (13,590) |
| ◑ | | 6.0 | 90.2 (308) | 7.79 (17,173) |

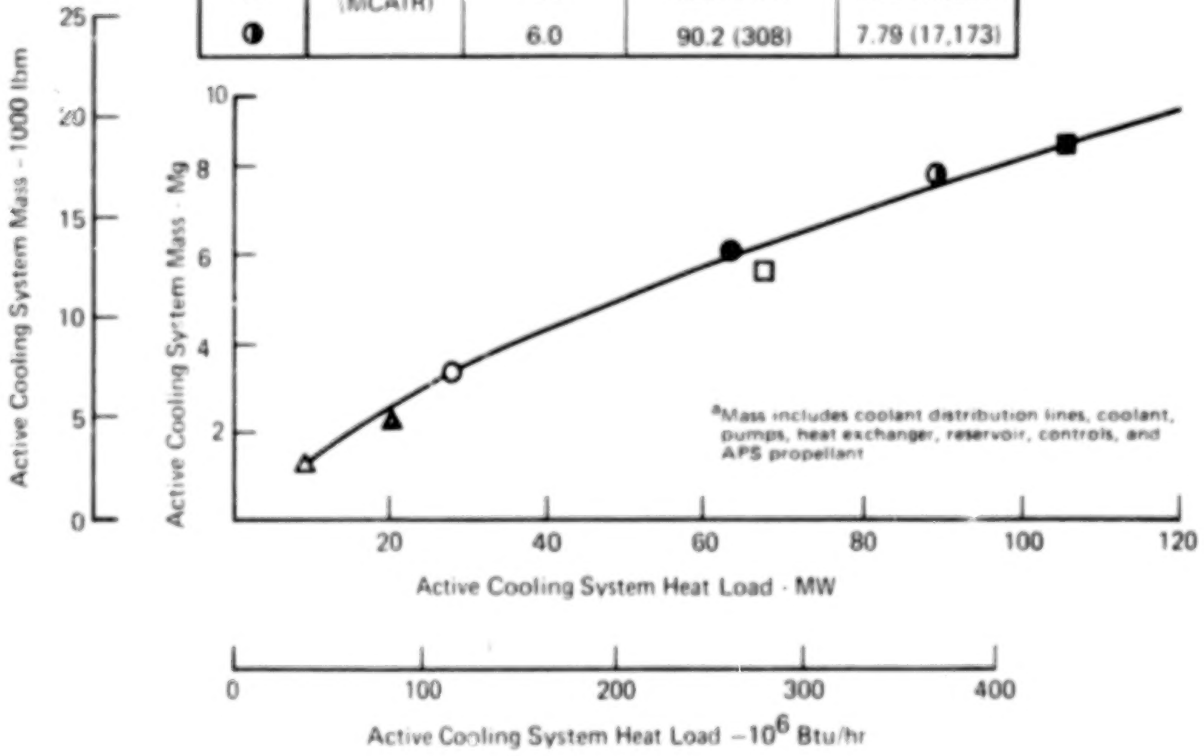


**FIGURE 44 - ACTIVE COOLING SYSTEM MASS TRENDS**

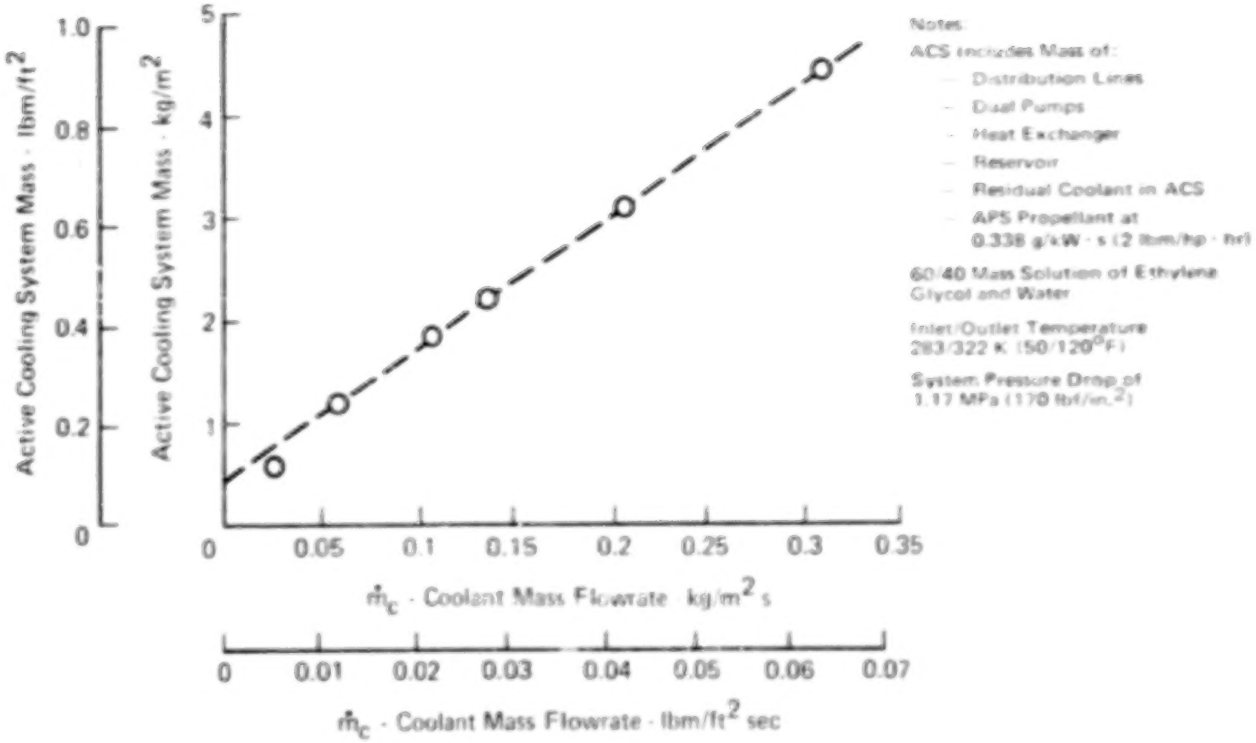


**FIGURE 45 ACTIVE COOLING SYSTEM MASS INCREASES LINEARLY WITH COOLANT MASS FLOWRATE**

mass analyses. The effect of system pressure (maximum pressure in ACS) on active cooling system mass, as shown in figure 46, was determined by the elemental equations of table 6. Figure 46 shows that the mass of the active cooling system decreases by approximately 30% when system pressures are increased from 689 kPa (100 lbf/in$^2$) to 1448 kPa (210 lbf/in$^2$). This reduction is primarily due to a decrease in distribution line coolant inventory as a result of higher system pressure drop and hence smaller line sizes. Increasing the system pressure above the 1448 kPa (210 lbf/in$^2$) level has a negligible impact as the reduction in coolant inventory is balanced by an increase in the mass of distribution lines. Therefore a system pressure of 1448 kPa (210 lbf/in$^2$) was selected. It should be noted that panel pressures are much less than system pressures due to pressure losses in the distribution lines.

Based on the correlations of table 6 and a system pressure of 1448 kPa (210 lbf/in$^2$) active cooling system mass as a function of absorbed heat flux for various values of coolant outlet

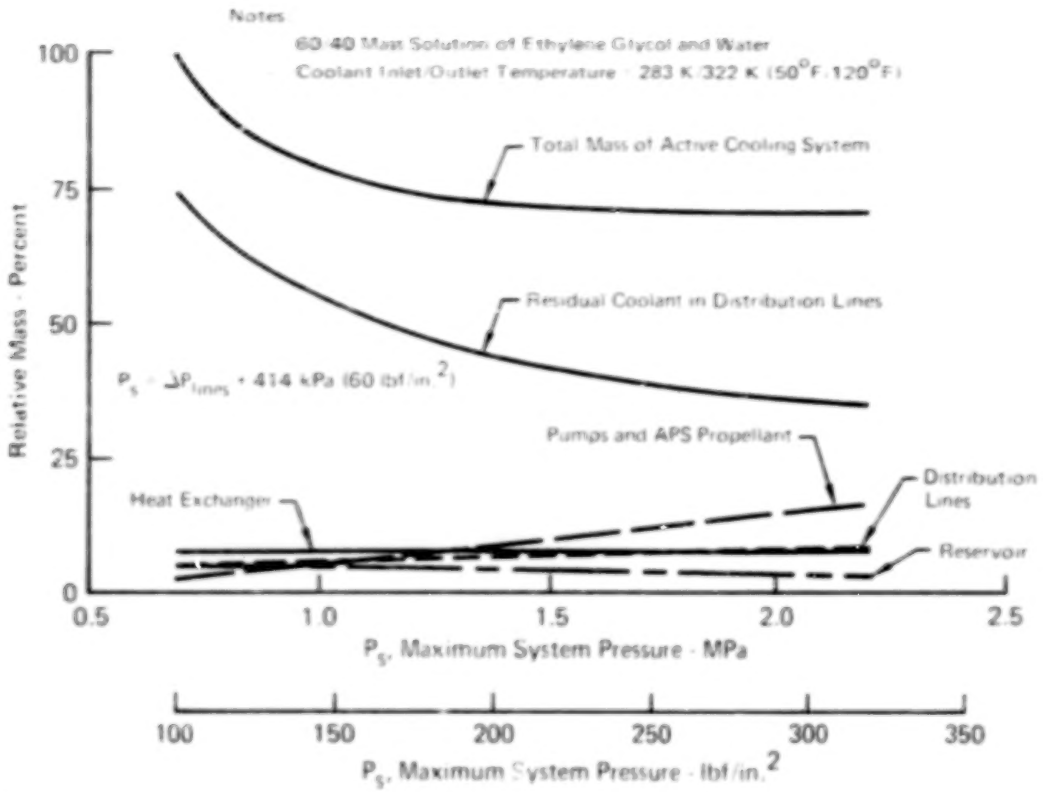


**FIGURE 46 - INCREASING PRESSURE REDUCES ACTIVE COOLING SYSTEM MASS**

temperature, is presented in figure 47. These design curves were used in detailed panel mass analyses. The decrease in active cooling system mass with increasing coolant outlet temperature is a direct result of the reduction in coolant mass flow rate.

## Abort Heating

The aerodynamic heating environment experienced during abort is presented in figure 48. These results are based on a minimum heat load/load factor limited abort trajectory discussed in Appendix B, assuming that failure of the active cooling system occurs at start of cruise and abort is initiated 15 seconds later. Local flow conditions used in determining turbulent adibatic wall temperatures and heat transfer coefficients (Spalding and Chi, reference 11) were computed based upon real gas conical flow relations at a location 3M (10 ft) aft on the lower surface centerline of the aircraft.

The adiabatic wall temperature continually decreases during

## TABLE 6 – EQUATIONS DEFINING THE MASS OF ACTIVE COOLING SYSTEM ELEMENTS

| Mass Element | Equation ~ Mass/Area |
|---|---|
| (1) Pumps (Dual/Wet) | $W_1 = C_1 (\dot{m}_c) (\Delta P_s)/\rho_c$ |
| (2) Heat Exchanger (Wet) | $W_2 = C_2 \dot{q}_{abs}$ |
| (3) Coolant in Lines | $W_3 = C_3 (\dot{m}_c)^{n1} (\mu_c)^{n2} (\rho_c)^{n3} \Delta P_s)^{n4}$ |
| (4) Distribution Lines (Dry) | $W_4 = C_4 (W_3) (P_s)/\rho_c$ |
| (5) Reservoir (Wet) | $W_5 = C_5 \Sigma$ Coolant Inventory<br>• Coolant in Lines ~ $W_3$<br>• Coolant in H/X ~ $0.4\, W_2$<br>• Coolant in Panel ~ $\dfrac{C'_5 (\rho_c) (D)^2}{P}$<br>$\Sigma$ Coolant Inventory |
| (6) APS Propellant @ F = 0.34 g/kW-s (2 lbm/hp-hr) | $W_6 = C_6 (\dot{m}_c) (\Delta P_s) (\theta)/\rho_c$ |

| Variables | | | |
|---|---|---|---|
| Symbol | Definition | Units | |
| | | SI | English |
| $W_i$ | Mass Element | $kg/m^2$ | $lbm/ft^2$ |
| $\dot{m}_c$ | Coolant Mass Flow | $kg/m^2 \cdot s$ | $lbm/ft^2 sec$ |
| $P_s$ | System Pressure | kPa | $lbf/in.^2$ |
| $\Delta P_s$ | Pressure Drop | kPa | $lbf/in.^2$ |
| $\rho_c$ | Coolant Density | $kg/m^3$ | $lbm/ft^3$ |
| $\dot{q}_{abs}$ | Absorbed Heat Flux | $kW/m^2$ | $Btu/ft^2 sec$ |
| $\mu_c$ | Coolant Viscosity | Pa·s | lbm/ft sec |
| $\theta$ | Time | hour | hour |
| D | Dee Tube I.D. | cm | inch |
| P | Tube Pitch | cm | inch |

| Constants | | |
|---|---|---|
| Symbol | Value in: | |
| | SI | English |
| $C_1$ | 0.44 | 0.19 |
| $C_2$ | 0.0105 | 0.0244 |
| $C_3$ | 2.49 | 3.9 |
| $C_4$ | 0.116 | 0.05 |
| $C_5$ | 0.06 | 0.06 |
| $C'_5$ | 0.00467 | 0.0389 |
| $C_6$ | 1.217 | 0.524 |
| $n_1$ | 0.75 | 0.75 |
| $n_2$ | 0.083 | 0.083 |
| $n_3$ | 0.583 | 0.583 |
| $n_4$ | –0.417 | –0.417 |

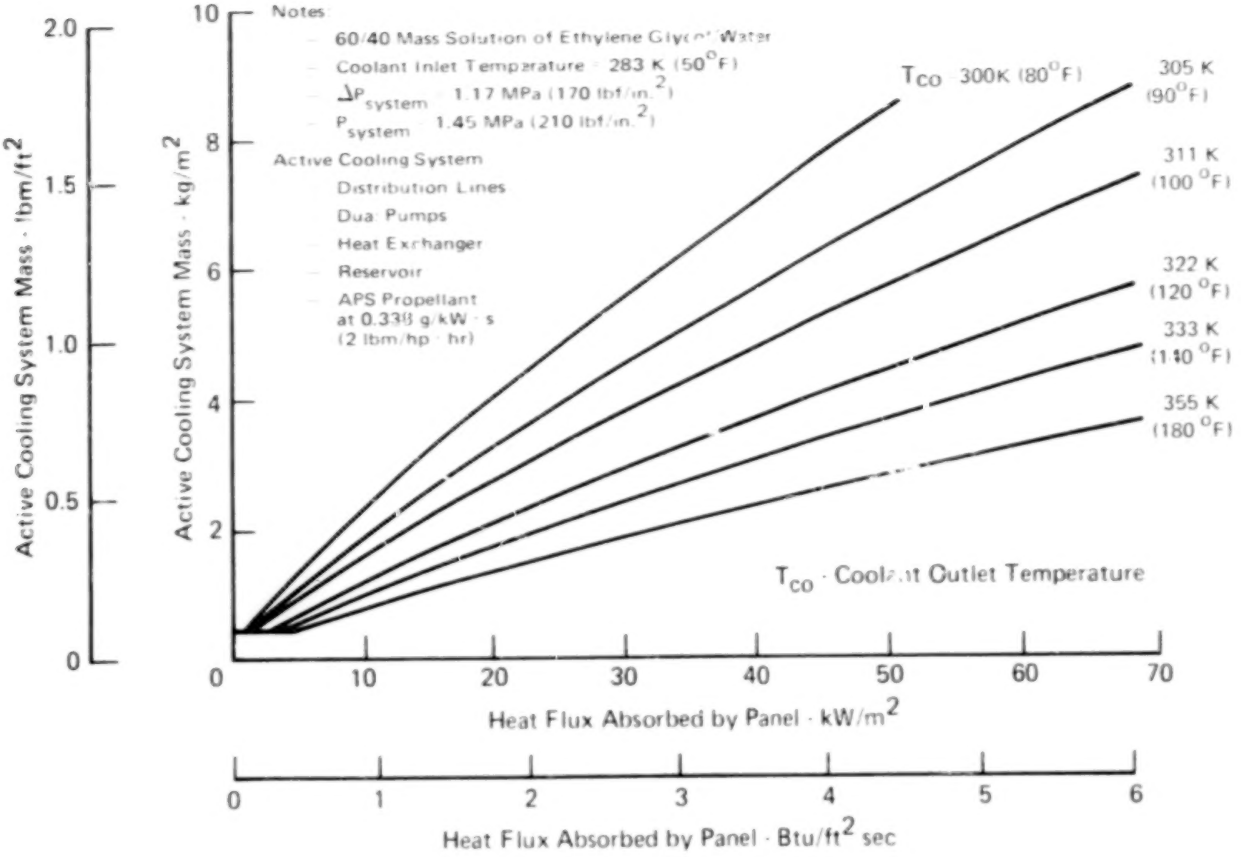


**FIGURE 47 - ACTIVE COOLING SYSTEM MASS vs ABSORBED HEAT FLUX**

abort, coincident with a continuing decrease in flight Mach number. The heat transfer coefficient oscillates due to variations in angle of attack, altitude, and Mach number.

The abort heating environment presented in figure 48 results in a total abort heat load (at a 422K (300°F) wall temperature) of about 21.6 MJ/m$^2$ (1900 Btu/ft$^2$). If unprotected, an aluminum structural mass of 390 kg/m$^2$ (80 lbm/ft$^2$) is necessary to absorb the abort heat load to limit structural temperatures to 478K (400°F). With a radiative thermal protection system, less than 4% of the abort heat load penetrates the thermal protection system and is absorbed by the panel. Analyses have shown that providing a fail-safe abort capability increases the mass of the radiative actively cooled panel by approximately 2.5%.

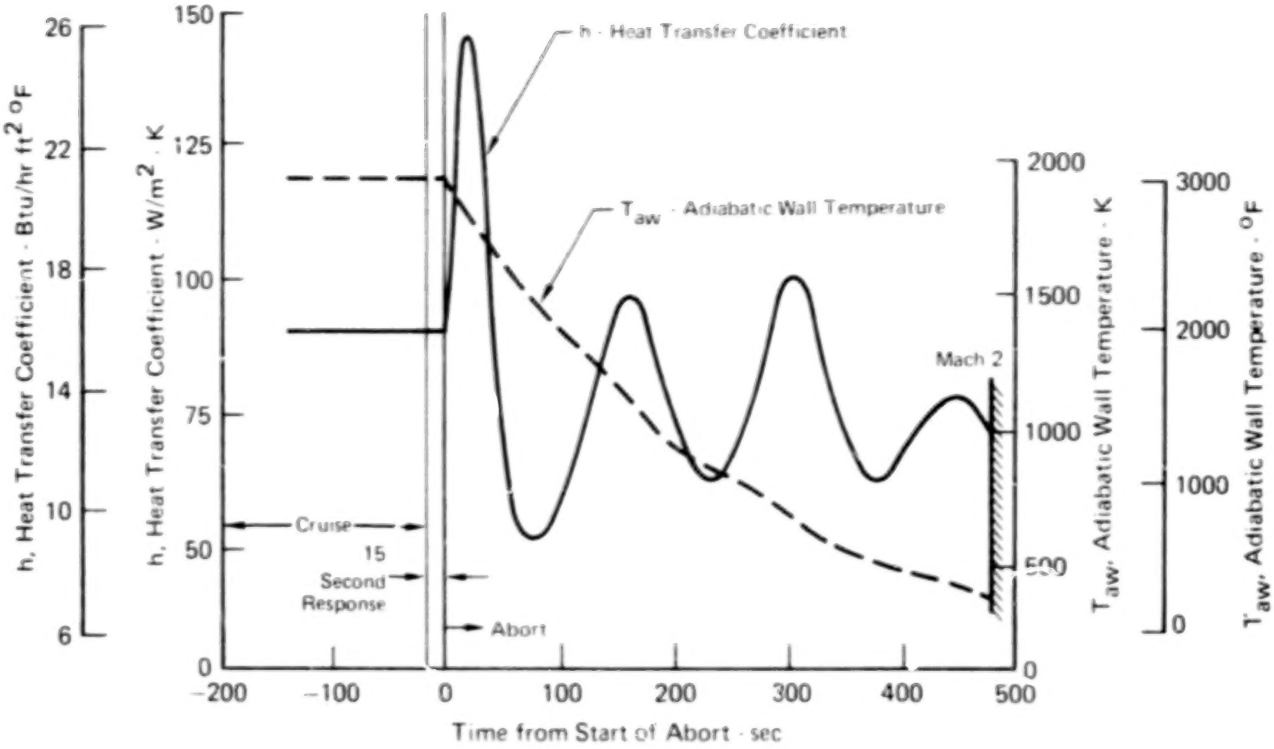


**FIGURE 48 - ABORT HEATING PROFILE**

Effect of Heat Shorts

Detailed thermal analyses determined the local increase in panel temperatures due to the heat short effect of heat shield attachments. Figure 49 presents panel temperatures around a heat shield attachment which passes through the longitudinal splice near the panel exit. Panel temperatures are presented at a location adjacent to the heat short (see sketch) and at a location 3.8 cm (1.5 in.) aft of the heat short. A maximum panel temperature of 422K (300°F) occurs on the outer longitudinal splice plate next to the heat shiled attachment. Comparison of actively cooled panel temperatures at the two locations shows that the maximum temperature difference, 19K (34°F) occurs in the outer splice plate. This temperature difference causes an average thermal gradient of only 5K/cm (23°F/in.). That is, due to the high thermal conductivity of aluminum, the effects of the heat short are distributed over a relatively large area which experiences a small increase in temperature rather than to a

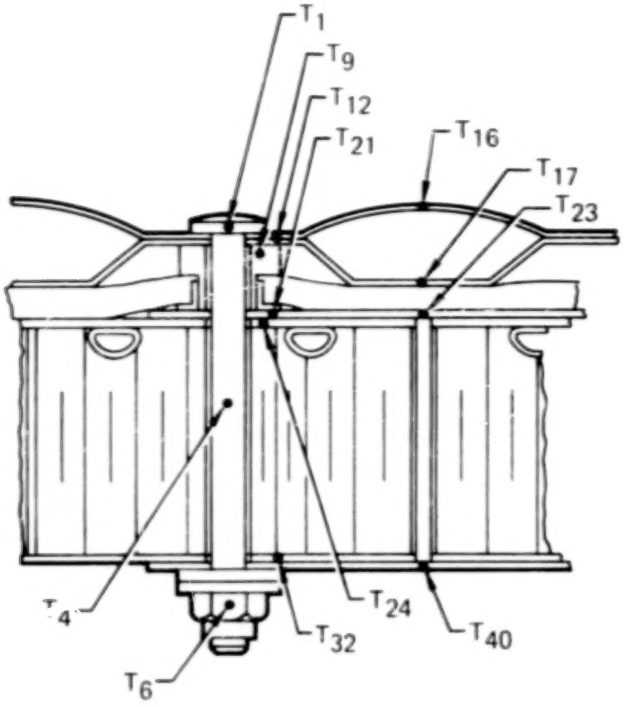


Note:
Full Scale Panel Longitudinal Splice Near Panel Exit

| Panel Element | Temperatures at | | | |
|---|---|---|---|---|
| | Heat Short | | 3.8 cm (1.5 in.) Away | |
| | K | °F | K | °F |
| $T_1$ · Head of Heat Shield Attachment | 892 | 1146 | – | – |
| $T_4$ · Bolt | 511 | 459 | – | – |
| $T_6$ · Nut | 445 | 341 | – | – |
| $T_9$ · Heat Shield Standoff | 781 | 945 | – | – |
| $T_{12}$ · Heat Shield Flat | 1039 | 1410 | 1081 | 1485 |
| $T_{16}$ · Heat Shield Bead | 1081 | 1485 | 1081 | 1485 |
| $T_{17}$ · Heat Shield Corrugation | 1030 | 1394 | 1030 | 1394 |
| $T_{21}$ · Longitudinal Splice Plate (Outer) | 422[a] | 300[a] | 403 | 266 |
| $T_{23}$ · Longitudinal Splice Plate (Outer) | 416 | 289 | 407 | 272 |
| $T_{24}$ · Panel Skin (Outer) | 413 | 283 | 399 | 258 |
| $T_{32}$ · Panel Skin (Inner) | 403 | 266 | 401 | 261 |
| $T_{40}$ · Longitudinal Splice Plate (Inner) | 402 | 264 | 401 | 261 |

[a]Maximum Temperature Experienced by Actively Cooled Panel

**FIGURE 49 - EFFECT OF HEAT SHIELD ATTACHMENT ON PANEL TEMPERATURES**

small region that experiences high temperatures and large thermal graidents.

As expected, moldline temperatures are reduced near the heat shorts. For example, heat shield temperatures adjacent to the attachment are 42K (75°F) lower than at a comparable location removed from the heat short. This effect increases thermal stresses in the heat shield, as discussed in the stress analysis section of this appendix.

To absorb the increased load due to heat shorts, the coolant mass flow rate must be increased. This causes a 44% increase in active cooling system mass, as shown in figure 50. Although this effect is significant, the overall increase in the mass of the radiative actively cooled panel design is less than 2%.

### Fluid Penalties

Coolant pressures, pressure drops, and fluid penalties for the radiative actively cooled panel design are presented in figure 51. The combined pressure drop of the inlet and exit manifold was calculated to be approximately 4% of the total pressure drop across the panel, indicating that the flow through any tube will not deviate by more than $\pm$2% from the mean (design) value. The total fluid penalty is 2.36 $kg/m^2$ (0.48 $lbm/ft^2$) and accounts for approximately 11% of the panel mass.

### Structural Analyses

The definition of the materials and geometry for the heat shields and the actively cooled panel resulted from parametric analyses and trade studies supported by detail analyses. Both mechanical and thermal loading were considered. Mechanical stresses and thermal stresses were computed separately and superimposed when additive. The following paragraphs present the analytical methods used and results from the detail strength analyses for the heat shields and the actively cooled panel.

Heat shield - The heat shield thermal stresses were calculated using elementary beam bending theory, accounting for elastic strains and two-dimensional temperature distributions, and assuming an infinitely long beam with constant temperature in

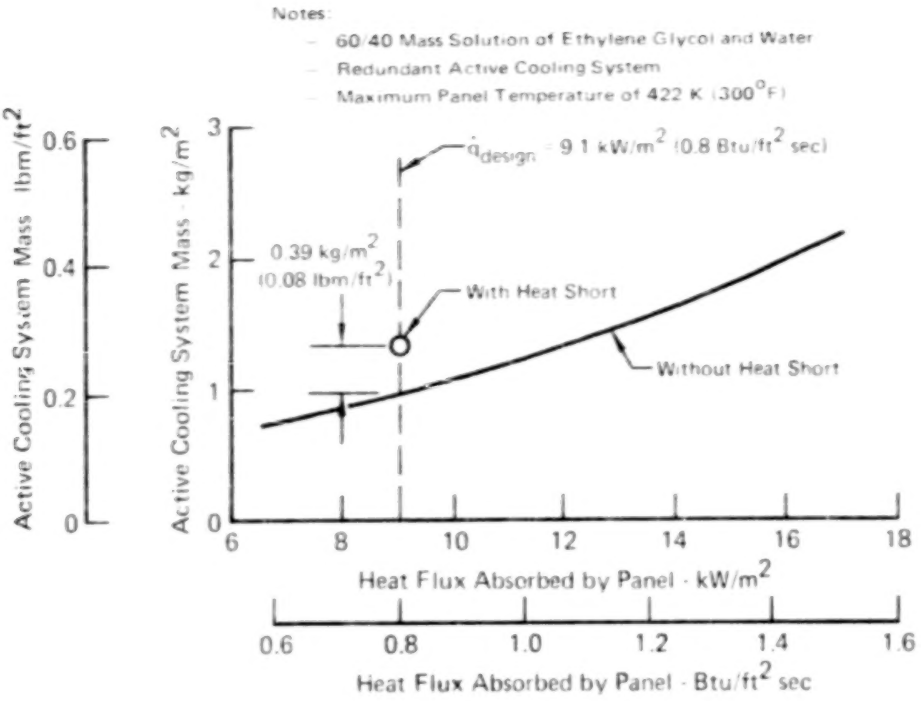


**FIGURE 50 - IMPACT OF HEAT SHORTS ON ACTIVE COOLING SYSTEM MASS**

each element. The thermal stresses were computed assuming zero slope at midspan, pinned ends at the heat shield ends, freedom to expand in the longitudinal direction, and rigid restraint in the transverse direction.

The mechanical stresses in the heat shield were computed assuming each bead/skin combination is an individual beam on three supports with the ends pinned and zero slope at midspan.

To optimize the heat shield, beaded skin crown and corrugation heights required to accommodate transverse thermal expansion were calculated for different skin gages. Using this initial geometry the support spacing in the longitudinal direction was varied and the heat shield dimension altered until a minimum mass heat shield was obtained.

Since the heat shield is restrained against transverse deflections by stand-off posts, the induced transverse stresses in the beaded skin and corrugations were calculated for different bead heights. Results of these calculations are presented in

Notes:

- 60/40 Mass Solution of Ethylene Glycol and Water
- Design Coolant Mass Flow Rate of 9.6 g/s (76 lbm/hr) per Tube

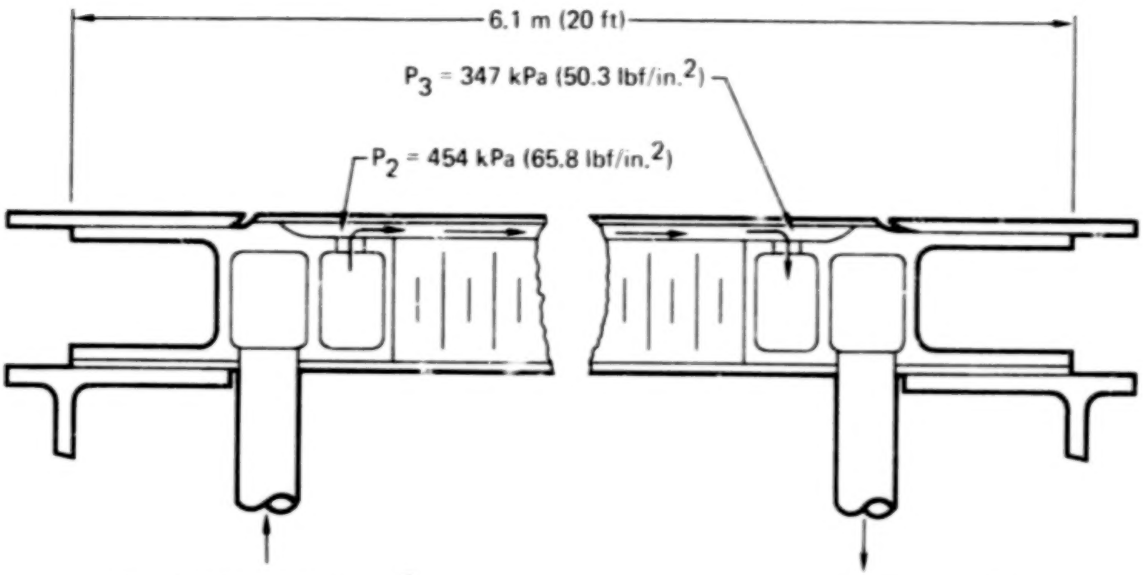


Coolant Pressure Drop

| | |
|---|---|
| Inlet Manifold | 2.8 kPa (0.4 lbf/in.$^2$) |
| Panel (24 Tubes) | 106.9 kPa (15.5 lbf/in.$^2$) |
| Exit Manifold | 2.1 kPa (0.3 lbf/in.$^2$) |
| Total | 111.8 kPa (16.2 lbf/in.$^2$) |

Fluid Penalties

| | |
|---|---|
| Coolant in Panel | 0.59 kg/m$^2$ (0.12 lbm/ft$^2$) |
| [a]Panel Plumbing | 0.39 kg/m$^2$ (0.08 lbm/ft$^2$) |
| APS Propellant (Panel) | 0.01 kg/m$^2$ (0.002 lbm/ft$^2$) |
| Subtotal (Panel) | 0.99 kg/m$^2$ (0.20 lbm/ft$^2$) |
| Redundant Active Cooling System | 1.37 kg/m$^2$ (0.28 lbm/ft$^2$) |
| Total Fluid Penalty | 2.36 kg/m$^2$ (0.48 lbm/ft$^2$) |

[a]Additional Plumbing Due to Redundant Active Cooling System

**FIGURE 51 - SUMMARY OF COOLANT PRESSURES AND FLUID PENALTIES FOR FULL SCALE PANEL DESIGN**

figure 52 and show, for a given corrugation height, that increasing the bead height reduces the stress levels in both the beaded skin and the corrugation. A bead height of 0.32 cm (0.125 in.) results in stresses of 620 MPa (90,000 psi) and 482 MPa (70,000 psi) in the corrugation and beaded skin, respectively, which are less than the 654 MPa (95,000 psi) fatigue allowable for a stress ratio of zero (R=0) and a $K_t$ = 1.0 for Rene'41 (see Appendix A). As shown, the stress levels in the lands are below the fatigue allowables for spot welds and for holes ($K_t$ = 3.0). The stress levels shown are based on assuming complete fixity at the standoff posts and restraint against an inward deflection of the corrugation provided by the insulation package.

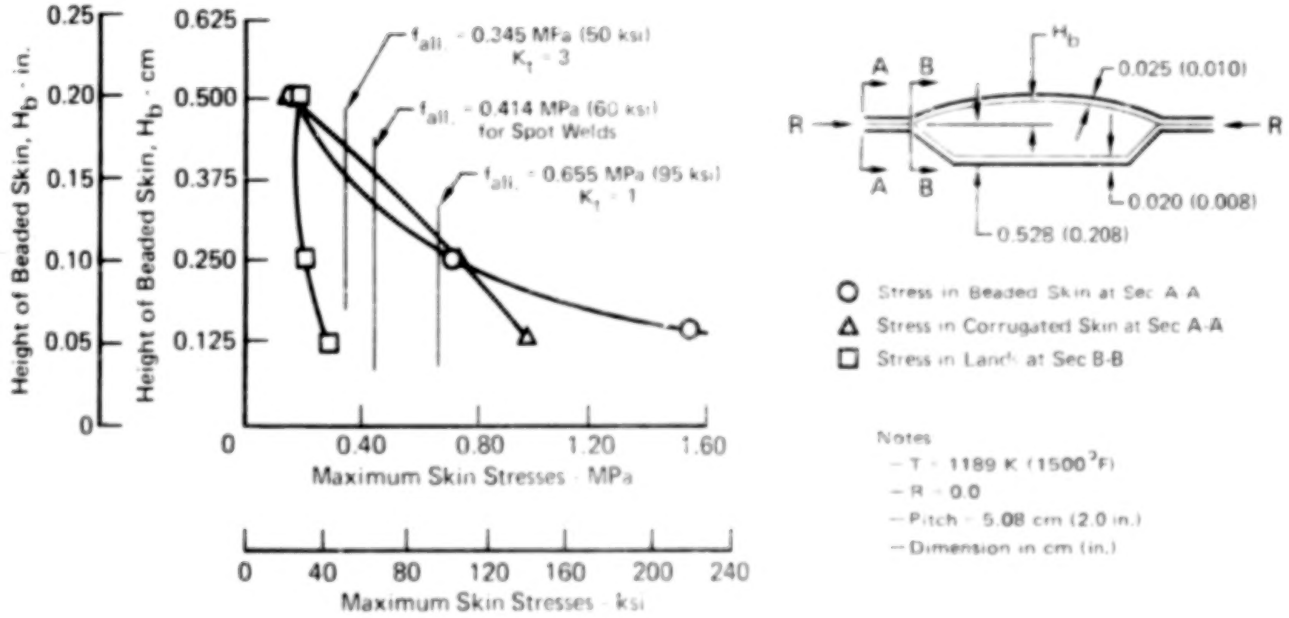


**FIGURE 52 - HEAT SHIELD SKIN STRESSES IN THE TRANSVERSE DIRECTION AS A FUNCTION OF BEAD HEIGHT**

Once the bead height was selected, the sensitivity of heat shield mass to support spacing was calculated. Figure 53 shows the results of this analysis. The mass discontinuities at 30.5, 40.6, 45.7, and 50.8 cm (12, 16, 18 and 20 in.) result from the fasteners that attach the actively cooled panel to the support

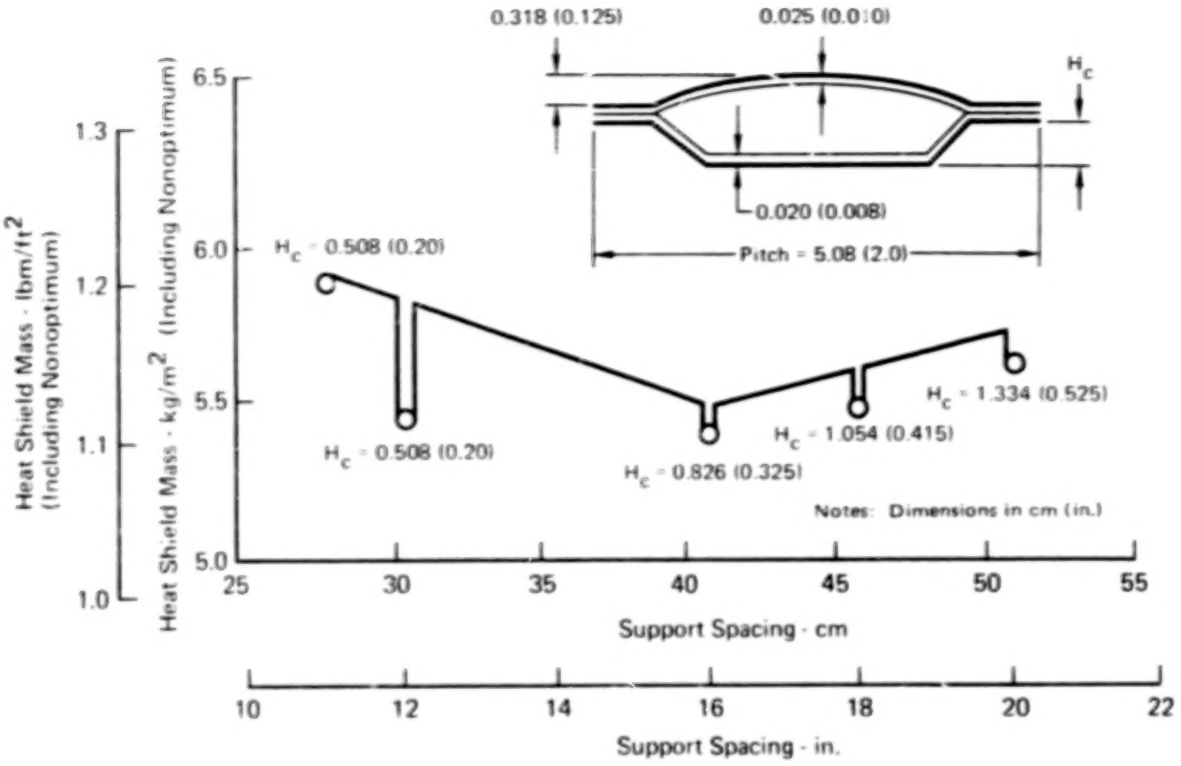


**FIGURE 53 - HEAT SHIELD MASS vs HEAT SHIELD SUPPORT SPACING**

frames. The corrugation height shown at the discrete support spacings yields a minimum mass design, when used with the 0.32 cm (0.125 in.) bead height and 5.08 cm (2 in.) pitch. A 30.5 cm (12 in.) support spacing was selected even though it was slightly heavier by 0.05 kg/m$^2$ (0.01 lbm/ft$^2$) than the 40.6 cm (16 in.) spacing because it enabled maximum use of existing fasteners at the panel support frames since the panel was supported at 60.9 cm (24 in.) spacing.

The heat shield reactions for the selected bead/corrugation pitch of 5.08 cm (2 in.), bead height of 0.32 cm (0.125 in.), corrugation height of 0.53 cm (0.208 in.), beaded skin thickness of 0.025 cm (0.01 in.) and corrugated skin thickness of 0.02 cm (0.008 in.) are shown in figure 54. The maximum concentrated reaction loads due to thermal loading result during climb and acceleration when a maximum $\Delta T$ of 106K (191°F) occurs between the beaded skin and the corrugation. The $\Delta T$ produces a compression stress in the beaded skin and a tension stress in the corrugation

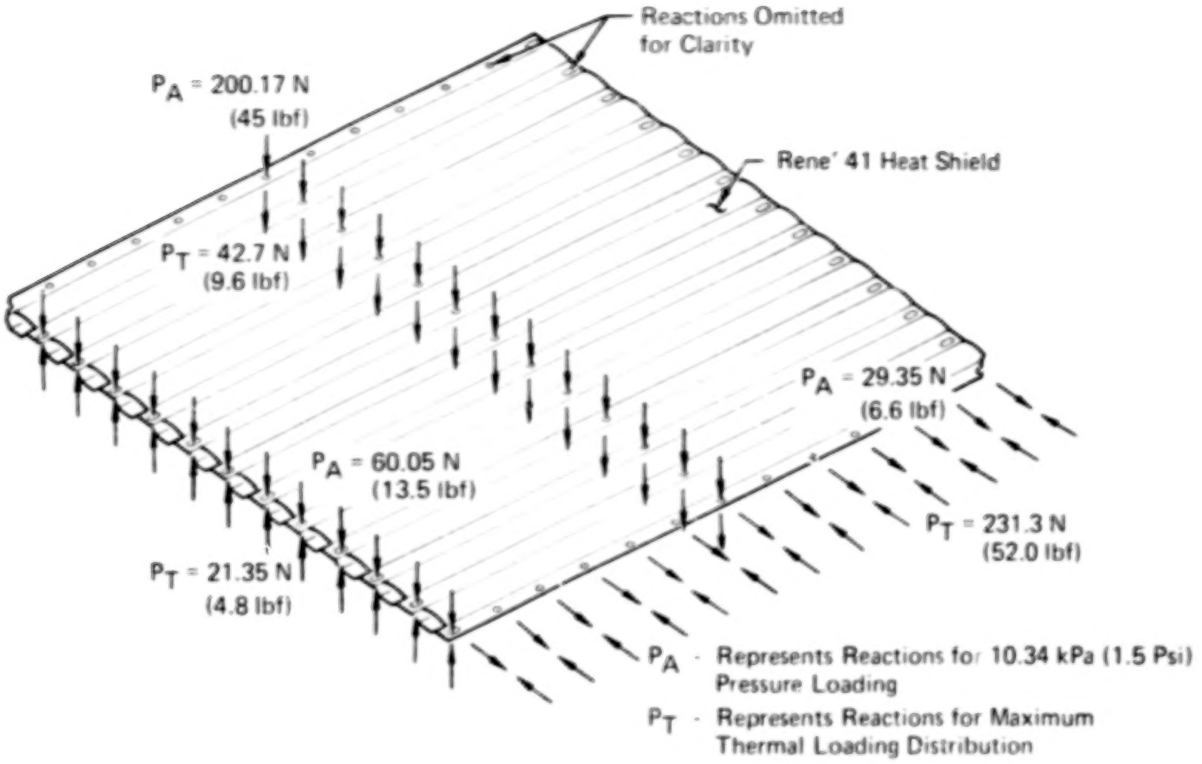


**FIGURE 54 - HEAT SHIELD REACTIONS**

and tends to bow the heat shield outward at midspan. This bowing is prevented by inward acting concentrated loads at the midspan supports and outward acting loads at the heat shield and supports.

The reactions shown for the airloads result from an outward acting 10.34 kPa (1.5 psi) ultimate pressure which produces maximum stresses at midspan when combined with the thermal stresses. The transverse loads result from rigid heat shield attachment to the substructure and adjacent heat shields. Slotting of the fastener holes along the transverse edge prevents inplane loads in the longitudinal direction.

The mechanical and thermal stress distributions in the heat shield at midspan are shown in figure 55. The thermal and mechanical stresses in the beaded skin are of the same order of magnitude.

Actively cooled panel - The actively cooled panel was analyzed as a continuous panel on multiple non-deflecting supports. The panel was assumed fixed (zero slope) along the loaded edges and

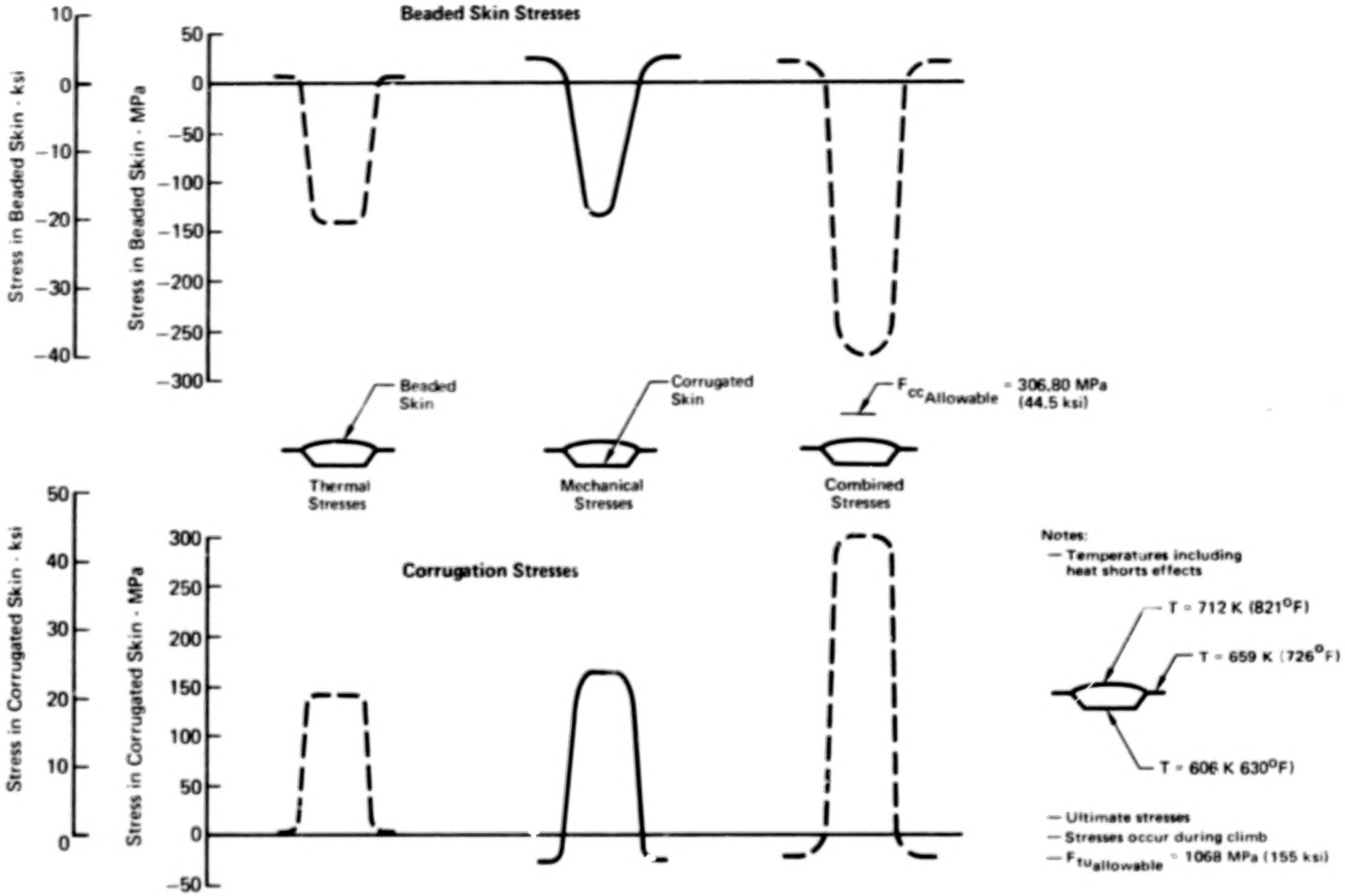


FIGURE 55 HEAT SHIELD THERMAL AND MECHANICAL LONGITUDINAL STRESSES



103

free along the unloaded edges. The panel was checked where the maximum stresses occurred, i.e., at the support and at midspan, for the critical combination of completely reversible inplane loads and normal pressures. Panel beam column checks, for the inplane loading only, treated the panel as simply supported at the transverse supports and free along the unloaded edges, with an initial manufacturing eccentricity, at midspan, of 0.102 cm (0.040 in.). For the combination of inplane loading and normal pressures, the beam column analysis treated the panel as fixed at the transverse supports and added the deflections, at midspan, due to the normal pressures to the assumed maximum 0.102 cm (0.040 in.) manufacturing eccentricities.

The failure modes included in the analysis were basic strength; local instability, such as facesheet wrinkling and facesheet dimpling; and overall panel buckling, including beam column effects. The beam column analysis included the effects of normal pressures and panel eccentricities, coupled with the uniaxial inplane loading. The allowables were computed using the equations given in reference 27, i.e.,

Face Sheet Wrinkling:

$$F_w = \frac{.82\sqrt{\frac{E_c E' t_s}{t_c}}}{1 + .64 \frac{\delta E_c}{t_c F_c}}$$

Face Sheet Dimpling:

$$F_c = \frac{2 E' t_s^2}{S^2(1-\mu^2)}$$

Panel Buckling:

$$N_{cr} = K \frac{\pi^2 EI}{b^2}$$

Beam Column Effects:

$$\psi = \frac{\psi_o}{1 - N/N_{cr}}$$

The actively cooled panel mass was minimized by calculating preliminary thermal stresses for a given cross section, using elementary beam bending theory and superimposing the mechanical stresses. If the resulting stresses were less than the allowables, the geometry was modified to obtain a lower margin of safety (and mass). The thermal stresses were then recalculated for the new geometry and the process continued until convergence of the applied and allowable stresses occured. Once the actively cooled panel geometry was selected, a finite element model was developed and the internal loads and stresses, both thermal and mechanical, were computed to substantitate the design.

As a part of the optimization the mass of the actively cooled panel was determined as a function of absorbed heat flux for a 2.54 cm (1.0 in.) tube pitch and various combinations of outer skin thickness and tube diameter. The tube pitch of 2.5 cm (1.0 in.) was used because this yielded a minimum mass panel that was less sensitive to variations in absorbed heat flux up to 22.7 $kW/m^2$ (2 $Btu/ft^2$ sec). The combination of outer skin thickness and tube diameter used with the 2.54 cm (1.0 in.) pitch were selected to prevent the outer skin temperature from exceeding the 422K (300°F) design temperature. The results, figure 56, show that panel mass is essentially constant for heat fluxes below 22.7 $kW/m^2$ (2 $Btu/ft^2$ sec.). Further, for constant tube diameter heat absorption can be increased by increasing outer skin thickness from 0.04 cm (0.016 in.) to 0.10 cm (0.04 in.) without a corresponding increase in panel mass; the structural mass can be redistributed to reduce the panel thickness and compensate for the increased mass of the facesheets by reducing the mass of the honeycomb. Outer skin thicknesses greater than 0.10 cm (0.04 in.) resulted in an increase in panel mass and were therefore not considered. Thus, an outer skin thickness of 0.10 cm (0.04 in.) was selected, rather than 0.04 cm (0.016 in.), since a thicker outer skin tends to decrease abort requirements, is less susceptible to damage, and can accept countersunk fasteners without a knife edge condition in the skin.

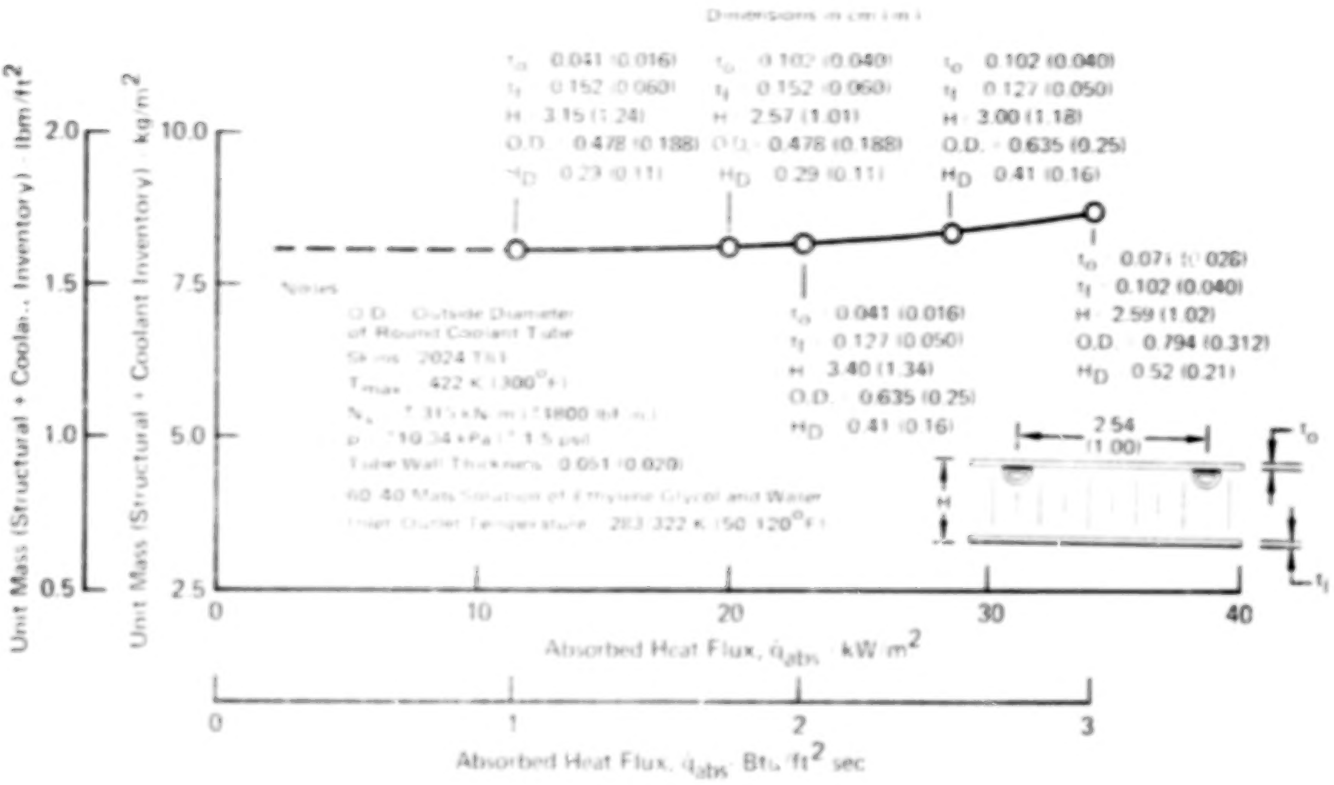


**FIGURE 56 - ACTIVELY COOLED PANEL MASS vs ABSORBED HEAT FLUX**

The concentrated loads occurring at the standoff posts and at the fasteners along the transverse edge of the actively cooled panel are shown in figure 57. The loads at the standoff posts result from the 10.34 kPa (1.5 psi) airload on the heat shields and the thermal loads due to the 106K (191°F) ΔT between the beaded skin and corrugation which occurs during climb and acceleration. The fastener loads along the transverse edge result from the uniformly applied 315K N/m (1800 lbf/in.) inplane loading, reaction of the panel pressures, and thermal loads in the actively cooled panel. The outer skin and coolant tube stress distribution near a standoff post is also shown in figure 57. As shown, a maximum compression stress of 149 MPa (21,700 psi) occurs in the outer skin adjacent to a standoff post fastener hole and results from superimposing the compressive stresses due to inplane loading and airloads and compressive thermal stresses. Reversing the inplane loads and airloads significantly reduces the outer skin compression stress. The

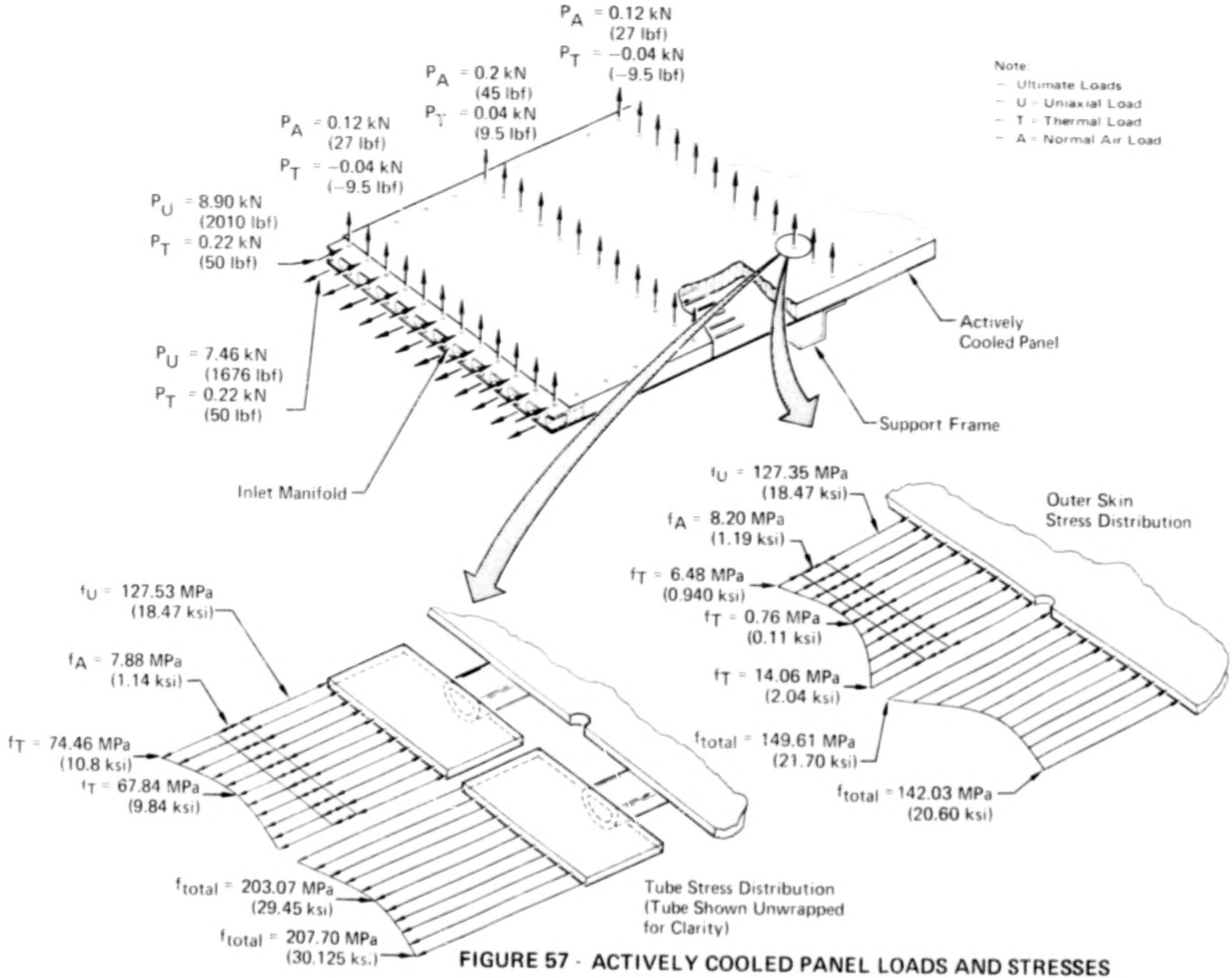


**FIGURE 57 - ACTIVELY COOLED PANEL LOADS AND STRESSES**



107

maximum tension stress occurs in the coolant tubes. The stress distribution in the tubes is shown in figure 57 (the tubes have been unwrapped and flattened to illustrate the stress distribution). A maximum tension stress of 208 MPa (30,125 psi) occurs at the apex of the tube which is imbedded in the honeycomb core. This maximum tension stress occurs when the stresses resulting from the inplane loads and airloads are superimposed with the thermal stresses.

The transverse thermal stresses at the panel centerline for both the inlet and exit manifolds are shown in figure 58. The maximum compression stresses occur in the outer skin near the exit manifold, and because they are small compared to stresses in the longitudinal direction do not impact the panel design. The effect of the heat shorts resulting from the heat shield standoff posts was negligible since it increased the compression stress in the transverse splice plate by only 17.2 MPa (2,500 psi).

A comparison of the thermal stresses in the longitudinal direction, at the panel edge, both close to and away from a heat short is shown in figure 59. A maximum compression stress occurs in the splice plates near a heat short and is only 11.0 MPa (1,600 psi) higher than in areas away from heat shorts. The heat shorts cause a slight sinusoidal stress distribution in the inner skin but have no effect on the design. Tension stress in the tubes is increased 10% by the heat shorts. These stresses were superimposed with mechanical stresses when additive.

## Sensitivity of ACP to Increased Loading

Effects on the actively cooled panel mass and geometry were calculated for increased inplane loading, combined biaxial loading, and combined inplane and shear loads. Figure 60 shows the effect of shear ($N_{xy} = .5\ N_x$) combined with axial loads ($N_x$) ranging from 315 kN/M $\leq N_x \leq$ 919 kN/m (1800 lbf/in. $\leq N_x \leq$ 5250 lbf/in.). Panel mass is more sensitive to the combination of axial and shear loads than to the combination of axial and transverse loads, i.e., biaxial loading because for $N_x$ loading only

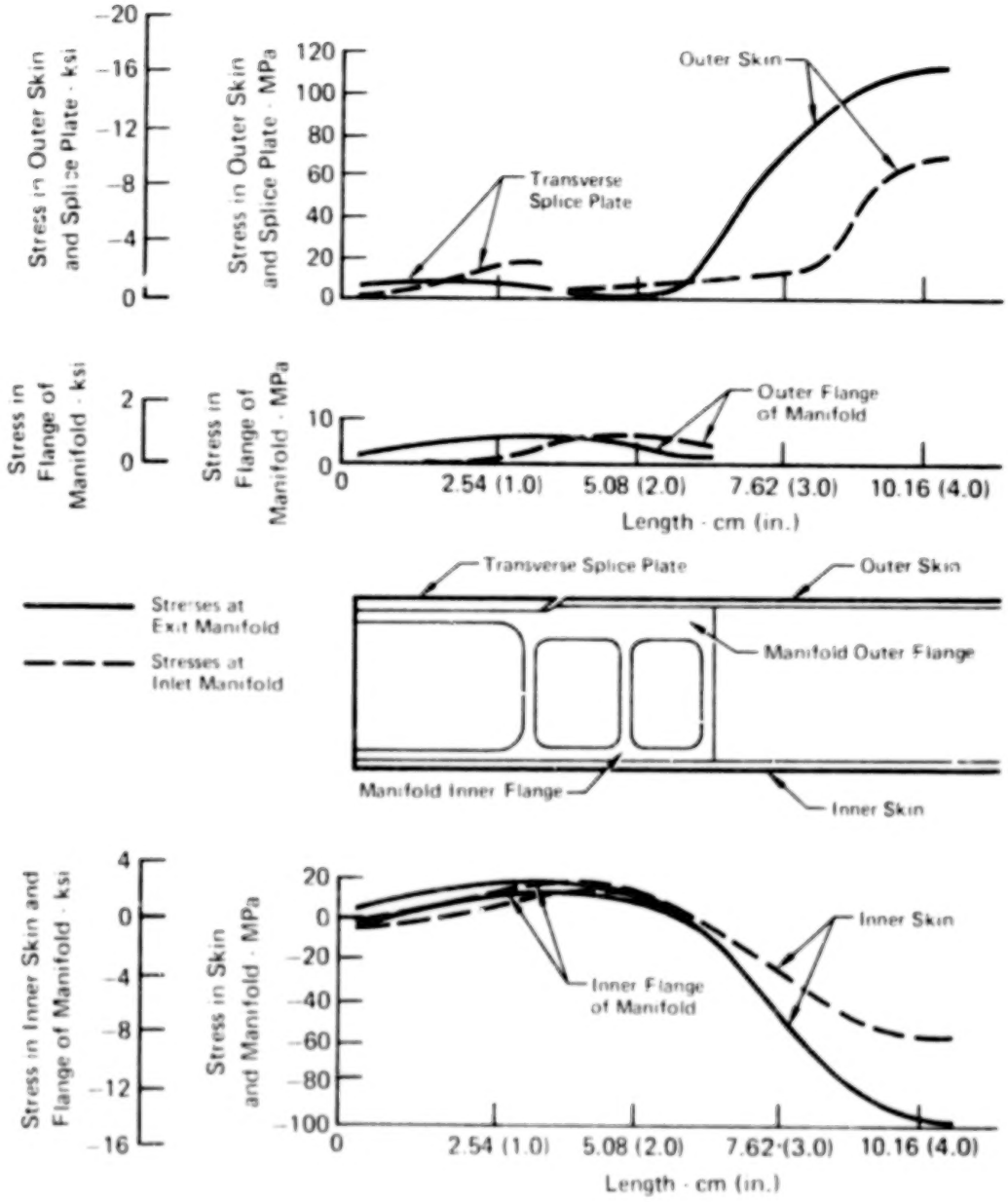


**FIGURE 58 - ACTIVELY COOLED PANEL TRANSVERSE THERMAL STRESSES AT THE MANIFOLDS**

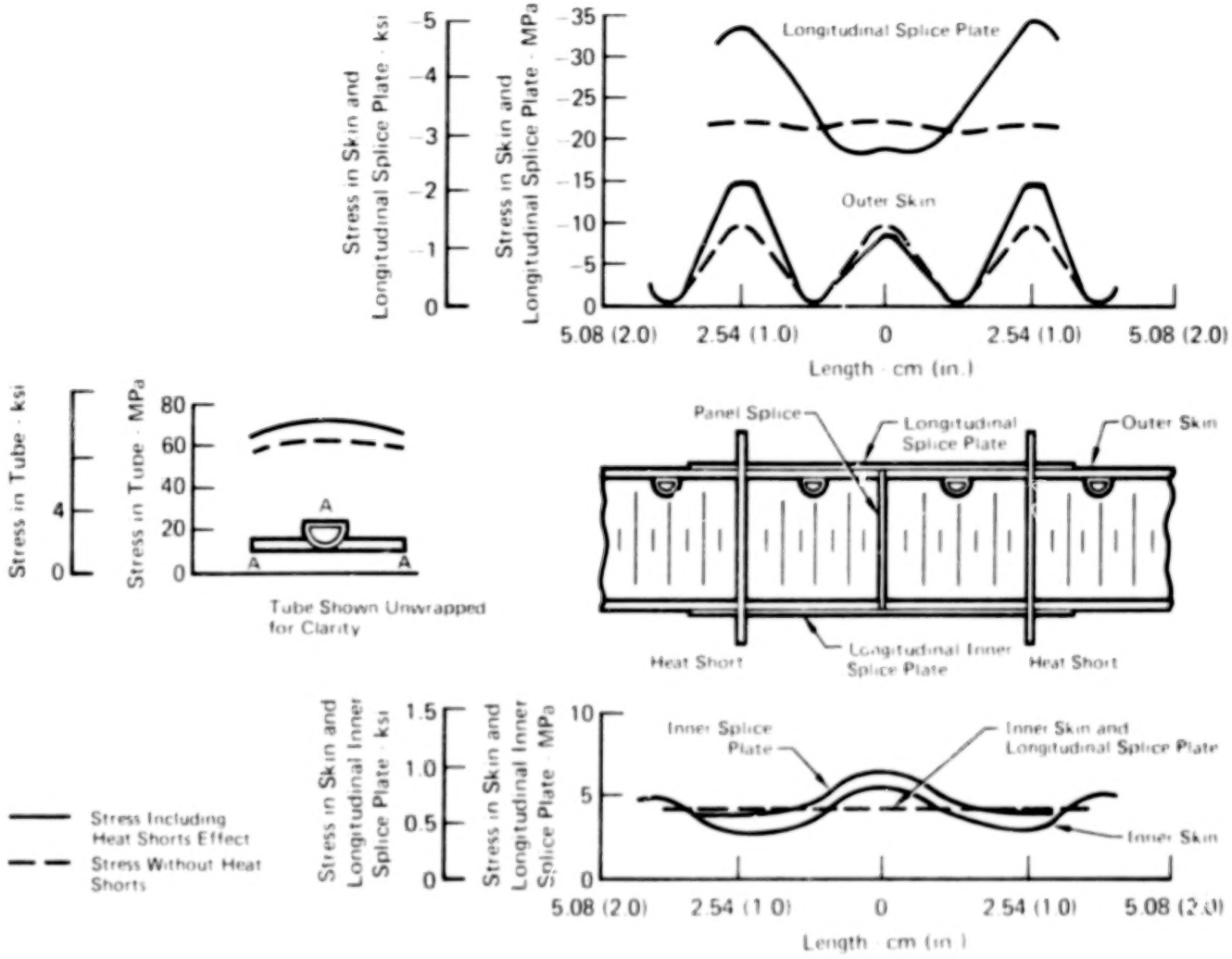


**FIGURE 59 ACTIVELY COOLED PANEL SKIN/TUBE/LONGITUDINAL SPLICE PLATE LONGITUDINAL THERMAL STRESSES**

| Condition | | $t_o$ & $t_i$ | H | Unit Mass[a] | |
|---|---|---|---|---|---|
| Points | Loading | cm (in.) | cm (in.) | $kg/m^2$ | ($lbm/ft^2$) |
| 1 | $N_x$ = 315 kN/m (1800 lbf/in.)<br>$N_y$ = 0.0 thru $N_y$ = 0.5 $N_x$<br>$N_{xy}$ = 0.0 | 0.102 (0.040) | 3.01 (1.185) | 7.23 | (1.48) |
| 2 | $N_x$ = 730 kN/m (3600 lbf/in.)<br>$N_y$ = 0.0 thru $N_y$ = 0.5 $N_x$<br>$N_{xy}$ = 0.0 | 0.204 (0.080) | 3.63 (1.430) | 13.28 | (2.72) |
| 3 | $N_x$ = 919 kN/m (5250 lbf/in.)<br>$N_y$ = 0.0 thru $N_y$ = 0.5 $N_x$<br>$N_{xy}$ = 0.0 | 0.305 (0.120) | 3.99 (1.57) | 19.04 | (3.90) |
| 4 | $N_x$ = 315 kN/m (1800 lbf/in.)<br>$N_y$ = 0.0<br>$N_{xy}$ = 0.5 $N_x$ | 0.127 (0.05) | 2.18 (0.857) | 8.59 | (1.76) |
| 5 | $N_x$ = 730 kN/m (3600 lbf/in.)<br>$N_y$ = 0.0<br>$N_{xy}$ = 0.5 $N_x$ | 0.236 (0.093) | 2.69 (1.060) | 14.65 | (3.00) |
| 6 | $N_x$ = 919 kN/m (5250 lbf/in.)<br>$N_y$ = 0.0<br>$N_{xy}$ = 0.5 $N_x$ | 0.360 (0.14) | 2.87 (1.13) | 20.99 | (4.30) |

Notes:
[a]Does not include coolant inventory
Dimensions in cm (in.)

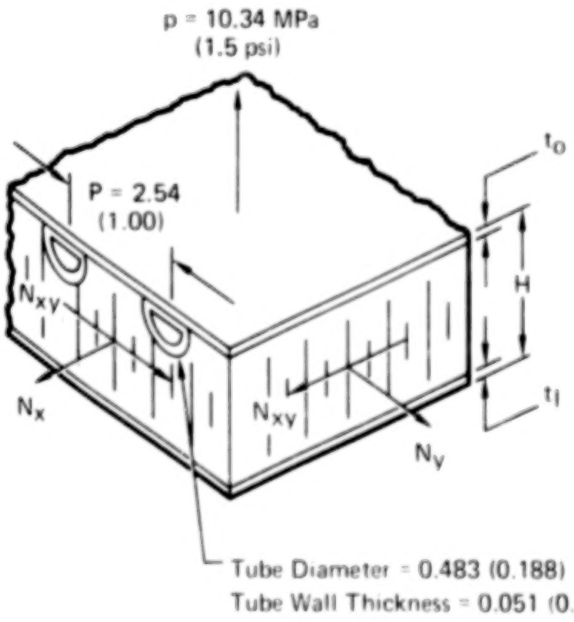


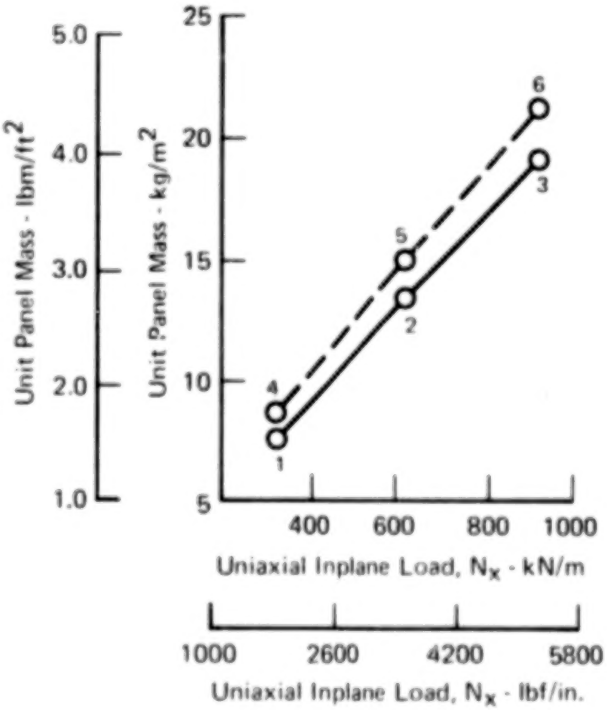


**FIGURE 60 - SENSITIVITY OF ACTIVELY COOLED PANEL MASS TO UNIAXIAL, BIAXIAL, AND SHEAR LOADING**

the panel is equally strength and beam column critical. It becomes strength critical when shear loads are added because the facesheet principal stresses increase. Consequently, the skin gages must be increased, over those required for $N_x$ loadings only, in order to satisfy basic strength requirements. This increase in skin thicknesses permitted some reduction in sandwich thickness but the reduced mass of the honeycomb could not offset the increased mass in the inner and outer skins. A minimum mass configuration is one with equal thickness inner and outer skins.

The mass shown reflects only the mass of the inner and outer skins and the honeycomb core. It does not include the adhesives, residual coolant, fasteners, bushings, splice plates, etc. However, these nonoptimums would be approximately the same as for the basic configuration designed for $N_x$ equal to 315 kN/m (1800 lbf/in.).

## APPENDIX E

## FATIGUE SPECIMENS AND TEST RESULTS

Three tube crack growth specimens (figure 61) were designed, fabricated, and fatigue tested at MCAIR to substantiate the design stress allowable used for the coolant tubes. This allowable, 163.27 MPa (23,680 psi), resulted from a crack growth analysis based on available da/dN for 6061-T6 material shown in Appendix A. The allowable developed for the 6061-T6 satisfied the requirement that cracks growing from a surface flaw would not grow through the tube wall thickness in 20,000 cycles. The method of analysis used for predicting crack growth induced by cyclic loading is a modification of the Wheeler model (reference 28) and the results, presented in figure 62, show approximately 20,000 cycles are required to propagate an 0.0228 cm (0.009 in.) deep circular surface crack through the 0.051 cm (0.02 in.) wall thickness.

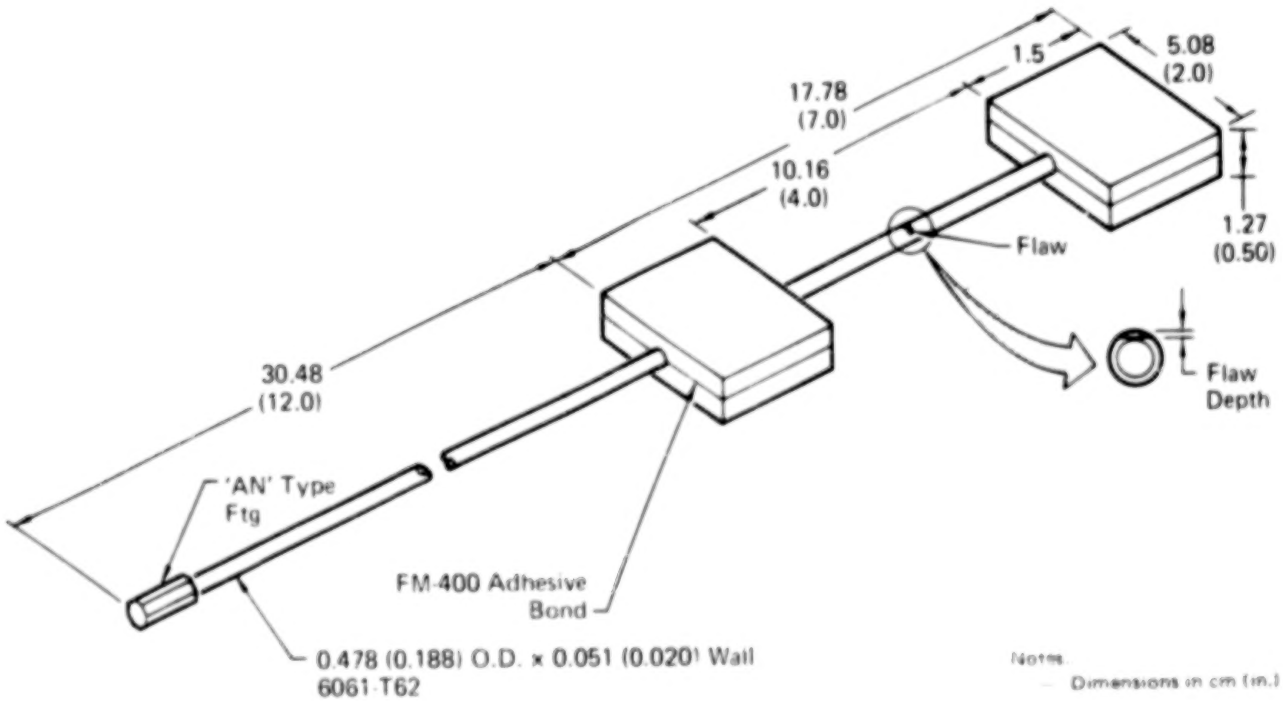


FIGURE 61 - TUBE CRACK GROWTH SPECIMEN

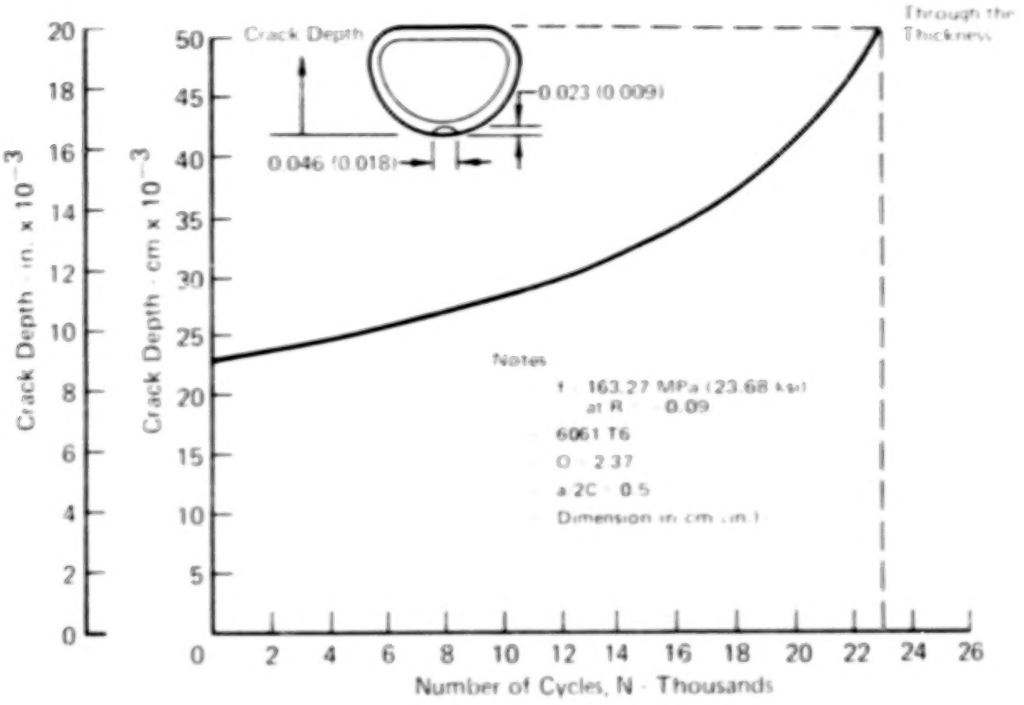


**FIGURE 62 - COOLANT TUBE CRACK GROWTH PREDICTION FOR DESIGN CYCLIC STRESS LEVELS AND FLAW SHAPE**

The test specimens consisted of three tubes with a 0.476 cm (0.188 in.) outside diameter and a 0.51 cm (0.02 in.) wall, sandwiched between and adhesively bonded to four aluminum loading plates. The first two specimens were flawed by scribing a sharp "V" notch across the tubes. The third specimen was similarly flawed using a triangular shaped jeweler's file. The flaw depths were determined by using a calibrated microscope which was used to focus on the tube outer surface and then on the surface at the tip of the flaw, while noting the change in focal length.

The test involved pressurizing specimens to the panel operating pressure of 0.655 MPa (95 psi) and cycling the loads such that the design limit stress level of 163.27 MPa (23,680 psi) and a R = -0.09 was developed in the tube. A pressure drop in the tube indicated when the crack propagated through the tube wall. The results of the tests are summarized in table 7. The first two specimens failed at the scribed flaw and the number of load cycles required to propagate the fatigue crack through the wall

## TABLE 7- RESULTS OF TUBE CRACK GROWTH FATIGUE TESTS[c]

| Specimen Identification | Preflaw Depth cm (in.) | Leak Detected (cycle) | Remarks |
|---|---|---|---|
| 1st | 0.0155 (0.0061) [a] | 28,000 | Specimen failed after 28,500 cycles. |
| 2nd | 0.0117 (0.0046) [a] | 43,000 | Test stopped at 46,000 cycles, tube was then static tested to failure. |
| 3rd | 0.0114 (0.0045) [b] | 167,000 | Specimen failed at an intergranular flaw on the surface away from the preflaw after 169,000 cycles. |

a. Tube flawed using scratch gage.
b. Tube flawed using jeweler's file.
c. Specimens tested using Sonntag machine at 1800 cycles/min.

thickness were 28,000 and 43,000 cycles, respectively. The third specimen, which was flawed with the jeweler's file, failed at an intergranular flaw (away from the scribed flaw) on the surface at 167,000 cycles.

The results of these tests show that with these types of flaws the tubes are able to withstand more than 20,000 cycles of design cyclic load levels before the crack grows through the tube wall thickness.

The failed surface of the second specimen was examined using the Scanning Electron Microscope to determine crack shape, crack initiation site, and crack growth rate. The results, figure 63, show the crack growth initiated from the 0.0117 cm (0.0046 in.) deep flaw after approximately 38,600 cycles, and that 4,400 additional cycles were needed to grow the crack through the remaining 0.039 cm (0.0154 in.) wall thickness. Even though the flaw depth was less than that used when developing the allowable, the crack shape was much more severe and the crack growth rates larger. It was predicted that approximately 5,800 cycles would be required to propagate a fatigue crack having the same flaw depth, crack shape, and cyclic stress levels as the second specimen through the tube wall thickness. The results of this analysis are shown in figure 63. Comparison of the predicted

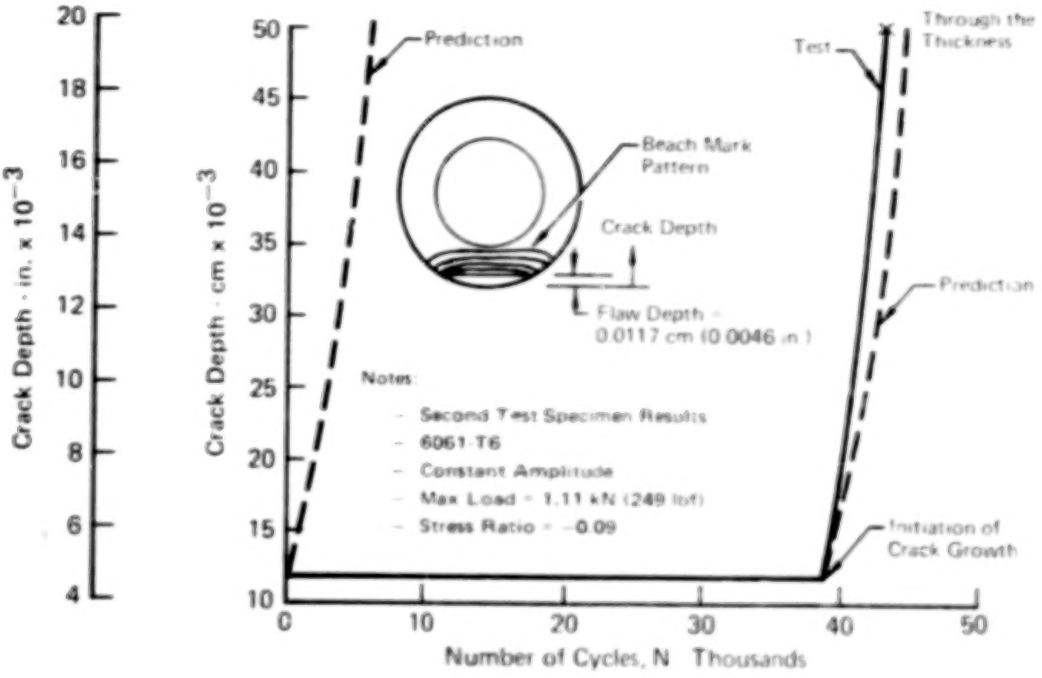


**FIGURE 63 - CRACK GROWTH ANALYSIS/TEST RESULTS**

to the actual crack growth curve at crack initiation reasonably substantiated the da/dN data and the analytical method used to develop the maximum design allowable for the coolant tube.

Figure 64 shows the failed second and third test specimens. The second specimen was static loaded to failure after the fatigue crack propagated through the thickness.

### Thermal Restraint Specimen

To determine if the Rene'41 heat shield design could survive 20,000 thermal cycles without fatigue failure, the thermal restraint specimen shown in figure 65 was fabricated and delivered to NASA for testing. Two areas of concern are the spot welds that attach the beaded skin to the corrugation and the cutouts in the beaded skin and corrugation at the lap splice joint. The test specimen was designed and a cyclic heating profile developed to simulate the structural and thermal responses of the full scale design heat shield.

The test specimen, 60.6 cm (23.88 in.) long and 23.3 cm (10.76 in.) wide, consists of a heat shield, insulation blanket, and a 1.27 cm (0.5 in.) thick aluminum support plate. Figure 66

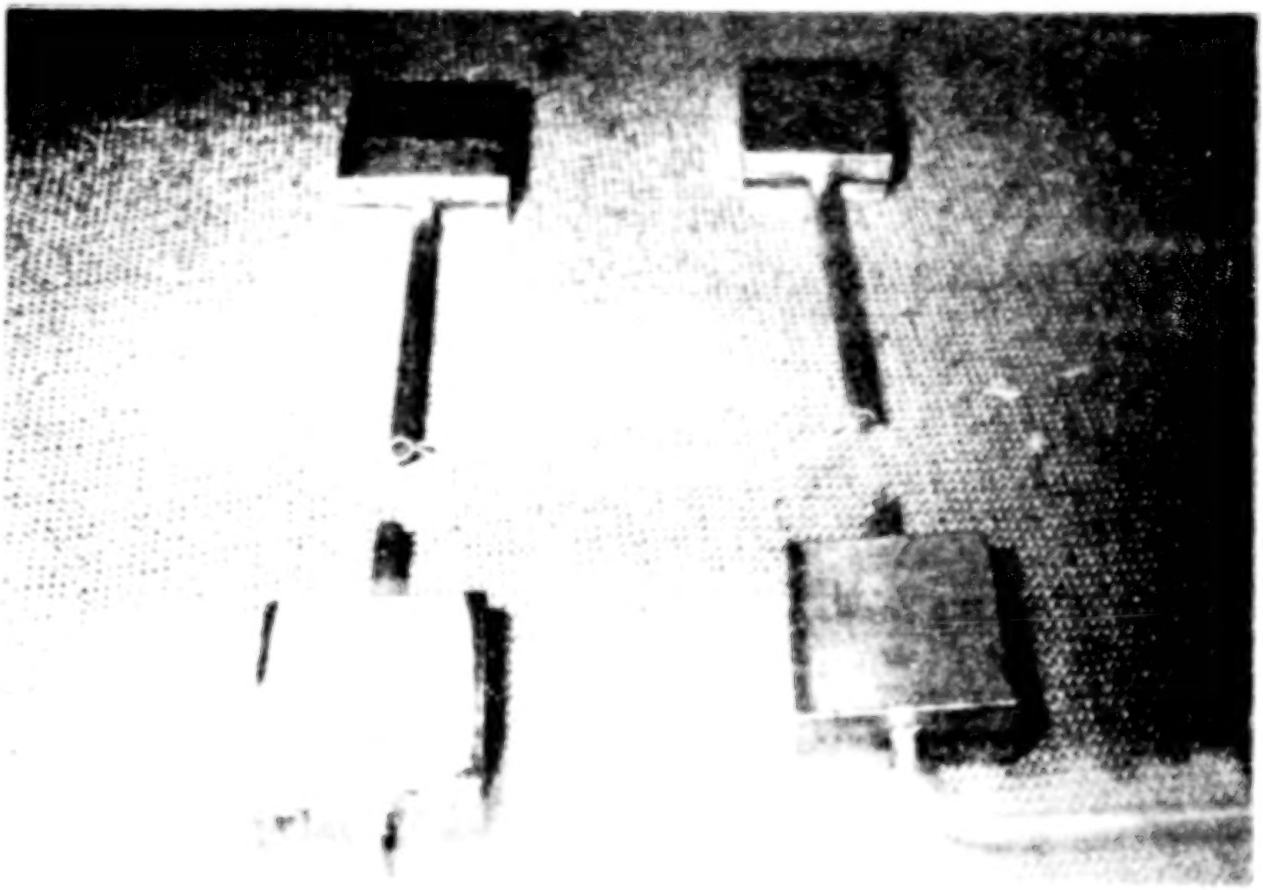

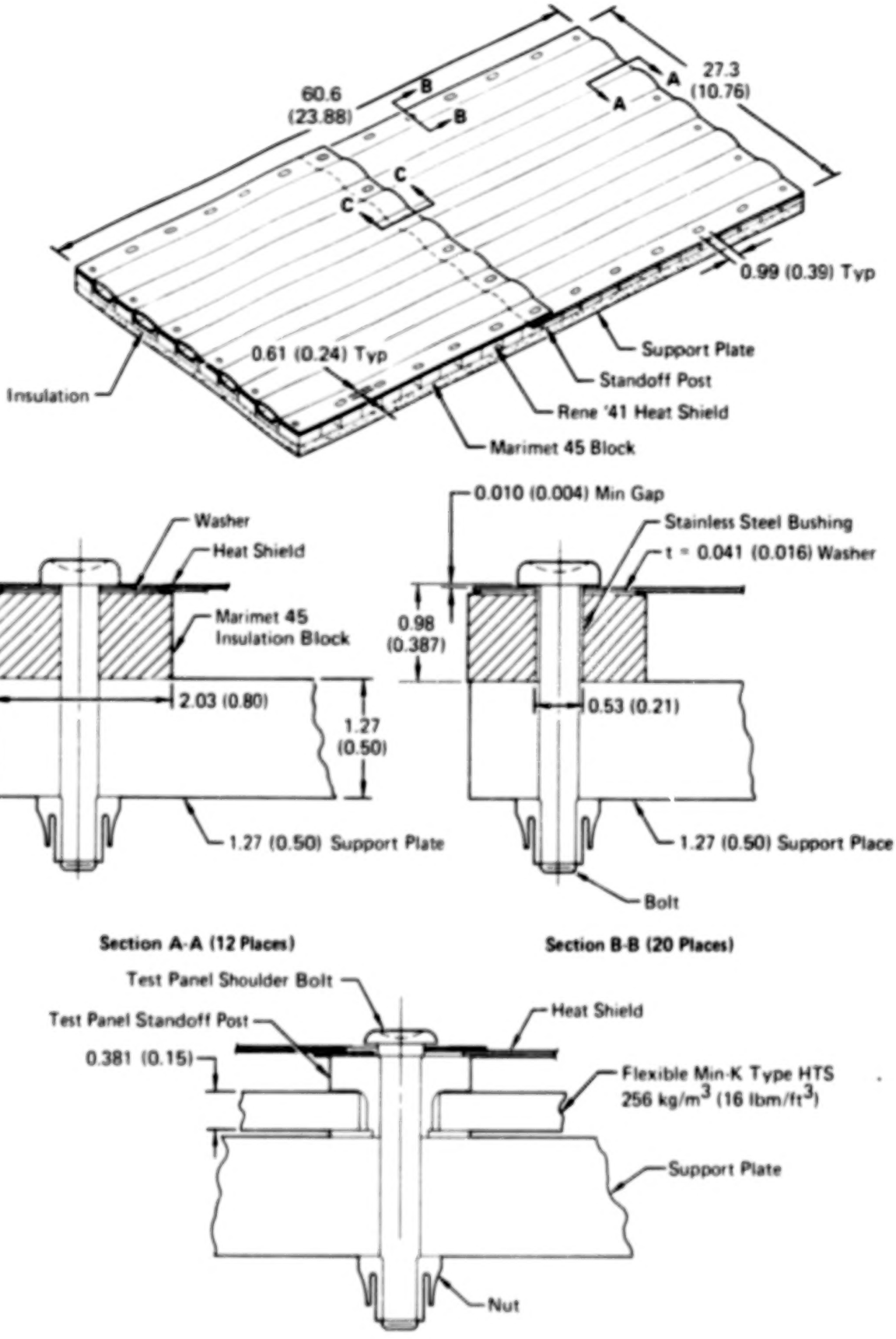


Note Dimensions in cm (in.)

**FIGURE 65 - THERMAL RESTRAINT SPECIMEN**

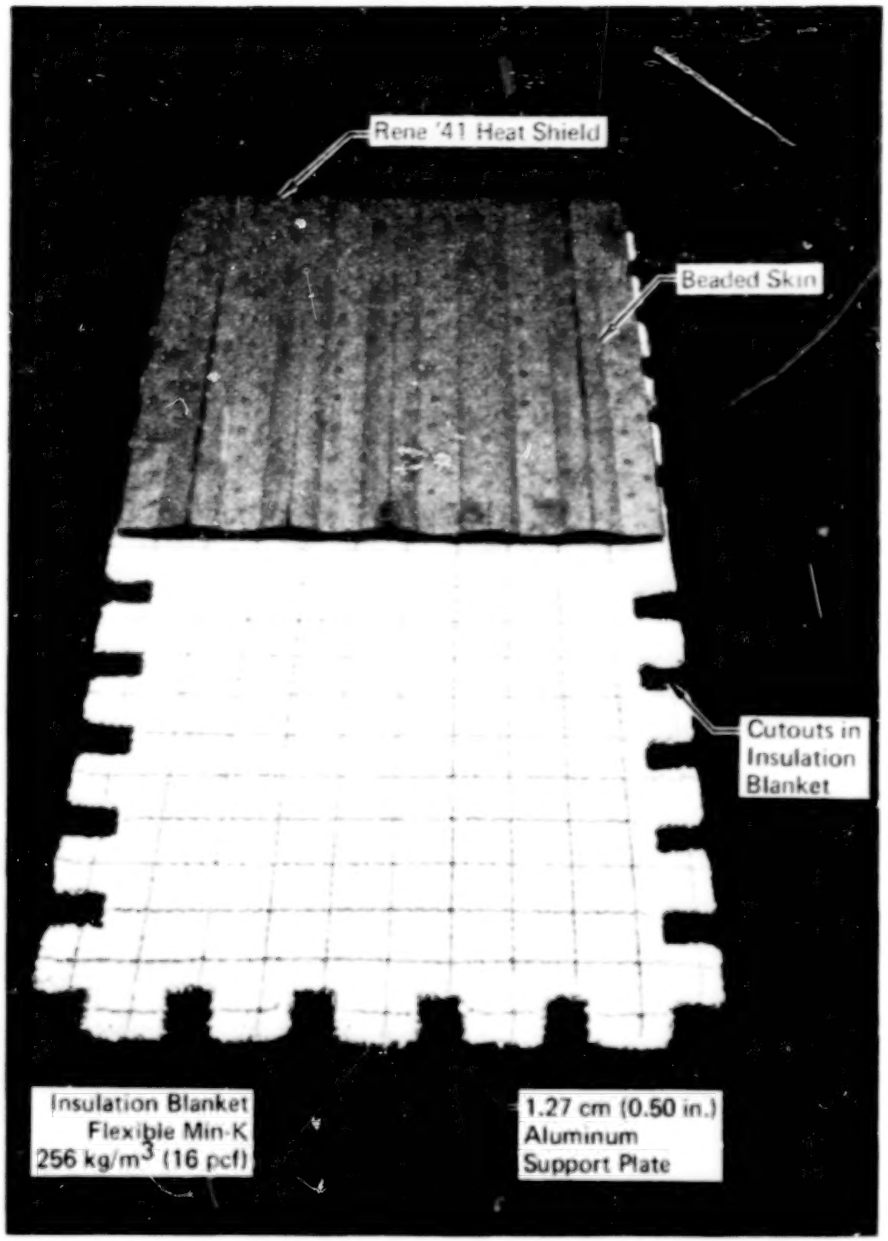


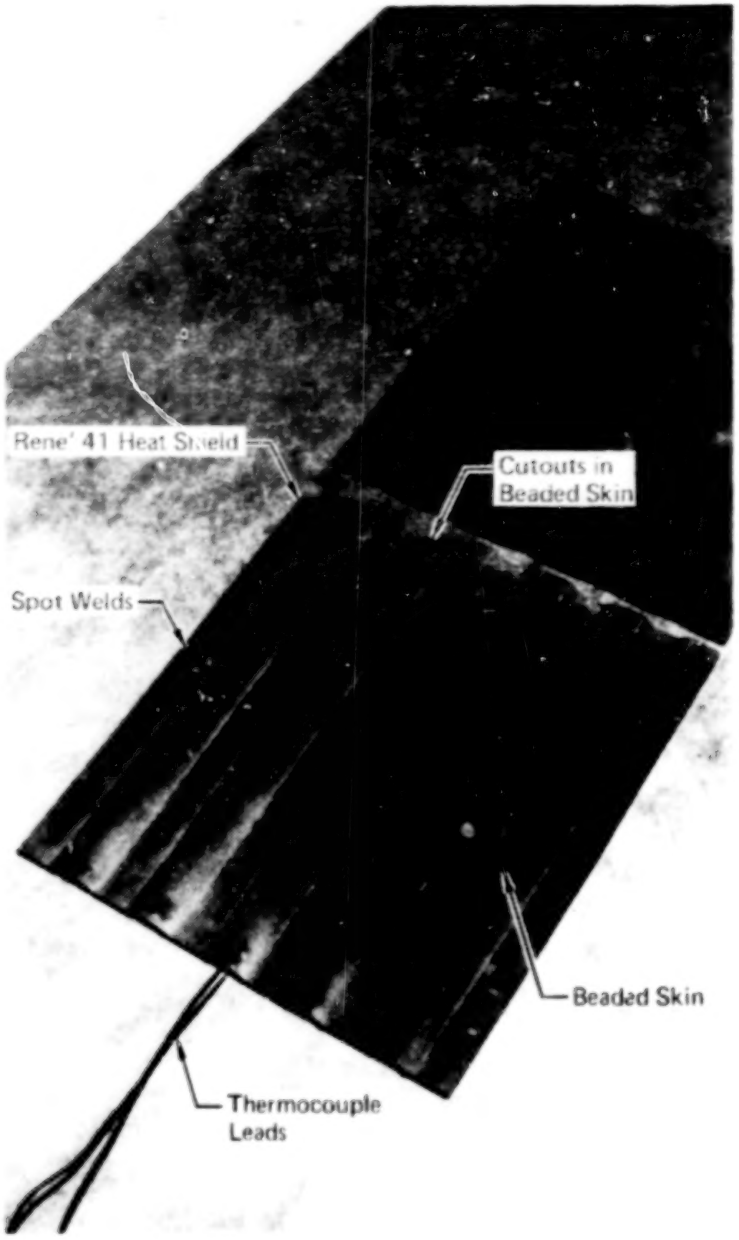


**FIGURE 66 - PARTIALLY ASSEMBLED TEST SPECIMEN**



119

blanket covered with Astroquartz cloth. The cloth covering the insulation was sewn together with Astroquartz thread in a 2.54 cm (1.0 in.) square quilted pattern. The cloth is sewn together along the trimmed edges to prevent the insulation from falling out during handling. Cutouts in the insulation blanket along the edges allow the Marimet 45 insulation blocks, shown in figure 66, to rest on the aluminum support plate and support the heat shield. The plate, which represents the actively cooled panel, supports the insulation and the heat shield and provides lateral restraint to the heat shield. The stainless steel bushings and shoulder bolts, similar to those in the test panel, prevent clamp-up and provide a gap between the fastener head and the heat shield to allow longitudinal thermal expansion.

Chromel-Alumel thermocouples were attached to the inner surface of the beaded and corrugated skins to monitor temperatures during testing.

Heat shield temperatures for a typical mission (see Appendix B) are compared in figure 67 with the recommended heat-up and cool-down rates for testing the thermal restraint specimen. During climb, flight heat shield temperatures increase at the rate of 2.8K (5°F) per second, which is duplicated during test.

This heat-up rate results in a maximum temperature difference across the heat shield of 127K (228°F) and 107K (193°F) for the first and subsequent test cycles, respectively, compared to a maximum temperature difference during climb of approximately 106K (191°F). Test cool-down rates are based upon natural convection with a room temperature environment. As shown, simulating flight cool-down rates would greatly increase the time required to complete a thermal cycle. The recommended natural convection cool-down reduces the thermal cycle to 12 minutes and will not jeopardize the structural integrity of the heat shield. Analyses have shown that forced air cooling and radiation to a room temperature environment, as defined on figure 67, limits the temperature of the aluminum support plate to 394K (250°F).

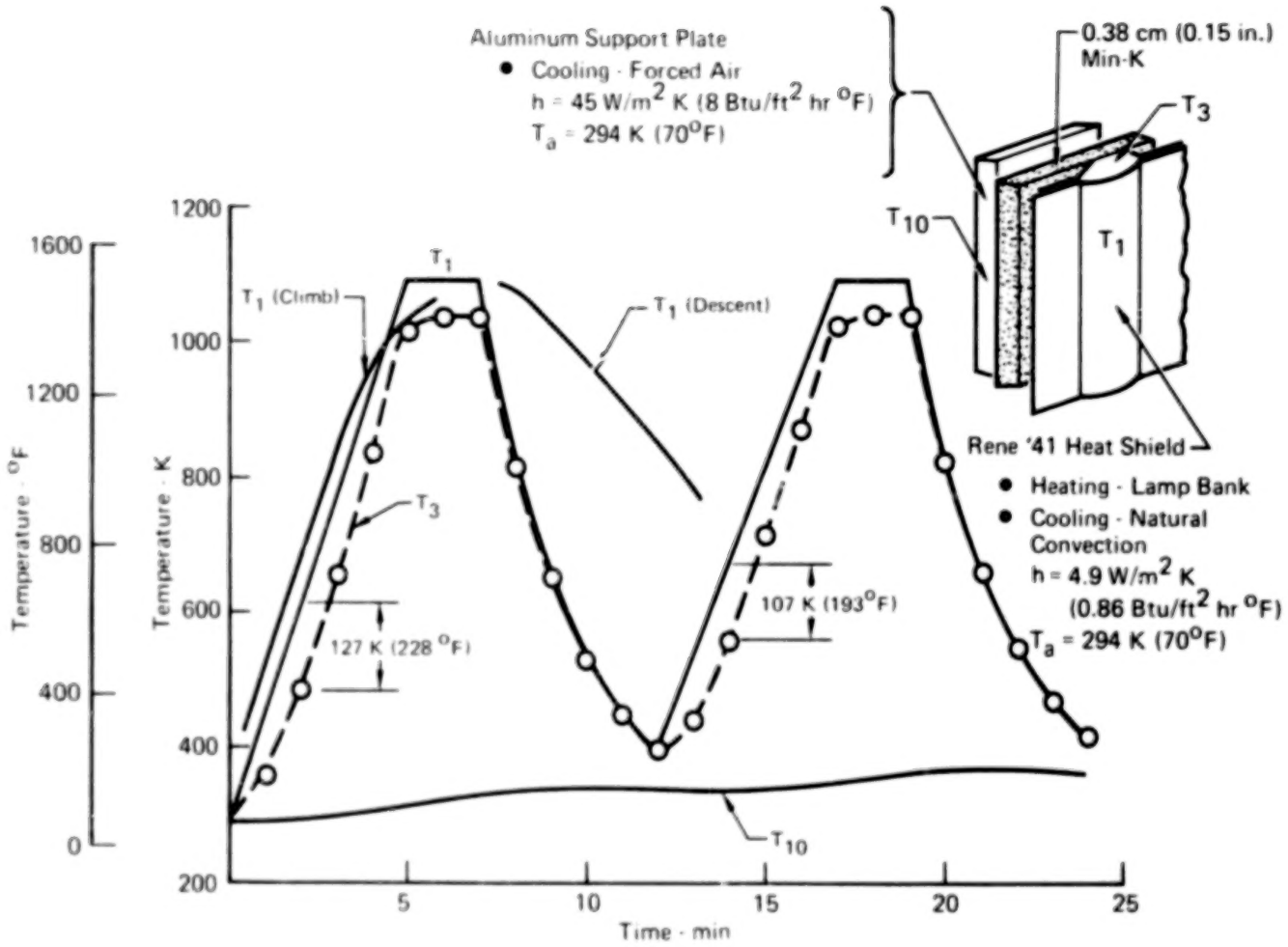


FIGURE 67 - PROPOSED THERMAL TEST CYCLE FOR THERMAL RESTRAINT SPECIMEN

Blank

Page

## APPENDIX F

## TEST PANEL SET-UP, TEMPEATURES AND STRESSES

The test panel is representative of a section at the end of the optimized full scale panel and consists of four Rene'41 corrugated stiffened beaded skin heat shield segments, two insulation blankets, an aluminum honeycomb sandwich actively cooled panel, and three support beams. It will be tested in NASA's fatigue/radiant heating facility and the 8 foot High Temperature Structures Wind Tunnel to evaluate the structural and thermal integrity of the full scale design. Following sections discuss the test panel set-up and the predicted panel temperatures and stresses.

### Fatigue/Radiant Heating Test Set-Up

The test panel, load adapters, side fairings, support fittings, and support frames for the fatigue/radiant heating configuration are illustrated in figure 68. The in-plane loads are applied to the actively cooled panel through the 3.18 cm (1.25 in.) thick aluminum load adapters attached to the transverse splice plate and a flange of the support frame by a row of fasteners installed in close tolerance holes.

Section A-A shows that the load adapter is machined down in the area of the load adapter/panel interface to minimize eccentric loading. An 0.081 cm (0.032 in.) strip of asbestos phenolic insulation is placed between the load adapter and the splice plate and the flange of the support frame to minimize heat loss from the panel to the load adapters.

Section B-B shows a typical panel cross section at the support frames. The support fittings are attached to NASA's structure which allows longitudinal panel displacement but prohibits deflection normal to the panel surface. The side fairings are attached to the longitudinal edge of the heat shield and extend beyond the actively cooled panel to protect the edges of the panel and the support fittings from direct exposure to the radiation.

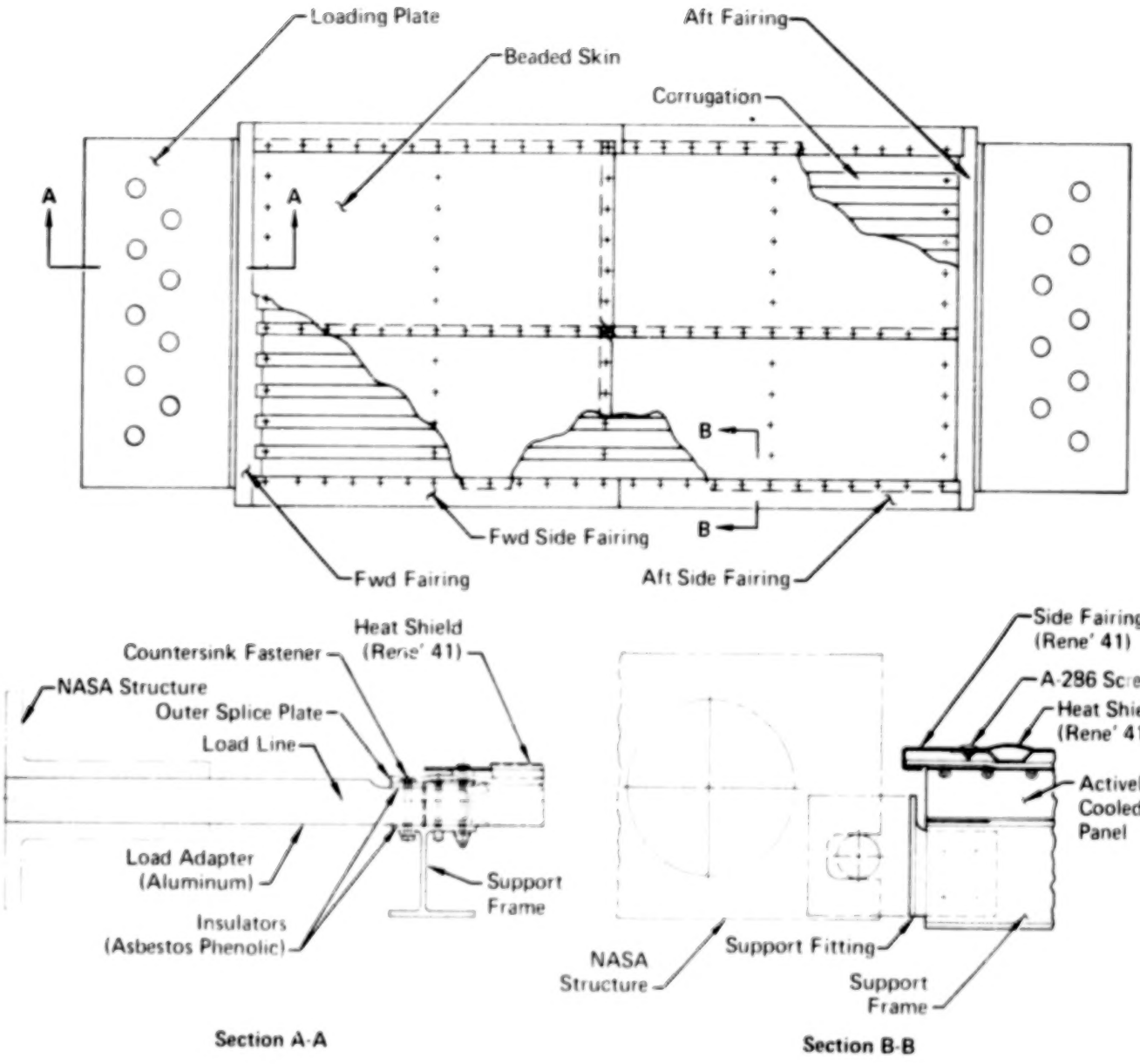


FIGURE 68 · TEST PANEL RADIANT HEAT/FATIGUE/STATIC TEST SET-UP

## Test Panel Wind Tunnel Set-Up

Figure 69 shows the test panel forward, aft, and side fairings, and the wind tunnel test fixture closeout fairing. The closeout fairing, designed to fit NASA's wind tunnel fixture, consists of 2.54 cm (1.0 in.) thick Thermo-Sil Castable 120 insulation which is bonded with RTV 560 adhesive to an aluminum framed substructure. The insulation protects the aluminum substructure from aerodynamic heating during wind tunnel testing.

Section A-A shows the interface between NASA's structure and the beaded skin of the heat shield at the forward end of the test panel. The 321 stainless steel forward fairing is flush with NASA's structure and extends over and mates with the contour of the beaded heat shield. Marimet 45 insulation blocks, covered with two plies of Astroquartz cloth to minimize airflow into the slots, support the slotted forward fairing.

Section B-B shows the interface of the longitudinal edge of the test panel and the wind tunnel closeout fairing. The Rene'41 side fairing is attached to the heat shield and is supported by the Castable 120 and the slotted L-shaped 321 stainless steel side retainer which is fastened to the aluminum support beam. An insulator strip isolates the side fairing from the side retainer and reduces the thermal gradients in the side fairing.

Section C-C shows the transition between the beaded skin and the wind tunnel closeout fairing at the aft end of the test panel. The flats between the beaded skin of the heat shield are at the same level as the leading edge of the tapered Castable 120. The flat 321 stainless steel aft fairing is sandwiched between the standoff posts and the beaded skin. This arrangement leaves the crown portion of the beaded skin open and provides venting of the heat shield to prevent overloading during wind tunnel startup.

## Test Panel Temperatures

Results from thermal analyses of the test panel were used to (a) establish test conditions that simulate full scale panel temperatures, and (b) predict panel temperatures in the region of the loading adapters. Since the test panel is only 1/5 the

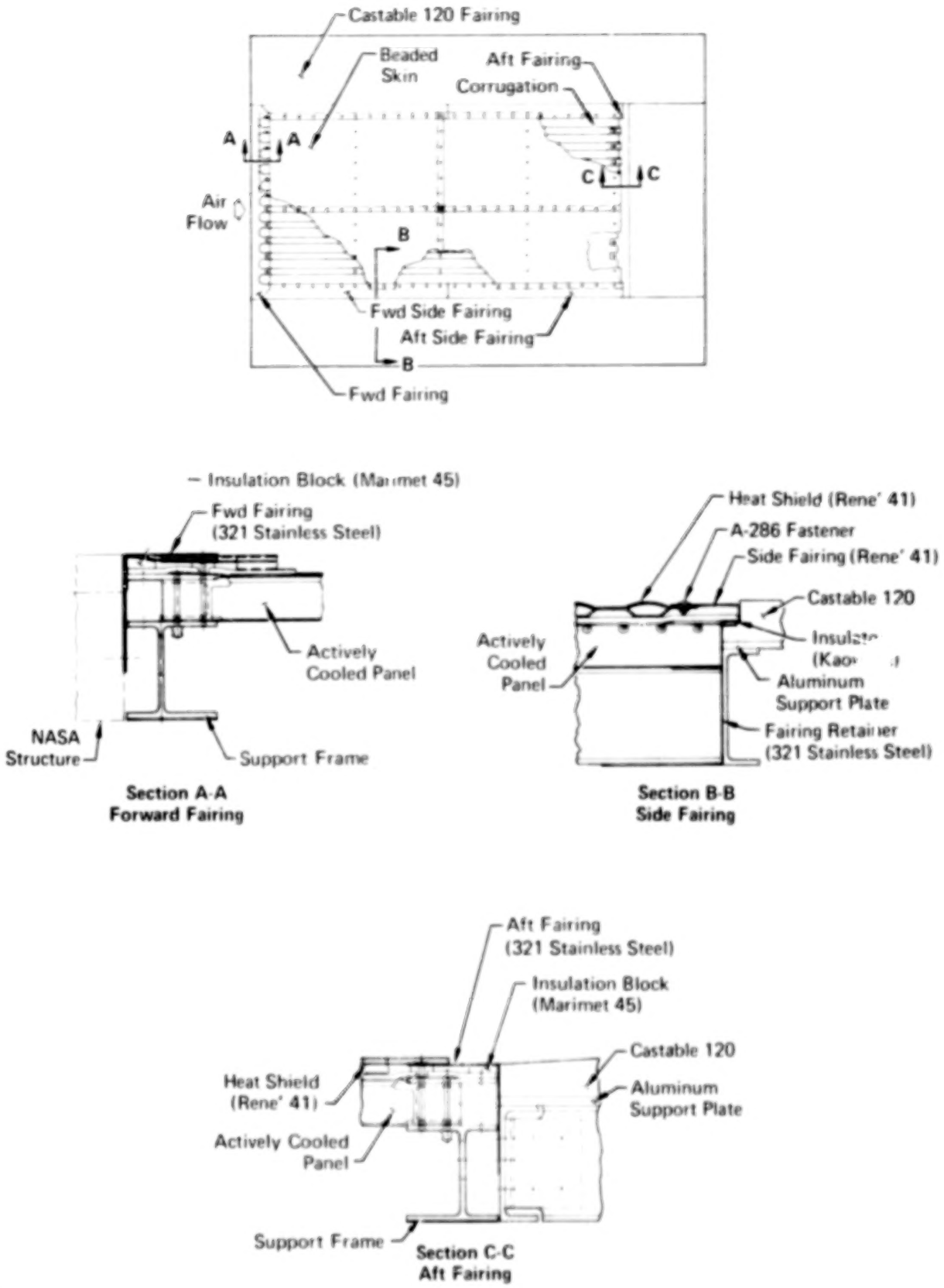


**FIGURE 69 - RADIATIVE ACTIVELY COOLED PANEL IN THE WIND TUNNEL CLOSEOUT FAIRING**

length of the full scale panel, and since the coolant side heat transfer coefficient (laminar flow) is inversely proportional to the cube root of the flow length, heat transfer coefficients are higher for the test panel than they are for the full scale panel. The higher heat transfer coefficients result in lower temperatures for the test panel than in the full scale design. However, panel temperatures can be readily increased (or decreased) by increasing (or decreasing) the test coolant temperature, as illustrated in figures 70 and 71 for simulated full scale inlet and exit conditions, respectively. A change in coolant temperature causes a nearly equal change in panel temperature. Conversely, as shown in figure 70, varying the coolant mass flow rate is very ineffective in controlling test panel temperatures. Reducing the coolant flow 50% increases test panel temperatures by only about 2.8K (5°F).

Sensitivity of test panel temperatures to variations in the coolant side heat transfer coefficient of $\pm$30 percent are presented in figure 72. Panel temperatures are insensitive to the variations considered and show a maximum increase of only 6.7K (12°F) when the coefficient is reduced 30% and a 3.3K (6°F) decrease when the coefficient is increased 30%.

Detailed thermal analyses of the test panel indicated that full scale manifold temperatures can be simulated when the test panel is attached to the loading grips. As shown in figure 73, the predicted test temperatures are in good agreement with full scale values for a simulated inlet condition. For a simulated exit condition (figure 74), predicted test temperatures are in good agreement with full scale panel temperature, except at the transverse splice plate, where predicted test temperatures are low due to the heat sink effect of the load grip.

## Test Panel Stresses

Figures 75 and 76 show the transverse thermal stresses in the transverse splice plates, inner and outer skins, and manifolds for simulated full scale panel inlet and exit conditions. These stresses were computed using the test panel temperatures shown in figures 73 and 74.

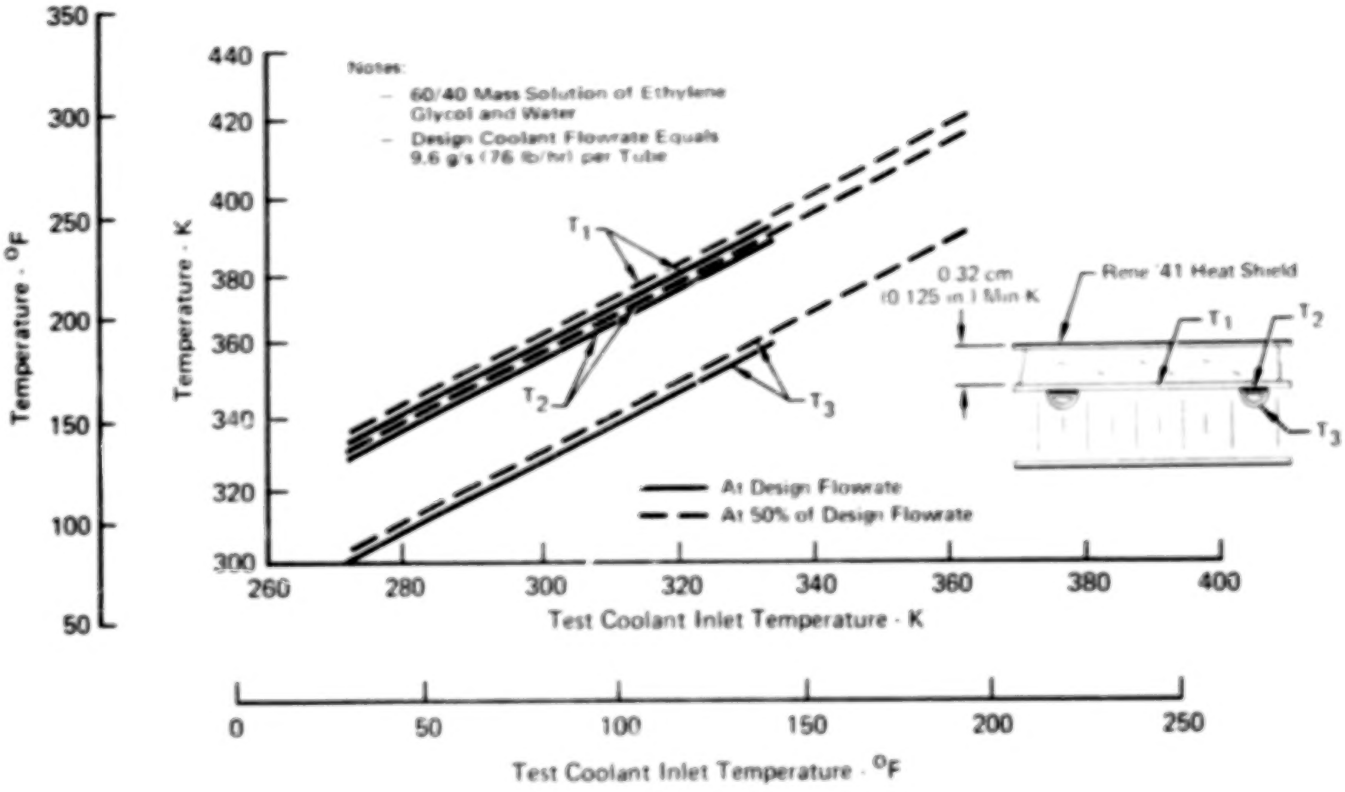


**FIGURE 70 - TEMPERATURES AT TEST PANEL INLET AS A FUNCTION OF COOLANT INLET TEMPERATURE**

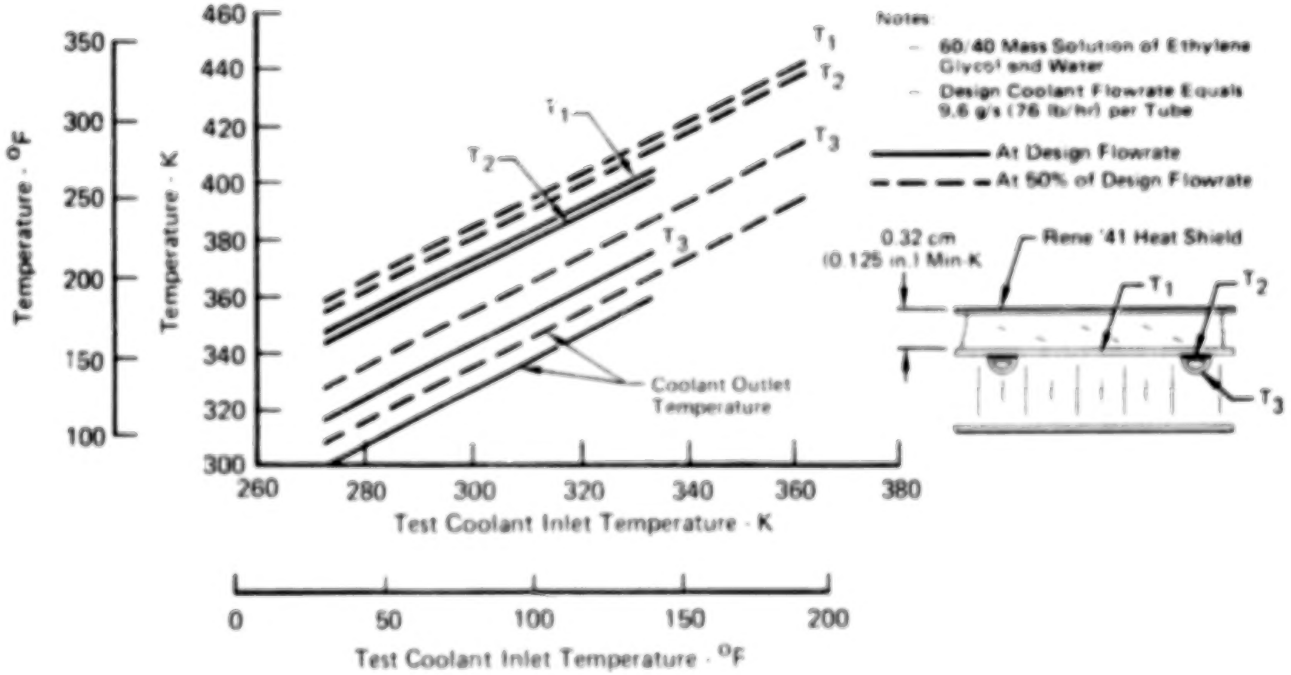


**FIGURE 71 - TEMPERATURES AT TEST PANEL EXIT AS A FUNCTION OF COOLANT INLET TEMPERATURE**

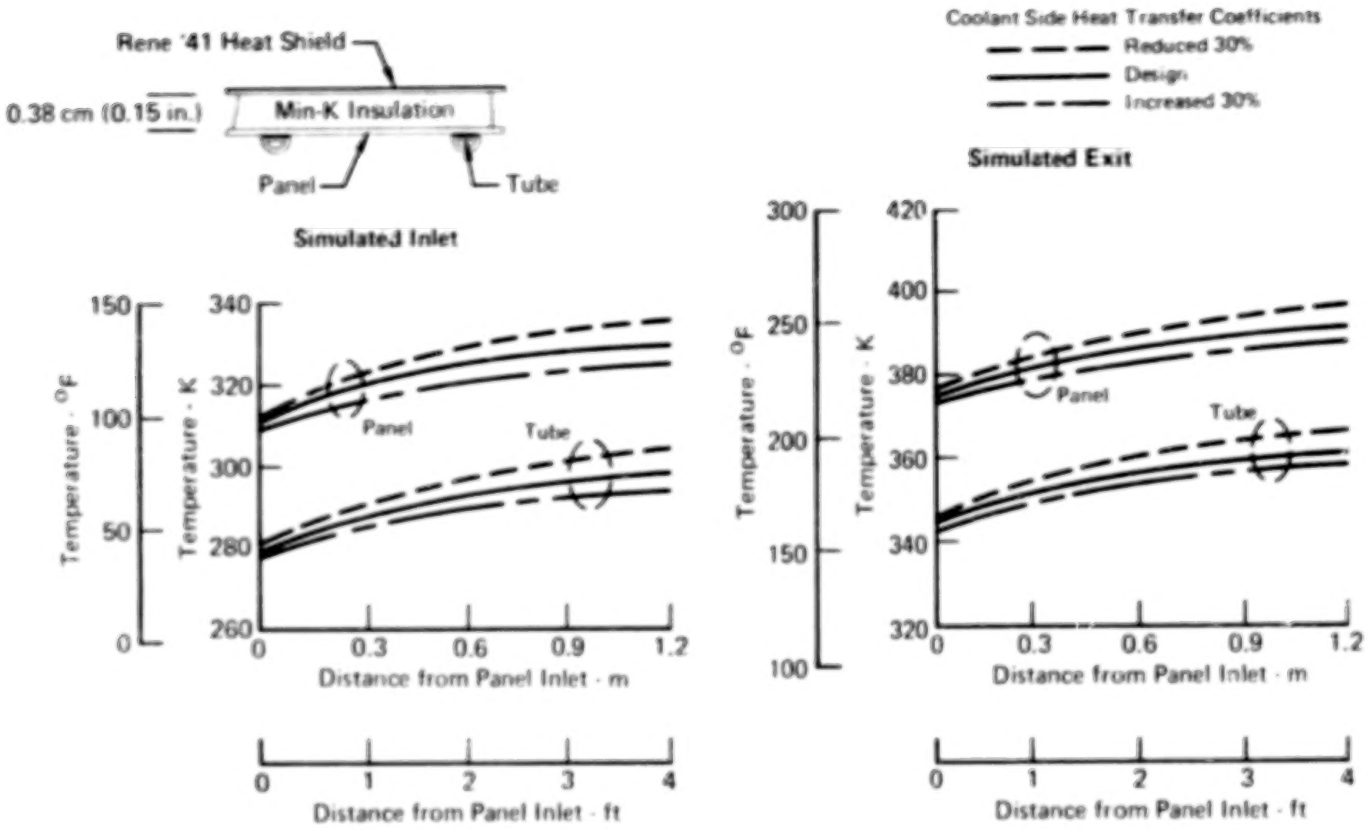


**FIGURE 72 - EFFECT OF COOLANT SIDE HEAT TRANSFER COEFFICIENT ON TEST PANEL TEMPERATURES**



129

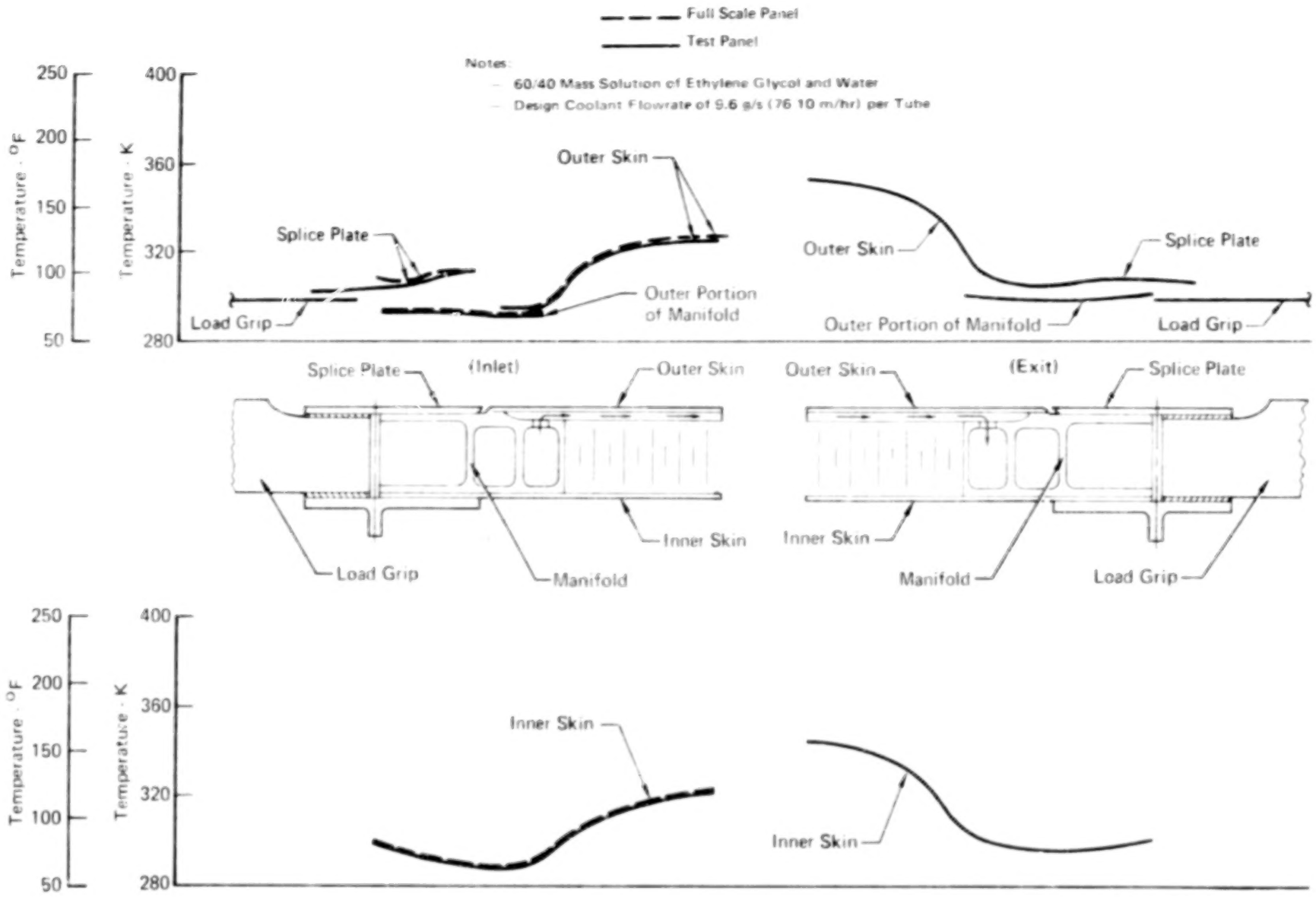


**FIGURE 73 - SIMULATION OF FULL SCALE INLET MANIFOLD TEMPERATURES**

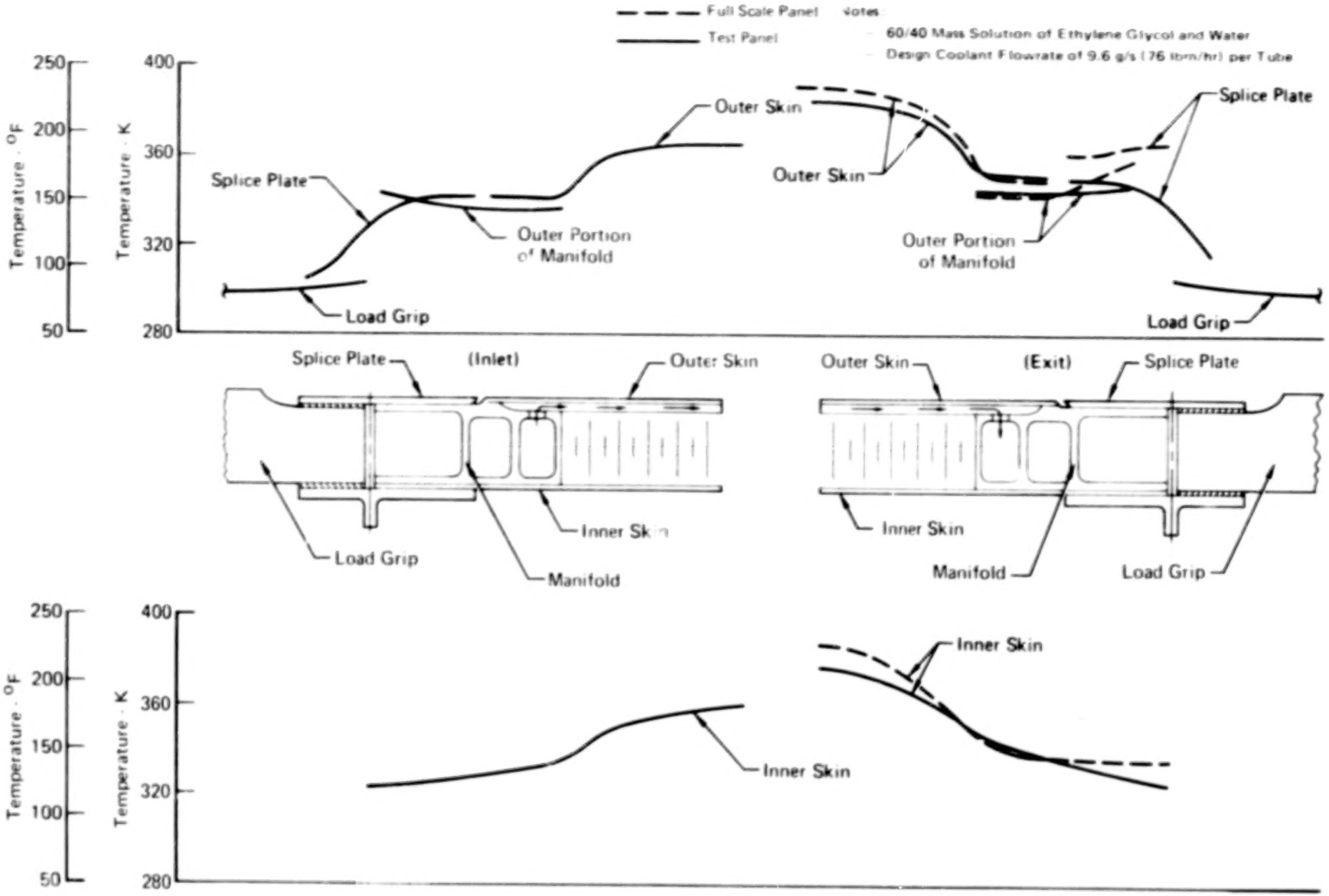


**FIGURE 74 - SIMULATION OF FULL SCALE EXIT MANIFOLD TEMPERATURES**



131

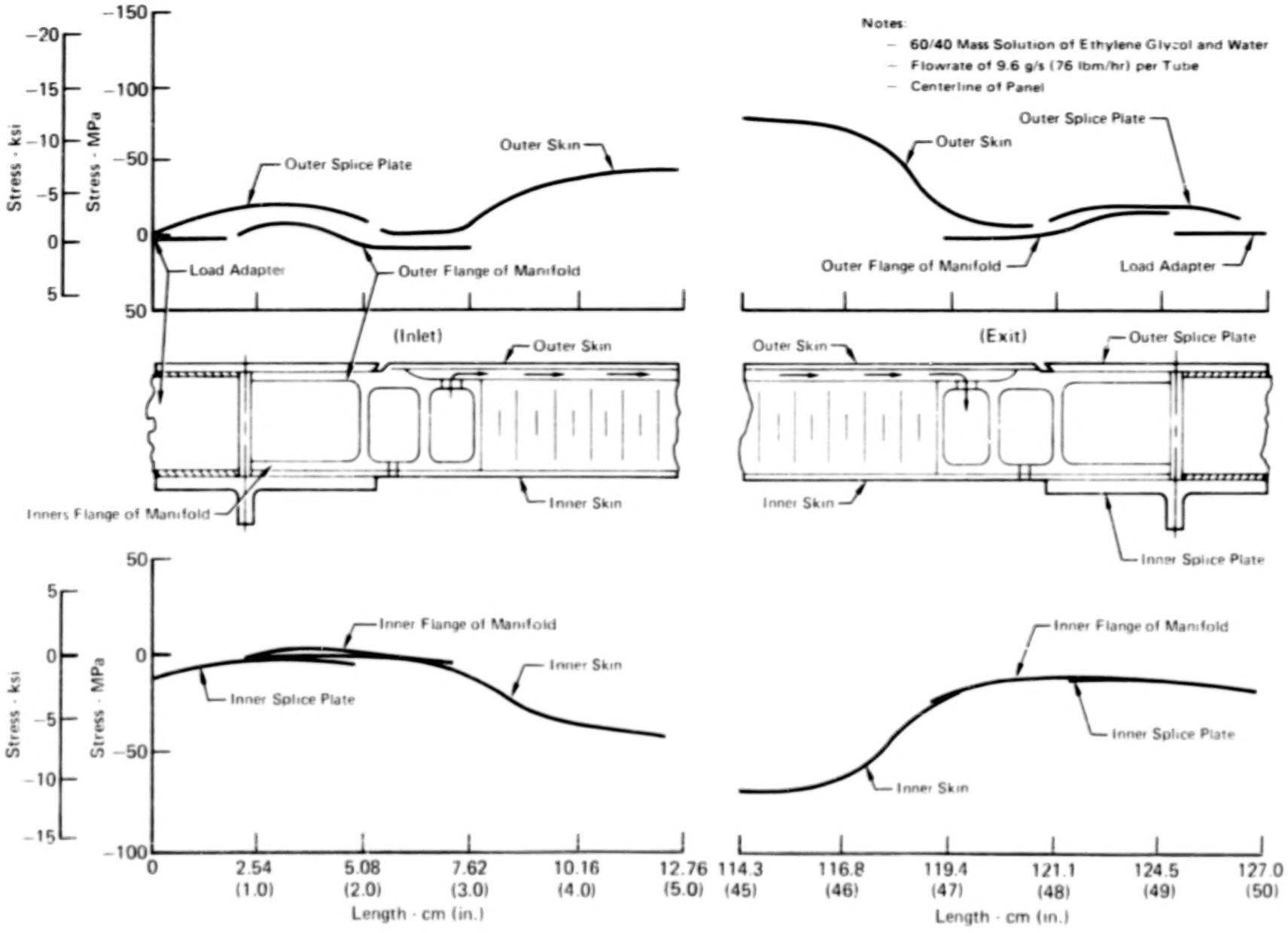


**FIGURE 75 - TEST PANEL TRANSVERSE THERMAL STRESSES AT THE MANIFOLDS FOR SIMULATED INLET CONDITION**

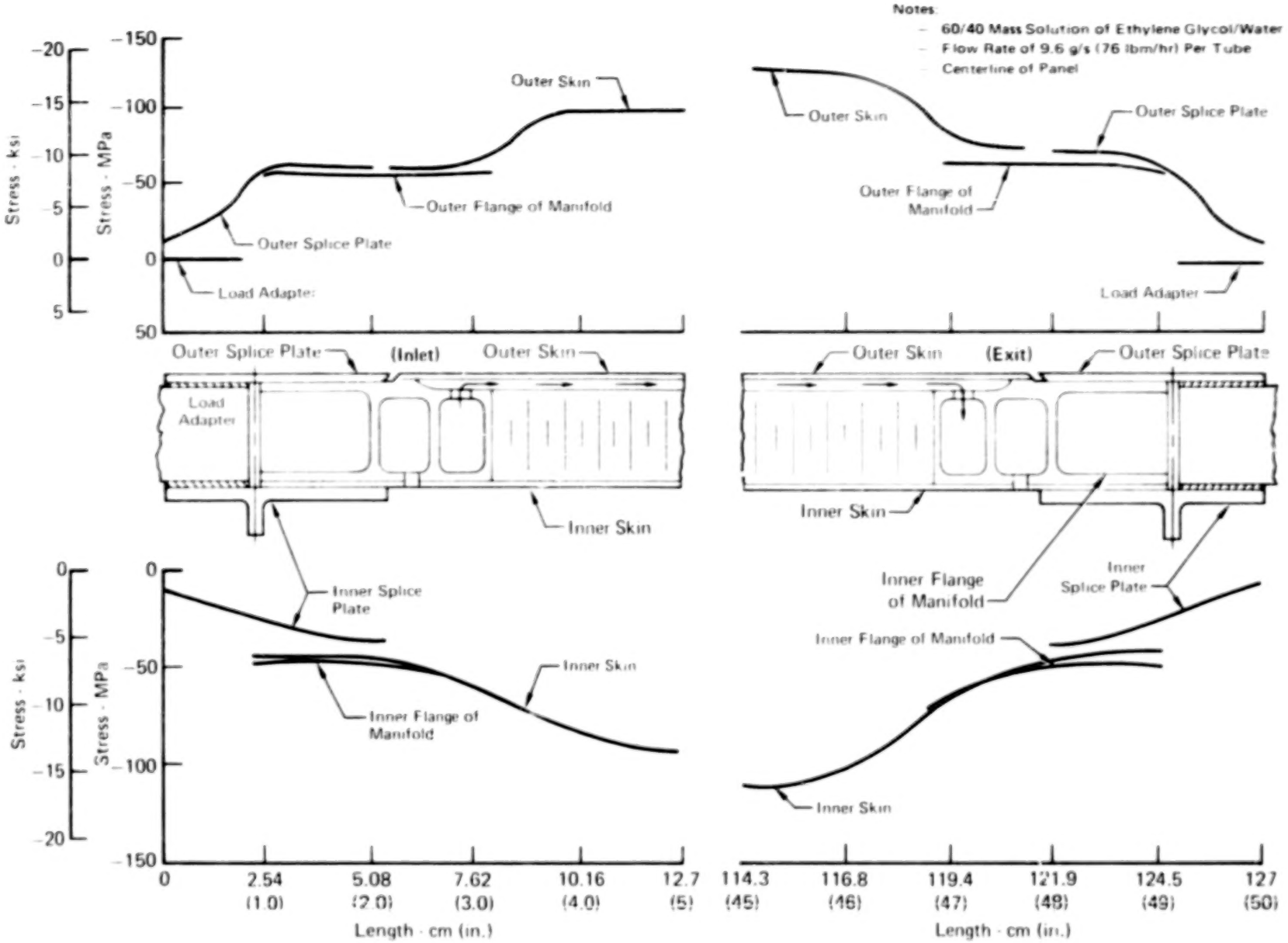


**FIGURE 76 - TEST PANEL TRANSVERSE THERMAL STRESSES AT THE MANIFOLDS FOR SIMULATED OUTLET CONDITION**



133

Figure 77 shows the longitudinal stresses in the inner and outer skins, and also the longitudinal splice strap for mechanical inplane loads and thermal loads, for simulated inlet and exit conditions.

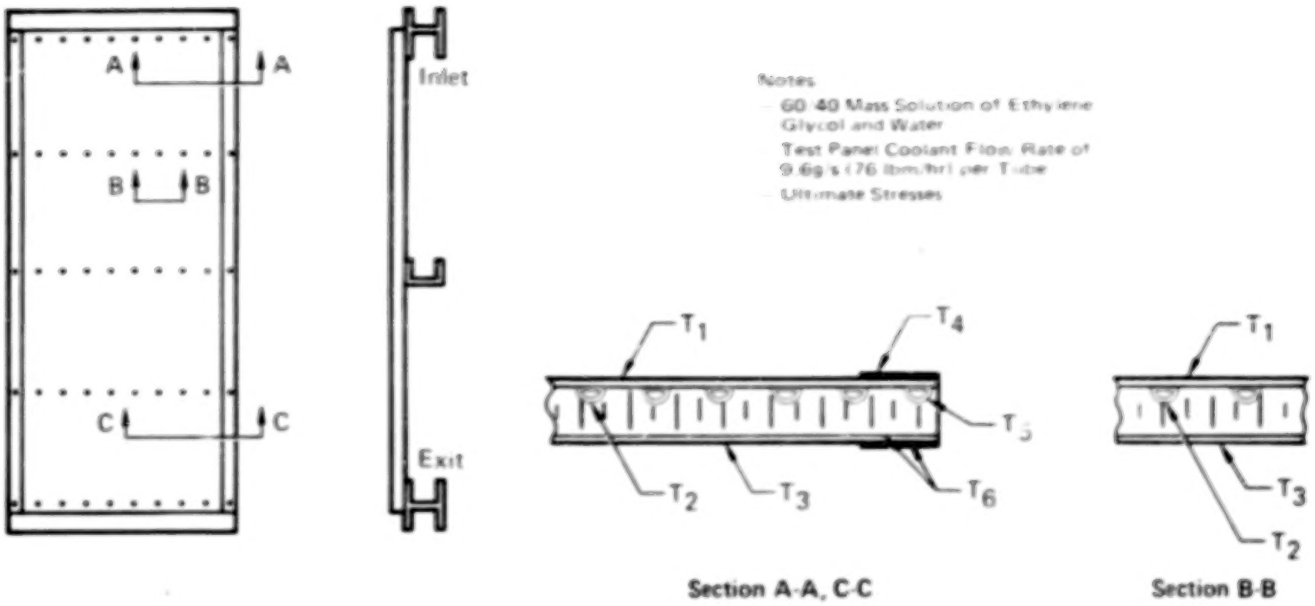


| Location | Mechanical Stresses | | Temperatures | | | | Thermal Stresses | | | |
|---|---|---|---|---|---|---|---|---|---|---|
| | | | Simulated Inlet | | Simulated Exit | | Simulated Inlet | | Simulated Exit | |
| | MPa | (ksi) | K | ($^{O}$F) | K | ($^{O}$F) | MPa | (ksi) | MPa | (ksi) |
| Section A-A | | | | | | | | | | |
| 1 | 129 | 18.7 | 332 | 138 | 381 | 225 | – 7.6 | –1.1 | – 8.6 | –1.3 |
| 2 | 129 | 18.7 | 299 | 79 | 352 | 174 | 43.4 | 6.3 | 38.6 | 5.6 |
| 3 | 131 | 19.0 | 337 | 130 | 375 | 215 | – 4.8 | –0.7 | – 4.1 | –0.6 |
| 4 | 129 | 18.7 | 346 | 162 | 394 | 249 | –24.8 | –3.6 | –24.8 | –3.6 |
| 5 | 129 | 18.7 | 298 | 76 | 351 | 171 | 52.4 | 7.6 | 39.3 | 5.7 |
| 6 | 131 | 19.0 | 340 | 127 | 373 | 212 | 8.3 | 1.2 | 10.3 | 1.5 |
| Section B-B | | | | | | | | | | |
| 1 | 128 | 18.6 | 337 | 147 | 391 | 235 | – 8.3 | –1.2 | – 8.3 | –1.2 |
| 2 | 128 | 18.6 | 304 | 88 | 359 | 186 | 41.4 | 6.0 | 36.5 | 5.3 |
| 3 | 130 | 18.8 | 342 | 138 | 381 | 226 | – 5.5 | –0.8 | – 3.4 | –0.5 |
| Section C-C | | | | | | | | | | |
| 1 | 129 | 18.7 | 344 | 160 | 392 | 246 | – 8.3 | –1.2 | – 7.6 | –1.1 |
| 2 | 129 | 18.7 | 313 | 104 | 366 | 199 | 41.4 | 6.0 | 36.5 | 5.3 |
| 3 | 131 | 19.0 | 350 | 153 | 387 | 237 | – 5.5 | –0.8 | – 4.1 | –0.6 |
| 4 | 129 | 18.7 | 359 | 186 | 407 | 275 | –25.5 | –3.7 | –26.9 | –3.9 |
| 5 | 129 | 18.7 | 311 | 100 | 364 | 195 | 50.3 | 7.3 | 37.9 | 5.5 |
| 6 | 131 | 19.0 | 353 | 150 | 386 | 234 | 8.9 | 1.3 | 12.4 | 1.8 |

**FIGURE 77 · ACTIVELY COOLED TEST PANEL TEMPERATURES AND LONGITUDINAL STRESSES FOR SIMULATED INLET AND EXIT CONDITIONS**

Blank

Page

# APPENDIX G

## TEST PANEL FABRICATION

This section describes the fabrication of the test panel and shows photographs of several components which are a part of the panel and the test apparatus.

Individual tube/tab assemblies were fabricated to assure the tube straightness needed to maintain a bondline thickness less than 0.025 cm (0.010 in.) and thus obtain the needed interface conductance between the tubes and outer skin. Fabrication of the tube/tab assemblies involved forming 0.48 cm (0.188 in.) diameter 6061-0 aluminum tubes into a Dee shape, cutting them to proper length, crimping and spot welding the ends, and torch brazing the machined tabs to each end of the tube. The tubes were formed by inserting an annealed round tube between two rotating wheels, one of which was machined to the desired semi-circular shape and the other machined to provide the flat surface of the tube.

Brazing of the Dee tubes to the machined tab was difficult because of porosity and poor wetting of the faying surfaces by the braze alloy. A slot was machined in the bottom of the tabs to improve wetting and allow the braze alloy to flow around the periphery of the tube at the tube/tab interface. Even then, the tube/tab rejection rate was high because of voids in the braze alloy. Exposed voids were rejected because entrapped brazing flux would cause corrosion if it came in contact with the coolant. Coolant passage holes were electrical discharge machined (EDM) rather than drilled to prevent burrs from entering the tubes and restricting coolant flow.

Figure 78 shows the fixture used to support one end of the tube/tab assembly during brazing. Also shown is the EDM hole. After EDM the tube/tab assemblies were solution treated, straightened by stretching approximately 2.5%, heat treated to the 6061-T6 condition, proof pressure checked to 1.31 kPa (190 psig), cleaned, and primed for bonding.

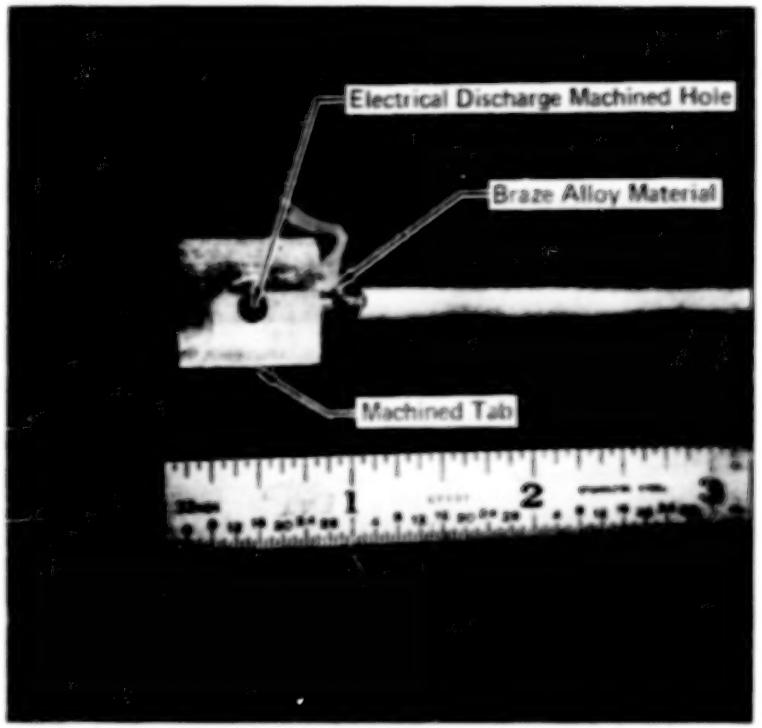


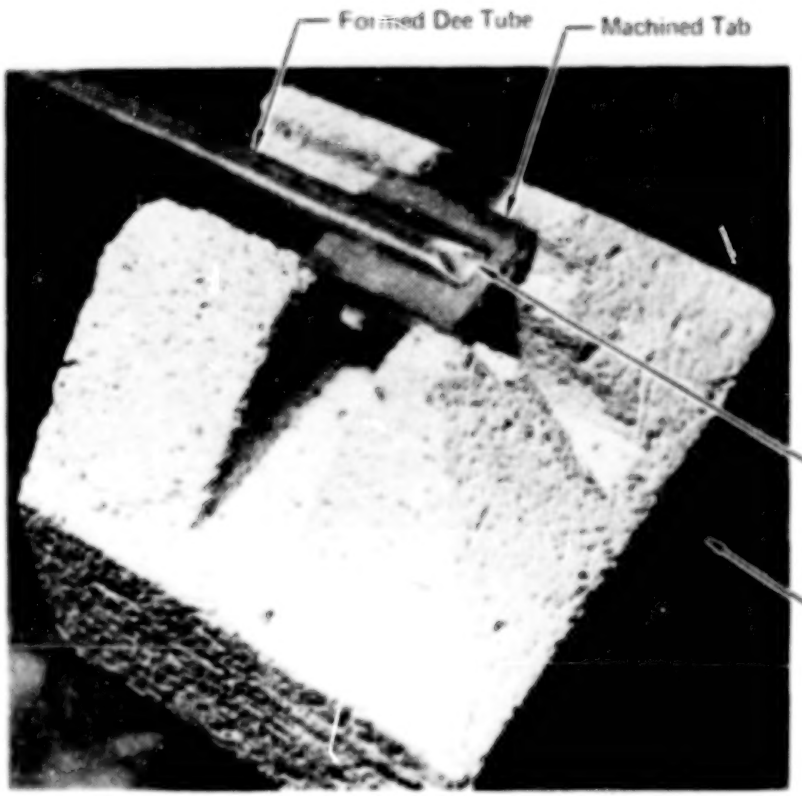


**FIGURE 78 · TUBE/TAB ASSEMBLY**

The test panel manifolds, shown in figure 79, were fabricated as a three piece weldment rather than an extrusion, because of the long procurement time involved in obtaining an extrusion. The manifold details were machined from 6061-T6511 bar stock and then automatic welded with 4043 filler rod to complete the manifold assembly. Figure 80 shows the welded manifolds being finish machined. Pockets were machined to accept the tabs of the tube/tab assemblies. Pockets were also machined in the transverse splice area to reduce the mass. The manifolds were then heat treated to the T6 condition, coolant passage holes drilled, and then cleaned. The manifold end caps and coolant ports were welded in place, the assembly proof pressure checked to 1.31 kPa (190 psig), and then primed for bonding.

The coolant passage holes in the machined pockets of the manifold are inline with holes provided on the opposite manifold surface so that neoprene plugs could be inserted in the coolant passage holes to prevent adhesive from entering the holes during the bonding operation.

Figure 81 shows the honeycomb core (ridigized with polyethylene glycol) being machined to accept the Dee tubes. After machining, the core was heated to 322K (120°F) to melt the polyethylene glycol. Next, the core was cleaned and primed for adhesive bonding and filled, as shown in figure 82, with Pro Seal 829 potting compound in areas where fasteners that do not have standoff posts pass through the panel. The Pro Seal hardens when the skins are bonded to the honeycomb.

Figure 83 shows the outer skin adhesively bonded with FM-400 film type adhesive to the tube/tab assemblies and the manifold assemblies. A sacrificial layer of FM-400 adhesive was provided on all surfaces to assure good adhesion of the honeycomb core during the next bonding operation.

The holes in the manifolds were then plugged with Lee plugs and the assembly was pressure tested before the second stage bonding operation. During the pressure check, numerous leaks were discovered between the manifolds and the tabs of the tube/tab assemblies. The leaks were sealed (figure 84) with Hysol EA956

FIGURE 79 WELDED COOLANT MANIFOLD

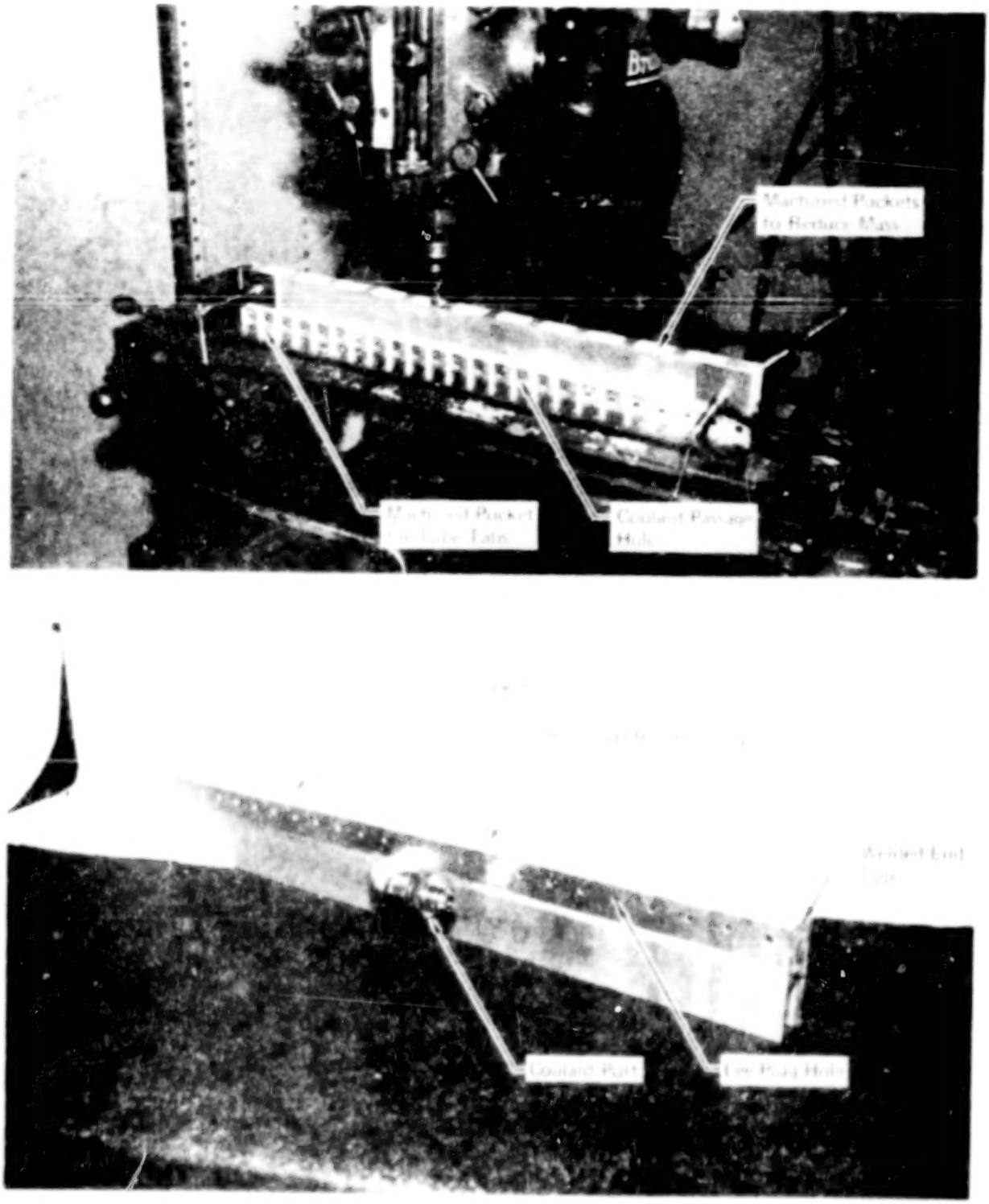


FIGURE 80 MACHINED COOLANT MANIFOLD

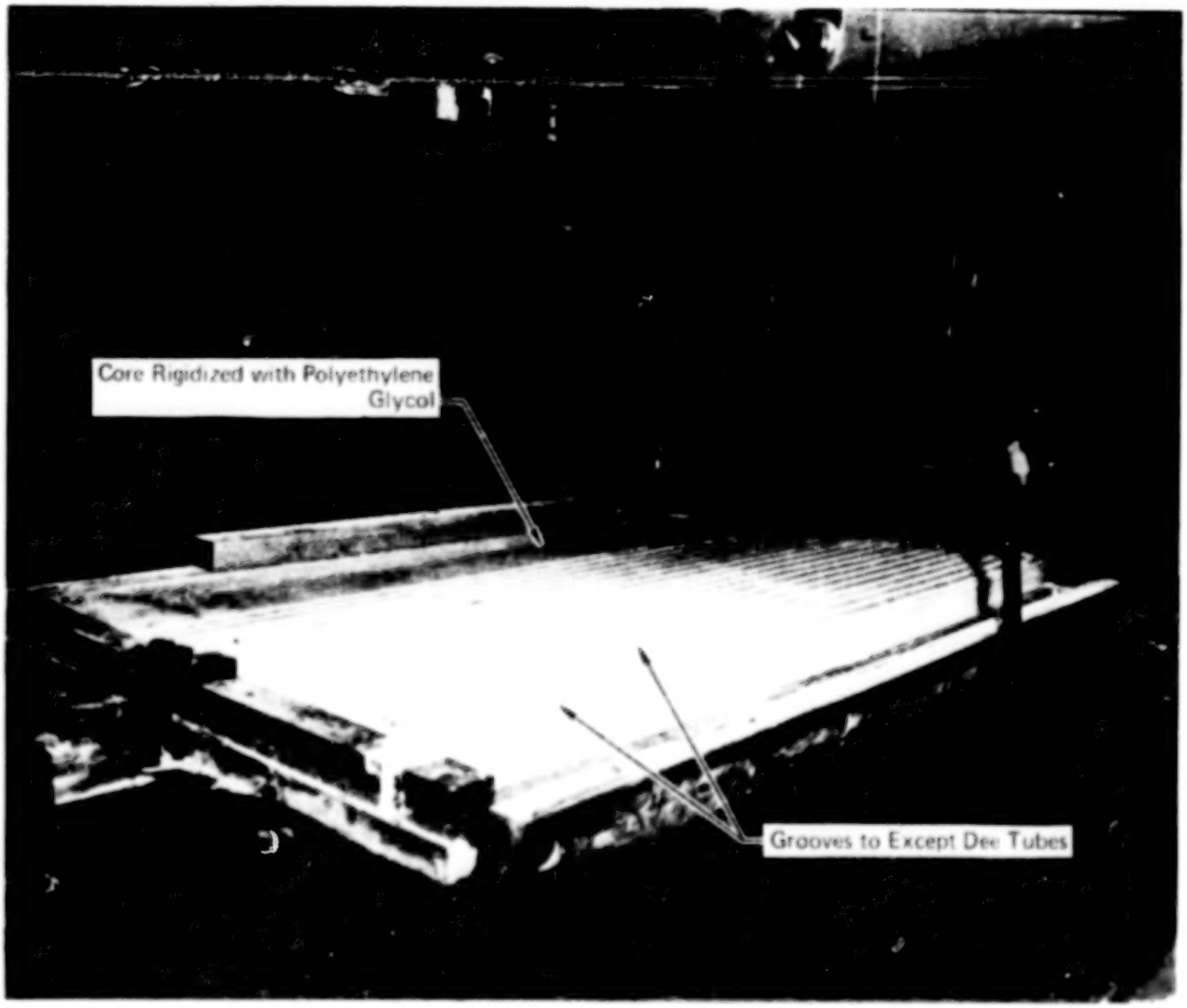


FIGURE 81 - MACHINING OF HONEYCOMB CORE

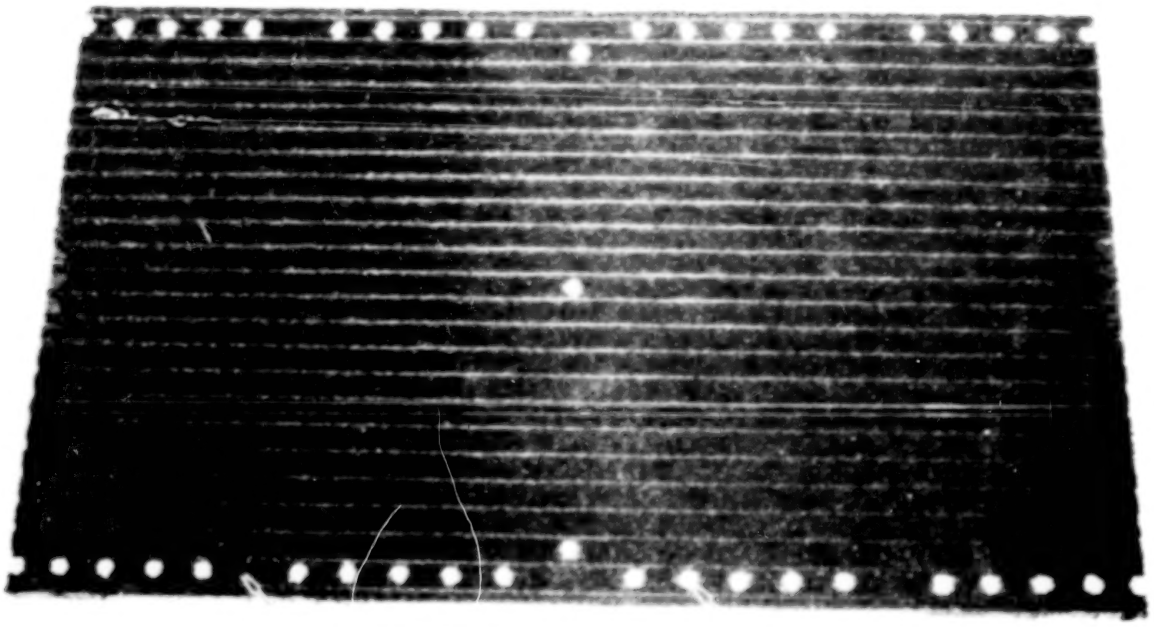

FIGURE 82 - POTTING COMPOUND IN HONEYCOMB CORE

Figure 85 shows the FM-404 foaming type adhesive placed over the sacrificial adhesive coverng the Dee tubes. The foaming adhesive was used in areas where poor fit-up could occur. During bonding, the adhesive foams into the honeycomb core, assuring bonding of the tubes to the core. After the second stage bonding operation, in which the honeycomb core and inner skin were bonded to the assembly shown in figure 83, the panel was proof pressure checked and radiographically inspected.

Figure 86 shows the completed actively cooled panel assembly with the transverse and longitudinal splice plates bonded in position with RTV 560. The exposed honeycomb edges of the test panel were filled with polysulfide sealant to prevent core damage during handling. Machined flanged bushings were used at the heat shield stand-off posts to prevent crushing of the honeycomb core during fastener installation.

Figure 87 shows four Chromel-Alumel thermocouple leads extending through the inner skin of the panel. Two thermocouples

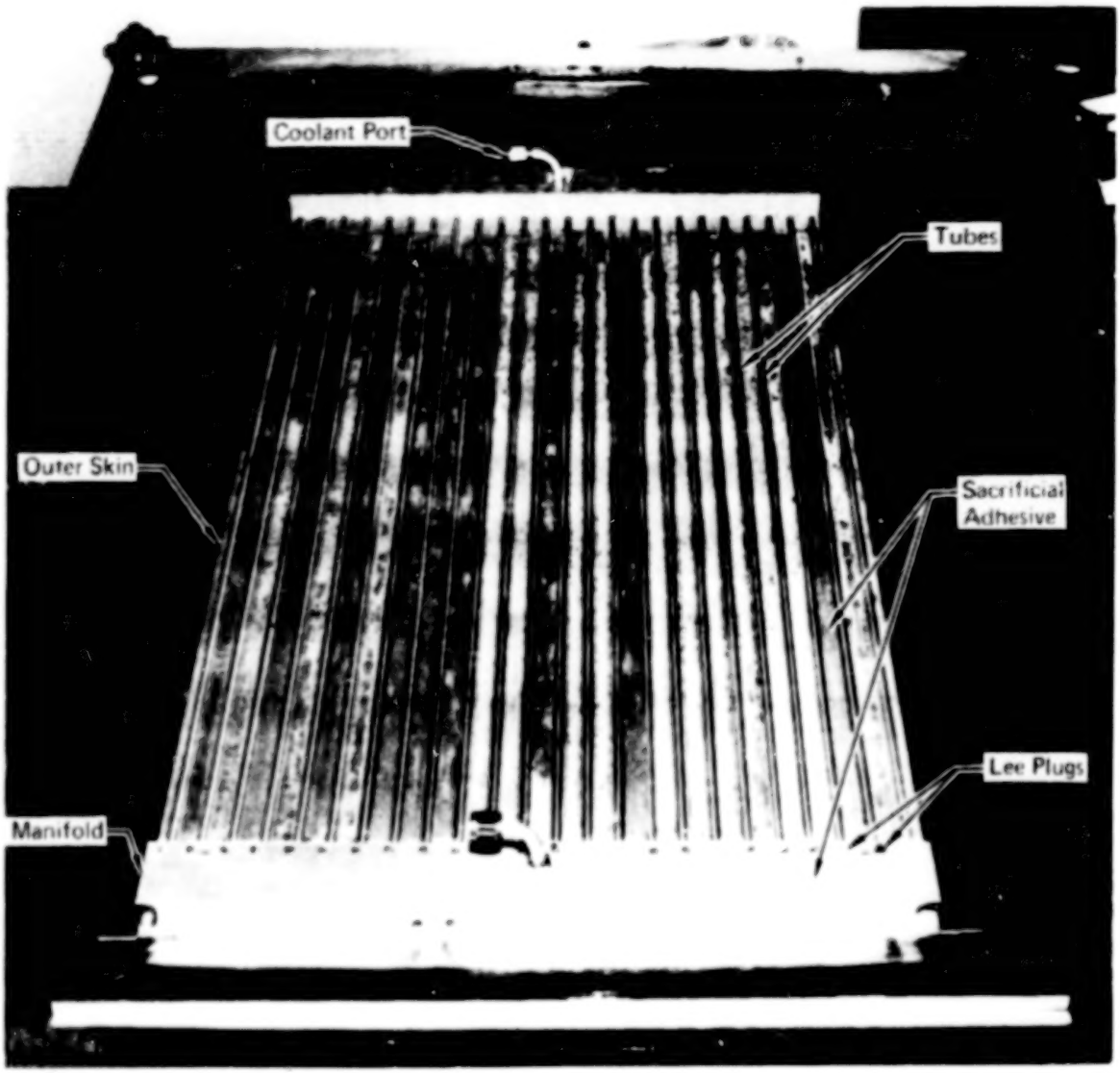


FIGURE 83 - BONDED OUTER SKIN AND TUBE/MANIFOLD ASSEMBLY

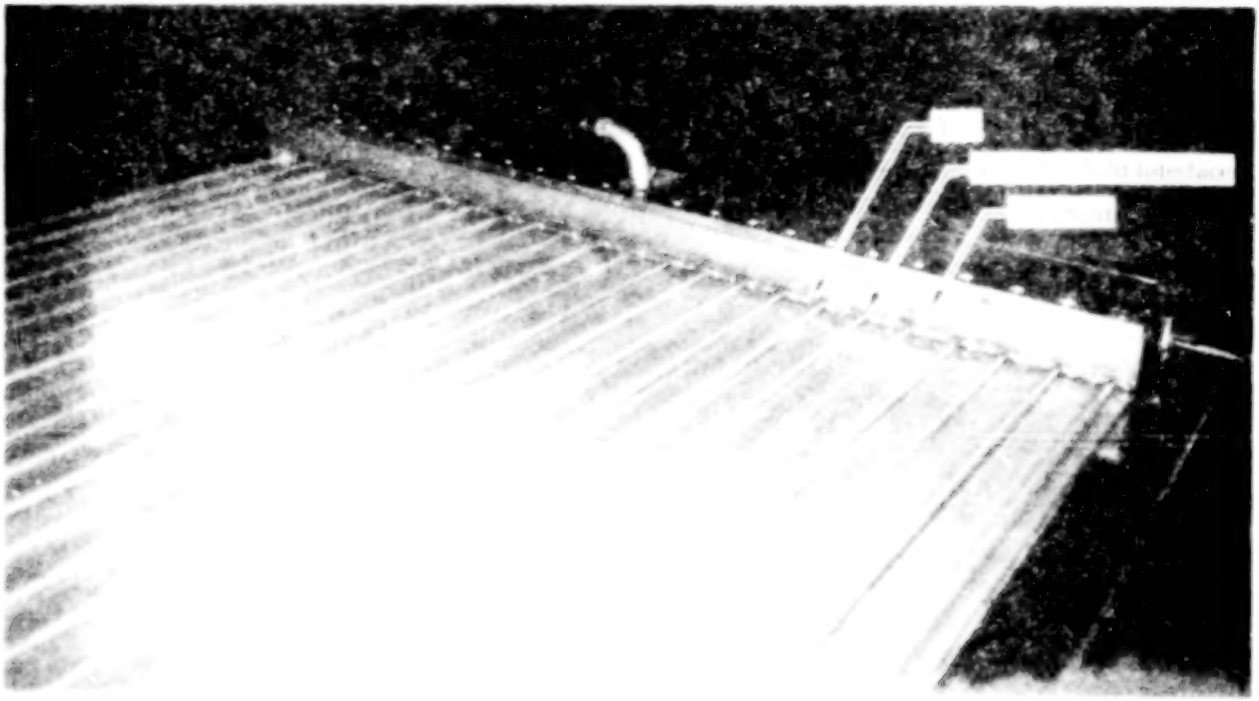

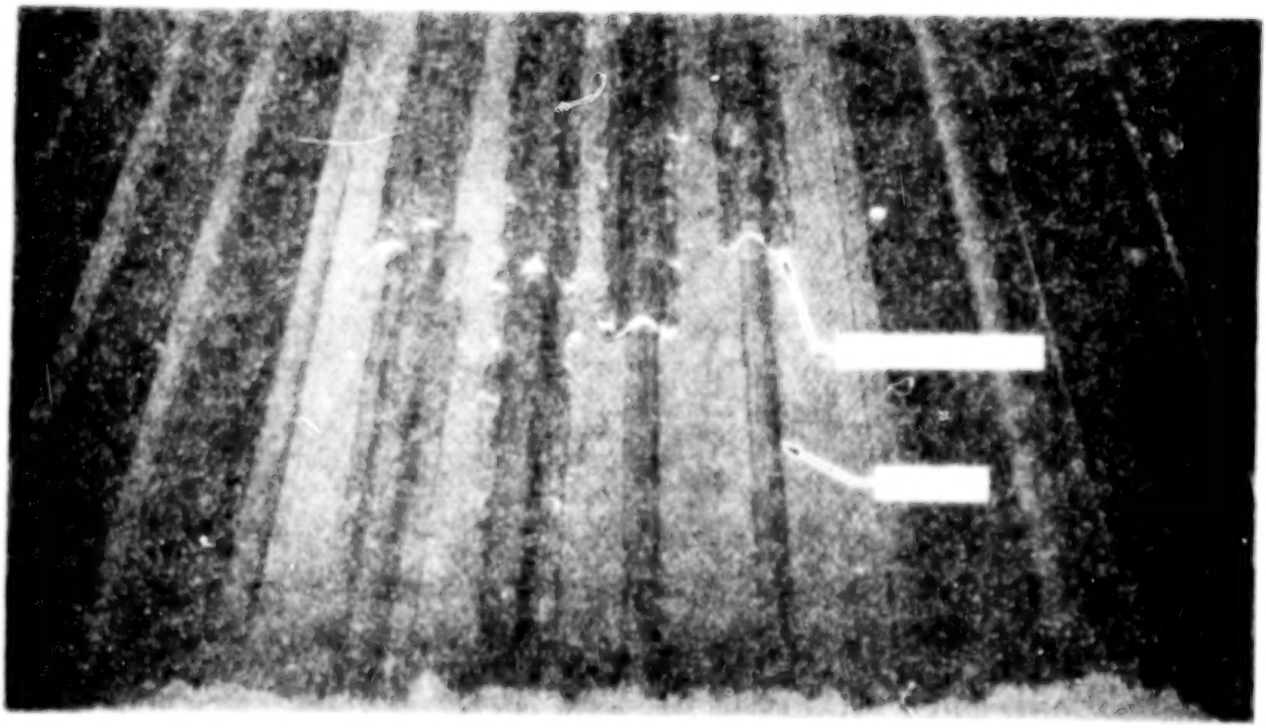

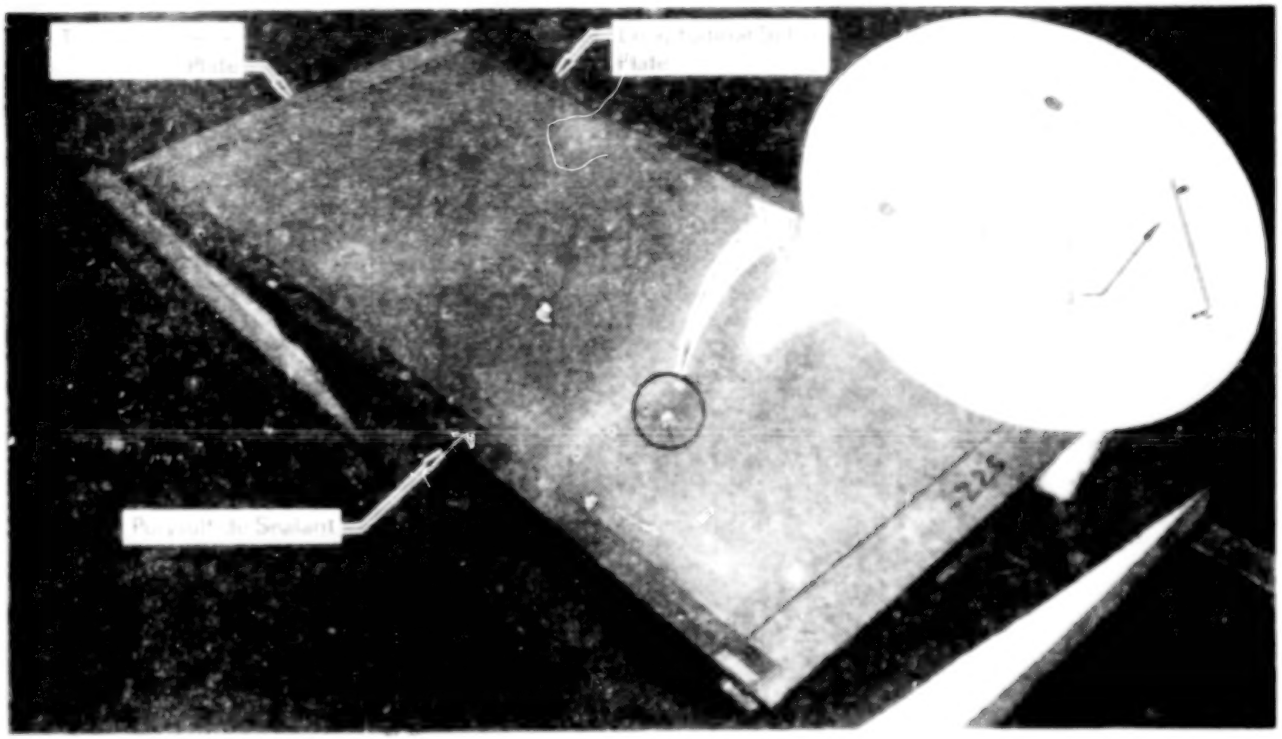

FIGURE 86 BONDED ACTIVELY COOLED PANEL

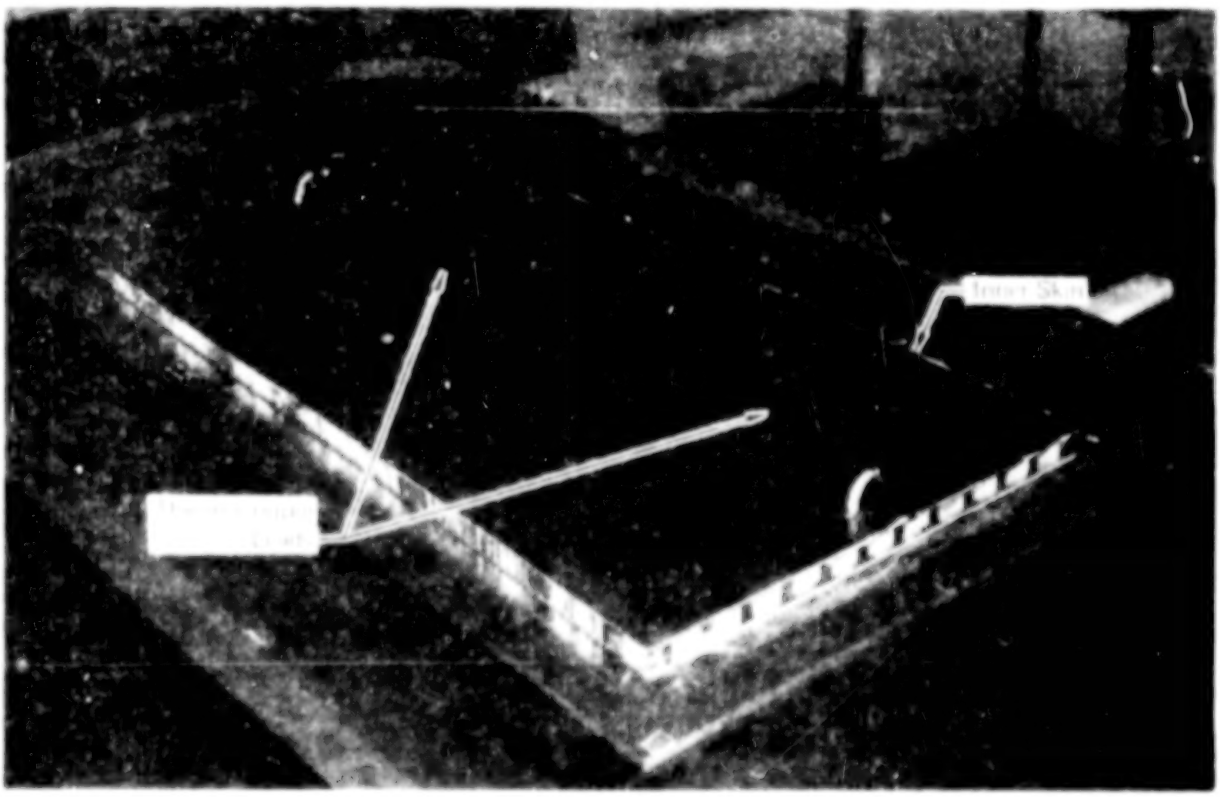

FIGURE 87 THERMOCOUPLE LEADS EXTEND THROUGH PANEL

were attached near the inlet and two near the exit manifold on the same Dee tube. The leads pass directly through the honeycomb and were potted with Pro Seal 829 potting compound to prevent damage during handling.

The superalloy Rene '41 beaded and corrugated heat shield skins were initially rubber formed at room temperature. Although rubber forming was successful for the beaded skins, it did not work for the corrugated skins because the corners of the corrugations did not completely conform to the female die. The corrugations were restruck with a steel male die (figure 88) to obtain the desired small radius at the bottom of the corrugations.

Examination of both the formed skins and corrugations showed a slight bow in the longitudinal direction. This bow was eliminated once the skins and corrugations were spot welded together.

The skins were cleaned with MEK (Methyl Ethyl Ketone) before spot welding. The following steps were then taken to minimize discoloration of the surfaces:

- The copper residue from spot welding was removed using a Bright Boy (Cratex Mfg. Co.) rubberized abrasive material.
- Surfaces were cleaned with MEK (Methyl Ethyl Ketone).
- Heat shields were ultrasonically cleaned in freon - P.C.A. (Precision Cleaning Agent)
- Heat shields were blown dry with nitrogen.

The heat shields were then aged at 1170 K (1650°F) for four hours and air-cooled. During aging, weights were placed on small stainless steel blocks located on the lands of the heat shield at 10.96 cm (4 in.) spacing to minimize distortion.

Figure 89 shows three of the heat shields positioned on the drill template which was used to align holes in the heat shields, insulation packages, and actively cooled panel.

Two insulation packages were fabricated for the test panel. Each package consisted of flexible 256 kg/m$^3$ (16 lbm/ft$^3$) Min-K insulation, covered with Astroquartz cloth. The Min-K insulation was inserted into an 0.0076 cm (0.003 in.) thick outer and an 0.00254 cm (0.001 in.) thick inner 321 stainless steel foil

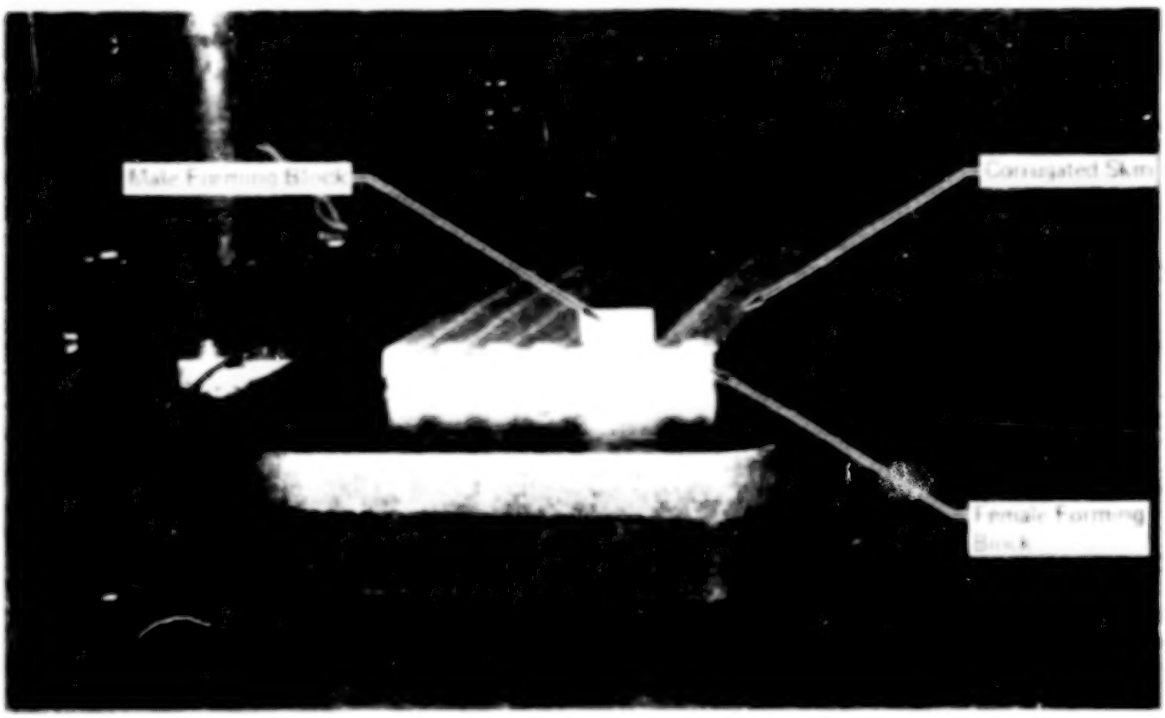


FIGURE 88 - FORMING RENE' 41 CORRUGATIONS

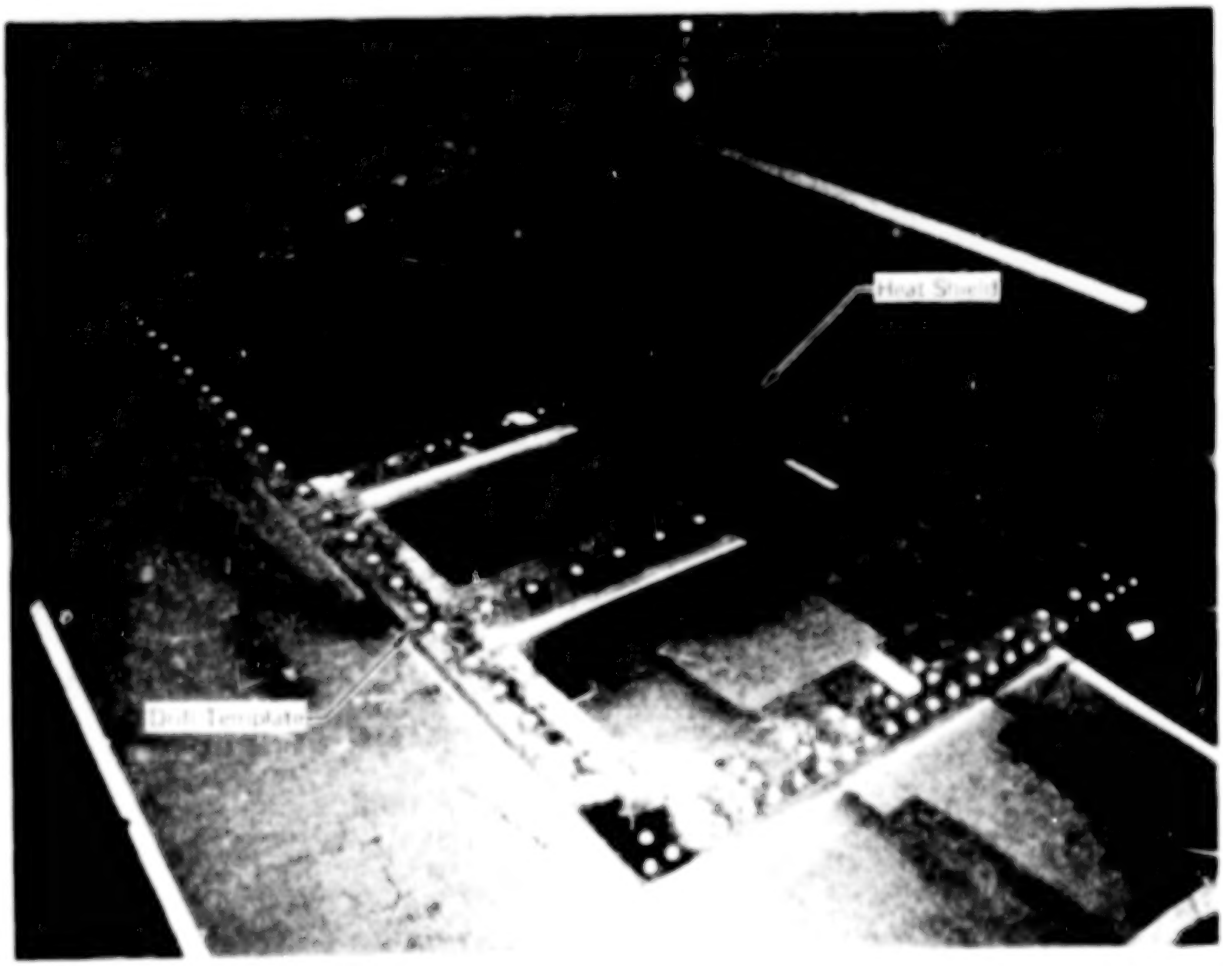


FIGURE 89 - RENE' 41 HEAT SHIELDS ON DRILL TEMPLATE

envelope. The 0.0076 cm (0.003 in.) thick foil was used on the outer surface because of concern of oxidation of the foil during high temperature thermal cycling. Figure 90 shows the strips of foil being spot welded together to form the envelope.

Figure 91 shows the partially completed wind tunnel close-out fairing, which consists of aluminum support beams, 0.635 cm (0.25 in.) thick aluminum support plates. and Thermo-Sil Castable 120 (fused silica) cover fairings. The support plates and the Castable 120 rest on the aluminum support beams, which mate with the NASA wind tunnel panel holder. The Castable 120 (not all shown) is bonded with RTV-560 adhesive to the aluminum support plates. The cutouts in the Castable 120 allow hoist fittings to be attached to the support beam for hoisting the assembly into the wind tunnel panel holder. The aluminum ACP support beams add stiffness to the fairing and support the actively cooled test panel (now shown) during hoisting.

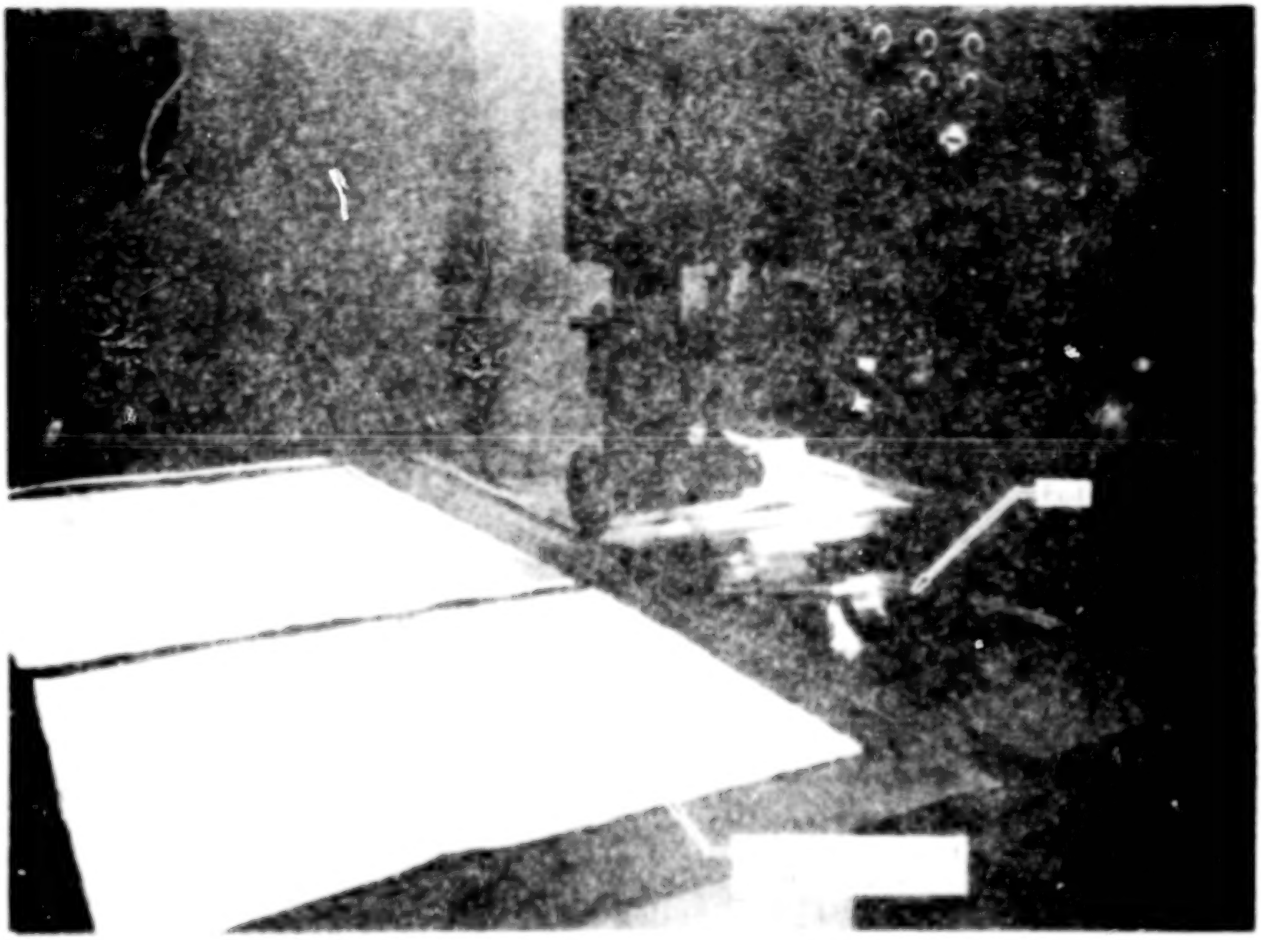

FIGURE 90 - INSULATION PACKAGES

FIGURE 91 - PANEL WIND TUNNEL SUPPORT STRUCTURE

## REFERENCES


1. Ellis, D. A.; and Pagel, L. L.: High Heat Flux Actively Cooled Honeycomb Sandwich Structural Panel for a Hypersonic Aircraft. NASA CR-2959, 1978.
2. Pirrello, C. J.; Baker, A. H.; and Stone, J. E.: A Fuselage Tank Structure Study for Actively Cooled Hypersonic Cruise Vehicles - Summary. NASA CR-2651, February 1976.
3. Military Specification, Airplane Strength and Rigidity Reliability Requirements, Repeated Loads and Fatigue. Department of Defense, MIL-A-008866A USAF, March 1971.
4. Federal Air Regulations. Volume III, Part 25 Airworthiness Standards, Transport Category Airplanes.
5. Brogren, E. W.; Brown, A. L.; Clinger, B. E.; Deringer, V.; and Jaeck, C. L.: Thermal-Structural Combined Loads Design Criteria Study. NASA CR-2102.
6. F-4 Fatigue and Damage Tolerance Assessment Program. MDC A2883, Volumes I and II, McDonnell Douglas Corporation, 28 June 1976.
7. Department of Defense, Aerospace Structural Metals Handbook. Volume 5, Code 4205 Rene'41, Revised December 1972.
8. Tims, D.: Evaluation of Adhesive of MMS-307. MDC A0884, McDonnell Douglas Corporation, 1971.
9. Mills, J. P.: Fatigue Tests on F-15 Honeycomb Panel with Spliced Core and Filled Honeycomb Core. MDC A1318, McDonnell Douglas Corporation, 3 October 1971.
10. Symposium on Reusable Surface Insulation for Space Shuttle. NASA TM X-2721, Volume III, Article 28, Pages 935-964, September 1973.
11. Spalding, D. B.; and Chi, S. W.: The Drag of a Compressible Turbulent Boundary Layer on a Smooth Flat Plate With and Without Heat Transfer. Journal of Fluid Mechanics, Volume 18, Part 1, January 1964.
12. Brewer, G. D.; and Morris, R. E.: Study of Active Cooling for Supersonic Transports. NASA CR-132573, February 1975.

13. Jones, Robert A.; Braswell, Dorothy O.; and Richie, Christine B.. Fail-Safe Systems for Actively Cooled Supersonic and Hypersonic Aircraft. NASA TM X-3125, January 1975.

14. Anthony, F. M.; Dukes, W. H.; Helenbrook, R. G.: Data and Results from a Study of Internal Convective Cooling Systems for Hypersonic Aircraft. NASA CR-132432, June 1974.

15. Stone, J. E.: A Fuselage/Tank Structure Study for Actively Cooled Hypersonic Cruise Vehicles. Volume III - Active Cooling System Analysis, NASA CR-132669, June 1975.

16. Pagel, L. L.; and Warmbold, W. R.: Active Cooling of a Hydrogen Fueled Scramjet Engine. AIAA Paper No. 68-1091, October 1968.

17. Peeples, M. E.; and Herring, R. L.: Study of a Fail-Safe Abort System for an Actively Cooled Hypersonic Aircraft. NASA CR-144920, Volume II, January 1976.

18. Symposium on Reusable Surface Insulation for Space Shuttle. NASA TM X-2719, Volume I, Article 1, Pages 1-16, September 1973.

19. Miller, R. C.: Metal Wool Heat Shields for Space Shuttle. NASA CR-132389, Hughes Aircraft Company, March 1974.

20. Kirlin, R. L.: Evaluation of Bond-On Insulation TPS Material for X-24C. AFFDL-TR-76-25, Vol. I, March 1976.

21. McAdams, W. H.: Heat Transmission, McGraw-Hill, Third Edition.

22. Rohsenow, W. M.; and Hartnett, J. P.: Handbook of Heat Transfer. McGraw-Hill.

23. SAE Aerospace Applied Thermodynamics Manual. Second Edition, October 1969.

24. Kays, W M.; and London, A. L.: Compact Heat Exchangers. McGraw-Hill, First Edition.

25. Kays, W. M.; and London, A. L.: Compact Heat Exchangers. McGraw-Hill, Second Edition.

26. Helenbrook, R. G.; and Anthony, F. M.: Design of a Convective Cooling System for a Mach 6 Hypersonic Transport Airframe. NASA CR-1918, December 1971.

27. Military Standardization Handbook, Structural Sandwich Composites. Department of Defense, MIL-HDBK-23A, December 1968.

28. Wheeler, O. E.: Crack Growth Under Spectrum Loading. FZM-5602, General Dynamics, 30 June 1970.

| 1. Report No. | 2. Government Accession No. | 3. Recipient's Catalog No. |
|---|---|---|
| NASA CR-2957 | | |

| 4. Title and Subtitle | 5. Report Date |
|---|---|
| DESIGN AND FABRICATION OF A RADIATIVE ACTIVELY COOLED HONEYCOMB SANDWICH STRUCTURAL PANEL FOR A HYPERSONIC AIRCRAFT | March 1978 |
| | 6. Performing Organization Code |
| 7. Author(s) | 8. Performing Organization Report No. |
| D. A. Ellis, L. L. Pagel, and D. M. Schaeffer | 10. Work Unit No. |
| 9. Performing Organization Name and Address | 11. Contract or Grant No. |
| McDonnell Douglas Corporation<br>P.O. Box 516<br>St. Louis, MO 63166 | NAS1-13939 |
| | 13. Type of Report and Period Covered |
| 12. Sponsoring Agency Name and Address | Contractor Report |
| National Aeronautics and Space Administration<br>Washington, D.C. 20546 | 14. Sponsoring Agency Code |

15. Supplementary Notes

Langley Technical Monitor: Charles P. Shore
Final Report

16. Abstract

This report presents the results of a study to design and fabricate a radiative actively cooled panel. The panel assembly consists of an external thermal protection system (metallic heat shields and insulation blankets) and an aluminum honeycomb structure. The structure is cooled to temperature 442K (300°F) by circulating a 60/40 mass solution of ethylene glycol and water through Dee shaped coolant tubes nested in the honeycomb and adhesively bonded to the outer skin. Rene'41 heat shields were designed to sustain 5000 cycles of a uniform pressure of ±6.89kPa (±1.0 psi) and aerodynamic heating conditions equivalent to 136 $kW/m^2$ (12 $Btu/ft^2$ sec) to a 422K (300°F) surface temperature. High temperature flexible Min-K insulation blankets were encased in stainless steel foil to protect them from moisture and other potential contaminates. The aluminum actively cooled honeycomb sandwich structural panel was designed to sustain 5000 cycles of cyclic in-plane loading of ±210 kN/m (±1200 lbf/in.) combined with a uniform panel pressure of ±6.89 kPa (±1.0 psi).

The total system (thermal protection system, actively cooled panel, and the active cooling system) was designed to be compatible with the available hydrogen fuel heat sink. A radiative actively cooled panel was determined to be 7% lighter than a bare actively cooled panel designed to the same conditions and constraints. One 0.61 x 1.22m (2 x 4 ft) radiative actively cooled test panel and one 0.30 x 0.61m (1 x 2 ft) heat shield fatigue specimen was fabricated by MCAIR and delivered to NASA for testing. A summary of the study and important conclusions is given in the body of the report (50 pages) and supporting details are presented in appendices.

| 17. Key Words (Suggested by Author(s)) | 18. Distribution Statement |
|---|---|
| Aluminum Actively Cooled Panel<br>Superalloy Heat Shields<br>Hypersonic Aircraft | Unclassified - Unlimited<br><br>Subject Category 39 |

| 19. Security Classif. (of this report) | 20. Security Classif. (of this page) | 21. No. of Pages | 22. Price |
|---|---|---|---|
| Unclassified | Unclassified | 161 | $8.00 |

* For sale by the National Technical Information Service, Springfield, Virginia 22161

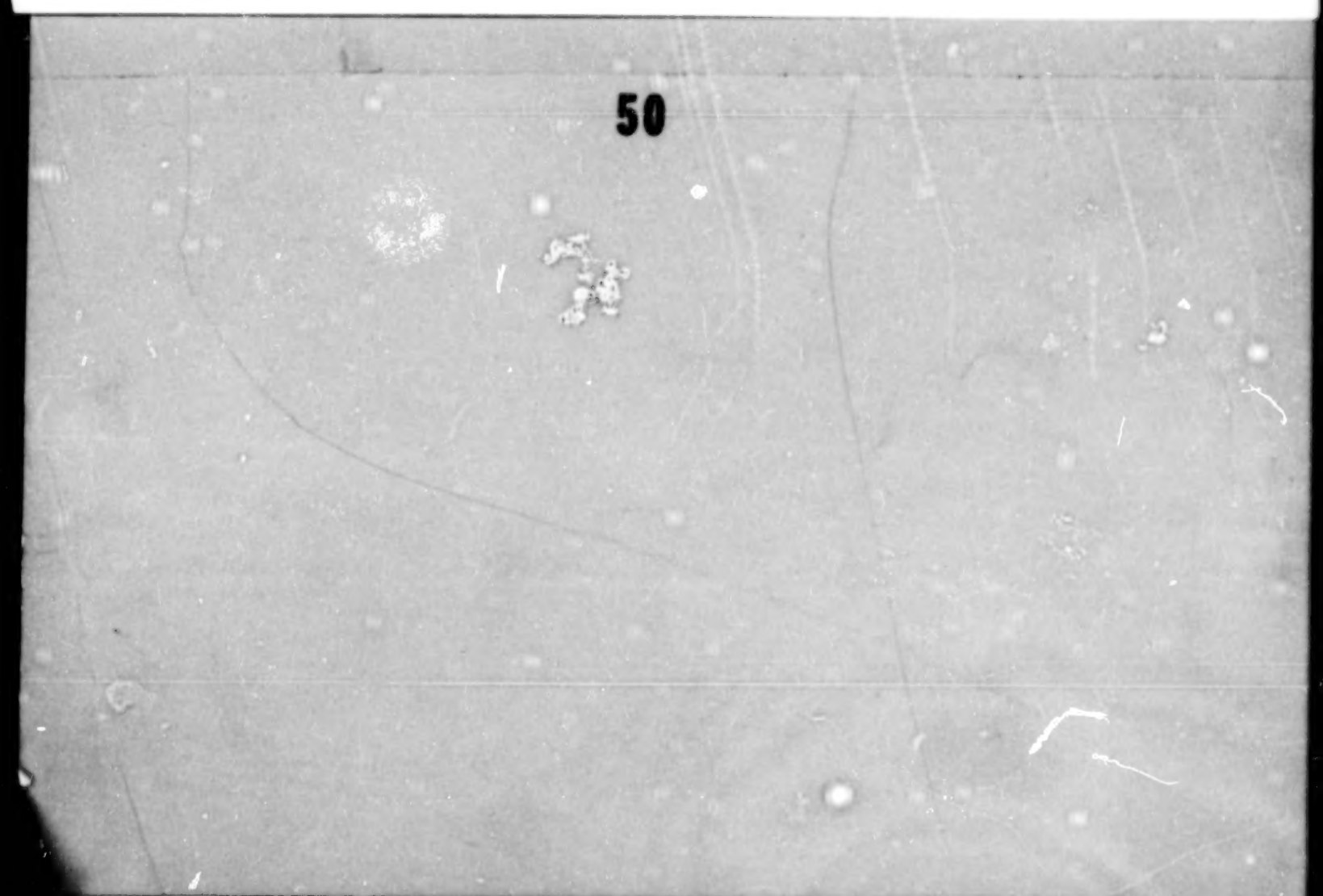
50

# END

DEC 11 1979